01 Dec 1992

Design of automotive structural components using high strength sheet steels influence of strain rate on the mechanical properties of sheet steels and structural performance of cold-formed steel members

Chi-Ling Pan

Wei-wen Yu
Missouri University of Science and Technology, wwy4@mst.edu

Civil Engineering Study 92-3
Cold-Formed Steel Series

Eighteenth Progress Report

DESIGN OF AUTOMOTIVE STRUCTURAL COMPONENTS USING HIGH STRENGTH SHEET STEELS

INFLUENCE OF STRAIN RATE ON THE MECHANICAL PROPERTIES OF SHEET STEELS AND STRUCTURAL PERFORMANCE OF COLD-FORMED STEEL MEMBERS

by

Chi-Ling Pan
Research Assistant

Wei-Wen Yu
Project Director

A Research Project Sponsored by the American Iron and Steel Institute

December 1992

Department of Civil Engineering
University of Missouri-Rolla
Rolla, Missouri

PREFACE

This report is based on a dissertation presented to the Faculty of the Graduate School of the University of Missouri-Rolla (UMR) in partial fulfillment of the requirements for the degree of Doctor of Philosophy in Civil Engineering.

The financial assistance granted by the Institute and the technical guidance provided by members of the AISI Task Force on Automotive Structural Design and the AISI Automotive Applications Committee and the AISI staff (S.J. Errera, D.C. Martin, A.L. Johnson, and L.A. Rysdrop) are gratefully acknowledged. Members of the Task Force are: Messrs. J. Borchelt, C. Haddad, C.M. Kim, R.W. Lautensleger, H. Mahmood, J.G. Schroth, T.N. Seel, M.Y. Sheh, and M.T. Vecchio. An expression of thanks is also due to Mr. D. L. Douty of Division of USX Steel Corporation, Mr. S.L. Caswell of National Steel Corporation, and Mr. J.D. Grozier of LTV Steel Company for their help.

All materials used in the experimental study were donated by LTV Steel Company, Inland Steel Company, and National Steel Corporation.

Appreciation is also expressed to Messrs. K. Haas, J. Bradshaw, F. Senter, and S. Gabel, staff of the Department of Civil Engineering, for their technical support and to Mr. M. Y. Shan for his valuable assistance in the preparation and performance of the tests.

ABSTRACT

The current design criteria for effective design width being used in the AISI Automotive Steel Design Manual[1] for the design of cold-formed steel members are based on tests under static loading condition. The primary objective of this investigation was to study the validity of these effective design width formulas for members subjected to dynamic loads. This report presents a detailed description of an experimental study. Selected steels with nominal yield strengths ranging from 25 ksi to 100 ksi were uniaxially tested under different strain rates. In order to study the structural behavior and strength of cold-formed steel members having stiffened and unstiffened compression elements, a total of 97 stub column specimens and 60 beam specimens were fabricated from 35XF and 50XF sheet steels and tested under dynamic loads. It was found from test results that the mechanical properties of sheet steels and strengths of cold-formed steel members increased with increasing strain rate. The amount of increase is dependent on the the material yield strengths, the stress-strain relationships, and the strain rates used in the tests. In the evaluation of the test data, it was found that the value of buckling coefficient, 0.43, used to calculate the effective width of unstiffened compression elements is conservative. For calculating the ultimate capacity of stub columns and beams, the values computed from Kalyanaraman's equations for unstiffened compression elements provide good agreements with test results. In addition, a better prediction for ultimate capacity of stub columns and beams can be obtained by using the dynamic yield strengths.

TABLE OF CONTENTS

TABLE OF CONTENTS (Cont'd)

TABLE OF CONTENTS (Cont'd)

TABLE OF CONTENTS (Cont'd)

TABLE OF CONTENTS (Cont'd)

LIST OF ILLUSTRATIONS

LIST OF ILLUSTRATIONS (Cont'd)

LIST OF ILLUSTRATIONS (Cont'd)

LIST OF ILLUSTRATIONS (Cont'd)

LIST OF ILLUSTRATIONS (Cont'd)

LIST OF ILLUSTRATIONS (Cont'd)

LIST OF ILLUSTRATIONS (Cont'd)

LIST OF ILLUSTRATIONS (Cont'd)

LIST OF ILLUSTRATIONS (Cont'd)

LIST OF ILLUSTRATIONS (Cont'd)

LIST OF TABLES

LIST OF TABLES (Cont'd)

LIST OF TABLES (Cont'd)

LIST OF TABLES (Cont'd)

LIST OF TABLES (Cont'd)

LIST OF TABLES (Cont'd)

LIST OF TABLES (Cont'd)

LIST OF TABLES (Cont'd)

I. INTRODUCTION

A. GENERAL

In recent years, more economic and lighter vehicles have been produced by automotive manufacturers for the sake of fuel economy. High strength sheet steels have been favorably used to accomplish the construction of such automobiles. The design information for using sheet steels is provided in the AISI Automotive Steel Design Manual[1].

In the "Guide for Preliminary Design of Sheet Steel Automotive Structural Components[2]" issued by American Iron and Steel Institute (AISI) in 1981, the design information was used only for sheet steels with yield strengths of up to 80 ksi. In order to provide more information on high strength sheet steels, a project entitled "Design of Automotive Structural Components Using High Strength Sheet Steel" has been conducted at University of Missouri-Rolla (UMR) since 1982 under the sponsorship of the American Iron and Steel Institute (AISI).

In the first phase of the UMR program, different grades of sheet steels with yield strengths ranging from 49 to 164 ksi were tested under static loads for the study of mechanical properties and stress-strain relationships. In the second phase of the UMR program, the research was concentrated on the investigation of the web crippling strength of beam webs and the strength of members consisting of flat and curved elements. The results were presented in ten progress reports[3-12]. In addition, the effective design widths of high strength cold-formed steel members were also investigated[13].

It has been recognized that material properties and stress-strain relationships of sheet steels can be influenced by the strain rate. Since the previous research was limited only to the tests subjected to static loads, additional studies of mechanical properties of sheet steels and strengths of cold-formed steel members under different strain rates were performed at UMR since 1988. The research findings were presented in seven progress reports[14-19].

B. PURPOSE OF INVESTIGATION

In view of the fact that in the current AISI Automotive Steel Design Manual[1], the design criteria for effective design width are based on the test results under static loading condition, this study involved primarily the investigation of the validity of these effective design width formulas for the design of cold-formed steel structural members subjected to dynamic loads. Prior to the member tests, the effects of strain rate on the mechanical properties of three selected sheet steels were also studied experimentally.

C. SCOPE OF INVESTIGATION

In the first phase of the investigation, three selected sheet steels (35XF, 50XF, and 100XF) have been studied. The test results of the static and dynamic mechanical properties in tension and compression under different strain rates were established. The nominal yield strengths of these three types of sheet steels ranged from 35 to 100 ksi and the range of strain rates varied from 10^{-4} to 1.0 in./in./sec.. The test results obtained from this study were presented in the Eleventh[14] and Twelfth[15] Progress Reports.

The structural behavior and strength of cold-formed steel members having both unstiffened and stiffened elements were studied experimentally and analytically for stub columns and beams subjected to dynamic loads in the second phase of the investigation. Both 35XF and 50XF sheet steels were used in this phase of study.

During the period from August 1989 through April 1990, eighteen (18) box-shaped stub columns and fifteen (15) hat-shaped beams were tested to study the strength of structural members having stiffened compression elements. For the study of unstiffened elements, seventeen (17) I-shaped stub columns and fifteen (15) channel beams were tested. These test specimens were fabricated from 35XF sheet steel. The test results were presented in the Thirteenth[16] and Fourteenth[17] Progress Reports.

From May 1990 through October 1990, fourty-eight (48) stub columns were fabricated from 50XF sheet steel for static and dynamic tests. In addition, twelve (12) stub columns fabricated from 35XF sheet steel were also tested for the study of large width-to-thickness (w/t) ratios of compression elements. The test results were presented in the Fifteenth Progress Report[18]. The study of beam specimens fabricated from 50XF sheet steel and subjected to dynamic loads was initiated in March 1991. Fifteen (15) channel sections and fifteen (15) hat sections were tested for the purpose of studying the behavior of beams having unstiffened and stiffened compression elements, respectively. The test results were presented in the Sixteenth Progress Report[19].

In Section II of this thesis, the literature review is related to (1) the effect of strain rate on mechanical properties of sheet steels,

(2) local buckling and postbuckling behavior of stiffened and unstiffened compression elements, and (3) the structural strength of steel members under dynamic loading conditions. The experimental investigations of the dynamic material properties of three selected sheet steels and the structural behavior of stub columns and beams subjected to dynamic loads are discussed in Section III. In Section IV, the test data of material properties, stub columns, and beam specimens are evaluated. Finally, the research findings are summarized in Section V.

II. REVIEW OF LITERATURE

A. GENERAL

It is well known that the mechanical properties of sheet steels, such as yield strength, ultimate tensile strength, and proportional limit can vary with the strain rate used in the test. Therefore, a review of mechanical properties of sheet steels and a survey of available literature concerning the effect of strain rate on the strengths of sheet steels in tension and compression are presented in Sections B and C of this Section, respectively.

For the design of cold-formed steel members, the current AISI design criteria for determining the effective design width of compression elements are based on the test results for static loading condition. In order to investigate the validity of these effective design width formulas for the members subjected to dynamic loads, it is necessary to review the literature relative to the following subjects:

(1) The structural behavior of compression elements under static loads (Sec. D).

* The analytical solutions of the elastic local buckling strengths of both stiffened and unstiffened compression elements (Sec. D.1).
* The inelastic buckling stress of flat compression elements (Sec. D.2).
* The theoretical background of the postbuckling behavior of stiffened and unstiffened compression elements (Sec. D.3).

* The development of effective width formulas for the prediction of maximum strength of stiffened and unstiffened compression elements (Sec. D.4).
* The current effective width formulas used in the AISI Automotive Steel Design Manual[1] (Sec. D.5).

(2) The available literature on the effect of impact loads or dynamic loads on the structural strengths of beams (Sec. E).

(3) The available literature related to the strengths of axially loaded members subjected to dynamic or impact loads (Sec. F).

B. MECHANICAL PROPERTIES OF SHEET STEELS

The mechanical properties of sheet steels such as proportional limit, yield strength, ultimate tensile strength, and rupture strength can be found from the stress-strain relationship. The engineering stress-strain curve which is different from the true stress-strain curve is commonly used for the purpose of engineering analysis and design.

Figure 2.1 shows two basic types of engineering stress-strain curves for high strength sheet steels. Figure 2.1(a) exhibits a well defined yield point, while Figure 2.1(b) does not. The classification of the stress-strain curve obviously comes from the yielding behavior of the steel. For most cases, hot-rolled sheet steels tend to be sharp yielding as shown in Figure 2.1(a), while the sheet steels which are cold-rolled or cold reduced in thickness are gradual yielding (Figure 2.1(b)).

For engineering stress-strain curve, the stress (σ) is defined by the load (P) divided by the original, unreduced area (A_o), of the specimen, i.e.

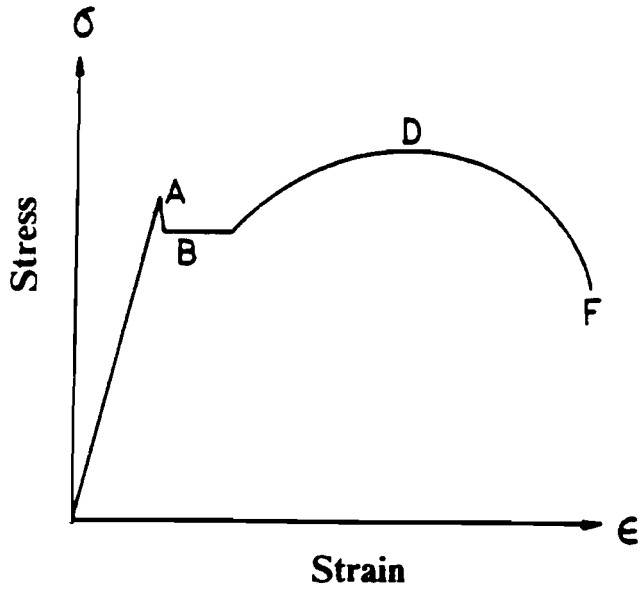

(a) Sharp-Yielding Steel

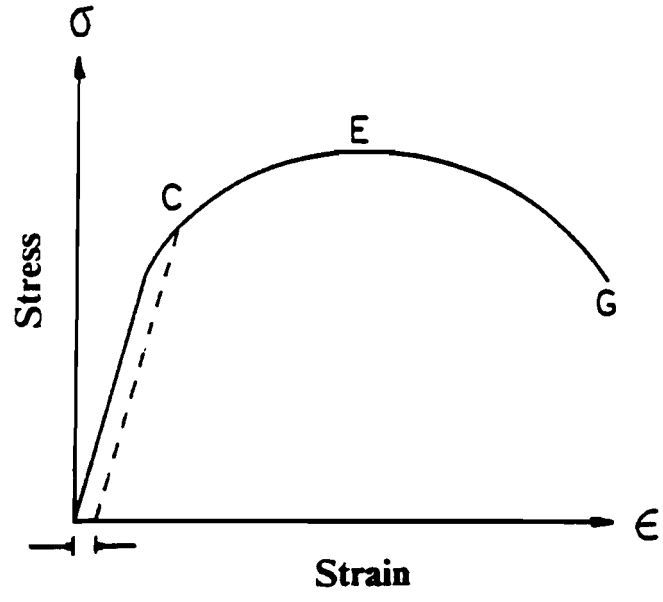

(b) Gradual-Yielding Steel

Figure 2.1 Stress-Strain Curves of Carbon Steel Sheets

$$\sigma = \frac{P}{A_o} \tag{2.1}$$

and the engineering strain (ε) can be obtained from dividing the elongation by the original, unreduced length as follows:

$$\varepsilon = \frac{\Delta L}{L_o} = \frac{L - L_o}{L_o} \tag{2.2}$$

where L = final length of specimen

L_o = original, unreduced length of specimen

The yield point is a stress, at which there is an appreciable elongation or yielding of the material without any corresponding increase of load. As shown in Figure 2.1(a), sharp yielding steels typically exhibit an upper (point A) and lower yield point (point B). Since the upper yield point is much more sensitive to strain rate, specimen alignment, and shape of the tested cross-section than the lower yield point, the lower yield point is customarily used to represent the yield stress of sharp yielding sheet steels subject to static loading[20,21]. It should be emphasized that the lower yield point depends on the machine stiffness[22].

Indeed, the load may actually decrease while the yielding occurs. However, the phenomenon of yielding is peculiar to structural steel; other grades of steels and steel alloys or other materials do not posses it, as is indicated by the typical stress-strain curve shown in Figure 2.1(b). This curve, incidentally, is typical for a first loading of material that contain appreciable residual stresses produced by manufacturing or aging processes. After repeated loading, these residual stresses are removed

and the stress-strain curve becomes practically straight[23]. Since gradual yielding steels do not have a well-defined yield point, their yield stress is defined by either an offset method or the strain-under-load method. The offset method consists of drawing a line parallel to the initial tangent of the stress-strain curve. A value of 0.2 percent is usually chosen to be an offset strain as shown in Figure 2.2(a)[24]. The strain-under-load method defines the yield point as the stress corresponding to some fixed value of strain. The strain usually chosen to be 0.5 percent as shown in Figure 2.2(b)[24].

Other material properties developed from the stress-strain curve are the following:

(1) The proportional limit (point C of Figure 2.1), that is, the stress beyond which the the strain is no longer proportional to the stress. For sheet steels, whether they are gradual or sharp yielding, the proportional limit may be determined by the 0.01 percent offset method.

(2) The modulus of elasticity (E), that is the slope of the linear portion of the stress-strain diagram.

(3) Working hardening, or strain hardening. Once the specimen is strained beyond the yield point, the load-carrying capacity of the steel continues to increase slightly in spite of the fact that the cross-sectional area of the specimen is continually decreasing. Since engineering stress is calculated based on the original area, there must be some other phenomenon occuring that causes the increase in load-carrying capacity. This phenomenon is commonly

referred to as work hardening and may be explained by dislocation theory[20].

(4) Ultimate tensile stress (points D and E of Figure 2.1), that is, the maximum stress of engineering stress-strain curve.

(5) Rupture stress (points F and G of Figure 2.1). For structural steel, it is somewhat lower than the ultimate tensile stress because the rupture strength is computed by dividing the rupture load by the orginal cross-sectional area which, although convenient, is incorrect. The error is caused by a phenomenon knowing as "necking".

As failure occurs, the material stretches very rapidly and simultaneously narrows down, so that the rupture load is actually distributed over a small area. If the rupture load is divided by the rupture area measured after failure occurs, the result is a reasonable value of the actual failure stress and this value is considerably higher than the ultimate stress[23].

As mention previously, the true stress-strain curve is different from the engineering stress-strain curve. The determination of the true stress ($\bar{\sigma}$), during a tensile test, is equal to the load (P) divided by the instantaneous cross-sectional area (A) as follows:

$$\bar{\sigma} = \frac{P}{A} \tag{2.3}$$

If the deformation in the gage length of the specimen is uniform, the instantaneous volume (AL) can be assumed equal to the initial volume (A_oL_o). Thus

$$V = A_o L_o = AL \tag{2.4}$$

Hence

$$A = \frac{A_o L_o}{L} \tag{2.5}$$

The true strain ($\bar{\varepsilon}$) is derived from the differential increment of strain ($d\bar{\varepsilon}$) as

$$d\bar{\varepsilon} = \frac{dL}{L} \tag{2.6}$$

The total unit elongation becomes

$$\bar{\varepsilon} = \int_{L_o}^{L} \frac{dL}{L} = \ln \frac{L}{L_o} \tag{2.7}$$

$$e^{\bar{\varepsilon}} = \frac{L}{L_o} \tag{2.8}$$

Using Equations 2.3, 2.5, and 2.8, thus

$$\bar{\sigma} = \frac{P}{A_o} e^{\bar{\varepsilon}} \tag{2.9}$$

As the load increases and thus the cross-sectional area decreases, the corresponding engineering stress will be smaller than the true stress computed for the same loading. The engineering and true stresses are practically identical in elastic range, because there is no appreciable change in area. However, as the stress reaches the inelastic range, the difference between the engineering and true stresses becomes apparent as

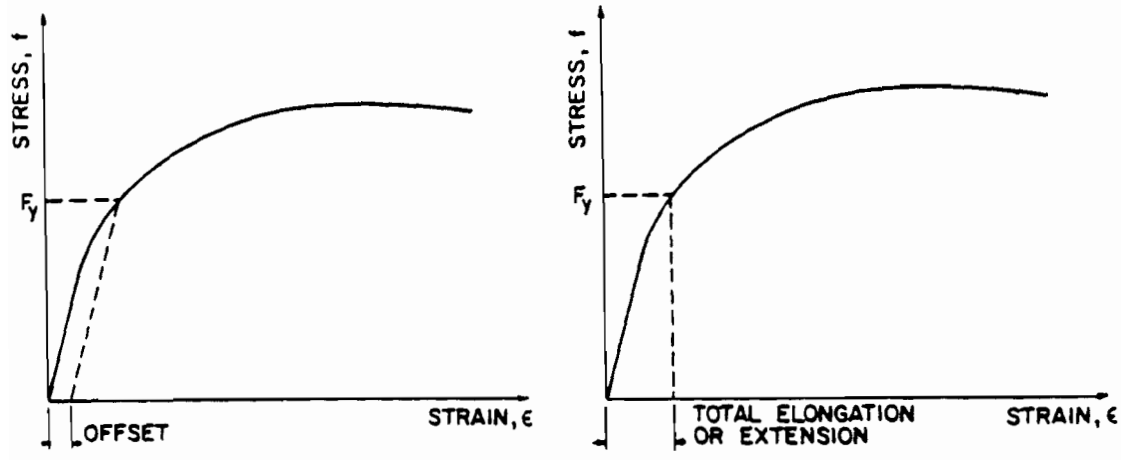

(a) Offset Method (b) Strain-under-Load Method

Figure 2.2 Determination of Yield Point for Gradual-Yielding Steel[24]

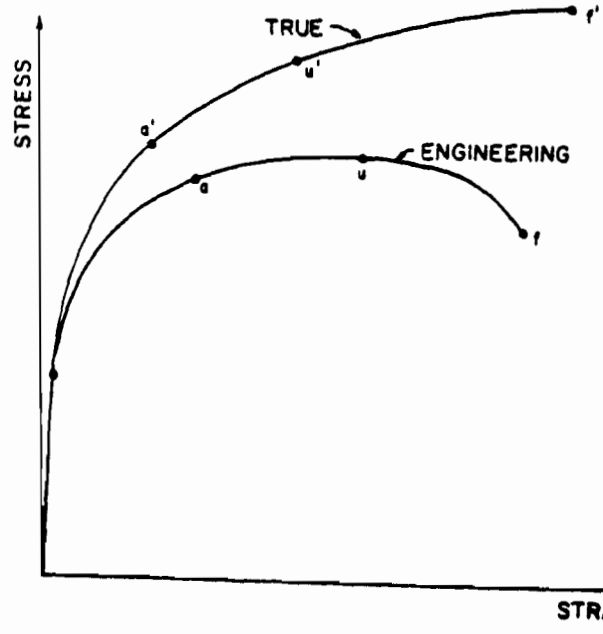

Figure 2.3 Comparison of Engineering and True Stress-Strain Curves[20]

can be seen in Figure 2.3[20]. By comparing the engineering and true stress-strain curves, it is noted that the true stress steadily increases until specimen fractures.

It is possible to correlate engineering and true values by substituting Equations 2.1 and 2.2 into Equation 2.9. Then, we get

$$\bar{\sigma} = \sigma(1 + \varepsilon) \qquad (2.10)$$

After specimen necks, the equations mentioned previously are not valid. Since the length changes within the gage length are now localized in the necked region, the engineering strain which assumes a uniform strain over the gage length can not be used to calculate the true stress and strain. An alternate method for computing the true stress in the necked region is described by Hosford et al. on page 53 of Reference 20.

C. EFFECT OF STRAIN RATE ON MECHANICAL PROPERTIES

1. Dynamic Strain Rate Testing. With the legislation requiring safer cars in the future, a good understanding of the effects of impact loading, controlled crush and energy absorption on automobile components is essential[25]. Since these design considerations involve dynamic loading, a knowledge of the effects of changing strain rate on the mechanical properties of sheet steels must be known in order for the engineer to design a safer and efficient vehicle[25,26].

The effect of strain rate on mechanical properties varies for each material. These general trends are well known, but because the magnitude of the change in properties with strain rate is so varied for each

material, no general quantitative theory exists that satisfactorily predict the mechanical behavior of materials over a wide range[27].

Strain rate ($\dot{\varepsilon}$) is the rate of change of strain (ε) with respect to time. Because strain is dimensionless, the units of strain rate are reciprocal of time (sec.$^{-1}$). The stress-strain relationships of the majority of metals are sensitive to the strain rate. Table 2.1 summarized by Lindholm[28] shows the range of strain rates for the different types of tests.

At strain rates of the order of 10^{-6} to 10^{-5} sec.$^{-1}$ the creep behavior of a material is the primary consideration, usually at elevated temperature for metals, for which the creep-type laws are used to describe the mechanical behavior. At a higher strain rate, in the range of 10^{-4} to 10^{-3} sec.$^{-1}$, the uniaxial tension, compression, or quasistatic stress-strain curve obtained from constant strain-rate test is used to describe the material behavior[29]. Strain rates ranged from 10^{-1} to 10^{2} sec.$^{-1}$ are generally referred to as the intermediate or medium strain-rate condition. Strain rates of 10^{3} sec.$^{-1}$ or higher are general treated as high strain rate.

Wave propagation becomes important in high strain-rate testing when the time interval of the applied force is so short and the dimensions of the specimen are such that the inertia force in the material is locally comparable to the local force for deformation. As the size of the specimen and strain rate increase, the effects of wave propagation generally become more significant, because the time availiable for a stress wave to propagate and reflect mutiple times become a significant portion of the test duration time[27]. At the strain rate of 10^{5} sec.$^{-1}$

Table 2.1

Dynamic Aspects of Mechanical Testing[22,28]

STRAIN RATE	COMMON TESTING METHODS	DYNAMIC CONSIDERATIONS	
10^{7} – 10^{6} – 10^{5}	HIGH VELOCITY IMPACT —Explosives —Pulsed laser —Projectile impact	SHOCK-WAVE PROPAGATION (See Section 15.3)	INERTIAL FORCES IMPORTANT
10^{4} – 10^{3}	IMPACT Hopkinson Bar (plane stress) Inclined parallel impact (shear)	PLASTIC WAVE PROPAGATION SHEAR WAVE PROPAGATION	
10^{2} – 10^{1}	DYNAMIC High-velocity hydraulic or pneumatic machines; cam plastometer	MECHANICAL RESONANCE IN SPECIMEN AND MACHINE IS IMPORTANT	
10^{0} – 10^{-1} – 10^{-2} – 10^{-3} – 10^{-4} – 10^{-5}	QUASI-STATIC Hydraulic, servo-hydraulic or screw-driven testing machines	TESTS WITH CONSTANT CROSS-HEAD VELOCITY STRESS THE SAME THROUGHOUT LENGTH OF SPECIMEN	INERTIAL FORCES NEGLIGIBLE
10^{-6} – 10^{-7} – 10^{-8} – 10^{-9}	CREEP AND STRESS-RELAXATION —Conventional testing machines —Creep testers	VISCO-PLASTIC RESPONSE OF METALS	

or higher, it is generally dealing with shock waves propagation through materials that are in a state of uniaxial strain. At these very high rates and the associated very short time scale involved, thermodynamic considerations become important[29].

To maintain a constant average strain rate during a test, large changes in crosshead speed usually are required from the beginning of the test beyond the yield point. Futhermore, for many materials, the onset of yielding is quite rapid, so that this large change in speed must be accomplished quickly. Thus, constant strain rate tests through yielding usually cannot be performed using screw-driven testing machines. Servohydraulic machines and eletromagnetic machines may be capable of conducting tests at constant strain rate for materials with a yield point[30]. Table 2.2[27] lists the experimental techniques which are used for various strain rate conditions.

2. Structural Steels and High Strength Steels. In view of the fact that mechanical properties of metals tend to increase at higher strain rates, the effect of strain rate on the mechanical properties of mild steels has been the subject of investigations since the beginning of this century. In this section, some of these investigations will be summarized in chronological order.

Ludwik was the first to study the effect of the speed of streching upon the stress at which a metal yields. He found a logarithmic relation between the stress at which a metal yields and the strain rate as early as 1909. In 1925, Korber and Storp compared impact tests with ordinary static tests for various metals. These tests showed a considerable

Table 2.2

Experimental Methods for High Strain Rate Testing[27]

MODE	APPLICABLE STRAIN RATE, S^{-1}	TESTING TECHNIQUE
Compression	<0.1	Conventional load frames
	0.1 to 100	Special servohydraulic frames
	0.1 to 500	Cam plastometer and drop test
	200 to 10^4	Hopkinson pressure bar in compression
	10^4 to 10^5	Taylor impact test
Tension	<0.1	Conventional load frames
	0.1 to 100	Special servohydraulic frames
	100 to 10^4	Hopkinson pressure bar in tension
	10^4	Expanding ring
	$>10^5$	Flyer plate
Shear	<0.1	Conventional shear test
	0.1 to 100	Special servohydraulic frames
	10. to 10^3	Torsional impact
	100 to 10^4	Hopkinson (Kolsky) bar in torsion
	10^3 to 10^4	Double-notch shear and punch
	10^4 to 10^7	Pressure-shear plate impact

increase in the yield stress in the more rapid tests. In 1932, Prandtl and his associates studied the effect of changing the speed of deformation on various metals. Their results were in agreement with the relation found by Ludwik. The effect of the rate of strain upon the yielding of deep-drawing sheet steel was investigated by Winlock and Leiter in 1937. Their results showed that the yield point and the corresponding elongation were considerably affected by the speed of deformation[31].

In the mid 1940's, Manjoine[32] studied the relationship between strain rate, temperature, and the material properties of mild steels. Figure 2.4[32] illustrates the true stresses at various strains versus strain rate for a low-carbon steel at room temperature. Figure 2.5[32] shows the similar plot as Figure 2.4 except for the tests under different temperature conditions. At room temperature, the ultimate strength decreases slightly at the very low strain rate and then increases with strain rate, showing a 40 percent increase at the highest strain rate. The lower yield point increases throughout the range of strain rates with an over-all increase of 170 percent. The total elongation for the higher strain rates is practically constant at 40 percent. At higher temperature, the yield stresses are greatly affected by strain aging. In general, as the strain rate is increased, a higher temperature and strain are necessary to accelerate strain aging. When the yield stress-strain rate curve has a negative slope, discontinuous yielding can be expected. The fluctuations of the load which occur during discontinuous yielding decrease in amplitude as the strain rate is increased. At 600° C, the influence of strain aging is reduced or

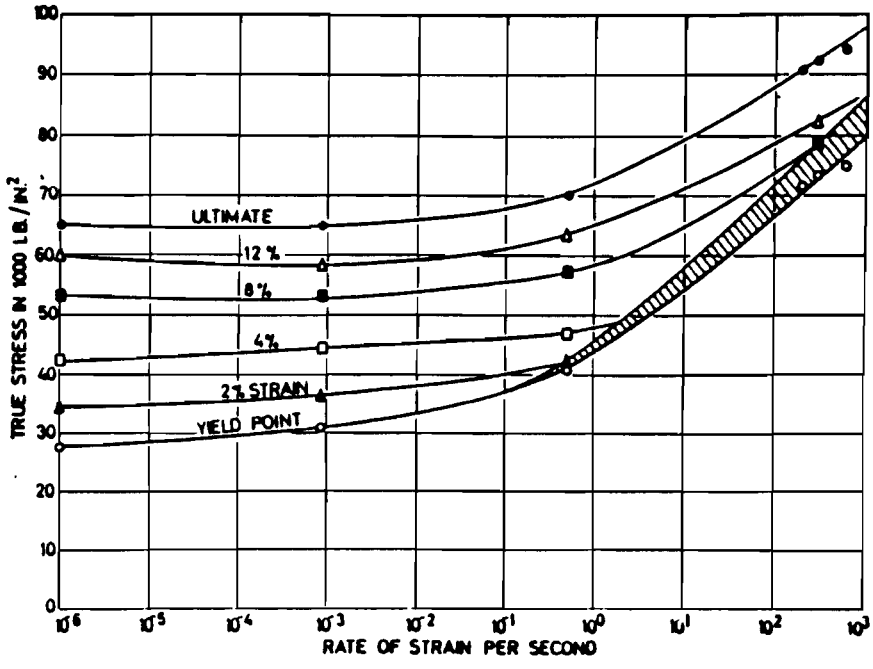

Figure 2.4 True Stresses at Various Strains Versus Strain Rate for a Low-Carbon Steel at Room Temperature[32]

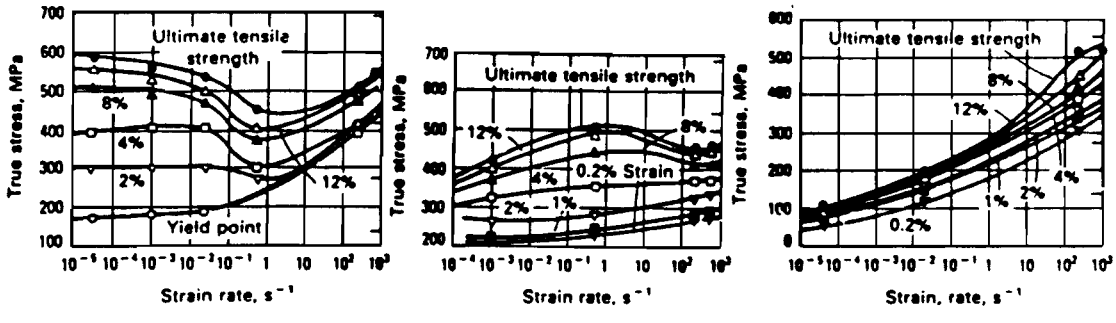

(a) (b) (c)

Figure 2.5 True Stresses at Various Strains Versus Strain Rate for a Low-Carbon Steel[32]

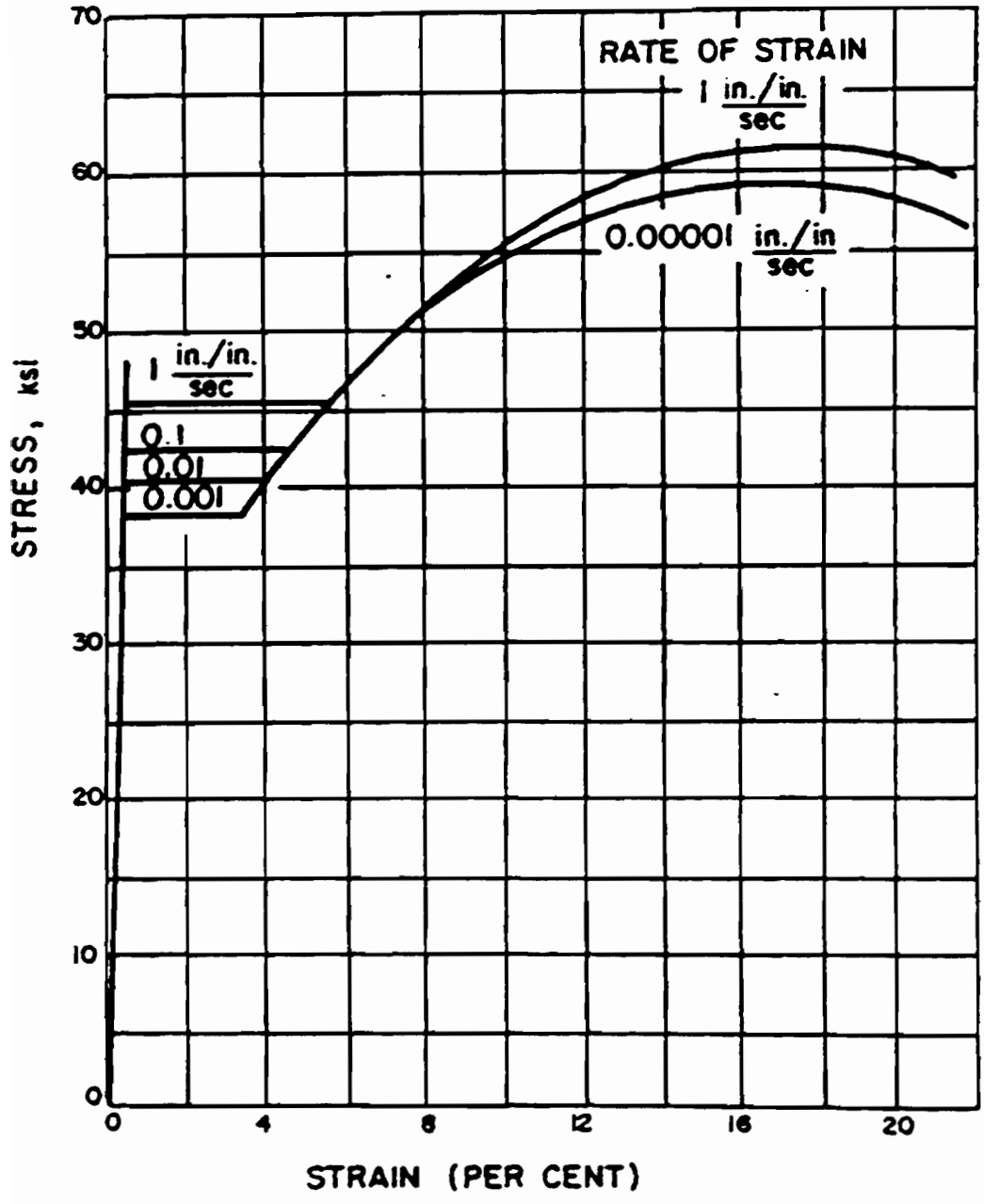

Figure 2.6 Effect of Strain Rate on Stress-Strain Curve for Structural Steel[33]

completely eliminated by annealing and recrystallization, and the yield stresses increase with strain rate over the entire range[32].

Figure 2.6 was published by Norris et al.[33] in 1959. It shows the effect of strain rate on the stress-strain curve of ordinary structural carbon steels. Based on a limited number of tests on ordinary structural carbon steels, Norris et al. stated the following phenomena as the rate of strain increases: (1) The yield stress increases to some dynamic value; (2) The yield-point strain increases; (3) The modulus of elasticity in the elastic range remains constant; (4) The strain at which strain hardening begins also increases; (5) The ultimate strength increases slightly.

In 1955, Alder and Phillips[34] studied the combined effects of strain rate and temperature on compressive mechanical properties of steel, copper, and aluminum. The stress-strain curves were determined for these three materials at constant true strain rates in the range from 1 to 40 in./in./sec.. The maximum compressive strain was 50 percent for temperatures ranging from 930° C to 1200° C. The tests were conducted by using the cam plastometer compression machine which was designed by Orwan and Los in 1950. They found that increase in strain rate or decrease in temperature resulted in an increase in the stress at any given compressive strain.

In 1957, Cook[35] used the cam plastometer machine to determine the compressive yield strengths for low, medium, and high carbon steels at 900°, 1000°, 1100°,and 1200°C combined with constant strain rates of 1.5, 8, 40, and 100 in./in./sec.. Similar results were found by Alder and

Phillips. Cook observed that the yield strengths of steels increase as the strain rate increases and/or the temperature decreases.

In 1963, Davies and Hunter[36] used the Split Hopkinson method to investigate the dynamic compressive mechanical behavior of some metals including steel. The compressive loading cycles were of 30 micro-seconds duration which generated strain rates in the range of 1000 to 10000 in./in./sec.. The results obtained from this investigation indicated that the ratio of the dynamic to static yield strength of the mild steel used in the study is 2.6.

In 1963, United States Steel Corporation[37] conducted numerous tests on high-strength, low-alloy steels (COR-TEN and TRI-TEN) for the purpose of studying the effects of the strain rate and temperature on the tensile properties of these steels. The results obtained from this investigation indicated that as the strain rate was increased at -50° F and 75° F (room temperature), the tensile strength and the 0.2 percent offset yield strength increased as shown in Figures 2.7 and 2.8[37]. However, as the strain rate increased at 600° F, the tensile strength decreased. The ductility of the COR-TEN steel, as measured by percent elongation and reduction of area, did not appear to be strain-rate sensitive at -50° F and room temperature, but at 600° F, the reduction of area for the fastest rate was higher than that for the slower rate. The percent elongation of the TRI-TEN steel appeared to be somewhat strain-rate dependent, decreasing slightly as the strain rate increased.

Chatfield and Rote[26](1974) completed a comprehensive report concerning the influence of strain rate on the mechanical properties of high strength, low alloy (HSLA) steels. In this investigation, six

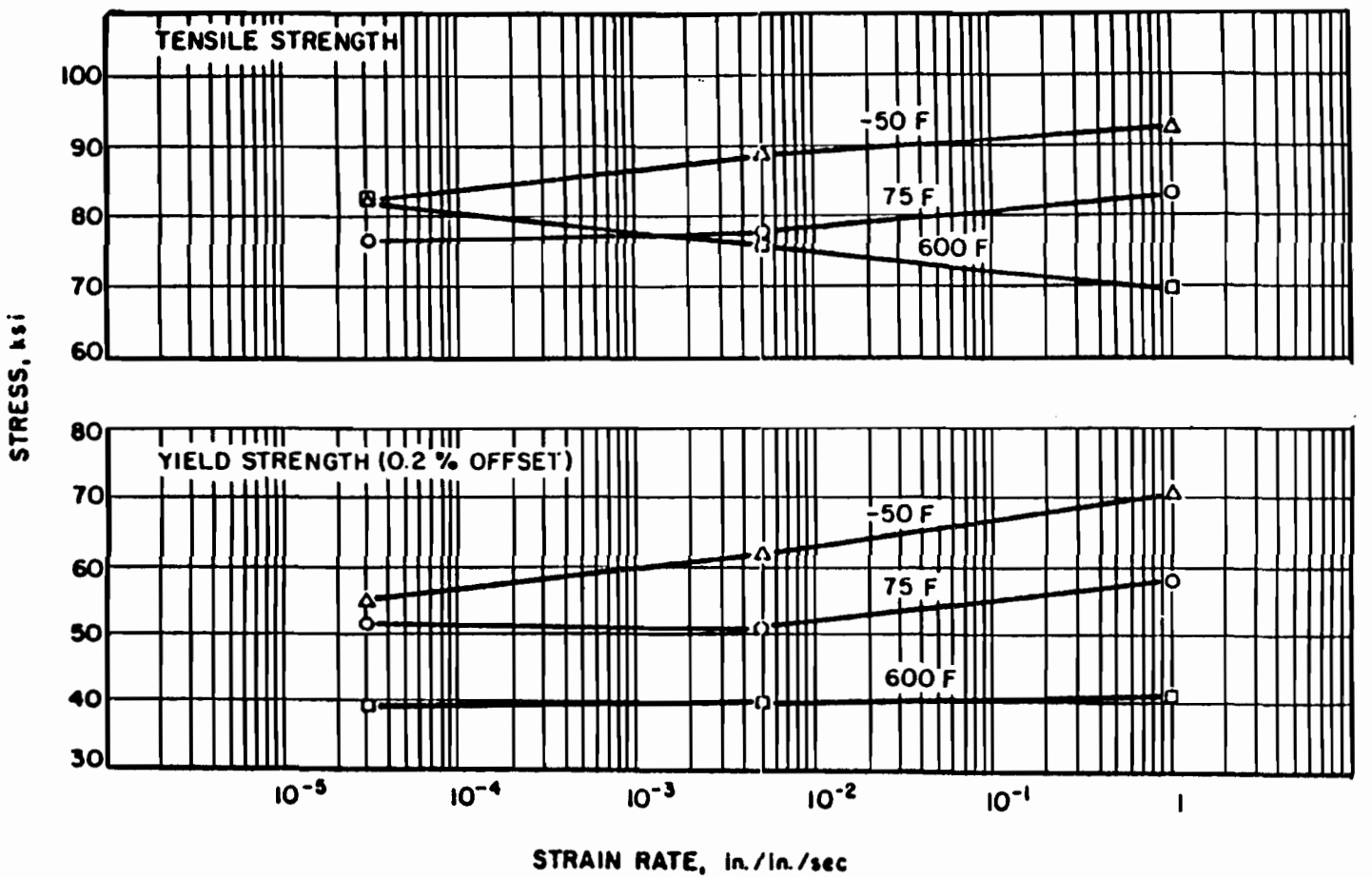

Figure 2.7 Effect of Strain Rate at Different Temperature on the Yield and Tensile Strengths of USS COR-TEN Steel[37]

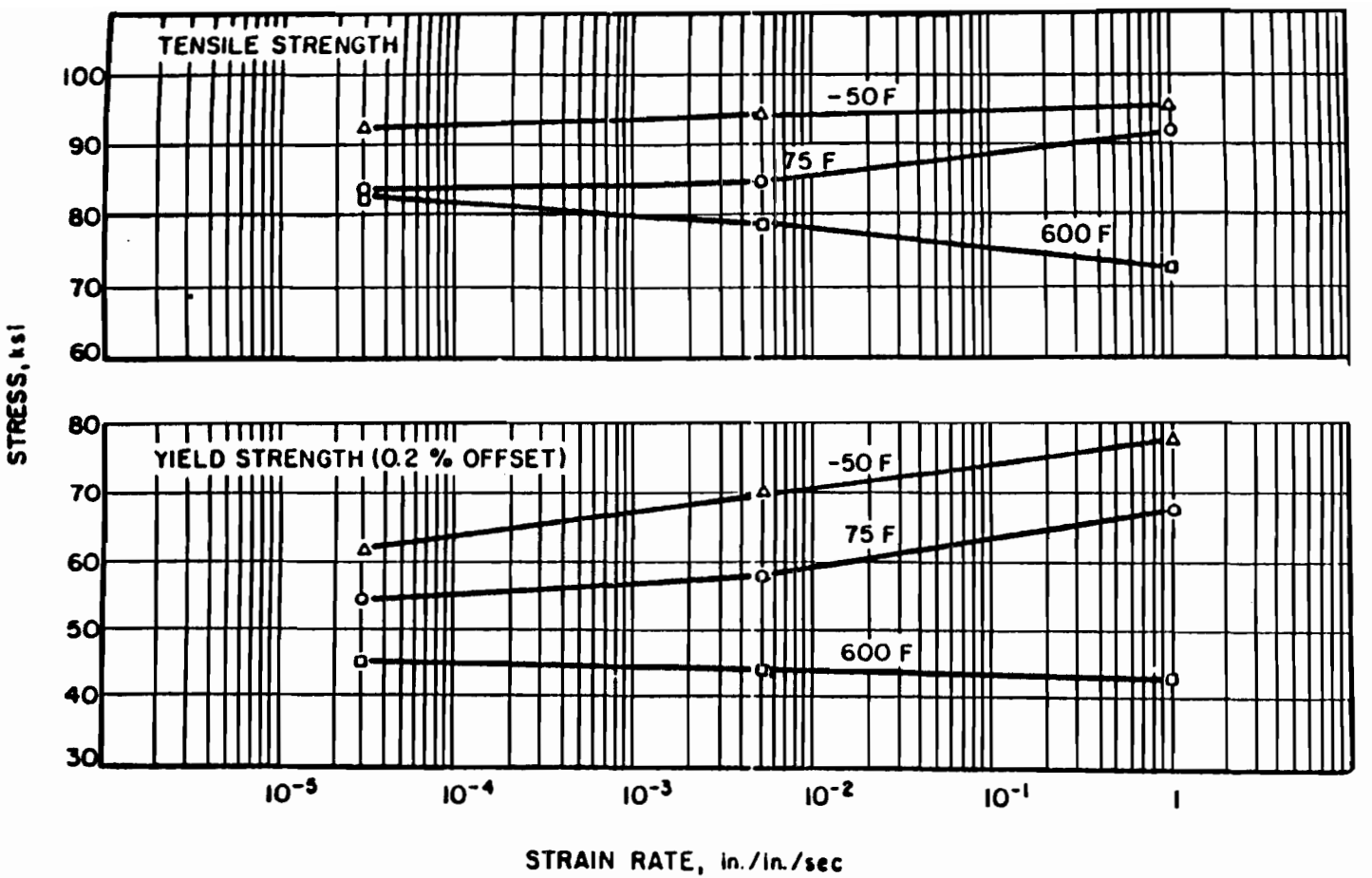

Figure 2.8 Effect of Strain Rate at Different Temperature on the Yield and Tensile Strengths of USS TRI-TEN Steel[37]

different HSLA steels were tested with yield strengths ranging from 40 to 80 ksi. They also tested three different aluminum alloys for comparison with the HSLA steels. All tests were performed at room temperature. The relationships of yield strength, tensile strength, and uniform elongation versus strain rate for a typical HSLA steel are shown in Figure 2.9[26]. From observing this figure, both the yield and tensile strengths increase substantially with increasing strain rate while the uniform elongation, which is the strain at the onset of necking, decreases sligtly. Total elongation, on the other hand, is relatively independent of strain rate. It seems that the absorbed energy of the HSLA steel increases with increasing strain rate.

Jump tests with steel were performed by Barraclough and Sellars in 1974. Rods of either of two steels were loaded in torsion at a temperature of about 1000° C. Typical stress strain curves for tests involving instantaneous changes in strain rate for both stainless and low alloy steels are shown in Figure 2.10[38]. Since the lowest strain rate was 2×10^{-3} sec.$^{-1}$ and the highest only 0.2 sec.$^{-1}$, it becomes evident that steel is strongly sensitive to strain rate (at least at this temperature). On the other hand, steel appears almost insensitive to strain rate history, as far as the jump test is concerned. It should be pointed out that Barraclough and Sellars carried their tests to very large strains because hot-working was the principal interest of their investigation. Jump tests to higher strain rates were performed by Wilson et al. (1979). Again they showed a strong strain rate sensitivity and again an insensitivity to strain rate history[38]. They also concluded that the

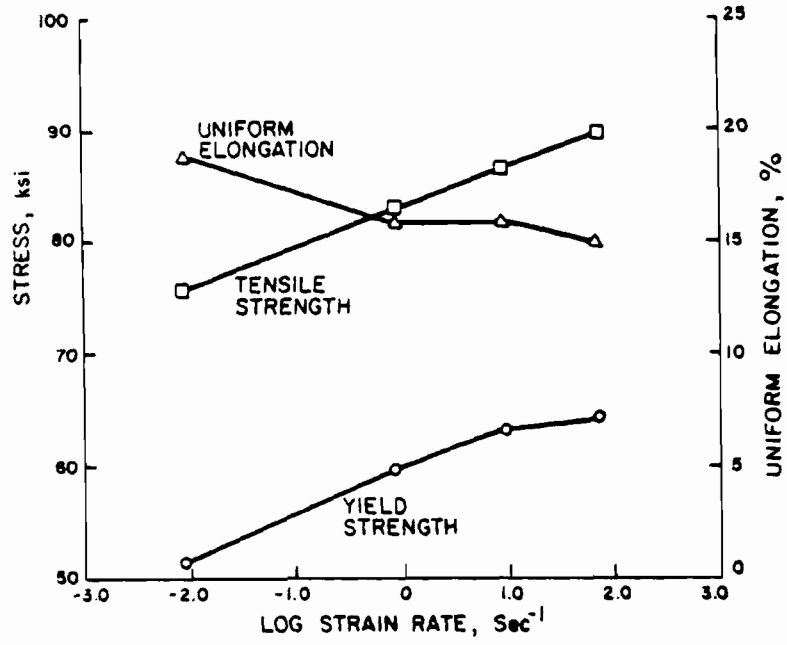

Figure 2.9 Effect of Strain Rate on Mechanical Properties of a HSLA Steel[26]

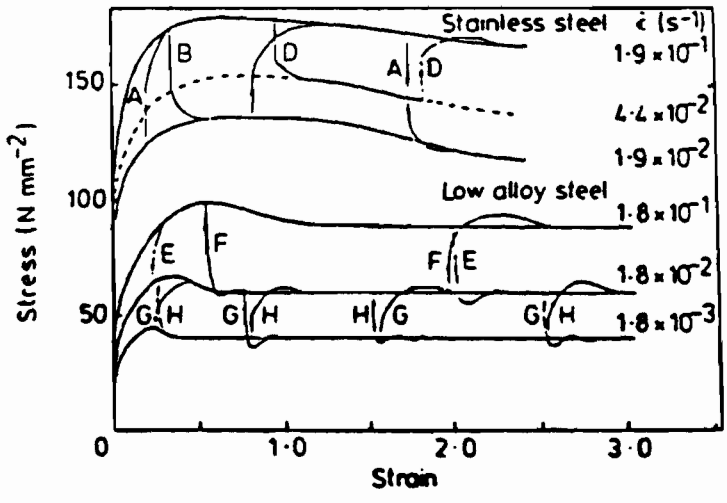

Figure 2.10 Typical Stress-Strain Curves for Tests Involving Instantaneous Changes in Strain Rate[38]

hot-rolled steel shows a somewhat greater strain rate sensitivity than does the cold-rolled steel[39].

The most extensive series of jump tests is probably that of Eleiche and Cambell[40] conducted in 1976. These investigators tested copper, titanium, and mild steel. The tests were performed over a range of temperatures and strains up to 60 percent in shear. They concluded that copper is sensitive to strain rate history, while titanium and steel are less sensitive to history, but more sensitive to direct effects of strain rate.

In 1982, Watanabe[41] studied the yield behavior of low-carbon steels at room temperature under the strain rates ranging from 10^{-4} to 10^{-1} $sec.^{-1}$ using an Instron type machine. The results showed another break point of the dependence of the yield stress on the strain rate of $3x10^{-3}$ $sec.^{-1}$, which is different from Majoine's strain rate of 10^{-1} $sec.^{-1}$. This means that the dependence of yield stress, yield point elongation, and tensile strength on the strain rate in the range of high strain rate above $3x10^{-3}$ $sec.^{-1}$ is larger than that at lower strain rates.

In 1984, Meyer[42] conducted tension tests on high strength sheet steel at strain rates between $5x10^{-4}$ $sec.^{-1}$ and $5x10^{3}$ $sec.^{-1}$. The stress-strain curves of the tested steel at different strain rates are shown in Figure 2.11[42]. It is observed that both yield and ultimate tensile strengths are increased with the increasing strain rate. However, the ductility decreased when the strain rate increased from $5x10^{-4}$ to $2x10^{3}$ $sec.^{-1}$. At higher strain rates above $2x10^{3}$ $sec.^{-1}$, the material becomes more ductile again.

The increase in stress (σ) is needed to cause a certain increase in plastic strain rate ($\dot{\varepsilon}$) at a given level of plastic strain (ε) and a given temperature (T). The strain-rate sensitivity (m) can be expressed in the following equation:

$$m = \left(\frac{\Delta \log \sigma}{\Delta \log \dot{\varepsilon}} \right) \tag{2.11}$$

Therefore, the effect of strain rate on the true stress in metals may be determined as follows[20,26]:

$$\sigma = C \dot{\varepsilon}^m \tag{2.12}$$

where C = material constant

According to Hosford and Caddel[20], the magnitude of the strain-rate sensitivity (m) for most metals is usually between 0.0 and 0.03. The value of material constant (C) depends on the strain, temperature, and type of material[20]. The value of m can be negative under some condition as shown in Figures 2.5(a) and 2.5(b). For a given material, the values of C and m can be determined empirically.

Another useful relationship between the true stress and true strain rate is given by Hosford[20] as:

$$\sigma_2 = \sigma_1 \left(\frac{\dot{\varepsilon}_2}{\dot{\varepsilon}_1} \right)^m \tag{2.13}$$

where σ_1 and σ_2 are the true stresses corresponding to strain rates $\dot{\varepsilon}_1$ and $\dot{\varepsilon}_2$, respectively. Therefore, if σ_1 and $\dot{\varepsilon}_1$ and m are known, then σ_2 can be found for any desired value $\dot{\varepsilon}_2$.

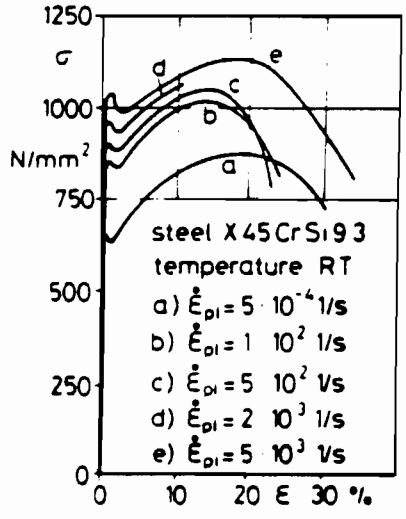

Figure 2.11 Stress-Strain Curves for High Strength Steel at Varying Strain Rate[42]

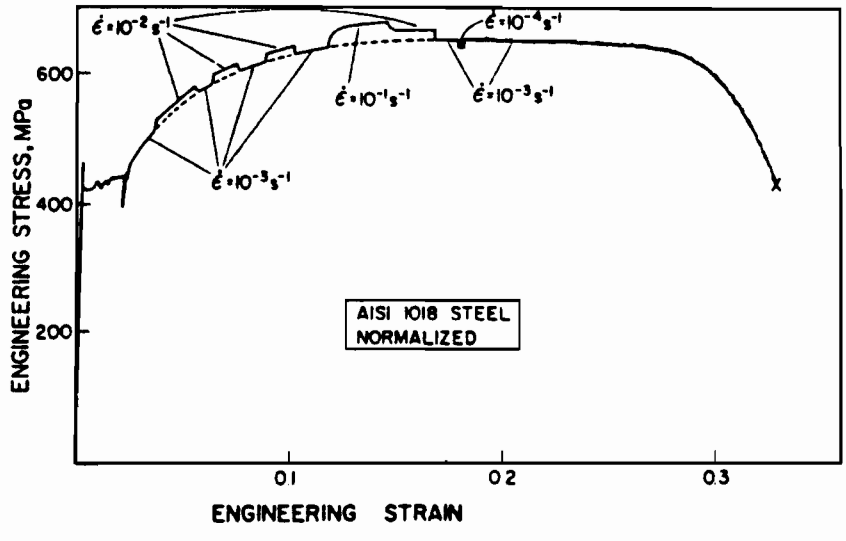

Figure 2.12 Strain-Rate Changes During Tensile Test, Four Strain Rates Shown are 10^{-1}, 10^{-2}, 10^{-3}, and 10^{-4} in./in./sec. (Ref.22)

According to Meyers[22], It is possible to determine the value of strain-rate sensitivity (m) by changing the strain rate suddenly and by measuring the instantaneous change in stress. This technique is illustrated in Figure 2.12[22]. Applying Equation 2.12 to different strain rates and eliminating C, we have

$$m = \frac{\ln(\sigma_2/\sigma_1)}{\ln(\dot{\varepsilon}_2/\dot{\varepsilon}_1)} \qquad (2.14)$$

In 1983, Sachdev and Wagonar[43] found that the strain rate sensitivity is strongly dependent on the strain rate for steel. This investigation included four types of steel : an interstitial free (IF), a hot rolled, plain carbon steel (HR), and two high strength steels (one with a ferrite-pearlite microstructure (HSLA) and the other with a ferrite-martensite (DP) microstructure). A new equation was developed to correlate the strain-rate sensitivity and the strain rate as follows:

$$m = b\ \dot{\varepsilon}^{a} \qquad (2.15)$$

In the above equation, a and b are constants to be determined from tests. Figure 2.13[43] shows the strain-rate sensitivity index (m) for the steels tested as a function of strain rate. The curves represent the best fits for Equation 2.15 for the steels tested under selected strain rate range[43].

Recently, Nagorka[44] (1987) conducted an experimental investigation to observe the effect of microstructure and strain rate on the stage III strain hardening and ductility of dual-phase steels. The five types of steels included in this investigation were cold-rolled, normalized,

martensitic, tempered martensitic, and ferrite-carbide. Based on the tested data, Nagorka concluded that the strain rate sensitivity of various microstructures are the same for any given strain rate and increase with increasing strain rate. These observations indicate that strain-rate sensitivity is insensitive to changes in microstructures. Also, it was concluded from this study that the uniform elongation increases slightly with increasing strain rate for most of the microstructures tested, whereas post-uniform elongation increases significantly with increasing strain rate.

If the strain rate sensitivity of a material is known as a design parameter, the engineer may use this property to his advantage and thus a more economical design may be obtained. For example, an automotive engineer that is concerned with designing a part to withstand impact loading without permanent deformation may take advantage of the increased yield point (if available) caused by the high strain rate associated with impact[26].

D. STRUCTURAL BEHAVIOR OF COMPRESSION ELEMENTS UNDER STATIC LOADS

1. Elastic Local Buckling of Flat Compression Elements. The compression flat elements may buckle locally in the elastic or inelastic range depending on the width-to-thickness ratio of the compression elements. The elastic local buckling stress, $(f_{cr})_E$, of compression elements subjected to a uniform compression can be determined by differential equations based on the small deflection theory of plates. Solving the differetial equation by using the energy method[45,46], the analytical solution for the buckling stress of compression elements can

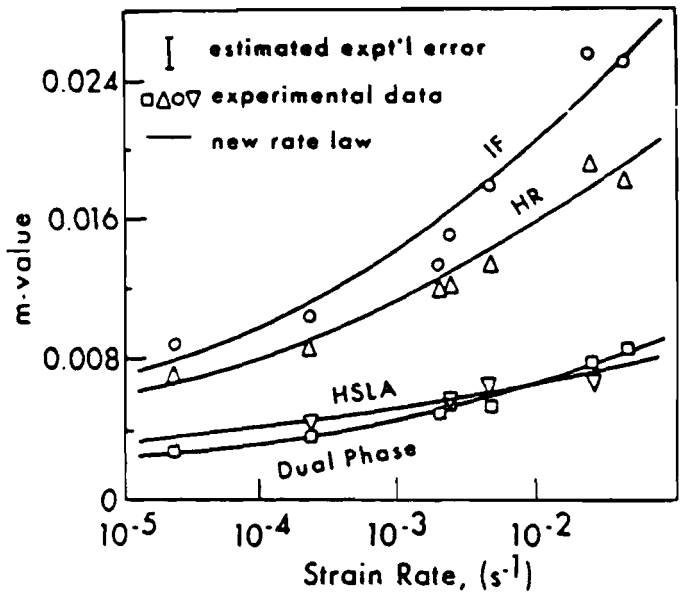

Figure 2.13 The Variation of the Strain Rate Sensitivity (m-value) with Strain Rate[43]

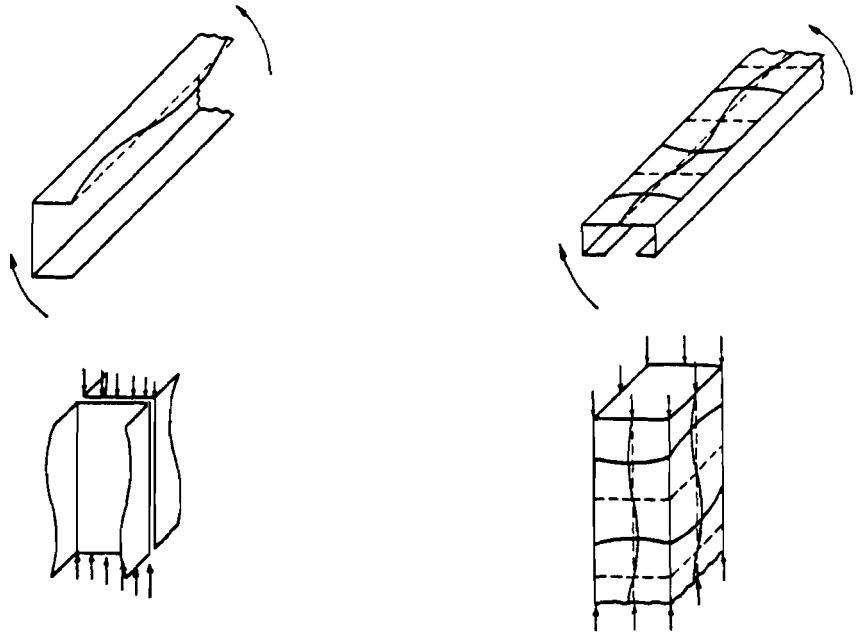

(a) Members with Unstiffened Compression Elements

(b) Members with Stiffened Compression Elements

Figure 2.14 Structural Members with Stiffened and Unstiffened Elements[24]

be obtained. A series of solutions of plate buckling for several different types of compression elements with various boundary conditions were derived by Timoshenko[45]. Figure 2.14[24] illustrates several different structural members with stiffened and unstiffened compression elements.

The following differential equation derived by Saint Venant[47] can be used for determination of the critical buckling stress of compression elements:

$$\frac{\partial^4\omega}{\partial x^4} + 2\frac{\partial^4\omega}{\partial x^2\partial y^2} + \frac{\partial^4\omega}{\partial y^4} = \frac{1}{D}\left[q + f_x t\frac{\partial^2\omega}{\partial x^2} + f_y t\frac{\partial^2\omega}{\partial y^2} + 2\tau_{xy}t\frac{\partial^2\omega}{\partial x\partial y}\right] \qquad (2.16)$$

where ω = lateral deflection of the plate

q = lateral uniform load applied to the plate

t = thickness of the plate

$D = Et^3/(12(1-\mu^2))$

E = modulus of elasticity

μ = Poisson's ratio = 0.3 for steel

f_x, f_y = stress components normal to the edges of the plate and lying in the x-y plane

τ_{xy} = shear stress component on the edges of the plate in the x-z and y-z plane

According to the loading conditions of the compression element, Bryan's differential equation (Equation 2.17) can be obtained by eliminating the nonexistent stress terms. The change of the sign in front of the f_x term indicates that the stress is considered to be positive for compression.

$$\frac{\partial^4 \omega}{\partial x^4} + 2\frac{\partial^4 \omega}{\partial x^2 \partial y^2} + \frac{\partial^4 \omega}{\partial y^4} = -\frac{f_x t}{D}\ \frac{\partial^2 \omega}{\partial x^2} \qquad (2.17)$$

a. Stiffened Elements. As shown in Figure 2.15, a retangular plate simply supported on four edges is compressed in its middle plane by stresses uniformly distributed along the side x=0 and x=a. The deflected surface of the buckled plate can be expressed by assuming a double Fourier series as follows:

$$\omega = \sum_{m=1}^{\infty} \sum_{n=1}^{\infty} A_{mn} \sin\left(\frac{m\pi x}{a}\right) \sin\left(\frac{n\pi y}{w}\right) \qquad (2.18)$$

where A_{mn} = coefficient

m = number of half sine waves in x-direction

n = number of half sine waves in y-direction

a = length of plate

w = width of plate

Equation 2.18 satisfies the boundary conditions along the four simply supported edges. The boundary conditions at the unload edges are

$$[\omega = 0]_{y=0,w}\ ,\quad \left[\frac{\partial^2 \omega}{\partial x^2} + \frac{\partial^2 \omega}{\partial y^2} = 0\right]_{y=0,w} \qquad (2.19)$$

By substituting Equations 2.18 and 2.19 into Equation 2.17 and assuming only one half sine wave in the y direction, the elastic buckling stress ($(f_{cr})_E$) can be obtained as follows:

$$(f_{cr})_E = f_x = \frac{k\pi D}{tw^2} \qquad (2.20)$$

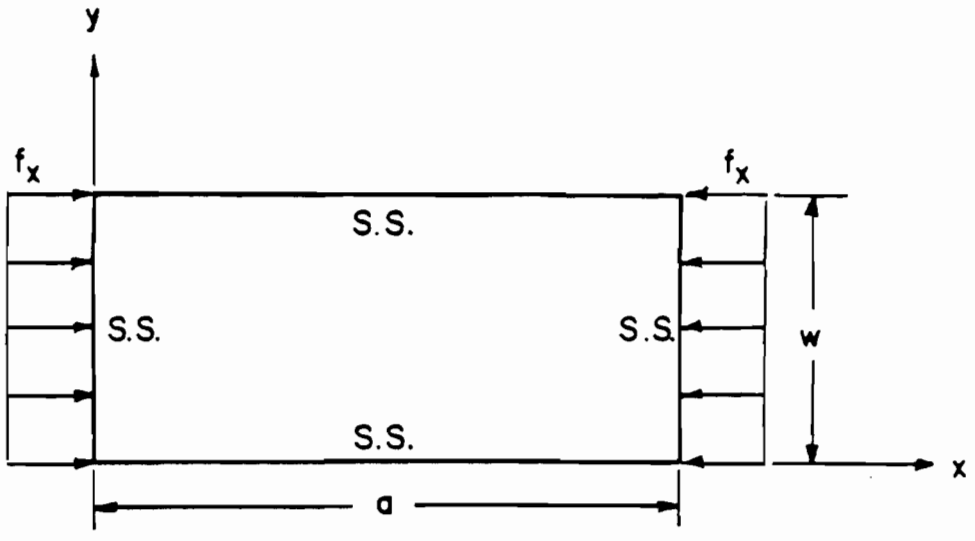

Figure 2.15 Rectangular Plate Simply Supported on Four Edges and Under Uniform Compression Stress[100]

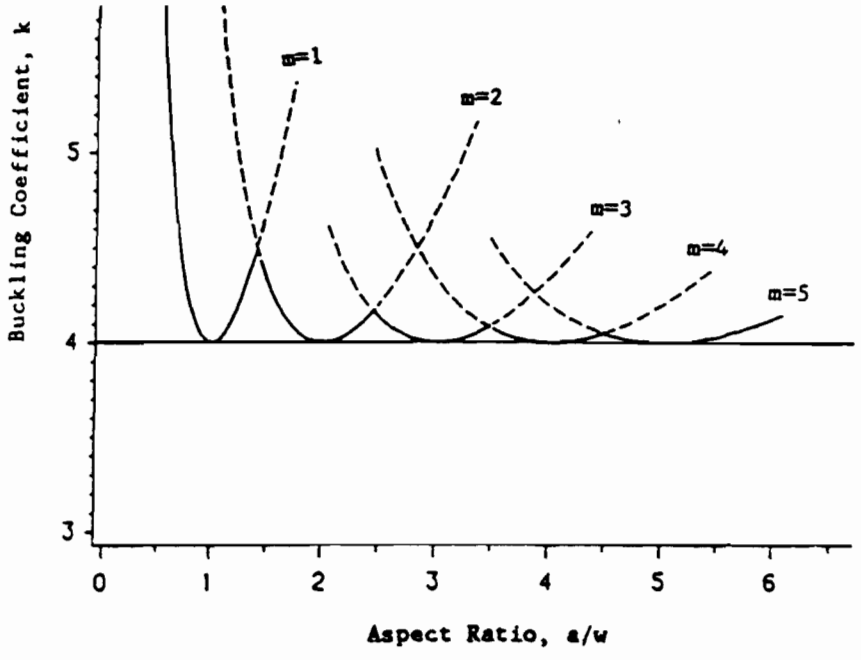

Figure 2.16 Buckling Coefficients for Flat Rectangular Stiffened Plates[100]

where $$k = [m(\frac{w}{a}) + (\frac{1}{m})(\frac{a}{w})]^2 \qquad (2.21)$$

By substituting the equation for D into Equation 2.20, the elastic buckling stress can be expressed as follows:

$$(f_{cr})_E = \frac{k\pi^2 E}{12(1-\mu^2)(w/t)^2} \qquad (2.22)$$

As can be seen from Figure 2.16, the value of k depends upon the magnitude of the aspect ratio (a/w) of the plate and the number of sine waves (m) in the direction of compression. It is noted that the k value is equal to four for a square plate and for any plate with an aspect ratio equal to an interger. It is also noted that the value approaches to four for a long plate with an aspect ratio larger than four. Therefore, a minimum value of k equal to four is conservatively used in practical design without considering the rotational restraint along the unload edges.

b. Unstiffened Elements. As shown in Figure 2.17, a retangular plate simply supported on three edges and the other edge free is compressed in its middle plane by a stress uniformly distributed along the side x= 0 and x=a. Timoshenko[45] assumed that a plate under the action of compression forces will buckle in m sinusoidal half-waves. The expression for the deflected surface of the buckled plate is

$$\omega = f(y)\sin(\frac{m\pi x}{a}) \qquad (2.23)$$

where f(y) = function of y alone

a = length of plate

Equation 2.23 satisfies the boundary conditions along the simply supported edges x=0 and x=a. The boundary conditions along the supported edge (y=0) and the free edge (y=w) are

$$[\omega = 0]_{y=0}, \quad \left[\frac{\partial^2\omega}{\partial y^2} + \mu\frac{\partial^2\omega}{\partial x^2} = 0\right]_{y=0} \tag{2.24a}$$

$$\left[\frac{\partial^2\omega}{\partial y^2} + \mu\frac{\partial^2\omega}{\partial x^2} = 0\right]_{y=w}, \quad \left[\frac{\partial^3\omega}{\partial y^3} + (2-\mu)\frac{\partial^3\omega}{\partial x^2\partial y} = 0\right]_{y=w} \tag{2.24b}$$

By substituting Equations 2.23 and 2.24 into Equation 2.17 and assuming only one half sine wave in the direction of compression regardless of the length of plate, the elastic buckling stress ($(f_{cr})_E$) can be obtained as follows:

$$(f_{cr})_E = f_x = \frac{k\pi D}{tw^2} \tag{2.25}$$

An approximate solution based on an energy method has been presented by both Timoshenko[45] and Bulson[46]. The buckling coefficient was found to be

$$k = \left(\frac{w}{a}\right)^2 + 6\frac{1-\mu}{\pi^2} \tag{2.26}$$

The value of k, as shown in Figure 2.18, depends upon the magnitude of the aspect ratio (a/w) of the retangular plate. It can be observed that the buckling coefficient (k) approaches to a constant of 0.425 as the aspect ratio of the plate approaches infinity. In the AISI Automotive Steel Design Manual, the buckling coefficient has been chosen equal to

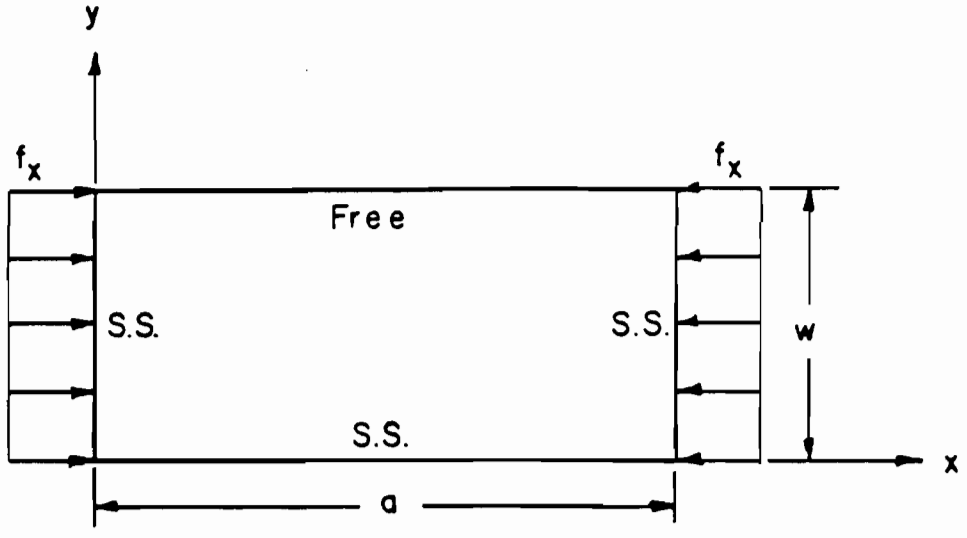

Figure 2.17 Rectangular Plate Simply Supported on Three Edges and under Uniform Compressive Stress[100]

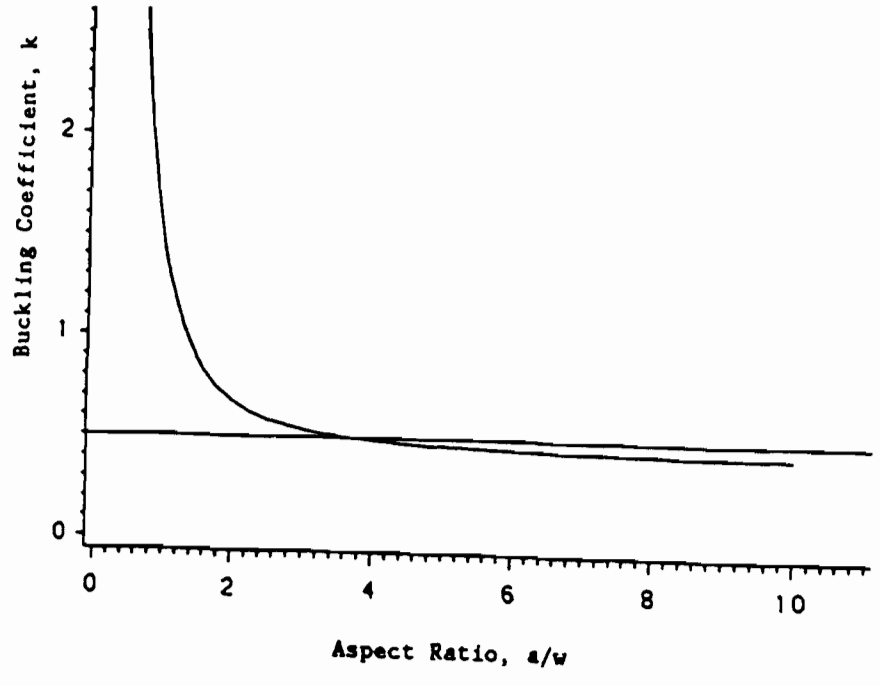

Figure 2.18 Buckling Coefficients for Flat Rectangular Unstiffened Plates[100]

0.43 for unstiffened compression elements and 4.0 for stiffened compression elements for conservative reason.

2. Inelastic Buckling of Flat Compression Elements. The preceding discussion on elastic local buckling is valid as long as the computed critical buckling stress is below the proportional limit of the material. When the flat width-to-thickness ratio is small, a plate will buckle at a stress level beyond the proportional limit. This type of buckling is referred to as inelastic buckling. The analytical study of local buckling in the inelastic range is rather complicated because of the anisotropic nature of the compression element. However, analytical studies of the plates buckled in the inelastic range have been performed by numerous researchers.[48-52]

In the late ninteenth century, the tangent modulus theory and the reduced modulus theory were proposed by Engesser. In 1924, Bleich[48] extended the theory of flat plate stability into the inelastic range by considering the plate as an anisotropic type and by introducing a reduced modulus in Equation 2.17. He assumed that the reduced modulus is applied only to a plate in the direction of the compressive stress, whereas the modulus of elasticity remains the same in the perpendicular direction to the compression stress. The differential equation proposed by Bleich[48] for inelastic buckling is

$$\tau \frac{\partial^4 \omega}{\partial x^4} + 2\sqrt{\tau}\ \frac{\partial^4 \omega}{\partial x^2 \partial y^2} + \frac{\partial^4 \omega}{\partial y^4} + \frac{f_x t}{D}\ \frac{\partial^2 \omega}{\partial x^2} = 0 \qquad (2.27)$$

where $\tau = E_t/E$

E_t = tangent modulus of steel

For a simply supported plate subjected to uniformly compressive stresses in one direction, the following equation can be given by the solution of Equation 2.28.

$$(f_{cr})_I = \eta(f_{cr})_E = \frac{\eta k \pi^2 E}{12(1-\mu^2)(w/t)^2} \qquad (2.28)$$

where $\eta = \sqrt{\tau} = \sqrt{E_t/E}$

It is noted that the inelastic buckling stress ($(f_{cr})_I$) is in terms of the elastic buckling stress ($(f_{cr})_E$) and the plasticity reduction factor (η).

3. Postbuckling Behavior of Flat Compression Elements. The compression elements of thin-walled structural members with relatively large w/t ratios can continue to carry additional loads after the attainment of elastic local buckling. The stresses in the compression elements will redistribute until the stresses along supported edges reach the yield stress of steel. Then, the maximum load-carrying capacity of the member will be reached.

A grid model shown in Figure 2.19[24] can be used for the deflected shape of a stiffened compression element in the postbuckling range. The transverse bars, which are anchored at the sides of grid, act as tie rods to support the deflection of the longitudinal struts. This meams that the tension membrane stress developed in the transverse direction restrains the lateral displacement caused by the longitudinal load. As a result, additional load can be carried by the plate after the elastic

buckling load is reached because of the transverse membrane stress and the redistribution of longitudinal stress. As shown in Figure 2.20(a)[24], the stress distribution is uniform prior to its buckling. After buckling, the stress distribution is nonuniform as shown in Figure 2.20(b)[24]. It is assumed that the maximum load is reached when the stress at the supported edges reaches the yield stress of the steel as shown in Figure 2.20(c)[24].

Because the membrane stresses are developed in the transverse direction and the deflection of the plate is usually much larger than its thickness after buckling, small deflection theory of plate bending can not be applied to the postbuckling behavior. Therefore, the large deflection theory of plates is used for the analysis of plates in the postbuckling range.

von Karman[53] developed large deflection equations for plates in the postbuckling range by taking the membrane stresses into account. The differential equation for the postbuckling behavior of a square plate is given by Timoshenko[45] in the following form:

$$\frac{\partial^4\omega}{\partial x^4} + 2\frac{\partial^4\omega}{\partial x^2\partial y^2} + \frac{\partial^4\omega}{\partial y^4} = \frac{t}{D}\left[\frac{\partial^2 F}{\partial y^2}\frac{\partial^2\omega}{\partial x^2} - 2\frac{\partial^2 F}{\partial x\partial y}\frac{\partial^2\omega}{\partial x\partial y} + \frac{\partial^2 F}{\partial x^2}\frac{\partial^2\omega}{\partial y^2}\right] \quad (2.29)$$

where F is a stress function. The median fiber stresses are defined as follows:

$$f_x = \frac{\partial^2 F}{\partial y^2}, \quad f_y = \frac{\partial^2 F}{\partial x^2}, \quad \tau_{xy} = -\frac{\partial^2 F}{\partial x\partial y} \quad (2.30)$$

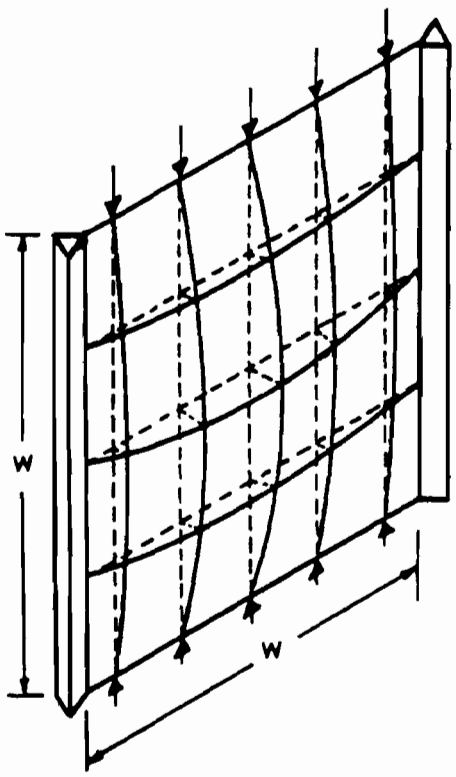

Figure 2.19 Strut and Bar Grid Model Simply Supported along Its Edges and Subjected to End Loading[24]

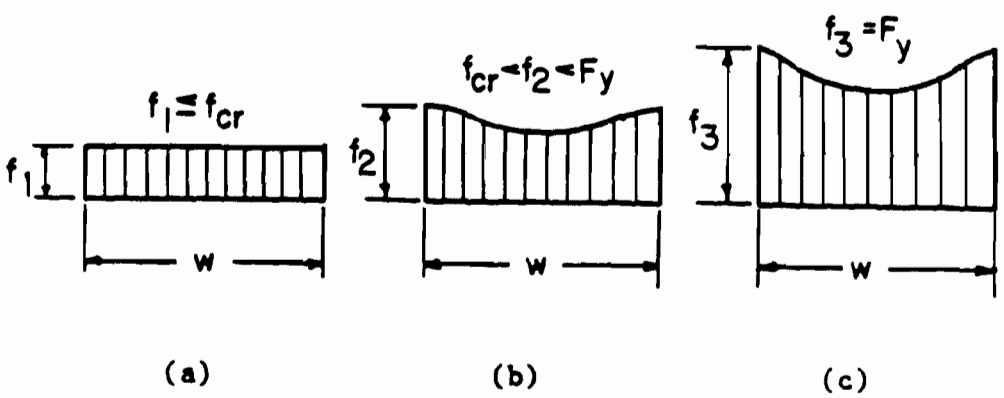

Figure 2.20 Consecutive Stages of Stress Distribution in a Stiffened Compression Element[24]

The exact solution for Equation 2.29 is difficult to achieve because the equation is a fourth-order nonlinear differential equation. Using the energy method and assuming a wave form of the deflected plate, approximate solutions for the differential equation have been proposed by Schnadel[54], Timoshenko[45], Cox[55], Marguerre[56], and Levy[57].

4. Development of Effective Width Formulas. A solution for the differential equation based on the large deflection theory was difficult for use in practical design because of its complexity. Therefore, the concept of "Effective Width" has been proposed by von Karman[58] to determine the ultimate strength of thin metal sheets in aeronautical structures in 1932. In the past, the effective width concept has been sucessfully used for the prediction of postbuckling strengths of stiffened and unstiffened elements.

In von Karman's[58] approach, it was assumed that the entire load is carried by two effective strips with a uniformly distributed stress equal to the edge stress, f_{max}, as shown in Figure 2.21[24], instead of using the full width of the compression element with actual, nonuniform stress distribution. The effective width can be considered as a particular width of the plate which just buckles when the compression stress reaches the yield strength of steel as shown in Equation 2.31. The effective width (b) of the stiffened element derived by von Karman is shown in Equation 2.32.

$$f_{cr} = F_y = \frac{\pi^2 E}{3(1-\mu^2)(b/t)^2} \qquad (2.31)$$

$$b = Ct\sqrt{\frac{E}{F_y}} = 1.9t\sqrt{\frac{E}{F_y}} \qquad (2.32)$$

where $C = \pi/\sqrt{3(1-\mu^2)} = 1.9$

Equation 2.33 can be derived from Equation 2.22 for a stiffened compression element with k=4.0.

$$w = Ct\sqrt{\frac{E}{f_{cr}}} \qquad (2.33)$$

From Equations 2.32 and 2.33, the following relationship of b and w can be obtained:

$$\frac{b}{w} = \sqrt{\frac{f_{cr}}{F_y}} \qquad (2.34)$$

For the study of effective design width, Winter[59-61] conducted extensive tests by using cold-formed steel sections. Based on his test results, Winter derived the following effective width formulas for the design of both stiffened and unstiffened compression elements under uniform compression:

(a) Stiffened Elements:

$$b = 1.9t\sqrt{\frac{E}{f_{max}}}\left[1 - 0.475\left(\frac{t}{w}\right)\sqrt{\frac{E}{f_{max}}}\right] \qquad (2.35)$$

(b) Unstiffened Elements:

$$b = 0.8t\sqrt{\frac{E}{f_{max}}}\left[1 - 0.202\left(\frac{t}{w}\right)\sqrt{\frac{E}{f_{max}}}\right] \qquad (2.36)$$

Equation 2.35 is similar to von Karman's equation with the addition of an empirical correction factor which accounts for the effect of initial imperfections of compression elements. The effective width of unstiffened elements can be calculated from Equation 2.36, in which the postbuckling strength of unstiffened elements is considered. In this approach, the entire load is assumed to be carried by an effective strip with a uniformly distributed stress equal to the edge stress (f_{max}) as shown in Figure 2.22[24], instead of using the full width of the compression element with a varying stress distribution. Additional research conducted by Kalyanaraman[62-64] has shown good agreement with Equation 2.36.

Based on the accumulated design experience with a restudy of original and additional test results, the following less conservative and more accurate equation was used in the AISI Specification for determination of the effective width of stiffened compression elements:

$$b = 1.9t\sqrt{\frac{E}{f_{max}}}\left[1 - 0.415\left(\frac{t}{w}\right)\sqrt{\frac{E}{f_{max}}}\right] \qquad (2.37)$$

or

$$\frac{b}{w} = \sqrt{\frac{f_{cr}}{f_{max}}}\left[1 - 0.22\sqrt{\frac{f_{cr}}{f_{max}}}\right] \qquad (2.38)$$

The effective width approach was used for the design of stiffened compression elements since 1946, whereas the reduced allowable stress method was used for the design of unstiffened compression elements until the 1986 revision of AISI Specification. Equation 2.35 was used for the design of cold-formed steel structural members until 1968. Equation 2.37 was used in the 1968 AISI Specification and retained in the 1980 AISI

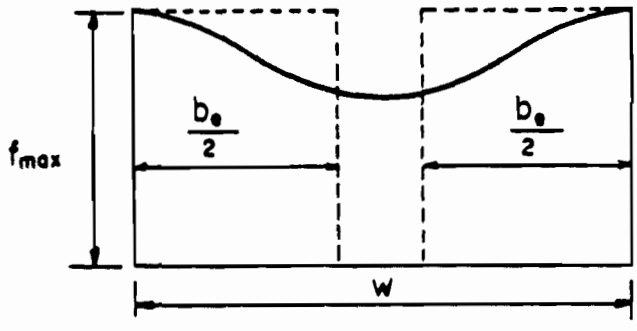

Figure 2.21 Effective Design Width of a Stiffened Compression Element[24]

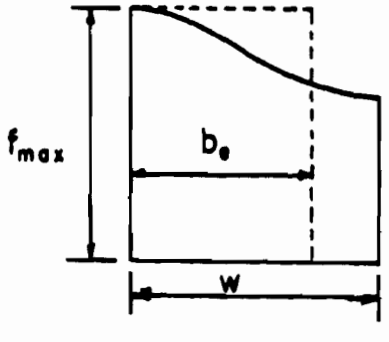

Figure 2.22 Effective Design Width of an Unstiffened Compression Element[24]

Specification. Based on the recent research[65], a new format of effective width formulas, which are based on Equation 2.38, has been used for the design of both stiffened and unstiffened compression elements in the AISI Specification since 1986. The effective width formulas used in the current AISI Specification and the AISI Automotive Steel Design Manual are presented in detail in the next section.

5. Current AISI Effective Width Formulas. According to the AISI Cold-Formed Steel Design Manual[66], the effective design widths of stiffened and unstiffened compression elements can be determined by using the following equations:

(a) For Load Capacity Determination: The effective width (b) for computing the load-carrying capacity of uniformly compressed elements can be determined from the following formulas:

$$b = w \qquad \text{when} \quad \lambda \leq 0.673, \tag{2.39a}$$

$$b = \rho w \qquad \text{when} \quad \lambda > 0.673, \tag{2.39b}$$

where b = effective width of a compression element

w = flat width of a compression element

$$\rho = (1 - 0.22/\lambda)/\lambda \tag{2.40}$$

λ = a slenderness factor

$$\lambda = \frac{1.052}{\sqrt{k}} \left(\frac{w}{t}\right)\left(\sqrt{\frac{f}{E}}\right) \tag{2.41}$$

where f = the edge stress

E = modulus of elasticity, 29500 ksi

k = plate buckling coefficient

= 4.0 for stiffened elements supported by a web on each longitudinal edge

= 0.43 for unstiffened elements supported by a web on one longitudinal edge and free on the other

(b) For Deflection Determination: The effective width (b_d) for computing deflections shall be determined from the following formulas:

$$b_d = w \qquad \text{when} \quad \lambda \leq 0.673, \qquad (2.42a)$$

$$b_d = \rho w \qquad \text{when} \quad \lambda > 0.673, \qquad (2.42b)$$

where ρ = reduction factor determined by either of the following two procedures:

(1) Procedure I.

A low estimate of the effective width may be obtained from Equations 2.40 and 2.41 where f_d is substituted for f. f_d is defined as the computed compressive stress in the element being considered (calculations are based on the effective section at the load for which deflections are determined).

(2) Procedure II.

For stiffened elements supported by a web on each longitudinal edge an improved estimate of the effective width can be obtained by calculating ρ as follows:

$$\rho = 1 \qquad \text{when} \quad \lambda \leq 0.673 \qquad (2.43a)$$

$$\rho = (1.358 - 0.461 / \lambda) / \lambda \qquad \text{when} \quad 0.673 < \lambda < \lambda_c \qquad (2.43b)$$

$$\rho = (0.41 + 0.59\sqrt{F_y/f} - 0.22/\lambda)/\lambda \qquad \text{when} \qquad \lambda \geq \lambda_c \tag{2.43c}$$

$$\text{where} \qquad \lambda_c = 0.256 + 0.328(w/t)(\sqrt{F_y/E}). \tag{2.44}$$

and λ is as defined by Equation 2.41 except that f_d is substituted for f.

For the uniformly compressed unstiffened elements, the effective width used in computing deflections shall be determined in accordance with Procedure I except that f_d is substituted for f.

The effective width formulas for computing the load-carrying capacity of uniformly compressed elements used in current AISI Automotive Steel Design Manual are similar to those used in AISI Cold-Formed Steel Design Manual for building construction. According to AISI Automotive Steel Design Manual, for stiffened and unstiffened compression elements with a higher yield strength than 80 ksi, It is recommended that a reduced yield strength can be used in the calculation of Equation 2.41. The reduced yield strengths for stiffened and unstiffened compression elements are given in Reference 1.

According to the AISI Automotive Steel Design Manual, the effective design width of compression elements is used for determining the load-carrying capacity of the member when the slenderness factor λ (Equation 2.41) of compression elements exceeds a limiting value of 0.673.

When $\lambda = 0.673$, the limiting width-thickness ratio (at which full capacity is achievable) can be evaluated as

$$\left[\frac{w}{t}\right]_{lim} = 0.64\sqrt{\frac{kE}{f}} \qquad (2.45)$$

For fully stiffened compression elements under a uniform stress, k = 4, which gives a limiting w/t value as follows:

$$\left[\frac{w}{t}\right]_{lim} = S = 1.28\sqrt{\frac{E}{f}} \qquad (2.46)$$

Using a buckling coefficient of 0.43, the limiting w/t ratio for the unstiffened compression elements can be derived as follows:

$$\left[\frac{w}{t}\right]_{lim} = S = 0.42\sqrt{\frac{E}{f}} \qquad (2.47)$$

When the w/t ratio exceeds the value of S, the effective width, b, is less than the actual width w. The value of b is calculated on the basis of Equation 2.39b.

E. RESPONSE OF FLEXURAL MEMBERS TO DYNAMIC LOADS

In this section, some of the developments resulted from the previous research for the response of structural members subjected to dynamic loads are reviewed. Particular attention is focused on those items related to beams.

Because material properties are influenced by impact loading, a large number of research projects were conducted for a variety of structures under specified loading conditions in the past three decades. Recent research has been directed to analytical procedures which take into account more precise constitutive relationships including strain rate

sensitivity, strain harding, and geometric change arising from overloads.

In 1955, Parkes[67] examined the permanent deformation of mild steel cantilever beams subjected to dynamic transvese loads and observed that a simple rigid, perfectly plastic analysis overestimated the final maximun deflections. In 1958, Parkes[68] examined encastre beams with impact loading applied transversely at any point on their span. The supports of beams were prevented from rotating but were free to move axially. Test specimens were made from mild steel, brass and duralumin. He found that the mild steel is the most sensitive to strain rate as compared with other two materials. Taking the strain-rate sensitivity into account one can improve the correlation between theoretical and experimental results. Similar discovery was also found by Ezra[69] in 1958. He developed a mathematical model to analyze the response of simply supported beams subjected to a concentrated impact load at midspan. His model allows the use of plastic moment, taking account of yield stress as affected by strain rate. His theoretical values showed increasingly better agreements with the test results as the impact speed of the test increases.

In 1962, Ting and Symonds[70] tested the cantilever beam with an attached tip mass subjected to a rapid transverse velocity change at the base. The predictions of plastic deformation showed good agreement with corresponding experimental results as considering the strain-rate dependence of yield stress and geometry changes. Bodner and Symonds[71] (1962) examined the plastic deformations of cantilever beams with tip mass under two loading conditions: (1) the base of the cantilever was impacted

against a solid support and (2) the tip mass was loaded either by an explosive charge, or being hit by a rifle bullet. Two materials (mild steel and aluminum alloy) were used to fabricate the specimens. Theoretical results were initially obtained from the use of a rigid-plastic theory. It was concluded that the strain rate effects gave good agreements with the test results.

Rawlings[72] (1963) reported on his experimental investigation of strain-rate effects on yield loads for beam tests. He tested a series of simply supported beams fabricated from mild steel using two-point loading system so that a plastic hinge could be formed in the central portion of a beam. All loads were applied by large falling masses. The results for the relationship between lower yield value and the time taken to yield obtained from beam tests showed good agreements with the relationship obtained from material tests.

Using the experimental results of Parkes, Ting[73] (1965) developed a formula for cantilever beams loaded dynamically on the basis of rigid-plastic theory, which took into account large geometric changes. His results compared very favorably with Parkes' experimental results. He concluded that not all of the errors between the theory and experimental results can be attributed to strain-rate effect, as had been previously assumed.

In 1965, Florence and Firth[74] tested the pinned and clamped beams without axial restraints, subjected to uniformly distributed impulses. It was concluded that a rigid-plastic analysis considering strain-hardening effect in an approximate manner during the second stage

of motion instead of considering strain-rate effect, gave somewhat better agreement with the experimental results than a rigid-plastic analysis.

Similar results were found by Jones[75] (1967). He developed the method for estimating the combined influence of strain-hardening and strain-rate sensitivity on the permanent deformation of rigid-plastic structures loaded dynamically. A study is made of the particular case of a beam supported at the ends by immovable frictionless pins and loaded with a uniform impulse. He found that when considering strain-hardening alone for beams with small L/H (half-length to thickness) ratios, or strain-rate sensitivity alone for physically small beams, then permanent deflections are predicted, which compare rather favorably with those given for the same value of λ (impulse parameter) by an analysis retaining their combined influence.

Aspden and Campbell[76] (1966) were the first to conduct dynamic flexural tests in which transient records were taken of moment -rotation characteristics. They used small-scale specimens, 0.75 inches long by 0.375 inches wide by 0.125 inches thick, supported at their ends by beams and loaded as four point loading system by a falling weight. They compared their high speed flexural test results with those obtained under dynamic compression using a hydraulically operated machine, and with slow speed tests in an Instron machine. Like Rawlings, Aspden and Campbell observed evidence of high initial peak moments of resistance. For the highest rate of strain in their beams, the dynamic 'upper yield moment' was about 80% higher than the corresponding moment in a low speed test. Figure 2.23 shows the variation of upper and lower yield moments with strain-rate at surface of specimen. They noticed that attaining the

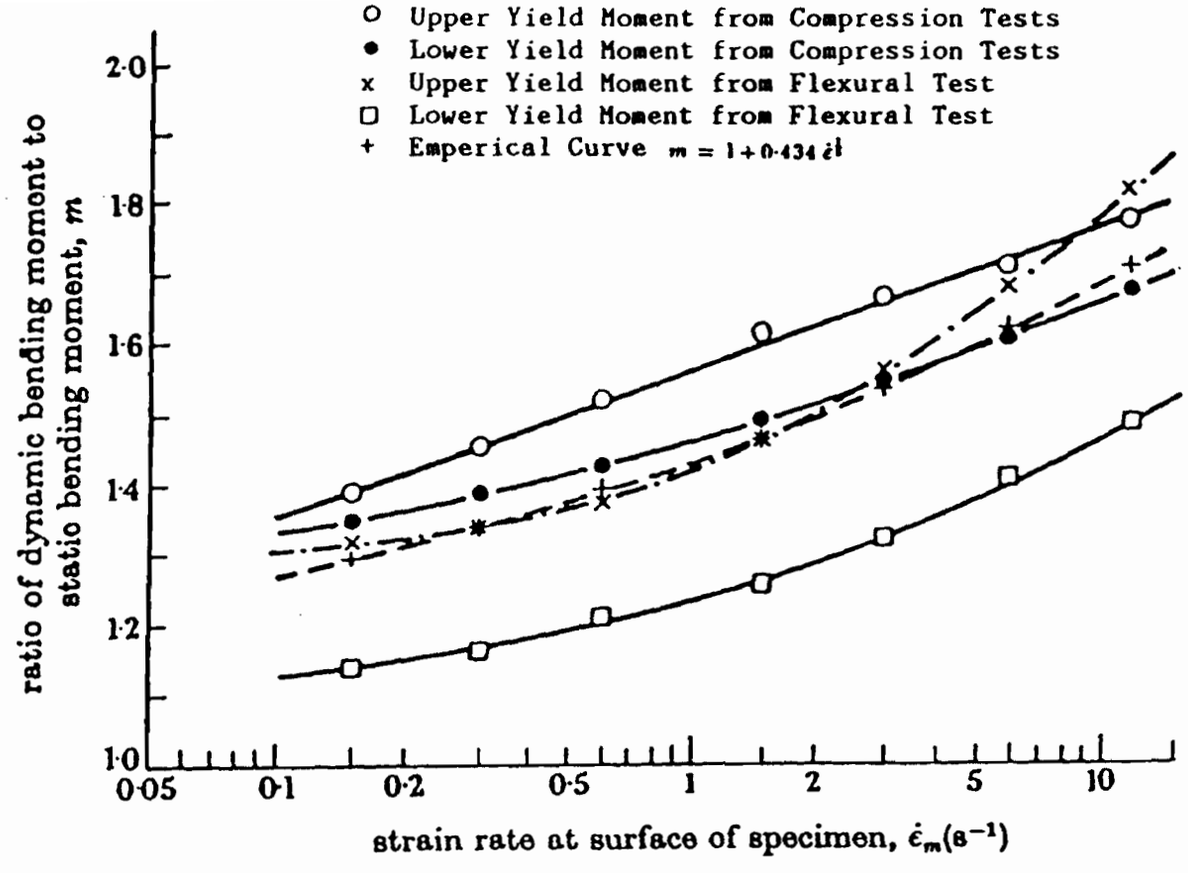

Figure 2.23 Variation of Upper and Lower Yield Moments with Strain Rate at Surface of a Specimen[76]

maximun peak moment of resistance, the value decreased below that which would be derived from test results by assuming plane sections remain plane. They attributed the difference of about 10% to non-uniform strain distribution throughout the experiment during the loading process. Based on the empirical equation (Equation 2.48) for prediction of dynamic yield stresses under constant strain rate derived by Cowper and Symonds, Aspden and Campbell integrated Equation 2.48 through the thickness of a beam and found that the dynamic bending moment is related to the associated beam curvature rate according to the expression given in Equation 2.49.

$$\frac{\sigma}{\sigma_0} = 1 + \left(\frac{\dot{\varepsilon}}{D}\right)^{1/p} \tag{2.48}$$

where σ = dynamic yield stress

σ_0 = static yield stress

$\dot{\varepsilon}$ = strain rate

D and p= strain-rate sensitivity coefficients

$$\frac{M}{M_0} = 1 + \frac{2p}{2P+1}\left(\frac{\dot{\kappa}H}{2D}\right)^{1/p} \tag{2.49}$$

where M = dynamic bending moment

$M_0 = \sigma_y H^2/4$, static collapse moment

$\dot{\kappa}$ = curvature rate

H = thickness of the beam

In 1971, Culver, Zanoni, and Osgood[77] of Carnegie-Mellon University reported on thin-walled beam sections subjected to dynamic loading, as part of a large program of dynamic loading on cold-formed steel structural sections. Two methods of analysis were used in this study. The linear

elastic and the non-linear methods including local buckling effects, were used to compare the test results. A comparision of results showed that it was sufficient to predict bending moments from nominal linear elastic analysis considering local buckling effects. It was also found that the effective design width formulas (Equation 2.37) satisfied both static and dynamic results to the same degree of accuracy.

Symonds and Jones[78] (1972) reviewed the earlier work on plastic response to impulsive loading of beams clamped against end rotations and axial displacements, taking account of small finite transverse displacements and of strain-rate dependence of the yield stress. New solutions were derived from the rigid-plastic analysis which included both effects and were compared with experimental results. They concluded that the rigid-plastic interation theory with simple strain-rate corrections provides satisfactory agreement with deflections measured in tests of small beams for deflections up to about seven times the beam thickness.

Forrestal, Wesenberg, and Sagartz[79,80] have developed a simple method for incorporating the approximate influence of material elasticity on the dynamic plastic response of beams. An exact elastic analysis was first undertaken for a dynamic beam problem which remains valid until the maximum stress reaches yield. If the beam material is strain-rate sensitive, then this yield stress is calculated from Cowper-Symonds constitutive law (Equation 2.48), using the corresponding strain-rate predicted by elastic analysis. The subsequent plastic behavior is controlled by a constant yield stress. There was an excellent agreement with the peak displacements recorded during experiments on simply

supported beams using 1018 steel and type 304 stainless steel as shown in Figure 2.24.

In 1989, Kassar[14-17] tested three different sheet steels (35XF, 50XF, and 100XF) and 30 beams fabricated from 35XF sheet steel under dynamic loads. Based on the test results, it was found that the mechanical properties of sheet steels (yield stress, proportional limit, and ultimate tensile strength) and the load-carrying capacity of beams increase with increasing strain rates.

F. RESPONSE OF AXIALLY LOADED MEMBERS TO DYNAMIC LOADS

Two current trends in automobile design have increased the complexity of material selection for automobiles. On the one hand, there has been the steady drive to develop designs that increase the safety of occupants during auto collisions. At the same time, in the interests of fuel and material economy, the steel industry has been developing high-strength steels for use by the automotive industry in designing lighter-weight steel components[81].

The crushing behavior of thin-walled sheet metal structures such as tubes, circular cylinders, and non-circular sections under both quasi-static and dynamic axial loading conditions has been studied over the past 30 years. These structures were used to study the mechanical energy absorption in the event of a vehicle collision or accident.

The dynamic plastic collapse of energy-absorbing structures is more difficult to understand than the corresponding quasi-static collapse, on account of two effects which may be described as the "strain-rate factor" and the "inertia factor" respectively. The first of these is material

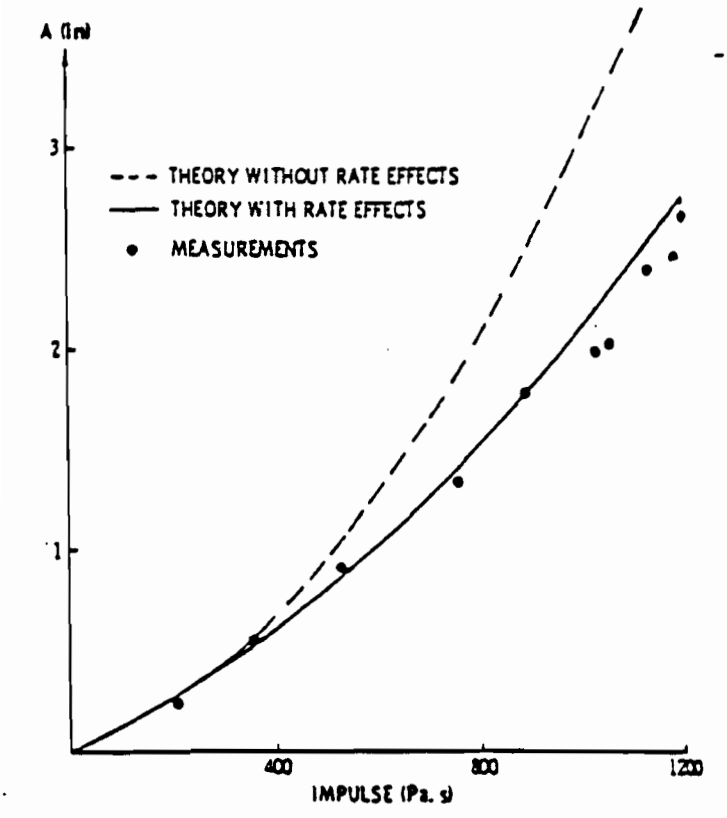

(a) AISI 1018 Steel Beams[80]

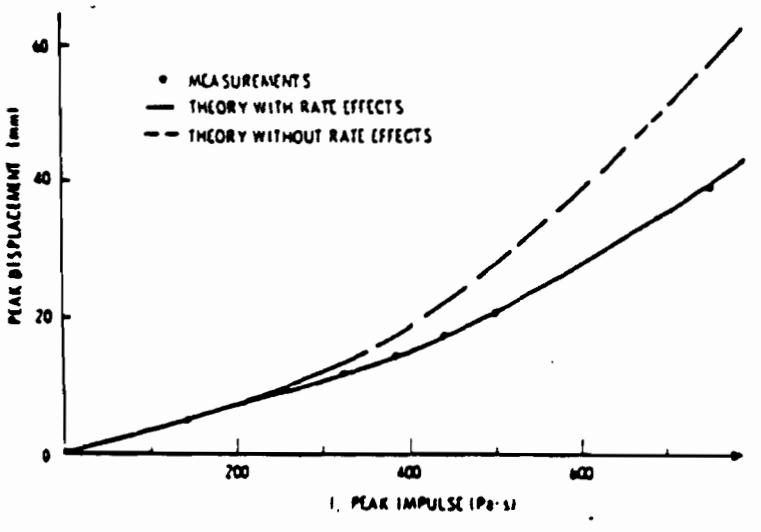

(b) Type 304 Stainless Steel Beams[79]

Figure 2.24 Peak Displacement Versus Impulse

property whereby the yield stress is raised, while the second can affect the collapse mode, etc[82].

The analysis of column behavior under impact loading conditions dates back to 1933, when Koning and Taub derived equations describing the axial and transverse oscillation of pin-ended columns subjected to dynamic axial loads. They considered loads having a rectangular pulse form, of magnitude less than, equal to, or greater than the static Euler load. However, they did not recognize the possibility of dynamic overloads[83].

Macaulay and Redwood (1964) examined the behavior of rods, square tubes and small-scale models to gain insight into the effect of axial impact on railway coaches. They found important differences between the static and dynamic buckling behavior and recognized a velocity effect with two components, geometry and strain rate[84].

Some of the most significant work on the analysis of strut behavior under dynamic loading is due to Hoff[85] (1965). His analysis was directed to study the dynamics of the buckling of elastic columns in a rapid compression test. In his study, he found that the lateral displacements of the column under rapid loading are less than those calculated from static considerations. As a consequence the load supported by the column can exceed the Euler load considerably.

Axial impact on thin-walled columns was examined theoretically by Culver and Vaidya[86] and experimentally by Logue[87], both were published in 1971. The theoretical work was applied to short duration impact loading which was defined by prescribing the time variations of the load

at the end of the columns. Nonlinearity due to local buckling was accounted for by using nonlinear axial load-curvature relations derived with the aid of the effective width concept. The results of the analytical study were shown as response spectra curves which described the effect of initial deflection, pulse duration, maximum dynamic load, and the static preload on the dynamic response. It was concluded from the experimental study that maximum loads in excess of the static failure loads may be carried dynamically.

Soden, Al-Hassani, and Johnson[88] (1974) studied the crushing behavior of circular tubes under static and dynamic axial loads. The loads and deformations of tubes with various thicknesses were recorded and three failure modes were observed and studied. The majority of tube tests collapsed by progressive folding into diamond shaped lobes, while thick tubes failed by collapsing into circumferential rings. The initial failure loads and postbuckling loads for various modes of deformation were predicted theoretically. They found that all stresses incresed with increasing strain rate.

In 1977, Van Kuren and Scott[81] studied a series of crushing tests performed to determine the energy absorption of a range of steels at testing speeds up to 40mph and temperatures of 70 and -40 F. Open-ended square and cylindrical tubes were axially loaded to produce accordionlike deformation patterns. For four-inch-diameter cylinders at 40mph impact, Figure 2.25 shows the effect of impact velocity on energy absorbed for two test thicknesses. Based on their investigation, the conclusions are: (1) the energy absorption of steel increases with impact velocity and at low temperature; (2) tube geometry significantly influences the amount

of energy absorbed. Specifically, a square tube absorbs a third less energy than a circular tube for an equal volume of material; and (3) high-strength steels absorb energy in proportion to their strength level, the significance being that they can be used in relatively thin material to reduce vehicle weight.

Van Kuren[89] (1980) also studied the energy absorption of several automotive materials, i.e., reinforced plastics, steel, and aluminum. These curved shell specimens were crushed at impact speeds up to 25mph and temperatures of 70 and -40 F. Figure 2.26 shows the effect of impact velocity on the energy absorption of several materials. He stated that steel absorbed up to 20 times more total energy than did the reinforced plastics and over twice that absorbed by aluminum for the same thickness. Aluminum absorbed more energy per unit weight than the other materials, but steel was considerably more cost-effective.

In 1977, Wierzbicki[90] studied the dynamic crushing strength of strain-rate sensitive box columns. The main purpose of his study was to identify material and geometrical parameters in the problem of impact loading for sheet metal and to derive an expression for the strain rate correction factor. As a particular structural component, a straight retangular box column was considered to be representive of front or rear longitudinal members of an automobile body. He stated that during a vehicle collision the strain rate in the zones of localized deformation can be of the order of 10 to 100 in./in./sec.. Consequently, dynamic forces in compressed mild steel members are much greater than static ones. An approximate analysis was presented to determine dynamic strength and energy absorption of axially loaded thin-walled box columns. In this

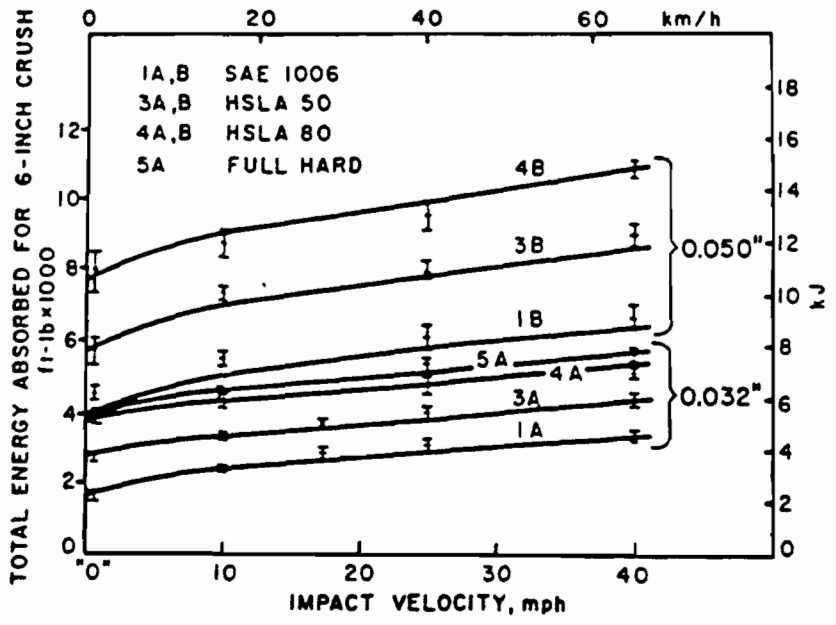

Figure 2.25 Effect of Impact Velocity on the Energy Absorbed for Several Steels[81]

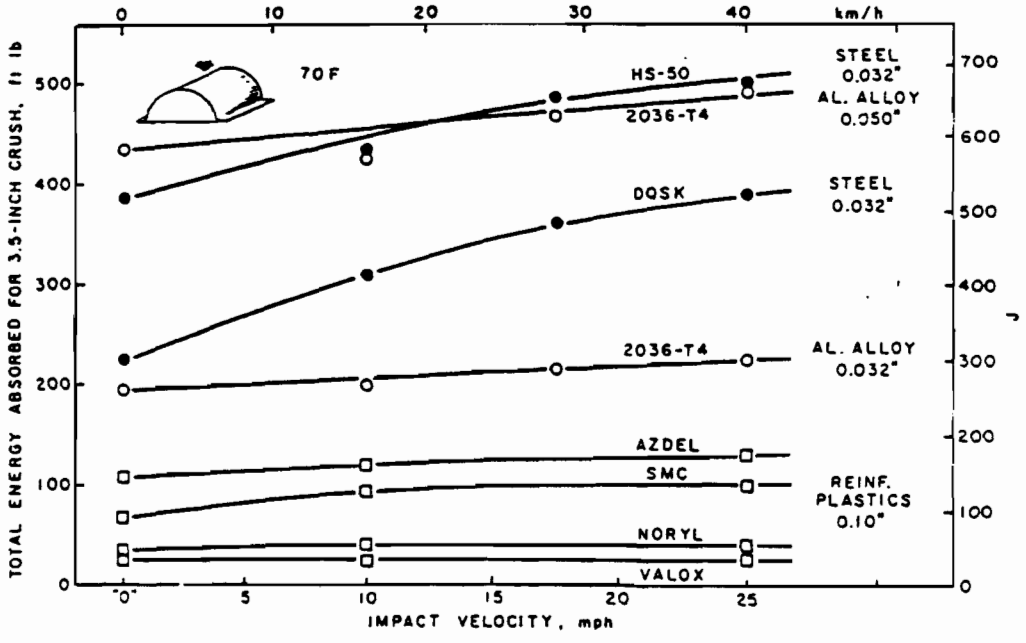

Figure 2.26 Effect of Impact Velocity on the Energy Absorption of Several Materials[89]

analysis, the dynamic compressive force is a product of a static crushing strength of the column and a strain-rate correction factor. The strain-rate correction factor was found to be dependent on the initial impact velocity and parameters describing the sensitivity of the material to strain rate.

In another work published in 1979, Wierzbicki and Abramowicz[91] used a simple method to calculate the dynamic correction factor for thin-walled, strain-rate sensitive structures. For the experiments run at two crushing speeds v1 and v2 with associated strain rates $\dot{\varepsilon}_1$ and $\dot{\varepsilon}_2$, the corresponding ratio of mean crushing forces P_m^1 and P_m^2 is equal to the dynamic correction factor given as follows:

$$R = \frac{P_m^1}{P_m^2} = \left(\frac{\dot{\varepsilon}_1}{\dot{\varepsilon}_2} \right)^{\frac{1}{\bar{n}}} = \left(\frac{v1}{v2} \right)^{\frac{1}{\bar{n}}} \qquad (2.50)$$

where $\bar{n}$ is the material strain-rate sensitivity calculated from the following equation:

$$\frac{\sigma}{\sigma_0} = \left(\frac{\dot{\varepsilon}}{\dot{\varepsilon}_0} \right)^{\frac{1}{\bar{n}}} \qquad (2.51)$$

It can be seen from Equation 2.50 that the dynamic correction factor does not involve any geometrical and material parameters except the constant $\bar{n}$.

In 1984, Abramowicz and Jones[92] conducted twenty-three experimental tests on 56mm-diameter steel tubes of various lengths subjected to dynamic axial loads. The columns were crushed axially on a drop hammer rig. The

effective crushing distance was considered in the analysis along with the influence of material strain-rate sensitivity. The ratio of the dynamic to quasi-static mean crushing forces for identical, straight tubes of mild steel can be expressed as below:

$$\frac{\dot{P}_m^d}{P_m^s} = 1 + \left(\frac{\dot{\varepsilon}}{6844} \right)^{\frac{1}{3.91}} \qquad (2.52)$$

where 3.91 and 6844 $sec.^{-1}$ are material constants.

They concluded that a modified version of Alexander's[93] theoretical analysis for axisymmetric, or concertina, deformations gives good agreements with the experimental results when the effective crushing distance is concerned and provided that the influence of material strain rate sensitivity is retained in the dynamic crushing case.

The crush strength characteristics and modes of collapse of thin-walled circular columns were mathematically formulated by Mahmood and Paluszny in 1984[94]. The formulation was based on the stability of shell structures subjected to axial crush, where various stages of collapse were identified and crush characteristics pertinent to column design were quantified. It was concluded that the crush characteristics of columns are functions of both column geometry (thickness to radius ratio (t/r)) and the elastic/yield properties of the material (elasticity modulus (E), poisson's ratio (ν), and yield strength (S_y)), whereas the mode of collapse (number of circumferential lobes) is governed predominantly by the geometry ratio (t/r).

Mamalis, Johnson, and Viegelahn[95] (1984) studied the uniformly thin circular cylinders and frusta (truncated circular cones) of low carbon steel subjected to axial loading at elevated strain rate. The initial axial length and the outside diameter of the cylinders and frusta (the larger top end) were kept constant while the uniform wall thickness of those specimens was varied. The load-deformation or compressive behavior of the cylinder and frusta for the two semi-apical angles used, 5° and 10°, were recorded and the modes of collapse were observed and discussed. In this investigation, they found that with increasing slenderness ratio, thickness to initial outside diameter ratio for cylinder and thickness to initial outside mean diameter for frusta, (effectively increasing wall thickness) both the peak and mean postbuckling loads increase in a broadly parabolic manner. With increase in semi-apical angle, both the peak and postbuckling load decrease.

Birch and Jones[84] conducted a series of axial impact and static crushing tests carried out on specimens manufactured from commercial structural mild steel tubing (seam welded) having an outside diameter D' of 64 mm, wall thickness H of 1.58 mm, a length of L of 150 mm, with stiffeners. An examination was made into the influence of stiffener depth (T), number of stiffeners (N), and the effect of placing the stiffeners externally or internally. Based on the test results, they found that the static and dynamic collapse modes are similar for plain unstiffened tubes. However, there are considerable differences between the static and dynamic collapse modes for the axially stiffened tubes which were even more pronounced in tubes with four axial stringers. The static collapse of tubes stiffened with four external stringers occurs in an unstable

overall buckling mode with peak collapse loads lower than those found in the specimens with four internal stringers. The dynamic collapse mode of the tubes stiffened with four internal stringers is generally a stable regular progressive type, while the dynamic collapse mode is an irregular progressive type, with some stability, when the tubes are stiffened with four external stiffeners.

In 1989, Kassar[14-17] also studied the box-shaped and I-shaped stub columns subjected to dynamic loads. A total of 35 stub columns were fabricated from 35XF sheet steel with a nominal yield strength of 35 ksi. Prior to the stub column tests, the effects of strain rate on the mechanical properties of three different sheet steels (35XF, 50XF, and 100XF) were studied experimentally. The results of the experimental study indicated that the mechanical properties of sheet steels (yield stress, proportional limit, and ultimate tensile strength) as well as the load-carrying capacity of stub columns increase with increasing strain rates.

III. EXPERIMENTAL INVESTIGATION

A. GENERAL

During the period from January 1988 through December 1991, the research project sponsored by the American Iron and Steel Institute (AISI) at the University of Missouri-Rolla was concentrated on a study of the effect of strain rate on mechanical properties of sheet steels and the structural behavior and strength of cold-formed steel members subjected to dynamic loads. In Sec. B of this section, the experimental investigation of material properties of three selected sheet steels is discussed in detail. The effects of strain rate on the structural strength of cold-formed steel stub columns and beams are presented in Sections C and D, respectively.

B. MATERIAL PROPERTIES

In order to study the effect of strain rate on the mechanical properties of high strength sheet steels, tension and compression coupon tests of three selected sheet steels (35XF, 50XF, and 100XF) were conducted by Maher Kassar under different strain rates ranging from 10^{-4} to 1.0 in./in./sec. The nominal yield strengths of these sheet steels varied from 35 to 100 ksi. Table 3.1 lists the thicknesses and chemical compositions for these sheet steels. All three virgin materials were uniaxially tested in the longitudinal (parallel to the direction of rolling) and transverse (perpendicular to the direction of rolling) directions in tension and compression under three different strain rates. Details of material tests were presented in the Eleventh[14] and Twelfth[15]

Progress Reports. Research findings of these two progress reports are summarized in Sec. B of Section III and Section IV.

1. Tension Tests. All tension tests followed the procedures outlined in the ASTM Specifications which are listed in Table 3.2. Two of these three sheet steels (35XF and 50XF) were also tested in both longitudinal and transverse directions to determine the combined effects of cold-stretching and strain rate. The amounts of the uniform cold-stretching used for the tests were 0.02 in./in. (20 mils) and 0.08 in./in. (80 mils). In order to determine the combined effects of aging and strain rate, half of the coupons (non-aged) were tested in an average of two days after cold stretching operation. The remaining half of the cold-stretching coupons (aged) were tested to failure under different strain rates at least 30 days after cold stretching operation. Three strain rates selected for the tension tests were 10^{-4}, 10^{-2}, and 1.0 in./in./sec..

a. Specimens. As can be seen from Figure 3.1, the test specimens were cut longitudinally and transversely from the quarter points of the steel sheets. All tensile specimens as shown in Figure 3.2 were prepared in the machine shop of the Department of Civil Engineering at the University of Missouri-Rolla. This figure also shows the dimensions of tension coupons. In this phase of study, 13 coupons were cut from the 100XF sheet steel, 56 coupons from the 50XF sheet steel, and 54 coupons from the 35XF sheet steel. A total of 22 different cases were conducted for the tension tests which are summarized in Table 3.3.

Table 3.1

Chemical Compositions of the Sheet Steels Used

AISI Designa.	Thick. in.	C	Mn	P	S	Si	V	Cu	Al	Cb	Zr
35XF	0.085	.070	.40	.007	.017	--	.08	--	--	--	--
50XF	0.077	.081	.96	.017	.003	.27	--	--	.04	--	--
100XF	0.062	.070	.43	.006	.023	--	--	.11	.056	.064	.08

Table 3.2

ASTM Specifications for Tension Tests

E8-69	Tension Testing of Metallic Materials
E83-67	Standard Method of Verification and Classification of Extensometers
E111-82	Standard Test Method for Young's Modulus, Tangent Modulus and Chord Modulus

Table 3.3

Number of Performed Tensile Coupon Tests

Cold-Stretched Condition	Type of Material	Number of Coupons Used
Virgin Materials		
Longitudinal Tension (LT)	100XF-LT	7
	50XF-LT	9
	35XF-LT	9
Transverse Tension (TT)	100XF-TT	6
	50XF-TT	9
	35XF-TT	6
2% Cold-Stretched Non-Aged Materials		
Longitudinal Tension (LT)	50XF-LT	6
	35XF-LT	6
Transverse Tension (TT)	50XF-TT	2
	35XF-TT	4
8% Cold-Stretched Non-Aged Materials		
Longitudinal Tension (LT)	50XF-LT	6
	35XF-LT	6
Transverse Tension (TT)	50XF-TT	4
	35XF-TT	4
2% Cold-Stretched Aged Materials		
Longitudinal Tension (LT)	50XF-LT	6
	35XF-LT	6
Transverse Tension (TT)	50XF-TT	4
	35XF-TT	4
8% Cold-Stretched Aged Materials		
Longitudinal Tension (LT)	50XF-LT	6
	35XF-LT	6
Transverse Tension (TT)	50XF-TT	4
	35XF-TT	4

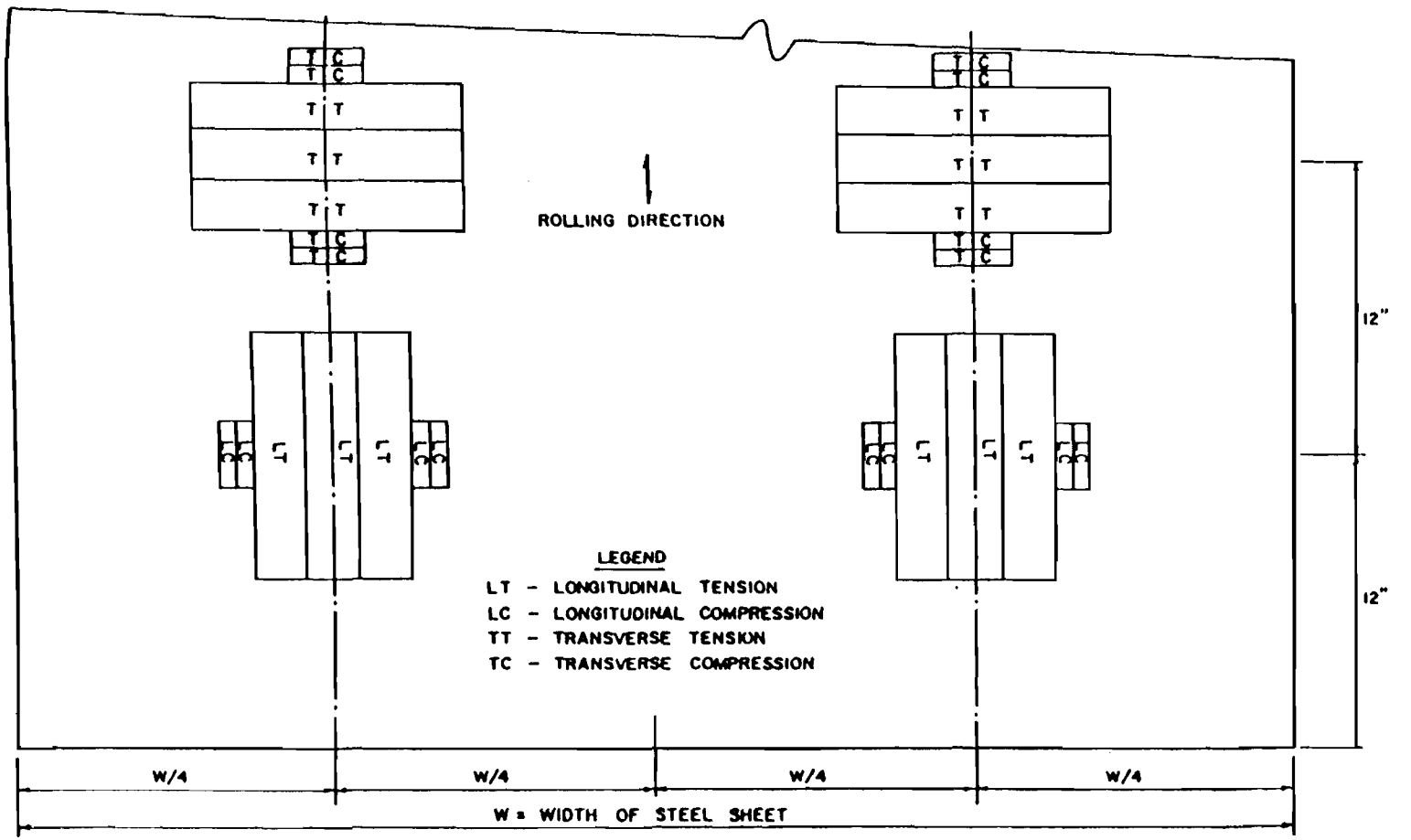

Figure 3.1 Location of Tension and Compression Coupons[8]

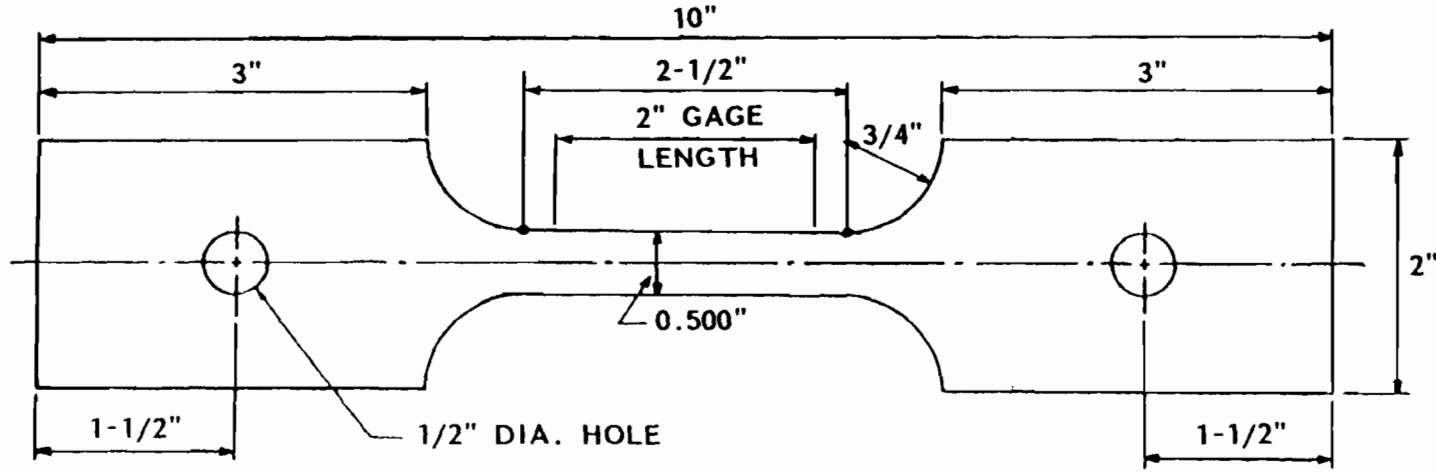

Figure 3.2 Nominal Dimensions of Tension Coupons Used for 35XF, 50XF, and 100XF Sheet Steels[8]

b. Instrumentation. All tests were performed by using a 110 kip MTS 880 Test System located at the UMR Engineering Research Laboratory. As shown in Figure 3.3, This test system consists of an MTS load frame, an MTS control console, and the CAMAC (Computer Automated Measurement and Control) Data Acquisition System. After the test data were acquired in the CAMAC Data Acquistion System, it was downloaded to the Data General MV-10000 Mini Computer for analysis purpose. Other equipment used to analyze the test data includes an IBM PS/2 Model 30 personal computer with an IBM color plotter and an NEC Pinwrite P5XL printer.

The loading apparatus was a servohydraulic closed-loop type. The moving position is driven by a double-action hydraulic cylinder, so that it can operate under tension and compression. The fluid pressure in the chamber is controlled by a servovalve, which responds to the difference between the measured signal and the desired signal. The signal is amplified to drive the valve so as to remove the error. The load was measured by an MTS System Model 380041-06 load cell and associated conditioning, which was calibrated prior to testing according to the procedure of the National Bureau of Standards.

The data acquisition used in this system conforms to the CAMAC standards. The main data acquisition module is a Kinetic Systems Model 4022 Transient Recorder. This unit has 64 simultaneous sampling input channels at a resolution of 12 bits. It is capable of acquiring the test data at the maximum rate of 25,000 sets of readings per second.

An MTS Model No. 732.25b-20 extensometer (Figure 3.4) with a 2-in. gage length was used to measure the strains from zero load to failure. The classification of this extensometer according to ASTM Designation

Figure 3.3 880 Material Test System (MTS) and Data Acquisition System

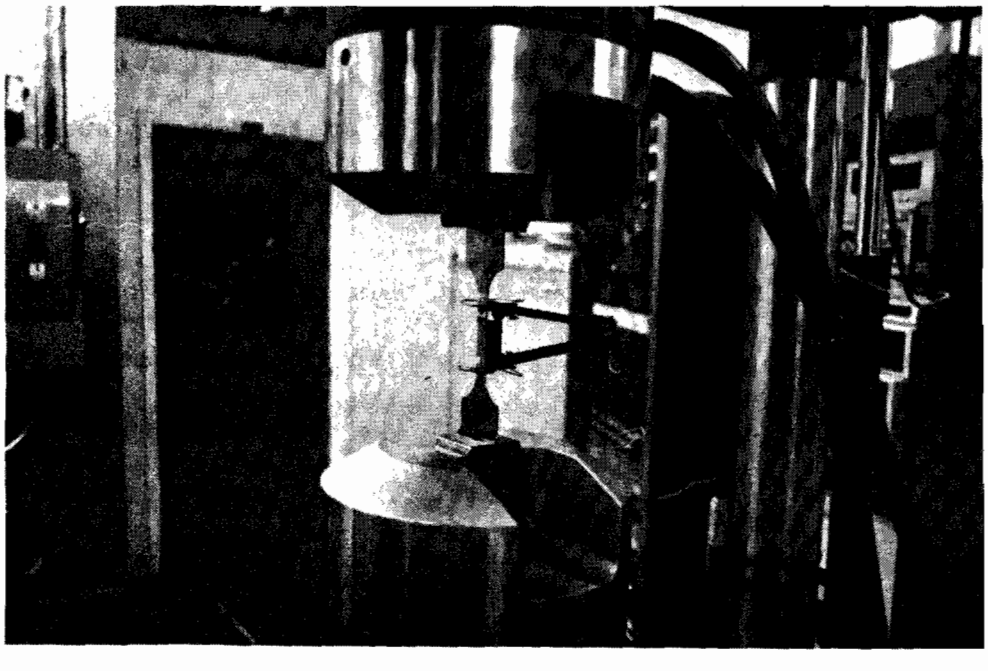

Figure 3.4 Test Setup Showing the Attachment of Extensometer

E-83 was found to be dependent on the extensometer range used in the test. Table 3.4 contains the classification of the four extensometer ranges according to the MTS transducer calibration data.

There are three modes of operating the machine, commonly referred to as load, strain, and stroke (displacement). There are four different ranges of operation (100%, 50%, 20%, and 10%) for each mode. Table 3.5 summarizes the transducer ranges and the corresponding load, strain, or displacement values. Under the stroke mode, the movement of the piston is the controlling variable. Under the load mode, it is the load acting on the test specimen. Under the strain mode, it is the strain, as read from the extensometer. For each of these three modes, different time functions can be established by the function generator to match the application needed. Tensile tests under a constant strain rate can be made by setting a ramp function under the strain mode. The slope of this ramp is the desired strain rate.

c. Test Procedure. All tensile coupons were cut and machined to the desired shapes. Prior to testing, the dimensions were measured to the nearest 0.001 inch. The specimen was then cleaned with acetone, and the gage length was marked in ink. The grips of the load frame were alligned by operating the machine under stroke mode. Then, the specimen was placed in the grips such that the longitudinal axis of the specimen coincided with the center line of the grips.

For most tension tests, load range 4, strain range 1, and stroke range 1 were selected. The function generator was programmed to produce the desired ramp. Ramp time 1 (RT1) was chosen for the desired strain-rate value and ramp time 2 (RT2) was chosen to give enough time

Table 3.4

Classification of the MTS Extensometer

Range	Maximum Strain in./in.	Maximum Error in./in.	ASTM Classification
100%	0.50	0.00065	Between Classes B-2 and C
50 %	0.25	0.00030	Between Classes B-2 and C
20 %	0.10	0.00011	Between Classes B-1 and B-2
10 %	0.05	0.00002	Between Classes A and B-1

Table 3.5

MTS Transducer Ranges and the Corresponding Load, Strain, or Displacement Values

Transducer	Range	Value
Load	1 100 %	100.0 kips
	2 50 %	50.0 kips
	3 20 %	20.0 kips
	4 10 %	10.0 kips
Strain	1 100 %	0.50 in./in.
	2 50 %	0.25 in./in.
	3 20 %	0.10 in./in.
	4 10 %	0.05 in./in.
Stroke	1 100 %	10.0 in.
	2 50 %	5.00 in.
	3 20 %	2.00 in.
	4 10 %	1.00 in.

to remove the extensometer and the specimen from the load unit as illustrated in Figure 3.5.

Before running the test, the load mode was selected to place the specimen in the grips. The extensometer was attached to the specimen such that the knife edges of extensometer lined up with the gage marks as shown in Figure 3.4. The load mode was then transferred to the strain mode before the test was started. After the test was completed, the test data was saved by the Data General Mini Computer for later plotting and determination of mechanical properties.

The cold-stretching coupons were loaded to the desired 2% strain or 8% strain by using strain as a control mode with the strain rate of 0.1 in./in./sec.. The span in the MTS system controller was used to stop the test when the desired strain was reached.

d. Test Results. A constant strain rate is very difficult to maintain with the conventional test machine especially at higher strain rate. For this series of tests, the strain rate was controlled electronically by the MTS 880 Test System, which allowed the exact strain rate to be maintained without any difficulty. Figure 3.6 shows the strain-time curve for the specimen fabricated from 50XF sheet steel and tested under 1.0 in./in./sec. strain rate. The stress-strain curves and mechanical properties of three types of materials obtained from tension tests are discussed below:

i) Stress-strain relationships. To illustrate the effect of strain rate on the mechanical properties, Figures 3.7 through 3.9 show the typical stress-strain curves for the three virgin materials (35XF, 50XF,

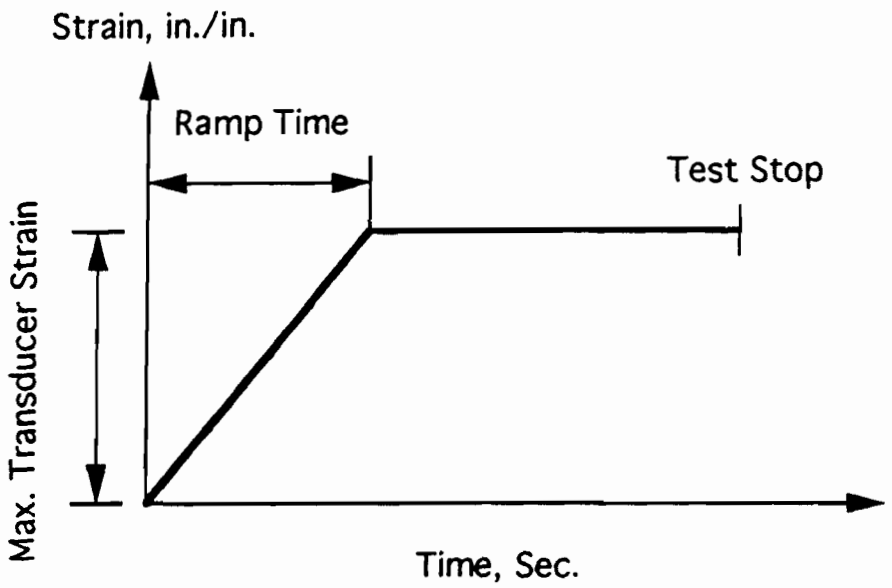

Figure 3.5 Typical Function Generator Ramp Waveform

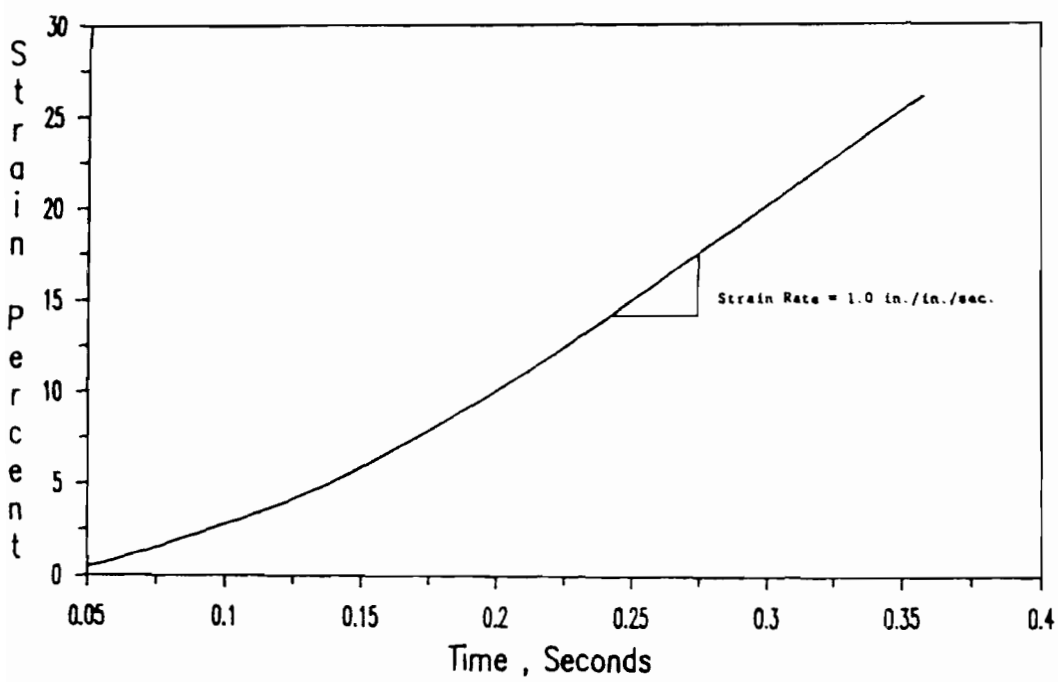

Figure 3.6 Strain-Time Curve for 50XF-LT-7 (Virgin Material)

and 100XF) tested in the longitudinal direction . Each figure includes three stress-strain curves representing the test data obtained from the same sheet steel using different strain rates (10^{-4}, 10^{-2}, and 1.0 in./in./sec.).

The stress-strain relationships were plotted by using the Data General graphics software named "Trendview" with the stress and strain data recalled from the computer storage. Because the stresses were calculated by dividing the loads by the original, unreduced areas of the specimens, they should be regarded as the engineering stress-strain curves.

In order to study the effect of aging on the mechanical properties of 50XF-LT steel, Figures 3.10 through 3.12 compare three typical stress-strain diagrams with different amounts of cold stretching tested under a constant strain rate. Other cases of stress-strain relationships were presented in Reference 14.

ii) Mechanical properties. The mechanical properties determined from tension tests are yield strength (F_y), ultimate tensile strength (F_u), and elongation in 2-in. gage length. The material properties derived from each individual test are presented in Tables 3.6 through 3.16. Tables 3.17 through 3.22 present the average values of the mechanical properties for each material tested in either longitudinal tension (LT) or transverse tension (TT), but with different amounts of cold stretching (virgin material, 2%, or 8%) under different strain rates (10^{-4}, 10^{-2}, or 1.0 in./in./sec.). The procedures used for determining the mechanical properties of sheet steels are discussed in the following paragraphs.

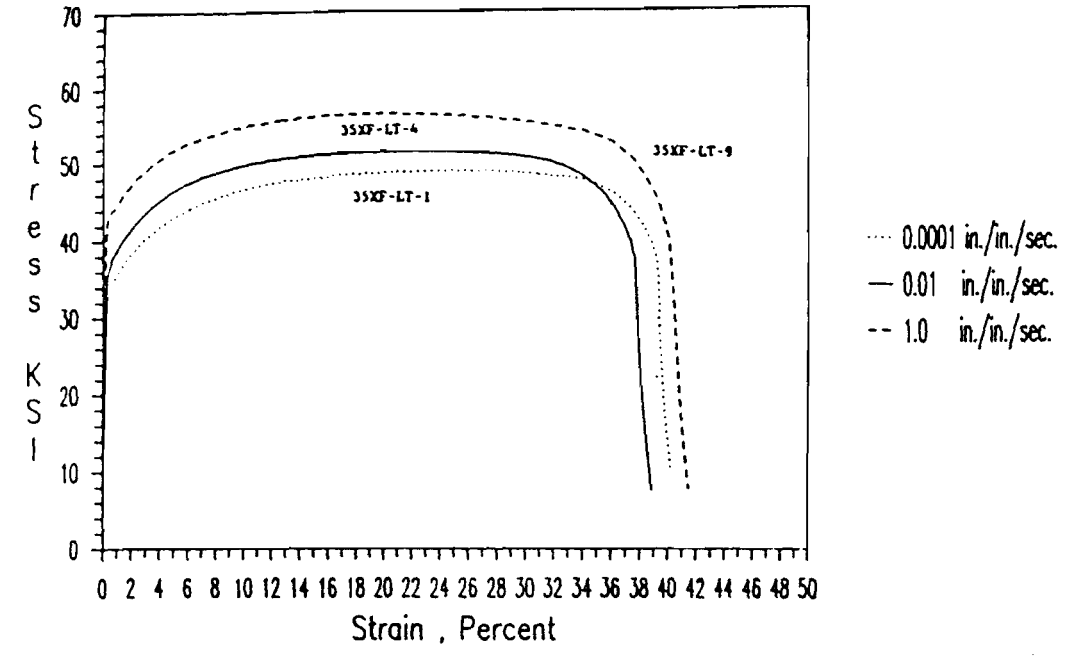

Figure 3.7 Stress-Strain Curves for 35XF-LT-1, 35XF-LT-4, and 35XF-LT-9, (Virgin Material)

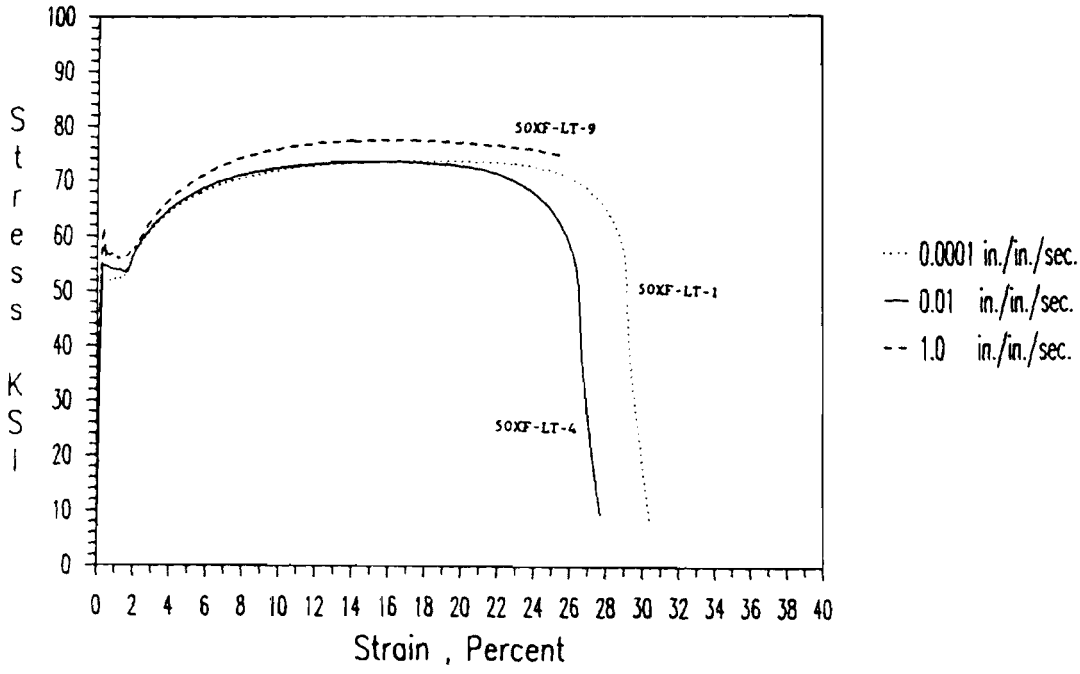

Figure 3.8 Stress-Strain Curves for 50XF-LT-1, 50XF-LT-4, and 50XF-LT-9, (Virgin Material)

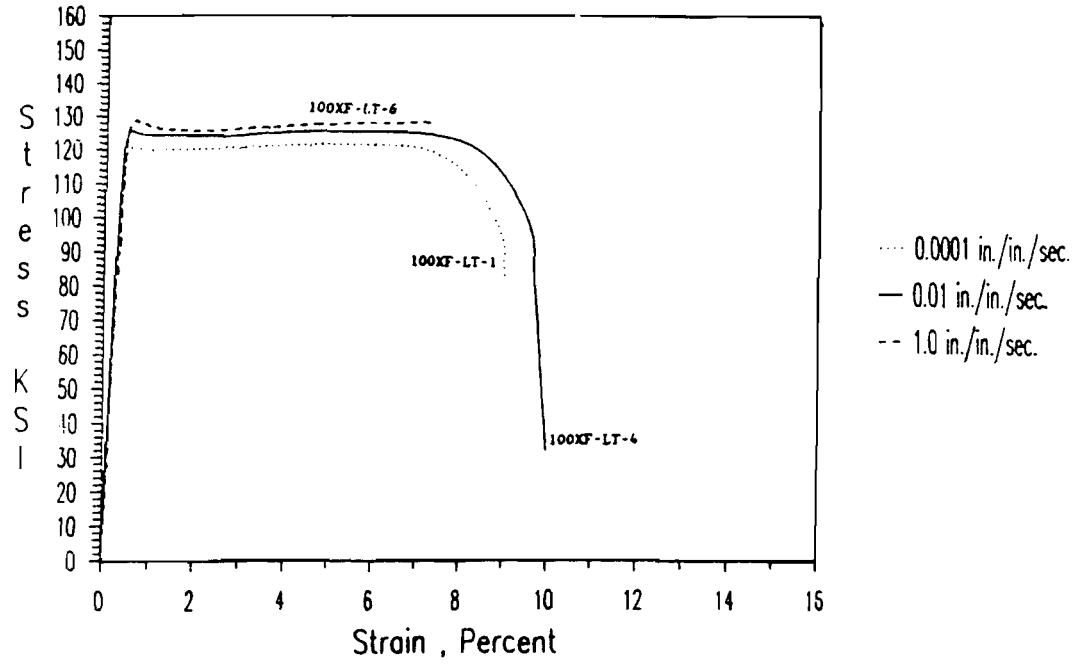

Figure 3.9 Stress-Strain Curves for 100XF-LT-1, 100XF-LT-4, and 100XF-LT-6, (Virgin Material)

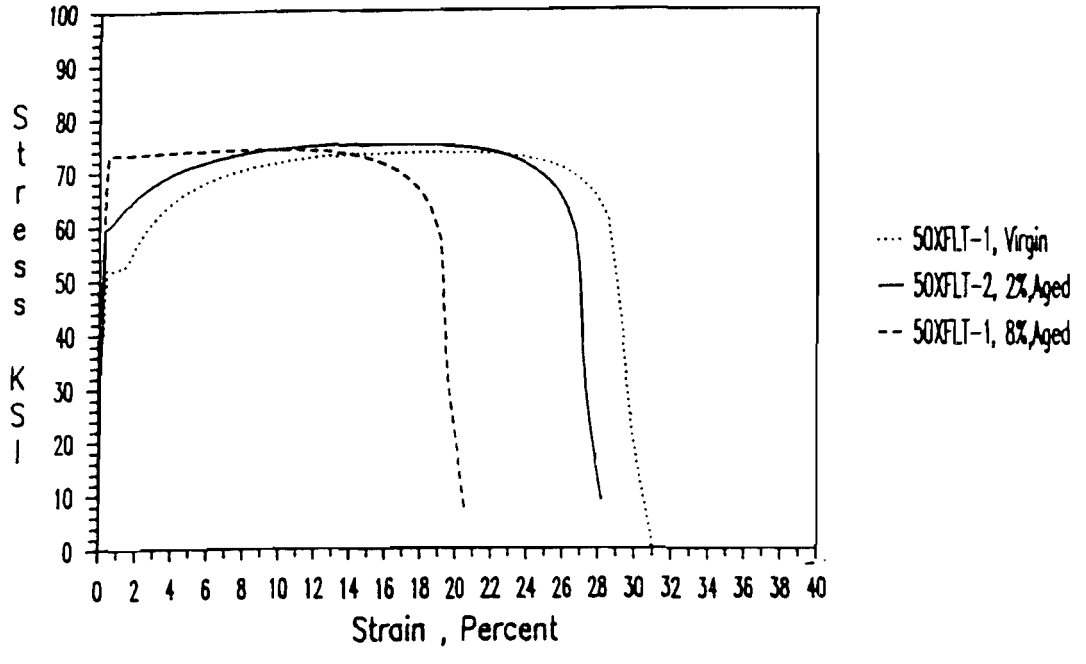

Figure 3.10 Stress-Strain Curves for 50XF-LT Steel at Strain Rate of 10^{-4} in./in./sec.

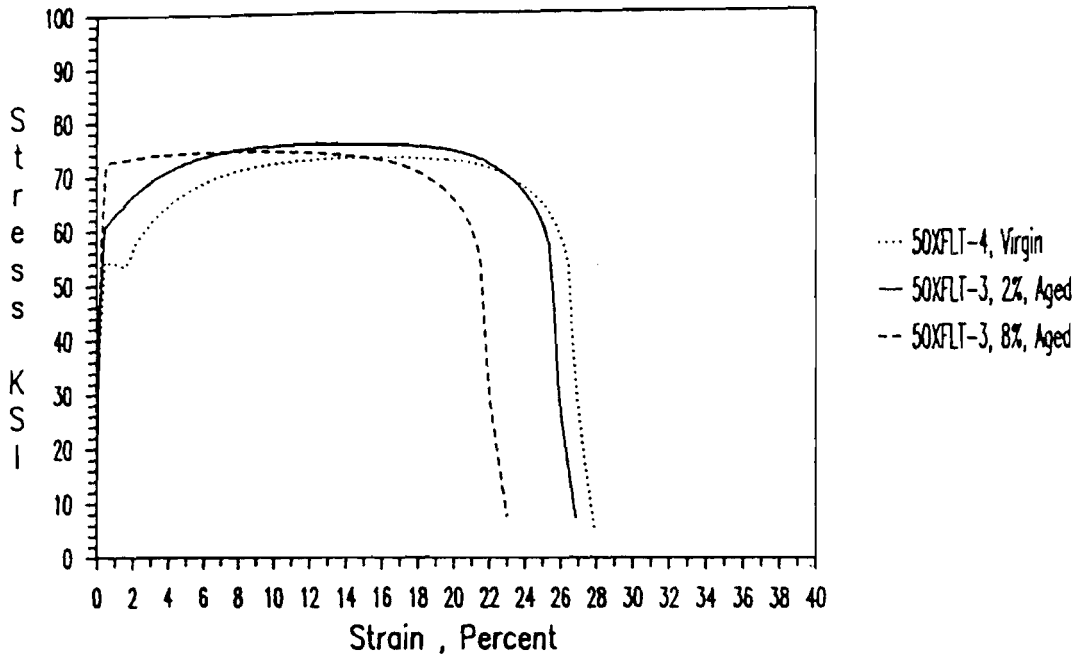

Figure 3.11 Stress-Strain Curves for 50XF-LT Steel at Strain Rate of 10^{-2} in./in./sec.

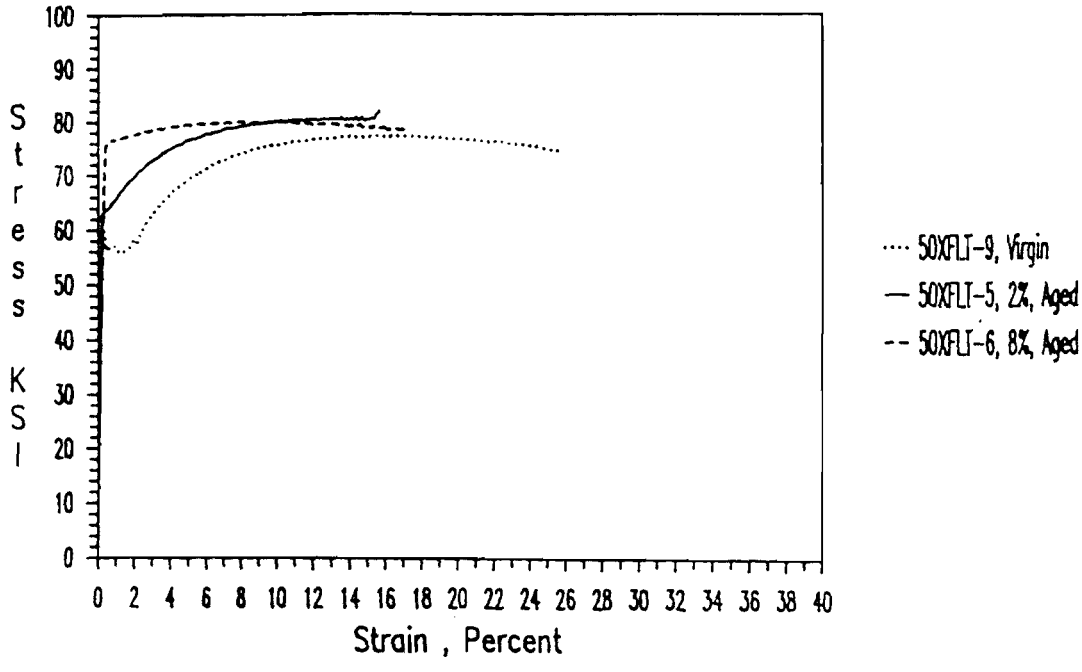

Figure 3.12 Stress-Strain Curves for 50XF-LT Steel at Strain Rate of 1.0 in./in./sec.

Table 3.6

Tested Mechanical Properties of 100XF Sheet Steel
Virgin Material

Test No.	Strain Rate in./in./sec.	F_y (ksi)	F_u (ksi)	Elongation in 2-in. Gage Length (percent)
LT-1	0.0001	122.44	122.44	9.4
LT-2	0.0001	126.07	126.07	9.7
LT-3	0.01	123.98	123.98	10.3
LT-4	0.01	125.91	125.91	10.3
LT-5	0.01	127.52	127.52	9.8
LT-6	1.0	129.06	129.06	---
LT-7	1.0	128.75	128.75	---
TT-1	0.0001	138.20	138.20	4.9
TT-2	0.0001	137.34	137.34	4.9
TT-3	0.01	140.11	140.11	6.1
TT-4	0.01	139.05	139.05	4.4
TT-5	1.0	144.11	144.11	8.0
TT-6	1.0	143.03	143.03	5.1

Table 3.7

Tested Mechanical Properties of 50XF Sheet Steel
Virgin Material

Test No.	Strain Rate in./in./sec.	F_y (ksi)	F_u (ksi)	Elongation in 2-in. Gage Length (percent)
LT-1	0.0001	49.80	73.87	29.9
LT-2	0.0001	49.39	72.54	32.0
LT-3	0.0001	49.32	72.51	31.0
LT-4	0.01	51.89	75.44	27.2
LT-5	0.01	50.83	74.07	27.4
LT-6	0.01	52.09	75.11	26.4
LT-7	1.0	54.71	79.18	26.2
LT-8	1.0	54.99	79.64	25.4
LT-9	1.0	54.29	77.36	25.7
TT-1	0.0001	50.38	73.73	26.8
TT-2	0.0001	51.13	73.39	28.3
TT-3	0.0001	50.25	73.21	24.8
TT-4	0.01	54.22	75.26	25.9
TT-5	0.01	52.77	74.80	26.7
TT-6	0.01	52.64	74.16	27.0
TT-7	1.0	56.21	79.86	28.3
TT-8	1.0	54.31	79.85	27.9
TT-9	1.0	56.13	80.03	27.1

Table 3.8

Tested Mechanical Properties of 50XF Sheet Steel
2% Cold Stretched, Non-Aged Material

Test No.	Strain Rate in./in./sec.	F_y (ksi)	F_u (ksi)	Elongation in 2-in. Gage Length (percent)
LT-1	0.0001	56.37	72.62	26.5
LT-2	0.0001	56.44	73.41	27.5
LT-3	0.01	58.46	74.81	25.4
LT-4	0.01	58.88	74.20	25.7
LT-5	1.0	63.19	80.58	26.1
LT-6	1.0	62.16	80.06	27.9
TT-1	0.0001	59.29	74.90	23.1
TT-2	1.0	68.48	81.29	24.6

Table 3.9

Tested Mechanical Properties of 50XF Sheet Steel
8% Cold Stretched, Non-Aged Material

Test No.	Strain Rate in./in./sec.	F_y (ksi)	F_u (ksi)	Elongation in 2-in. Gage Length (percent)
LT-1	0.0001	71.22	73.73	24.6
LT-2	0.0001	71.86	73.99	23.8
LT-3	0.01	73.87	76.21	21.6
LT-4	0.01	75.06	76.81	20.3
LT-5	1.0	77.00	80.77	21.6
LT-6	1.0	78.18	81.55	19.8
TT-1	0.0001	72.59	74.90	20.0
TT-2	0.0001	74.71	76.86	23.6
TT-3	1.0	77.90	82.07	19.4
TT-4	1.0	77.78	81.94	17.5

Table 3.10

Tested Mechanical Properties of 50XF Sheet Steel
2% Cold Stretched, Aged Material

Test No.	Strain Rate in./in./sec.	F_y (ksi)	F_u (ksi)	Elongation in 2-in. Gage Length (percent)
LT-1	0.0001	58.78	74.84	30.3
LT-2	0.0001	59.68	75.31	27.7
LT-3	0.01	60.49	76.05	26.4
LT-4	0.01	60.55	76.27	26.7
LT-5	1.0	63.45	81.39	----
LT-6	1.0	62.97	81.16	28.8
TT-1	0.0001	60.33	74.96	26.5
TT-2	0.0001	60.20	75.13	28.9
TT-3	1.0	65.43	83.62	22.1
TT-4	1.0	64.15	82.57	22.1

Table 3.11

Tested Mechanical Properties of 50XF Sheet Steel
8% Cold Stretched, Aged Material

Test No.	Strain Rate in./in./sec.	F_y (ksi)	F_u (ksi)	Elongation in 2-in. Gage Length (percent)
LT-1	0.0001	73.33	74.41	20.1
LT-2	0.0001	72.94	73.21	20.0
LT-3	0.01	72.51	74.49	22.4
LT-4	0.01	73.80	75.92	20.5
LT-5	1.0	75.60	77.19	----
LT-6	1.0	75.93	80.69	----
TT-1	0.0001	75.06	75.41	17.1
TT-2	0.0001	73.54	74.49	21.5
TT-3	1.0	78.11	81.82	19.1
TT-4	1.0	77.26	81.47	16.4

Table 3.12

Tested Mechanical Properties of 35XF Sheet Steel
Virgin Material

Test No.	Strain Rate in./in./sec.	F_y (ksi)	F_u (ksi)	Elongation in 2-in. Gage Length (percent)
LT-1	0.0001	32.42	49.22	39.7
LT-2	0.0001	32.57	49.19	40.2
LT-3	0.0001	33.63	49.64	36.7
LT-4	0.01	36.42	51.68	38.1
LT-5	0.01	36.65	52.02	36.0
LT-6	0.01	36.12	51.59	36.5
LT-7	1.0	42.53	56.82	41.6
LT-8	1.0	41.87	56.48	40.2
LT-9	1.0	42.70	56.60	40.9
TT-1	0.0001	33.53	49.41	34.9
TT-2	0.0001	33.49	49.19	37.5
TT-3	0.01	36.21	50.98	39.0
TT-4	0.01	36.57	51.10	35.3
TT-5	1.0	43.00	55.70	36.9
TT-6	1.0	43.47	56.15	34.1

Table 3.13

Tested Mechanical Properties of 35XF Sheet Steel
2% Cold Stretched, Non-Aged Material

Test No.	Strain Rate in./in./sec.	F_y (ksi)	F_u (ksi)	Elongation in 2-in. Gage Length (percent)
LT-1	0.0001	39.20	49.08	36.2
LT-2	0.0001	39.89	49.86	39.3
LT-3	0.01	42.62	52.11	31.4
LT-4	0.01	42.29	52.44	33.5
LT-5	1.0	47.44	57.05	39.8
LT-6	1.0	47.20	57.05	38.7
TT-1	0.0001	38.06	47.73	32.7
TT-2	0.0001	38.14	48.18	34.5
TT-3	1.0	46.36	55.81	32.1
TT-4	1.0	46.45	56.04	37.5

Table 3.14

Tested Mechanical Properties of 35XF Sheet Steel
8% Cold Stretched, Non-Aged Material

Test No.	Strain Rate in./in./sec.	F_y (ksi)	F_u (ksi)	Elongation in 2-in. Gage Length (percent)
LT-1	0.0001	46.05	49.41	29.9
LT-2	0.0001	46.57	49.08	29.7
LT-3	0.01	48.54	52.00	30.0
LT-4	0.01	49.75	52.67	29.5
LT-5	1.0	53.23	57.72	31.5
LT-6	1.0	52.57	56.71	38.5
TT-1	0.0001	44.77	47.84	29.0
TT-2	0.0001	46.14	47.73	22.1
TT-3	1.0	52.35	56.26	28.5
TT-4	1.0	52.59	56.49	26.9

Table 3.15

Tested Mechanical Properties of 35XF Sheet Steel
2% Cold Stretched, Aged Material

Test No.	Strain Rate in./in./sec.	F_y (ksi)	F_u (ksi)	Elongation in 2-in. Gage Length (percent)
LT-1	0.0001	40.02	49.32	31.8
LT-2	0.0001	39.89	50.10	35.7
LT-3	0.01	41.80	51.77	37.3
LT-4	0.01	41.25	51.16	36.1
LT-5	1.0	47.52	56.91	35.9
LT-6	1.0	47.28	56.80	40.9
TT-1	0.0001	38.89	48.73	29.8
TT-2	0.0001	39.27	48.90	31.8
TT-3	1.0	45.02	55.78	34.3
TT-4	1.0	45.23	55.34	32.6

Table 3.16

Tested Mechanical Properties of 35XF Sheet Steel
8% Cold Stretched, Aged Material

Test No.	Strain Rate in./in./sec.	F_y (ksi)	F_u (ksi)	Elongation in 2-in. Gage Length (percent)
LT-1	0.0001	45.69	48.19	34.8
LT-2	0.0001	46.61	49.11	30.7
LT-3	0.01	48.85	51.74	30.6
LT-4	0.01	49.70	52.34	30.7
LT-5	1.0	53.82	57.52	32.0
LT-6	1.0	53.53	57.55	31.1
TT-1	0.0001	45.25	47.60	25.3
TT-2	0.0001	45.64	47.65	28.7
TT-3	1.0	50.83	55.48	28.5
TT-4	1.0	51.25	56.01	28.1

Table 3.17

Average Tested Mechanical Properties of 100XF Sheet Steel
Longitudinal Tension, Virgin Material

Strain Rate in./in./sec.	F_y (ksi)	F_u (ksi)	Elongation (percent)
0.0001	124.25	124.25	9.5
0.01	125.80	125.80	10.2
1.0	128.91	128.91	----

Table 3.18

Average Tested Mechanical Properties of 100XF Sheet Steel
Transverse Tension, Virgin Material

Strain Rate in./in./sec.	F_y (ksi)	F_u (ksi)	Elongation (percent)
0.0001	137.77	137.77	4.9
0.01	139.58	139.58	5.3
1.0	143.57	143.57	6.6

Table 3.19

Average Tested Mechanical Properties of 50XF Sheet Steel
Longitudinal Tension

Amount of Cold Stretching	Strain Rate in./in./sec.	F_y (ksi)	F_u (ksi)	Elongation (percent)
Virgin	0.0001	49.50	72.97	31.0
Virgin	0.01	51.60	74.87	27.0
Virgin	1.0	54.66	78.73	25.8
2%, Non-Aged	0.0001	56.40	73.01	27.0
2%, Non-Aged	0.01	58.67	74.50	25.5
2%, Non-Aged	1.0	62.67	80.32	27.0
8%, Non-Aged	0.0001	71.54	73.86	24.2
8%, Non-Aged	0.01	74.47	76.51	20.9
8%, Non-Aged	1.0	77.59	81.16	20.7
2%, Aged	0.0001	59.23	75.07	29.0
2%, Aged	0.01	60.52	76.16	26.5
2%, Aged	1.0	63.21	81.27	28.8
8%, Aged	0.0001	73.13	73.81	20.0
8%, Aged	0.01	73.15	75.20	21.5
8%, Aged	1.0	75.77	78.94	-----

Table 3.20

Average Tested Mechanical Properties of 50XF Sheet Steel
Transverse Tension

Amount of Cold Stretching	Strain Rate in./in./sec.	F_y (ksi)	F_u (ksi)	Elongation (percent)
Virgin	0.0001	50.59	73.44	26.7
Virgin	0.01	53.21	74.74	26.5
Virgin	1.0	55.55	79.91	27.8
2%, Non-Aged	0.0001	59.29	74.90	23.1
2%, Non-Aged	1.0	68.48	81.29	24.6
8%, Non-Aged	0.0001	73.65	75.88	21.8
8%, Non-Aged	1.0	77.84	82.00	18.5
2%, Aged	0.0001	60.27	75.05	27.7
2%, Aged	1.0	64.79	83.09	22.1
8%, Aged	0.0001	74.30	74.95	19.3
8%, Aged	1.0	77.69	81.65	17.7

Table 3.21

Average Tested Mechanical Properties of 35XF Sheet Steel
Longitudinal Tension

Amount of Cold Stretching	Strain Rate in./in./sec.	F_y (ksi)	F_u (ksi)	Elongation (percent)
Virgin	0.0001	32.87	49.35	38.9
Virgin	0.01	36.40	51.76	36.8
Virgin	1.0	42.37	56.63	40.9
2%, Non-Aged	0.0001	39.55	49.47	37.7
2%, Non-Aged	0.01	42.45	52.27	32.5
2%, Non-Aged	1.0	47.32	57.05	39.3
8%, Non-Aged	0.0001	46.31	49.25	29.7
8%, Non-Aged	0.01	49.15	52.33	29.8
8%, Non-Aged	1.0	52.90	57.21	35.0
2%, Aged	0.0001	39.95	49.71	33.8
2%, Aged	0.01	41.53	51.47	36.7
2%, Aged	1.0	47.40	56.85	38.4
8%, Aged	0.0001	46.15	48.65	32.7
8%, Aged	0.01	49.27	52.04	30.7
8%, Aged	1.0	53.67	57.53	31.5

Table 3.22

Average Tested Mechanical Properties of 35XF Sheet Steel
Transverse Tension

Amount of Cold Stretching	Strain Rate in./in./sec.	F_y (ksi)	F_u (ksi)	Elongation (percent)
Virgin	0.0001	33.51	49.30	36.2
Virgin	0.01	36.39	51.04	37.1
Virgin	1.0	43.23	55.93	35.5
2%, Non-Aged	0.0001	38.10	47.95	33.6
2%, Non-Aged	1.0	46.41	55.93	34.8
8%, Non-Aged	0.0001	45.45	47.79	25.6
8%, Non-Aged	1.0	52.47	56.37	27.7
2%, Aged	0.0001	39.08	48.81	30.8
2%, Aged	1.0	45.13	55.56	33.5
8%, Aged	0.0001	45.45	47.63	27.0
8%, Aged	1.0	51.04	55.75	28.3

Table 3.23

ASTM Specifications for Compression Tests

E9-70	Standard Method of Compression Testing of Metallic Materials at Room Temperature
E83-67	Standard Method of Verification and Classification of Extensometers
E111-82	Standard Test Method for Young's Modulus, Tangent Modulus and Chord Modulus

* Yield strength. The method commonly used to determine the yield strength of sheet steels depends on whether the stress-strain curve is the gradual-yielding or sharp-yielding type. For the types of sheet steels tested in this phase of study, the stress-strain curves of 50XF and 100XF sheet steels are the sharp-yielding type, while the stress-strain curves of 35XF sheet steel are the gradual-yielding type. Because the 50XF sheet steel exhibited a considerable amount of strain hardening, the stress-strain curves became the gradual-yielding type after the material was cold-stretched to a selected strain of either 2% or 8%.

The yield strength of sharp-yielding sheet steel was determined by the lower yield point, for which the stress-strain curve becomes horizontal. For the stress-strain curves of gradual-yielding type, the yield strength was determined by the intersection of the stress-strain curve and the straight line drawn parallel to the elastic portion of the stress-strain curve at an offset of 0.2 percent.

* Ultimate tensile strength. The ultimate tensile strength was determined from each of the tension tests as the maximum stress that the given tension coupon could withstand before fracture.

* Ductility. In this study, ductility was determined by the total elongation in a 2-in. gage length. For this method, the maximum strain recorded by the computer before fracture was taken as the ductility. The maximum elongation was also verified by placing the fractured ends of the specimen together and measuring the distance between the gage marks.

2. Compression Tests. The materials used for the tension tests, were also unaxially tested in compression in the longitudinal and transverse directions under three different strain rates of 10^{-4}, 10^{-2}, and 1.0 in./in./sec.. All compression tests followed the procedures outlined in the ASTM Specifications listed in Table 3.23.

a. Specimens. All test specimens were cut from the steel sheet and prepared in the Machine Shop of the Department of Civil Engineering at the University of Missouri-Rolla. Figure 3.13 shows the shape and dimensions of the specimen used for the compression test. The specimen dimensions were selected to fit a Montgomery-Templin compression test fixture as shown in Figure 3.14. The notches along one edge were for the installation of the knife edges of the compressometer. Special care was taken to ensure that the ends of the specimens were parallel and thus the same length was used for both longitudinal sides of the specimen. Eighteen (18) coupons cut from each of 100XF, 50XF, and 35XF sheet steels were tested in this phase of study. These specimens are summarized in Table 3.24.

b. Intrumentation. All compression tests were performed in the same MTS 880 machine as discussed for the tension tests. Two compression platens were installed for conducting the compression tests.

Figure 3.14 shows the assembly of the test specimen and the test fixture. The load was applied to the compression coupon by means of a specially made subpress as shown in Figure 3.15. The subpress base and ram are constructed of a hardened steel in order to minimize their deformation when applying the load. The compression specimen was placed

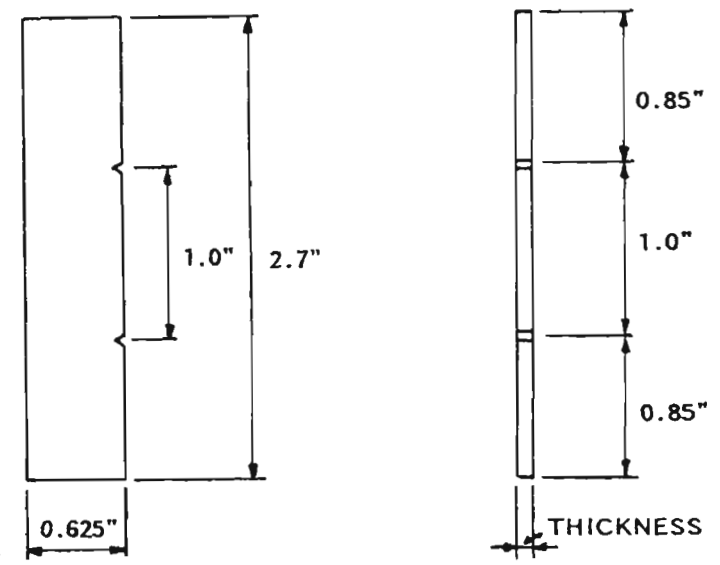

Figure 3.13 Nominal Dimensions of Compression Coupons Used for All Sheet Steels

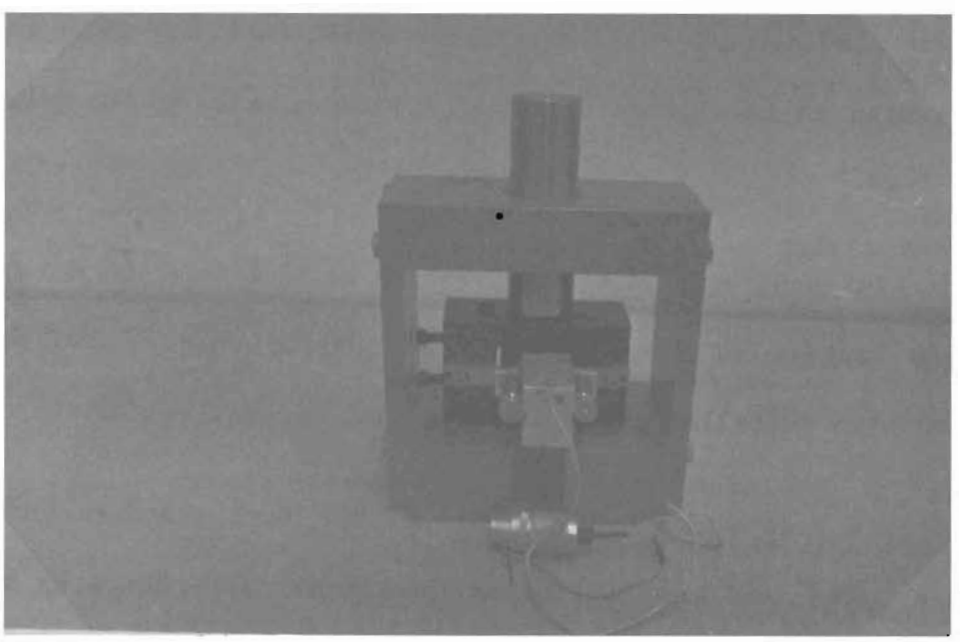

Figure 3.14 Assembly of Compression Subpress, Jig, and Compressometer

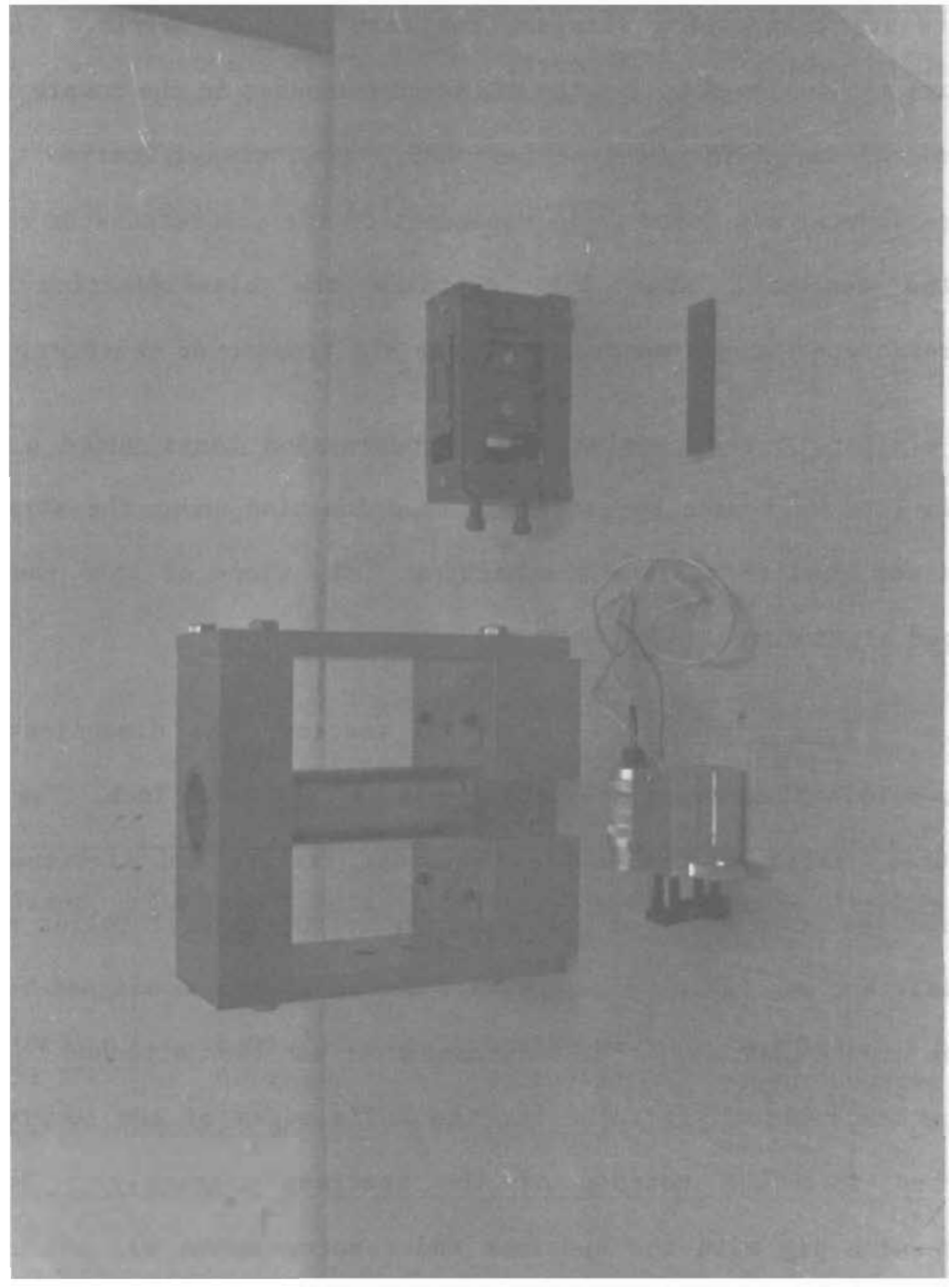

Figure 3.15 (A) Compression Subpress, (B) Compression Jig, (C) Compressometer, and (D) Specimen Used for Compression Tests

in a Montgomery-Templin compression test fixture, which contains a series of rollers to prevent buckling as can be seen from Figure 3.14.

An MTS compressometer (Figure 3.15) with a 1-in. gage length was used to measure compression strains from zero to 0.02 in./in.. A special fixture was designed to fit the MTS compressometer in the compression jig. According to ASTM Designation E83, the classification of this compressometer was found to be dependent on the compressometer range used in the tests. Table 3.25 contains the classification of four compressometer ranges according to the MTS transducer calibration data.

Similar to the tension tests, compression tests under a constant strain rate were made by setting a ramp function under the strain mode, which was used to operate the machine. The slope of this ramp is the desired strain rate.

c. Test Procedure. Prior to testing, the dimensions of the compression coupons were measured to the nearest 0.001 inch. The specimen was then placed in the compression test fixture and tightened firmly against the both sides of the specimen by the lateral roller supports. Special care was taken to ensure that the specimen was aligned vertically in the compression jig. The compressometer was then attached to one side of the compression jig such that the knife edges of the compressometer inserted into the notches of the specimen correctly. Next, the compression jig with the specimen and compressometer was placed in the compression subpress. A small stub is provided on each side of the bottom surface of compression jig. These stubs fit into indentations on the base of the subpress in order to ensure proper alignment of the subpress ram with the longtidinal axis of specimen. Next step was to place the entire

Table 3.24

Number of Performed Compressive Coupon Tests

Direction of Testing	Type of Material	Number of Coupons Used
Longitudinal Compression (LC)	100XF-LC	9
	50XF-LC	9
	35XF-LC	9
Transverse Compression (TC)	100XF-TC	9
	50XF-TC	9
	35XF-TC	9

Table 3.25

Classification of the MTS Compressometer

Range	Maximum Strain in./in.	Maximum Error in./in.	ASTM Classification
100%	0.20	0.000100	Class B-1
50 %	0.10	0.000050	Between Classes A and B-1
20 %	0.04	0.000012	Between Classes A and B-1
10 %	0.02	0.000008	Class A

test unit between two compression platens in the loading frame such that the longitudinal axis of the subpress lined up with the center of the platens.

For all the compression tests, the strain mode was selected to maintain a constant strain rate. Range 4 was chosen for the load, strain, and stroke modes in the MTS control console. The function generator was programmed to produce the desired ramp. The test data was recorded in the Data General Mini Computer for later plotting and analysis.

d. Test Results. As pointed out in preceding section, a constant strain rate was conducted for each compression test by using the MTS 880 Test System without any difficulty. The stress-strain curves and mechanical properties of three types of sheet steel were obtained from compression tests as discussed below:

i) Stress-strain relationships. Figures 3.16 through 3.18 present the typical stress-strain curves for the three different sheet steels tested in the longitudinal direction. Each figure includes three stress-strain curves representing the test data obtained from the same sheet steel but using different strain rates (10^{-4}, 10^{-2}, and 1.0 in./in./sec.). Reference 14 contains the typical compressive stress-strain curves for the same materials tested in the transverse direction.

ii) Mechanical properties. The mechanical properties determined from compression tests included proportional limit (F_{pr}), and yield strength (F_y). The material properties derived from each individual test are presented in Tables 3.26 through 3.31. Tables 3.32 through 3.37

present the average values of the mechanical properties for each material tested in either longitudinal compression (LC) or transverse compression (TC) under different strain rates. The procedures used for determining the mechanical properties of sheet steels are discussed in the subsequent paragraphs.

* Proportional limit. The proportional limit is usually defined as the point above which the stress-strain curve becomes nonlinear. Because it is often difficult to determine the exact location of the true proportional limit in the stress-strain diagram, the proportional limit can be determined by the 0.01 percent offset method for sheet steel.

As illustrated in Figure 3.19, the proportional limit of 35XF sheet steel tested in the transverse compression under the strain rate of 10^{-4} in./in./sec. was obtained by using the 0.01 percent offset method. Because of the waving effect of the impact load on the stress-strain curves of the tests conducted at the strain rate of 1.0 in./in./sec., reliable values for the proportional limit were difficult to obtain.

* Yield strength. The yield strength of sharp-yielding sheet steel was determined by the stress where the stress-strain curve becomes horizontal. Therefore, the lower yield point of stress-strain diagram was used to determine the yield strengths listed in the tables for 50XF and 100XF sheet steels. For the gradual-yielding type stress-strain curves (35XF sheet steel), the yield strength was determined by the intersection of the stress-strain curve and the straight line drawn parallel to the elastic portion of the stress-strain curve at an offset of 0.2 percent.

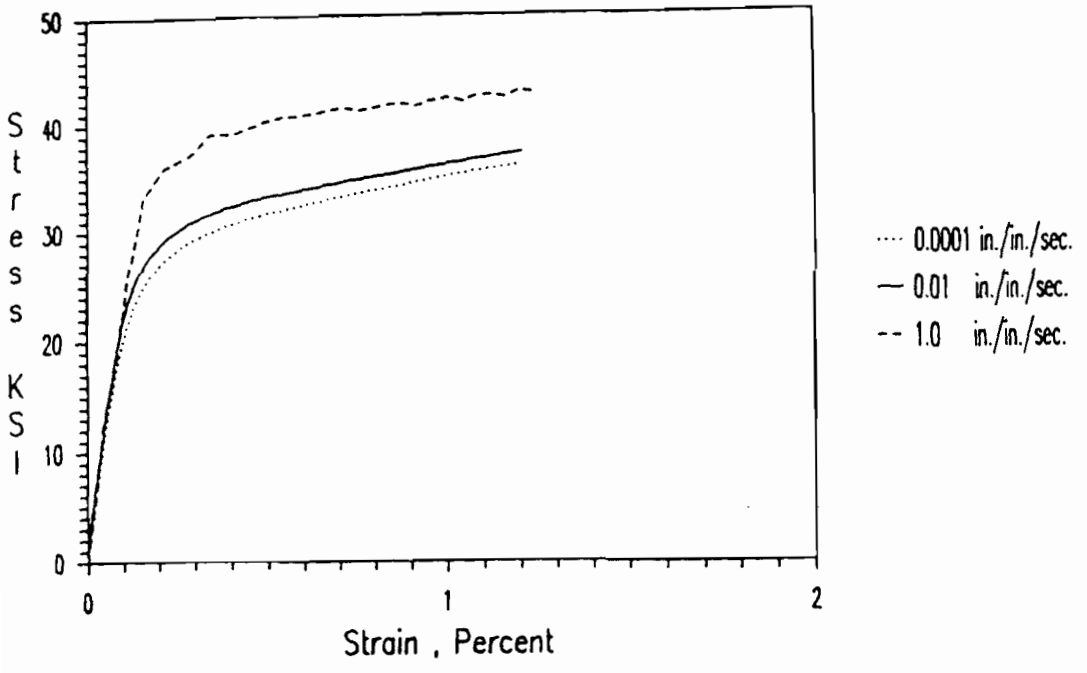

Figure 3.16 Stress-Strain Curves for 35XF-LC Steel under Different Strain Rate

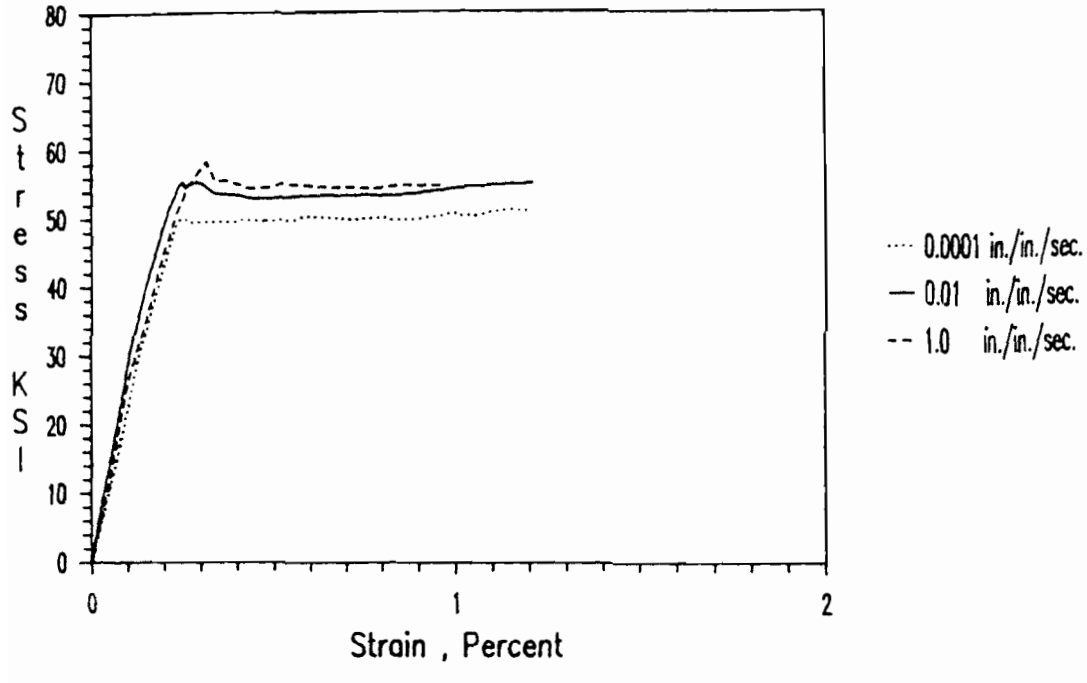

Figure 3.17 Stress-Strain Curves for 50XF-LC Steel under Different Strain Rate

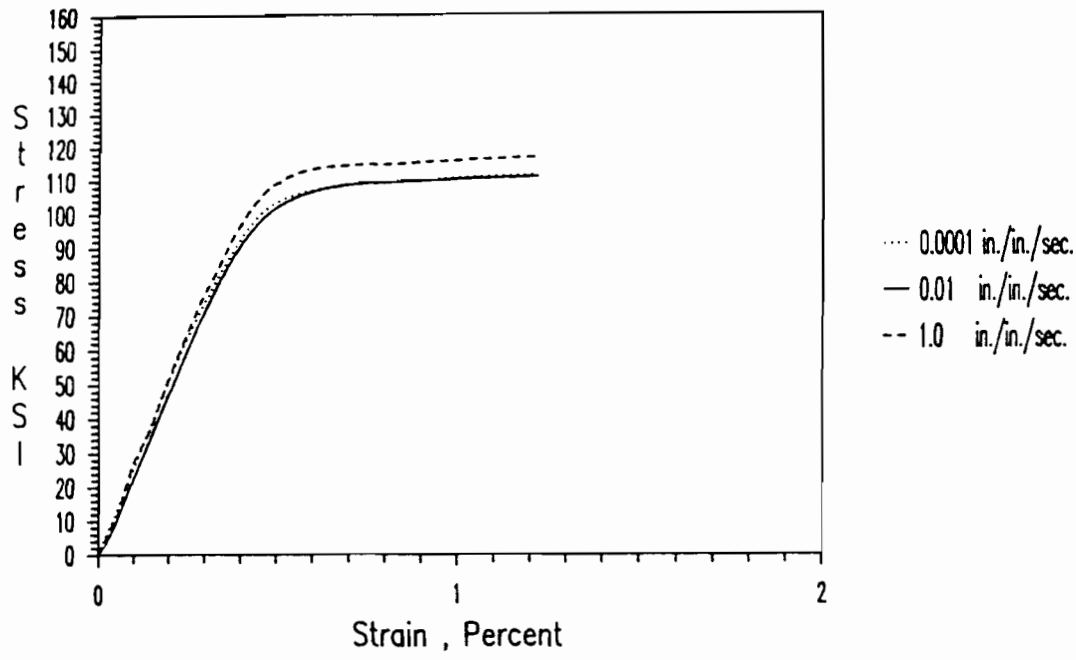

Figure 3.18 Stress-Strain Curves for 100XF-LC Steel under Different Strain Rate

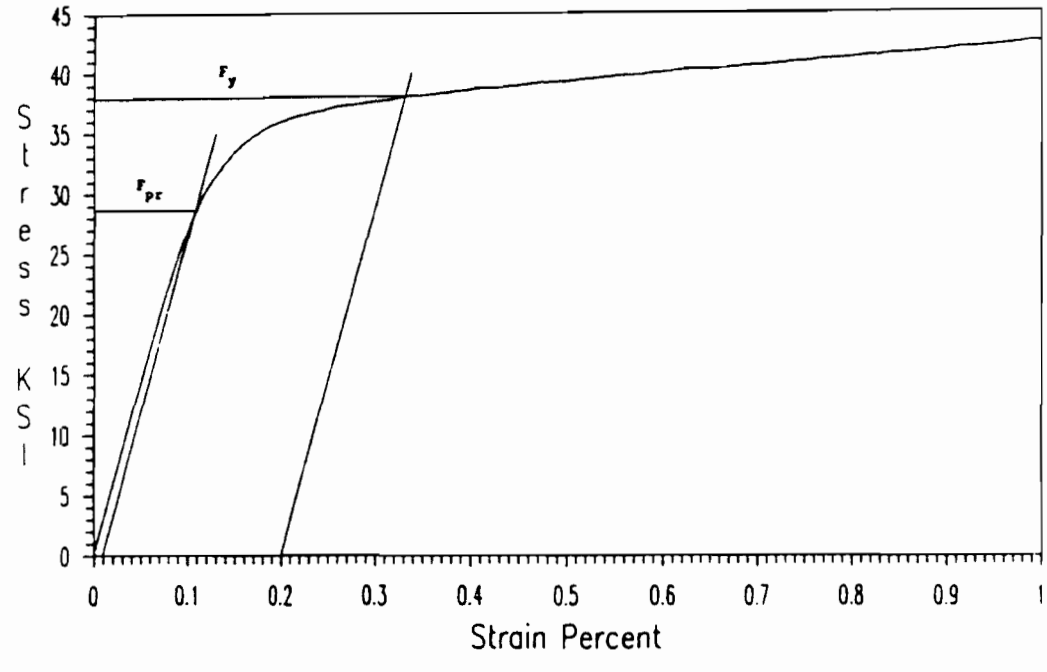

Figure 3.19 Stress-Strain Curve for Determination of Mechanical Properties of 35XF-TC-4

Table 3.26

Tested Mechanical Properties of 100XF Sheet Steel
Longitudinal Compression

Test No.	Strain Rate in./in./sec.	F_{pr} (ksi)	F_y (ksi)	F_{pr}/F_y
LC-1	0.0001	72.87	107.28	0.68
LC-2	0.0001	71.17	108.23	0.66
LC-3	0.0001	69.71	106.37	0.65
LC-4	0.01	87.90	110.51	0.79
LC-5	0.01	88.98	112.18	0.79
LC-6	0.01	*****	111.08	****
LC-7	1.0	*****	115.16	****
LC-8	1.0	*****	116.61	****
LC-9	1.0	*****	112.97	****

Table 3.27

Tested Mechanical Properties of 100XF Sheet Steel
Transverse Compression

Test No.	Strain Rate in./in./sec.	F_{pr} (ksi)	F_y (ksi)	F_{pr}/F_y
TC-1	0.0001	103.82	123.66	0.84
TC-2	0.0001	102.53	120.41	0.85
TC-3	0.0001	104.63	126.91	0.82
TC-4	0.01	113.27	126.42	0.90
TC-5	0.01	113.18	125.14	0.90
TC-6	0.01	113.91	126.91	0.90
TC-7	1.0	******	129.98	****
TC-8	1.0	******	132.62	****
TC-9	1.0	******	132.59	****

Table 3.28

Tested Mechanical Properties of 50XF Sheet Steel
Longitudinal Compression

Test No.	Strain Rate in., in./sec.	F_{pr} (ksi)	F_y (ksi)	F_{pr}/F_y
LC-1	0.0001	37.63	49.95	0.75
LC-2	0.0001	39.05	49.70	0.79
LC-3	0.0001	39.24	49.40	0.79
LC-4	0.01	42.92	52.82	0.81
LC-5	0.01	41.25	52.82	0.78
LC-6	0.01	35.99	51.90	0.69
LC-7	1.0	*****	54.88	****
LC-8	1.0	*****	54.50	****
LC-9	1.0	*****	54.99	****

Table 3.29

Tested Mechanical Properties of 50XF Sheet Steel
Transverse Compression

Test No.	Strain Rate in./in./sec.	F_{pr} (ksi)	F_y (ksi)	F_{pr}/F_y
TC-1	0.0001	38.69	51.07	0.76
TC-2	0.0001	42.65	51.04	0.84
TC-3	0.0001	43.19	51.13	0.84
TC-4	0.01	50.00	53.46	0.93
TC-5	0.01	50.47	53.38	0.94
TC-6	0.01	51.47	53.36	0.96
TC-7	1.0	*****	55.52	****
TC-8	1.0	*****	55.88	****
TC-9	1.0	*****	55.22	****

Table 3.30

Tested Mechanical Properties of 35XF Sheet Steel
Longitudinal Compression

Test No.	Strain Rate in./in./sec.	F_{pr} (ksi)	F_y (ksi)	F_{pr}/F_y
LC-1	0.0001	17.76	29.95	0.59
LC-2	0.0001	17.98	29.79	0.60
LC-3	0.0001	17.63	29.74	0.59
LC-4	0.01	23.15	32.50	0.71
LC-5	0.01	17.94	31.52	0.57
LC-6	0.01	19.00	31.73	0.60
LC-7	1.0	*****	36.69	****
LC-8	1.0	*****	36.27	****
LC-9	1.0	*****	37.76	****

Table 3.31

Tested Mechanical Properties of 35XF Sheet Steel
Transverse Compression

Test No.	Strain Rate in./in./sec.	F_{pr} (ksi)	F_y (ksi)	F_{pr}/F_y
TC-1	0.0001	23.48	32.76	0.72
TC-2	0.0001	22.45	32.44	0.69
TC-3	0.0001	23.42	32.67	0.72
TC-4	0.01	28.60	37.95	0.75
TC-5	0.01	30.34	36.71	0.83
TC-6	0.01	27.26	35.40	0.77
TC-7	1.0	*****	43.17	****
TC-8	1.0	*****	41.00	****
TC-9	1.0	*****	46.17	****

Table 3.32

Average Tested Mechanical Properties of 100XF Sheet Steel
Longitudinal Compression

Strain Rate in./in./sec.	F_{pr} (ksi)	F_y (ksi)	F_{pr}/F_y
0.0001	71.25	107.29	0.66
0.01	88.44	111.26	0.79
1.0	*****	114.91	****

Table 3.33

Average Tested Mechanical Properties of 100XF Sheet Steel
Transverse Compression

Strain Rate in./in./sec.	F_{pr} (ksi)	F_y (ksi)	F_{pr}/F_y
0.0001	103.66	123.66	0.84
0.01	113.45	126.16	0.90
1.0	*****	131.73	****

Table 3.34

Average Tested Mechanical Properties of 50XF Sheet Steel
Longitudinal Compression

Strain Rate in./in./sec.	F_{pr} (ksi)	F_y (ksi)	F_{pr}/F_y
0.0001	38.64	49.68	0.78
0.01	40.05	52.51	0.76
1.0	*****	54.79	****

Table 3.35

Average Tested Mechanical Properties of 50XF Sheet Steel
Transverse Compression

Strain Rate in./in./sec.	F_{pr} (ksi)	F_y (ksi)	F_{pr}/F_y
0.0001	41.51	51.08	0.81
0.01	50.65	53.40	0.95
1.0	*****	55.54	****

Table 3.36

Average Tested Mechanical Properties of 35XF Sheet Steel
Longitudinal Compression

Strain Rate in./in./sec.	F_{pr} (ksi)	F_y (ksi)	F_{pr}/F_y
0.0001	17.79	29.83	0.60
0.01	20.03	31.92	0.63
1.0	*****	36.91	****

Table 3.37

Average Tested Mechanical Properties of 35XF Sheet Steel
Transverse Compression

Strain Rate in./in./sec.	F_{pr} (ksi)	F_y (ksi)	F_{pr}/F_y
0.0001	23.12	32.62	0.71
0.01	28.73	36.69	0.78
1.0	*****	43.45	****

C. STUB COLUMN SPECIMENS

As pointed out in Section I, the current design criteria used in the AISI Automotive Steel Design Manual[1] for the effective design width are based on the test results under static loading condition. The primary objective of this investigation was to study the validity of these effective design width formulas for the design of members subjected to dynamic loads.

All stub column tests were performed in the MTS 880 Test System located in the Engineering Research Laboratory at the University of Missouri-Rolla. The materials used in this phase of study were 35XF and 50XF sheet steels with nominal yield strengths of 35 ksi and 50 ksi, respectively. Since May 1989, a total of 24 box-shaped stub columns were fabricated from 35XF sheet steel and 22 box-shaped stub columns were fabricated from 50XF sheet steel. These specimens were tested to study the strength of stiffened elements. For the strength of unstiffened elements, 25 I-shaped stub columns were fabricated from 35XF sheet steel and 26 I-shaped stub columns were fabricated from 50XF sheet steel. These specimens were cold-formed to shape by Butler Manufacturing Company in Grandview, Missouri and Holloway Machine Company in Springfield, Missouri. The configurations of stub column specimens having stiffened and unstiffened elements are shown in Figures 3.20 and 3.21, respectively. The designation of test specimens is presented in Table 3.38. Two groups of test specimens were used for each sheet steel, i.e. 35XF or 50XF. Group I is for box-shaped stub columns and Group II is for I-shaped stub columns. In each group, four cases of w/t ratios were studied. Cases A, B, C, and D represent the small, medium, large, and extra large w/t

ratios, respectively. Tables 3.39 to 3.42 show the specimen number, test speed, strain rate, w/t ratio, and the slenderness ratio, L/r, of each individual test specimen. A total of 97 stub column specimens were tested and are discussed in this study.

1. Material Properties. The mechanical properties of 35XF and 50XF sheet steels were presented in the previous section. The average values of mechanical properties tested under different strain rates for 35XF and 50XF sheet steels include yield stress (F_y) in tension and compression, proportional limit (F_{pr}), tensile strength (F_u), and elongation in 2-in. gage length as given in Tables 3.43 and 3.44. The thicknesses of 35XF and 50XF sheet steels are 0.085 in. and 0.077 in., respectively.

From Figures 3.7 to 3.9 and 3.16 to 3.18, it can be seen that the effect of strain rate on material properties varies for each material. The empirical equations derived on the basis of the material test results are discussed in Section IV, which are used to predict longitudinal tensile and compressive yield stresses.

2. Stub Column Tests for Stiffened Elements

a. Specimens. Stub column tests were used to study the local and postbuckling strengths of compression elements. For the design of cold-formed steel members, the effective design width formula has been employed for the determination of the structural strength. The length of stub column specimens was designed long enough (more than 3 times the largest dimension of the cross section) to develop the buckling wave and short enough (less than 20 times the least radius of gyration) to prevent overall bucking of the entire member as recommended in Reference 96 and

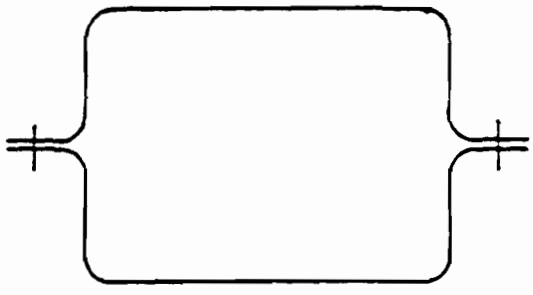

Figure 3.20 Configuration of Test Specimens for Members Having Stiffened Compression Flanges

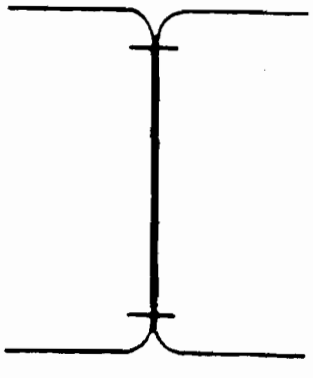

Figure 3.21 Configuration of Test Specimens for Members Having Unstiffened Compression Flanges

Table 3.38

Designation of Stub Column Specimens Used in This Study

1st Digit	1st Letter	2nd Digit	2nd Letter
Section Type (Group)	w/t Ratio (Case)	Strain-Rate (in./in./sec.)	Test No.
1- Box-Shaped Section	A- Small Ratio	0- 0.00001	A- 1st Test
Stub-Column Test	B- Medium Ratio	1- 0.0001	B- 2nd Test
2- I-Shaped Section	C- Large Ratio	2- 0.01	
Stub-Column Test	D- Extra Large Ratio	3- 0.1	

Note: The fifth character (X) in the designation of test specimens represents the specimen fabricated from 50XF sheet steel.

Table 3.39

Number of Performed Stub Column Tests
Box Sections Having Stiffened Compression Elements
(35XF Sheet Steel)

Spec. No.	Test Speed in./min.	Strain Rate (in./in./sec.)	w/t	L/r	No. of Tests Performed
1A1A	0.072	0.0001	27.15	12.26	1
1A1B	0.072	0.0001	27.39	12.26	1
1A2A	7.2	0.01	26.92	12.26	1
1A2B	7.2	0.01	27.06	12.26	1
1A3A	72.0	0.1	27.31	12.26	1
1A3B	72.0	0.1	27.40	12.26	1
1B1A	0.084	0.0001	38.93	10.98	1
1B1B	0.084	0.0001	38.17	10.98	1
1B2A	8.4	0.01	38.86	10.98	1
1B2B	8.4	0.01	39.10	10.98	1
1B3A	84.0	0.1	38.86	10.98	1
1B3B	84.0	0.1	38.96	10.98	1
1C1A	0.09	0.0001	52.69	11.27	1
1C1B	0.09	0.0001	52.96	11.27	1
1C2A	9.0	0.01	52.20	11.27	1
1C2B	9.0	0.01	53.06	11.27	1
1C3A	90.0	0.1	53.15	11.27	1
1C3B	90.0	0.1	53.39	11.27	1
1D1A	0.18	0.0001	100.68	12.52	1
1D1B	0.18	0.0001	100.35	12.46	1
1D2A	18.0	0.01	100.49	12.52	1
1D2B	18.0	0.01	100.62	12.54	1
1D3A	89.9	0.05	100.85	12.56	1
1D3B	89.7	0.05	100.72	12.49	1
Total					24

Table 3.40

Number of Performed Stub Column Tests
Box Sections Having Stiffened Compression Elements
(50XF Sheet Steel)

Spec. No.	Test Speed in./min.	Strain Rate (in./in./sec.)	w/t	L/r	No. of Tests Performed
1A1AX	0.0896	0.0001	23.89	13.21	1
1A1BX	0.0899	0.0001	23.15	13.17	1
1A2AX	9.00	0.01	23.15	13.18	1
1A2BX	8.97	0.01	22.94	13.20	1
1A3AX	44.9	0.05	23.10	13.15	1
1A3BX	44.9	0.05	22.92	13.15	1
1B1AX	0.0899	0.0001	35.15	11.00	1
1B1BX	0.0898	0.0001	34.59	10.98	1
1B2AX	8.94	0.01	34.50	10.96	1
1B2BX	9.01	0.01	34.96	10.99	1
1B3AX	36.0	0.04	34.97	10.95	1
1B3BX	35.9	0.04	34.79	10.97	1
1C1AX	0.0896	0.0001	52.76	10.29	1
1C1BX	0.0896	0.0001	53.40	10.31	1
1C2AX	8.96	0.01	53.06	10.33	1
1C2BX	8.96	0.01	52.23	10.28	1
1C3AX	35.9	0.04	51.67	10.32	1
1C3BX	35.9	0.04	52.90	10.26	1
1D1AX	0.156	0.0001	97.99	12.12	1
1D2AX	15.5	0.01	98.21	12.10	1
1D3AX	46.7	0.03	98.01	12.10	1
1D3BX	46.7	0.03	98.07	12.08	1
Total					22

Table 3.41

Number of Performed Stub Column Tests
I-sections Having Unstiffened Compression Elements
(35XF Sheet Steel)

Spec. No.	Test Speed in./min.	Strain Rate (in./in./sec.)	w/t	L/r	No. of Tests Performed
2A1A	0.054	0.0001	8.93	18.73	1
2A1B	0.054	0.0001	9.04	18.73	1
2A2A	5.4	0.01	8.93	18.73	1
2A2B	5.4	0.01	9.10	18.73	1
2A3A	54.0	0.1	8.93	18.73	1
2A3B	54.0	0.1	8.96	18.73	1
2B1A	0.06	0.0001	13.34	17.65	1
2B1B	0.06	0.0001	13.41	17.65	1
2B2A	6.0	0.01	13.40	17.65	1
2B2B	6.0	0.01	13.37	17.65	1
2B3A	60.0	0.1	13.34	17.65	1
2B3B	60.0	0.1	13.42	17.65	1
2C0A	0.0084	0.00001	20.69	15.64	1
2C1A	0.084	0.0001	20.85	15.64	1
2C1B	0.084	0.0001	20.76	15.64	1
2C2A	8.4	0.01	20.97	15.64	1
2C2B	8.4	0.01	20.81	15.64	1
2C3A	84.0	0.1	20.93	15.64	1
2C3B	84.0	0.1	20.87	15.64	1
2D1A	0.144	0.0001	44.60	16.57	1
2D1B	0.144	0.0001	44.50	16.55	1
2D2A	14.4	0.01	44.62	16.69	1
2D2B	14.4	0.01	44.59	16.64	1
2D3A	71.7	0.05	44.51	16.85	1
2D3B	71.8	0.05	44.60	16.58	1
Total					25

Table 3.42

Number of Performed Stub Column Tests
I-sections Having Unstiffened Compression Elements
(50XF Sheet Steel)

Spec. No.	Test Speed in./min.	Strain Rate (in./in./sec.)	w/t	L/r	No. of Tests Performed
2A1AX	0.0418	0.0001	8.41	19.01	1
2A1BX	0.0419	0.0001	8.38	19.12	1
2A2AX	4.19	0.01	8.40	19.08	1
2A2BX	4.18	0.01	8.38	19.08	1
2A3AX	33.6	0.08	8.29	19.39	1
2A3BX	33.4	0.08	8.36	19.16	1
2B1AX	0.0539	0.0001	11.68	20.20	1
2B1BX	0.0536	0.0001	11.60	20.29	1
2B1CX	0.0054	0.00001	11.63	20.37	1
2B2AX	5.38	0.01	11.58	20.43	1
2B2BX	5.40	0.01	11.54	20.61	1
2B2CX	0.54	0.001	11.53	20.51	1
2B3AX	43.2	0.08	11.65	20.34	1
2B3BX	43.1	0.08	11.50	20.53	1
2C1AX	0.0896	0.0001	22.84	16.85	1
2C1BX	0.0898	0.0001	22.73	16.99	1
2C2AX	8.96	0.01	22.77	16.91	1
2C2BX	8.97	0.01	22.76	16.94	1
2C3AX	44.9	0.05	22.72	16.97	1
2C3BX	44.8	0.05	22.79	16.90	1
2D1AX	0.108	0.0001	35.37	15.31	1
2D1BX	0.108	0.0001	35.33	15.32	1
2D2AX	10.8	0.01	35.26	15.30	1
2D2BX	11.8	0.01	35.21	15.29	1
2D3AX	43.1	0.04	35.29	15.32	1
2D3BX	43.1	0.04	35.15	15.28	1
Total					26

Table 3.43

Average Mechanical Properties of 35XF Sheet Steel Used in the Experimental Study Under Different Strain Rates

Strain Rate in./in./sec.	$(F_y)_c$ (ksi)	$(F_{pr})_c$ (ksi)	$(F_y)_t$ (ksi)	$(F_u)_t$ (ksi)	Elongation (%)
0.0001	29.83	17.79	32.87	49.35	38.90
0.01	31.92	20.03	36.40	51.76	36.80
1.0	36.91	*****	42.37	56.63	40.90

Table 3.44

Average Mechanical Properties of 50XF Sheet Steel Used in the Experimental Study Under Different Strain Rates

Strain Rate in./in./sec.	$(F_y)_c$ (ksi)	$(F_{pr})_c$ (ksi)	$(F_y)_t$ (ksi)	$(F_u)_t$ (ksi)	Elongation (%)
0.0001	49.68	38.64	49.50	72.97	31.00
0.01	52.51	40.05	51.60	74.87	27.00
1.0	54.79	*****	54.66	78.73	25.80

Notes:

1) $(F_y)_c$ and $(F_{pr})_c$ are based on longitudinal compression coupon tests.
2) $(F_y)_t$ and $(F_u)_t$ and Elongation are determined from longitudinal tension coupon tests.
3) Elongation was measured by using a 2-in. gage length.

Part VII of the 1986 AISI Cold-Formed Steel Design Specification[66]. In order to investigate the behavior and strength of stiffened compression elements, the webs and unstiffened flanges of all hat sections were designed to be fully effective. Tables 3.45 and 3.46 give the lengths and dimensions of stub column test specimens fabricated from 35XF and 50XF sheet steels, respectively.

Prior to April 1990, a total of 18 stub column specimens fabricated from 35XF sheet steel were tested and reported in the Thirteenth Progress Report. These specimens had stiffened elements with w/t ratios ranging from 26.92 to 53.39. Since May 1990, six additional stub column specimens were fabricated from 35XF sheet steel and tested to study the strength of stiffened elements with the w/t value of 100.62. In addition, a total of 22 stub column test specimens were fabricated from 50XF sheet steel and tested to study the local buckling and postbuckling strengths of stiffened elements with w/t ratios ranging from 22.89 to 98.21. Due to lack of 50XF sheet steel material, only four stub column specimens were fabricated and tested for box sections having stiffened flanges with a w/t ratio of approximately 98.0. In this study, strain rates for the tests ranged from 10^{-4} to 10^{-1} in./in./sec..

As shown in Figure 3.22, two hat sections were assembled by connecting two unstiffened flanges to form a box-shaped stub column. To avoid the failure of bolts, 1/4"-diameter, Grade 8 high strength bolts were used to fabricate the test specimens. The spacing between bolts was chosen to satisfy the requirements of the AISI Specification[66]. To ensure a better contact between the ends of test specimens and compression

platens of the test machine, all specimens were milled in the machine shop to make both ends of stub column flat and parallel.

b. Strain Measurements. There were several reasons for mounting strain gages on the test specimens: (1) to ensure the alignment of stub-column specimens, (2) to detect the local buckling load, (3) to determine the stress at the location of strain gage, and (4) to determine the strain rate used in the test. For specimens with small w/t ratios (cases A and B of Group I for using 35XF and 50XF sheet steels), eight foil strain gages were mounted at midheight of stub column specimens. For the stub columns with large w/t ratios (cases C and D of Group I for using 35XF and 50XF sheet steels), additional eight strain gages were mounted above and below the midheight of stub column at the location equal to one-half of the overall width of the stiffened elements. The arrangements of strain gages are shown in Figures 3.23 and 3.24.

All strain gages were used to check the alignment. The load-strain diagrams obtained from paired strain gages (No. 1-2, 5-6, and 9 through 16) were used to determine the local buckling load by means of the modified strain reversal method, which is discussed in Reference 97. For some specimens, additional paired strain gages were placed on the edges of stiffened elements of stub columns to measure the maximum edge strains.

c. Instrumentation and Test Procedure. All stub column tests were performed by using an 880 Material Test System with a capacity of 110 kips. For all tests, the maximum load range of 100 kips and the maximum stroke ranges of 1 or 0.5 inches were selected for the function generator of the test machine. The ramp time was programmed to have a constant speed, which was calculated by the product of the selected strain rate

Table 3.45

Dimensions of Stub Columns with Stiffened Flanges
Fabricated from 35XF Sheet Steel
(35XF Sheet Steel)

Specimen	BF (in.)	BW (in.)	BL (in.)	w/t	Gross Area ($in.^2$)	L (in.)	$(P_u)_{test}$ (kips)
1A1A	2.790	1.492	0.916	27.15	1.2060	12.03	46.12
1A1B	2.811	1.482	0.915	27.39	1.2060	12.02	44.89
1A2A	2.771	1.484	0.918	26.92	1.2010	12.03	50.02
1A2B	2.783	1.482	0.916	27.06	1.2060	12.03	49.29
1A3A	2.804	1.470	0.916	27.31	1.2009	12.03	53.54
1A3B	2.812	1.467	0.915	27.40	1.2009	12.03	54.37
1B1A	3.792	1.990	0.922	38.93	1.5477	14.99	49.19
1B1B	3.812	1.985	0.918	39.17	1.5480	13.97	53.54
1B2A	3.786	1.978	0.918	38.86	1.5412	13.84	56.28
1B2B	3.806	1.982	0.919	39.10	1.5463	13.94	57.01
1B3A	3.786	1.992	0.919	38.86	1.5463	13.84	64.78
1B3B	3.794	1.982	0.918	38.96	1.5440	13.94	60.87
1C1A	4.961	2.523	0.919	52.69	1.9266	15.06	56.76
1C1B	4.984	2.513	0.922	52.96	1.9282	15.06	56.52
1C2A	4.920	2.524	0.920	52.20	1.9203	14.81	61.02
1C2B	4.993	2.519	0.922	53.06	1.9317	15.12	64.58
1C3A	5.000	2.526	0.919	53.15	1.9343	15.09	73.96
1C3B	5.021	2.510	0.922	53.39	1.9334	15.00	69.27
1D1A	9.041	3.008	1.024	100.68	2.8207	29.91	63.85
1D1B	9.012	3.026	1.019	100.35	2.8203	29.92	63.90
1D2A	9.024	3.011	1.018	100.49	2.8169	29.93	70.35
1D2B	9.035	3.009	1.020	100.62	2.8188	29.94	69.22
1D3A	9.055	3.002	1.021	100.85	2.8202	29.95	74.06
1D3B	9.044	3.014	1.009	100.72	2.8183	29.91	72.45

Note : * For symbols BF, BW, and BL, see Figure 3.22.

* The nominal thickness of the stub column specimens fabricated from 35XF sheet steel is 0.085 inch.

Table 3.46

Dimensions of Stub Columns with Stiffened Flanges
Fabricated from 50XF Sheet Steel
(50XF Sheet Steel)

Specimen	BF (in.)	BW (in.)	BL (in.)	w/t	Gross Area ($in.^2$)	L (in.)	$(P_u)_{test}$ (kips)
1A1AX	2.229	1.963	0.923	22.89	1.1569	14.94	57.89
1A1BX	2.249	1.982	0.921	23.15	1.1652	14.99	57.65
1A2AX	2.249	1.960	0.921	23.15	1.1584	15.00	59.82
1A2BX	2.233	1.967	0.923	22.94	1.1587	14.95	60.23
1A3AX	2.245	1.963	0.927	23.10	1.1605	14.98	63.95
1A3BX	2.231	1.961	0.938	22.92	1.1612	14.95	62.04
1B1AX	3.173	1.969	0.926	35.15	1.3050	14.98	62.19
1B1BX	3.130	1.978	0.926	34.59	1.3012	14.97	61.75
1B2AX	3.123	1.983	0.919	34.50	1.2995	14.99	68.88
1B2BX	3.158	1.977	0.926	34.95	1.3052	15.01	67.86
1B3AX	3.159	1.979	0.921	34.97	1.3044	14.98	71.42
1B3BX	3.145	1.975	0.934	34.79	1.3050	14.94	71.52
1C1AX	4.529	1.967	0.923	52.76	1.5123	14.94	60.09
1C1BX	4.578	1.962	0.936	53.40	1.5223	14.94	60.67
1C2AX	4.552	1.968	0.928	53.06	1.5177	14.94	64.00
1C2BX	4.488	1.971	0.928	52.23	1.5087	14.93	66.44
1C3AX	4.445	1.972	0.923	51.67	1.5009	14.97	66.54
1C3BX	4.540	1.975	0.926	52.90	1.5174	14.96	69.47
1D1AX	8.012	2.719	1.014	97.99	2.3083	25.94	76.94
1D2AX	8.029	2.719	1.009	98.21	2.3094	25.92	82.22
1D3AX	8.013	2.725	1.018	98.01	2.3115	25.94	82.46
1D3BX	8.018	2.727	1.018	98.07	2.3129	25.92	80.85

Note : * For symbols BF, BW, and BL, see Figure 3.22.

* The nominal thickness of the stub column specimens fabricated from 50XF sheet steel is 0.077 inch.

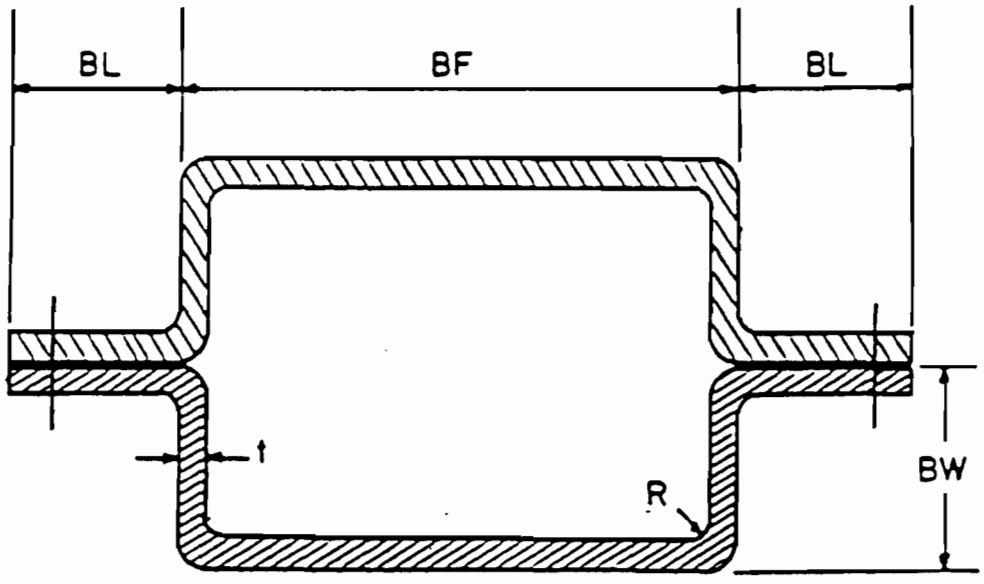

Figure 3.22 Cross Section of Box-Shaped Stub Columns Used for the Study of Stiffened Elements

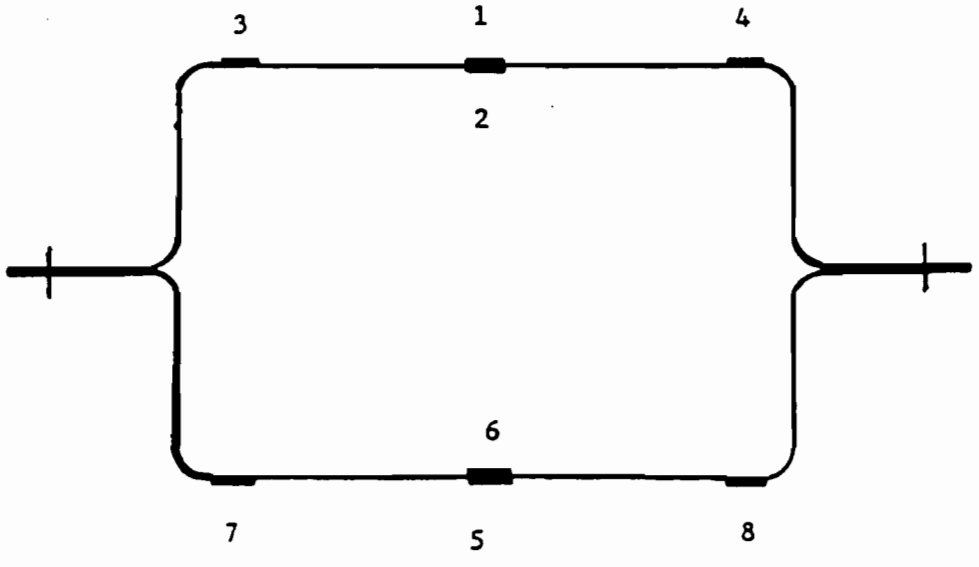

Figure 3.23 Locations of Strain Gages at Midheight of Box-Shaped Stub Columns

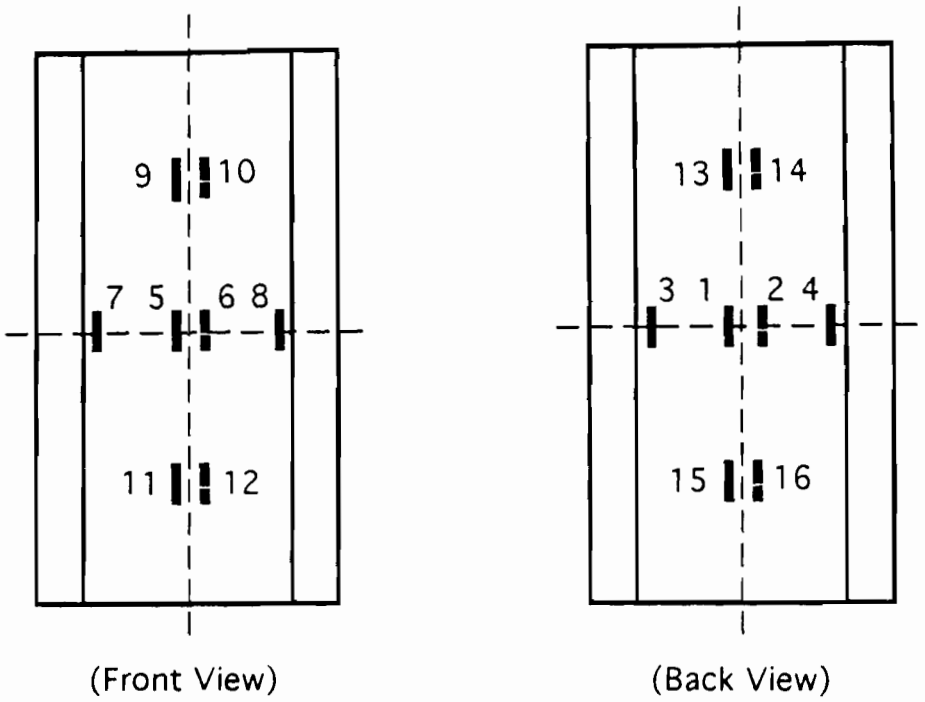

Figure 3.24 Locations of Strain Gages along the Specimem Length for Box-Shaped Stub Columns Having Large w/t Ratios

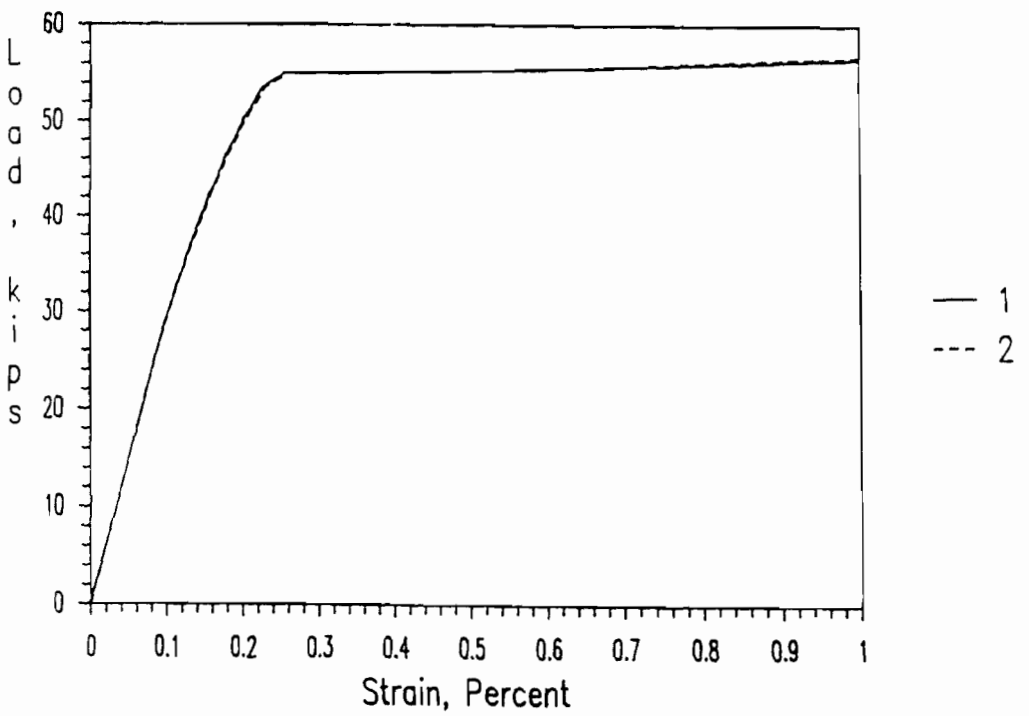

Figure 3.25 Load-Strain Curves of Strain Gages # 1 and 2 Installed at the Center of Stiffened Elements (Spec. 1A1AX)

and the overall length of the specimen. The CAMAC Data Acquisition System was used to record all the data during tests. After the data was acquired, it was downloaded to the Data General Mini Computer for analysis purpose.

In order to obtain good test results, a small amount of preload was applied to the stub column for the purpose of checking the alignment of specimens prior to testing. If necessary, thin aluminum foils were placed at the end of the specimen in the regions of low strain until the load is uniformly distributed over the whole cross section.

d. Test Results. It is well known that the local buckling stress depends on the width-to-thickness ratio of the stiffened compression element. As shown in Figure 3.25, no local buckling occurred in the specimens with small w/t ratios (case A of Group I for using both 35XF and 50XF sheet steels). For specimens with medium w/t ratios, (i.e., case B of Group I for using 35XF and 50XF sheet steels), the stiffened flanges normally buckled in the inelastic range as shown in Figure 3.26. The local buckling occurred in the elastic range for the specimens having large w/t ratios (cases C and D of Group I for using 35XF and 50XF sheet steels). When local buckling occurred in the test specimens, the stresses in the compression flanges redistributed over the cross section until the edge stress reached to the maximum value. Typical load-strain relationship for the specimens with large w/t ratios is shown in Figure 3.27.

The location of local buckling for the box-shaped stub columns with small or medium w/t ratios was found to be either at the end or at midheight or both. However, the sections with large w/t ratios failed

locally at or near the midheight of specimens regardless of the strain rate for most cases. Figure 3.28 is an example of locally buckled test specimen with large w/t ratio of 98.07.

Figures 3.29 to 3.32 show typical load-displacement diagrams for box-shaped stub columns fabricated from 35XF sheet steel and tested under different strain rates. The average w/t ratio of stiffened elements and the strain rates used in the tests are indicated in each figure. Similarly, Figures 3.33 to 3.36 show four typical load-displacement curves for box-shaped stub columns fabricated from 50XF sheet steel. Although a constant speed was applied to the test specimens during the test, however, the strain rate could not be retained constant after the ultimate load was reached in the specimen. Therefore, the value of strain rate was defined as the slope of the strain-time relationship before the attainment of the ultimate load. A typical strain-time diagram for an intermediate strain rate is shown in Figure 3.37. The tested ultimate loads are presented in Tables 3.45 and 3.46 for the box-shaped stub columns fabricated from 35XF and 50XF sheet steels, respectively.

3. Stub Column Tests for Unstiffened Elements

a. Specimens. In this phase of experimental investigation, I-shaped stub columns made of 35XF and 50XF sheet steels were tested to study the local buckling and postbuckling strength of unstiffened elements affected by strain rate. A total of 19 stub column test specimens fabricated from 35XF sheet steel were tested and reported in the Thirteenth Progress Report. These specimens have unstiffened elements with w/t ratios ranging from 8.93 to 20.97. Six additional stub column specimens fabricated from

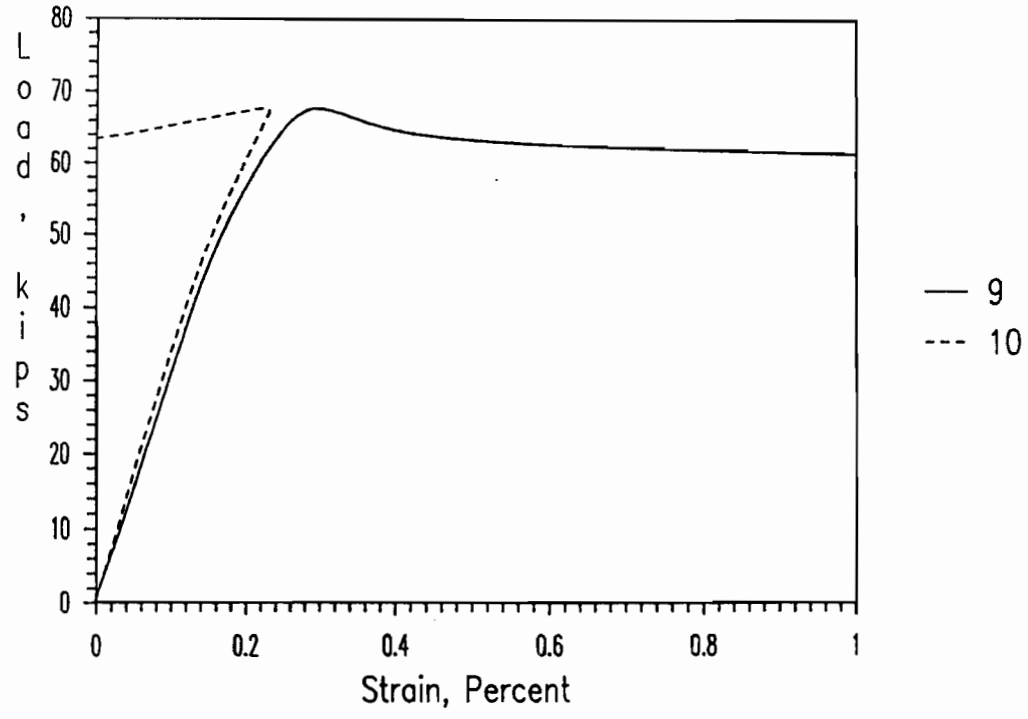

Figure 3.26 Load-Strain Curves of Strain Gages # 9 and 10 Installed at the Center of Stiffened Elements (Spec. 1B2BX)

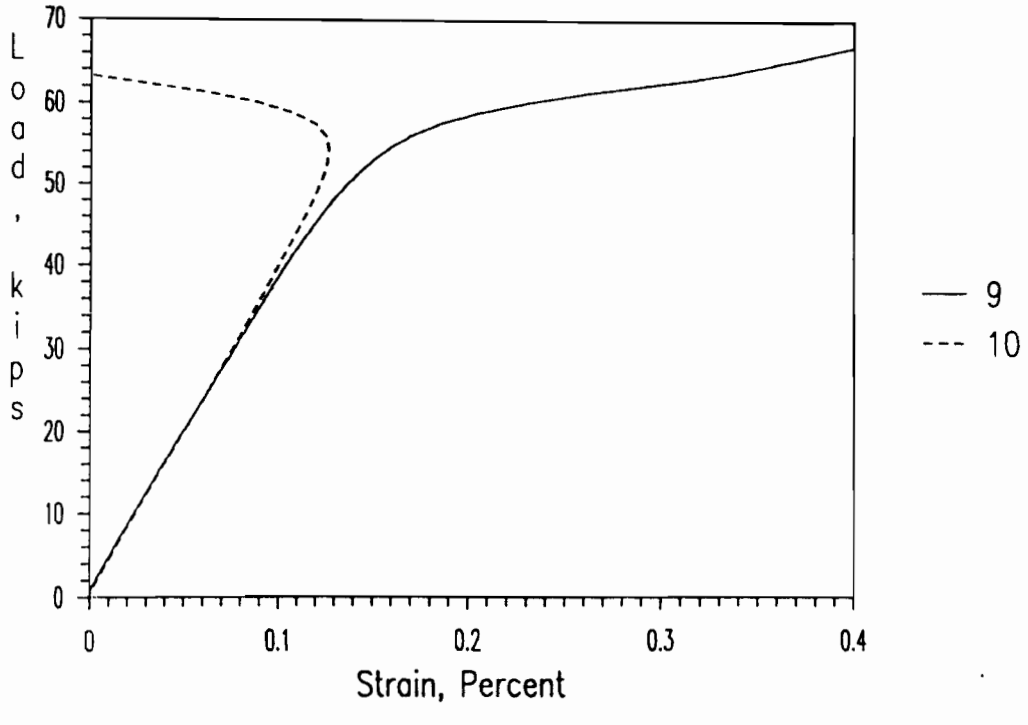

Figure 3.27 Load-Strain Curves of Strain Gages # 9 and 10 Installed at the Center of Stiffened Elements (Spec. 1C3BX)

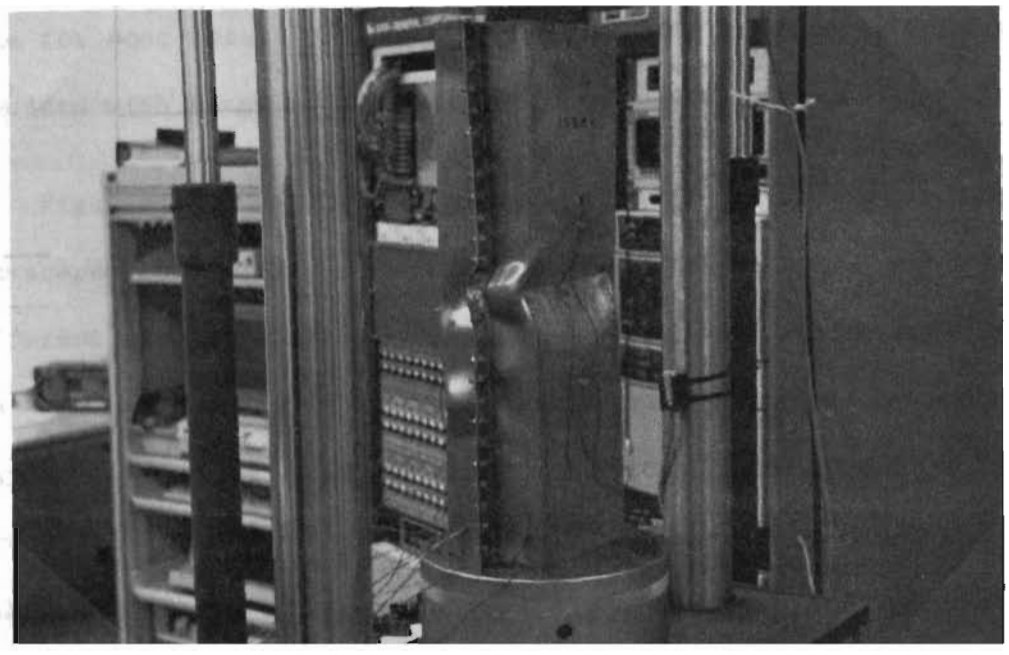

Figure 3.28 Typical Failure of Stub Columns with Large w/t Ratios

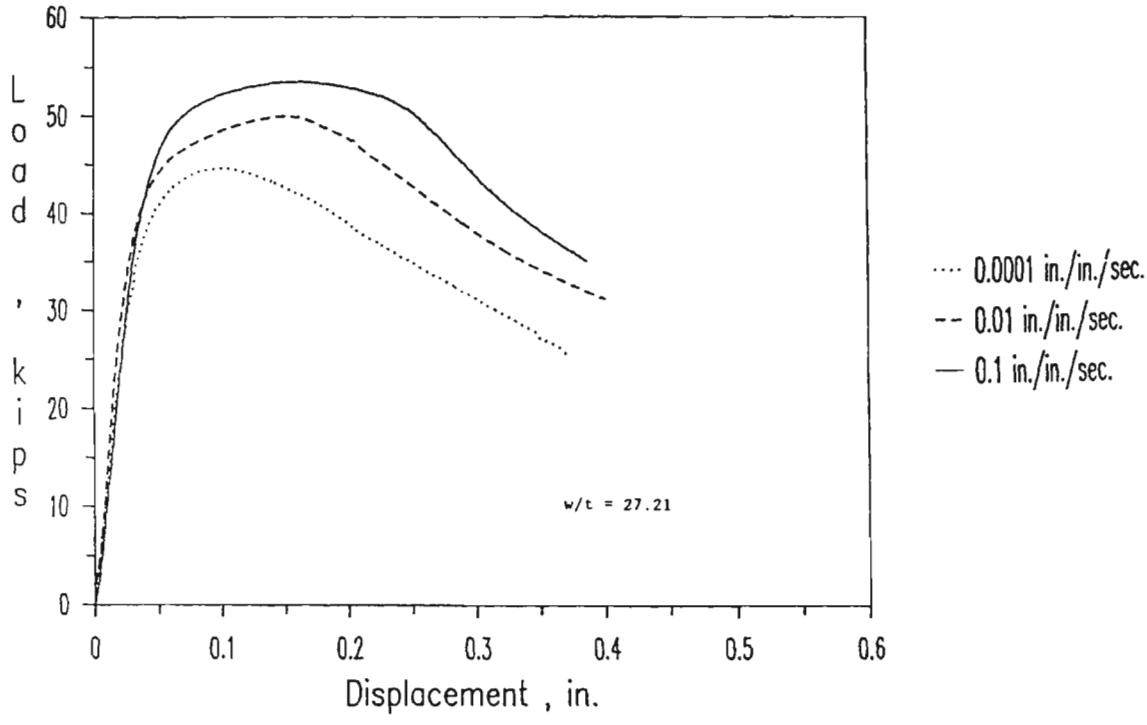

Figure 3.29 Load-Displacement Curves for Stub Column Specimens (35XF) 1A1A, 1A2A, and 1A3A

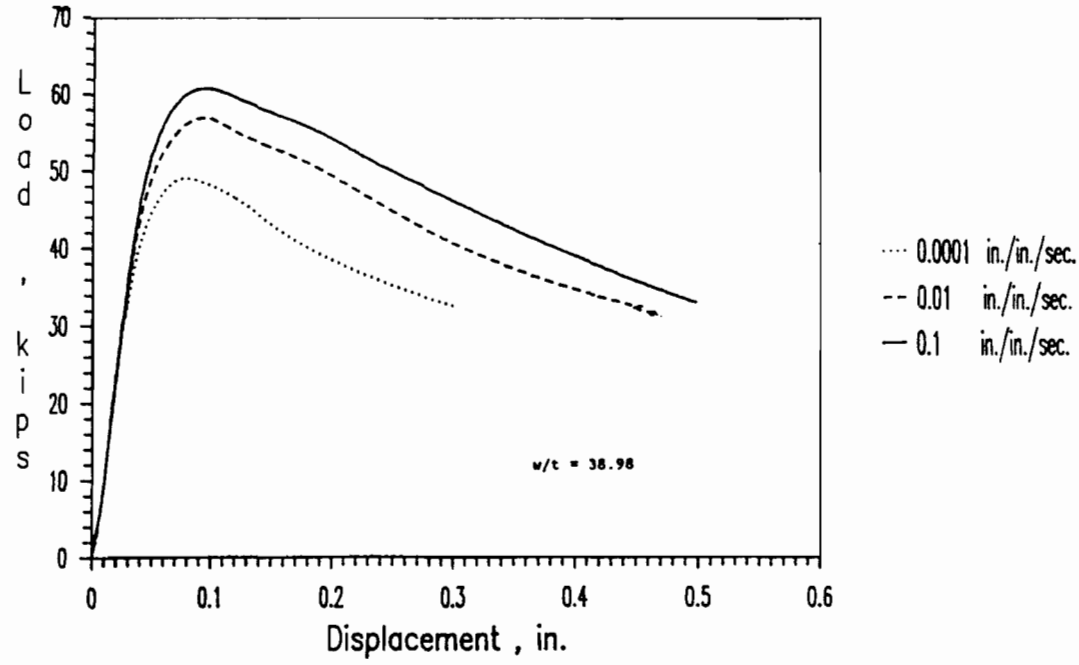

Figure 3.30 Load-Displacement Curves for Stub Column Specimens (35XF) 1B1A, 1B2A, and 1B3A

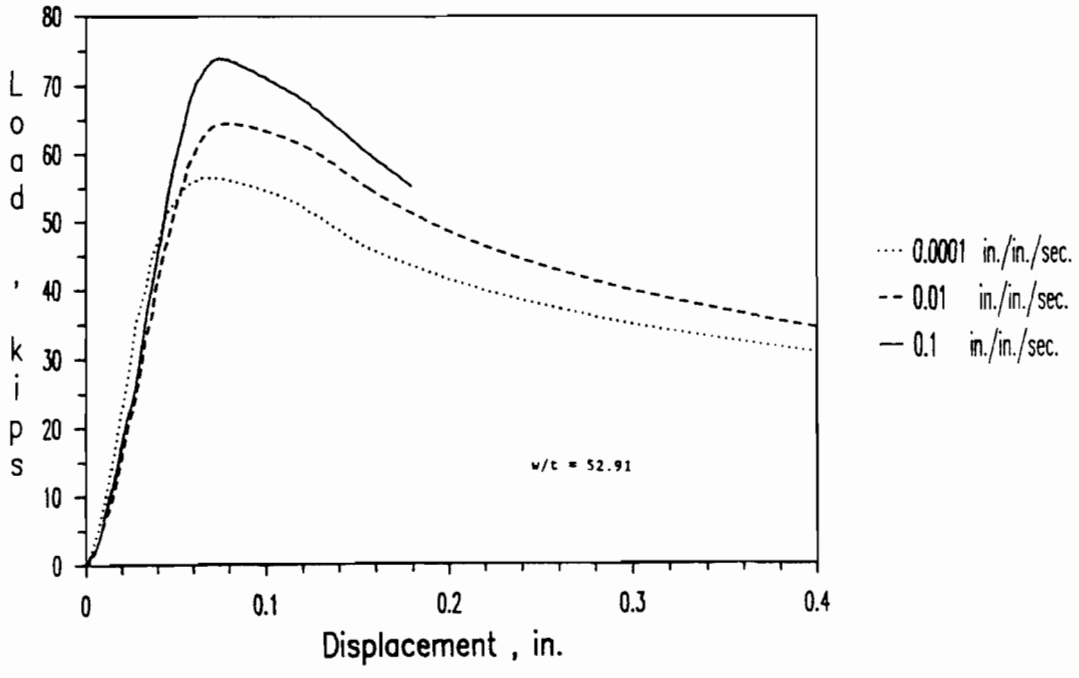

Figure 3.31 Load-Displacement Curves for Stub Column Specimens (35XF) 1C1A, 1C2A, and 1C3A

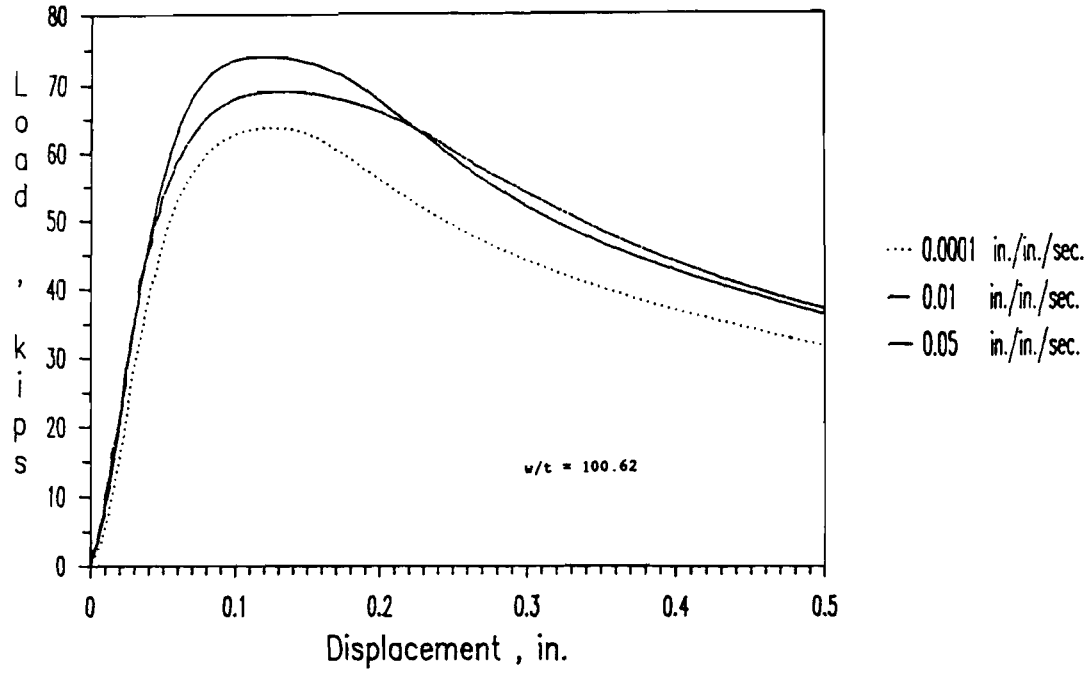

Figure 3.32 Load-Displacement Curves for Stub Column Specimens (35XF) 1D1A, 1D2A, and 1D3A

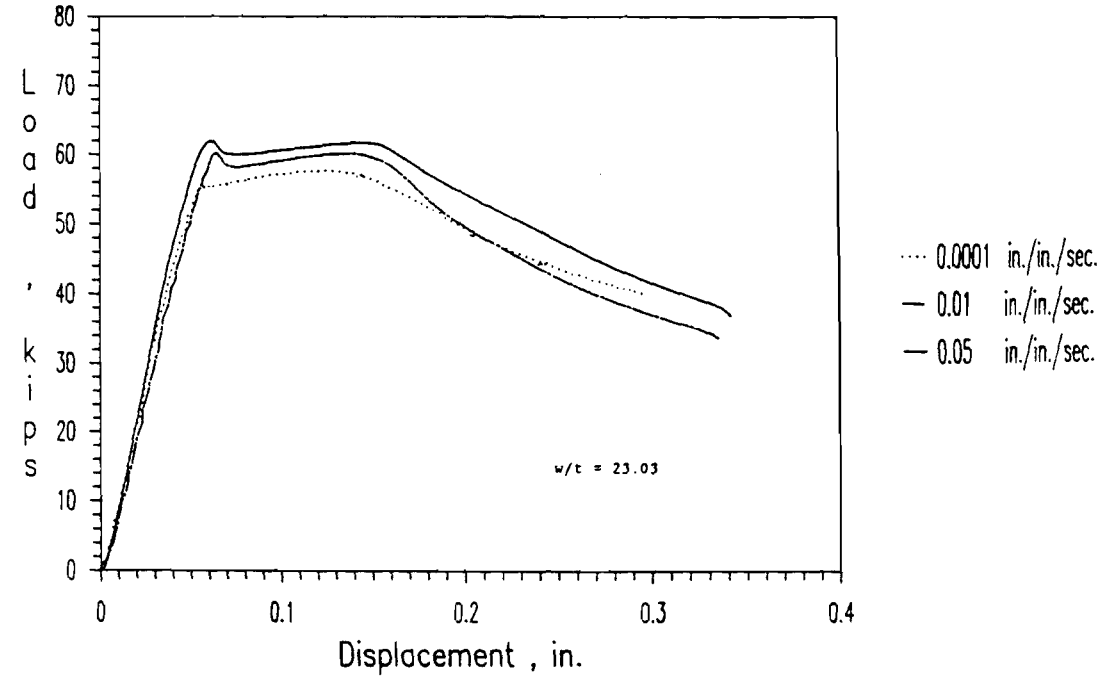

Figure 3.33 Load-Displacement Curves for Stub Column Specimens (50XF) 1A1BX, 1A2BX, and 1A3AX

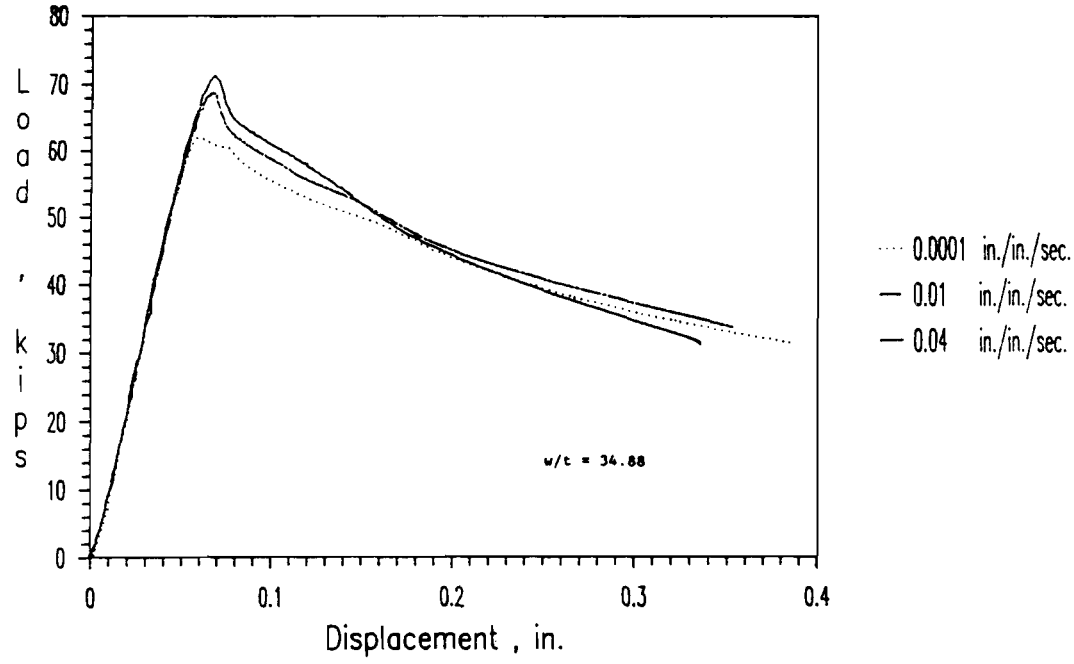

Figure 3.34 Load-Displacement Curves for Stub Column Specimens (50XF) 1B1AX, 1B2AX, and 1B3AX

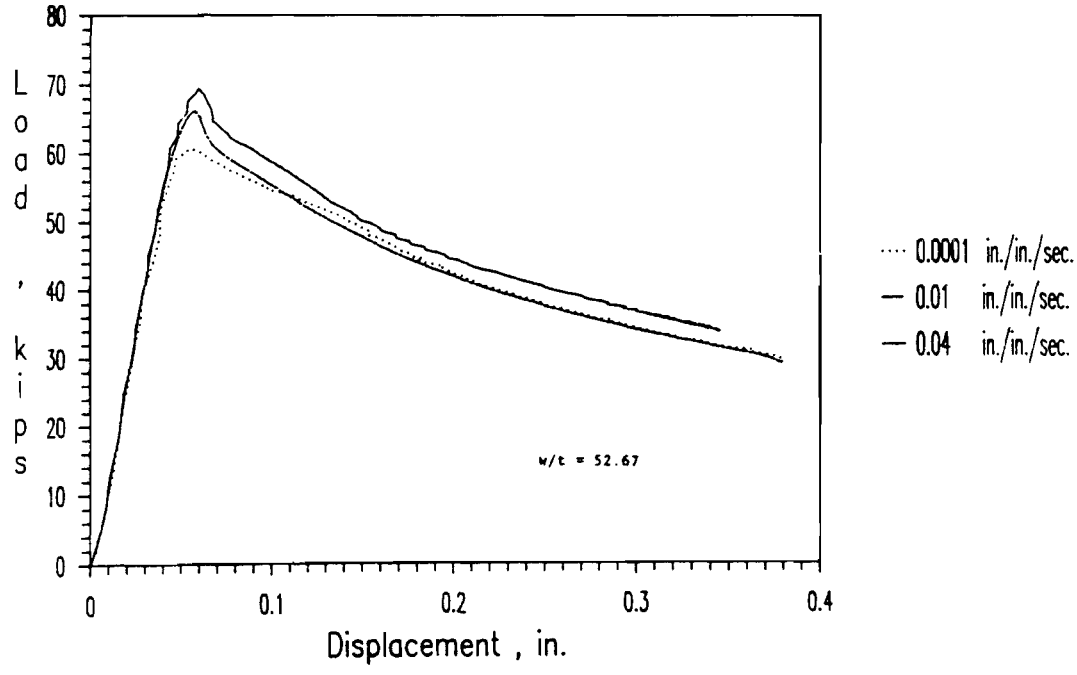

Figure 3.35 Load-Displacement Curves for Stub Column Specimens (50XF) 1C1AX, 1C2BX, and 1C3BX

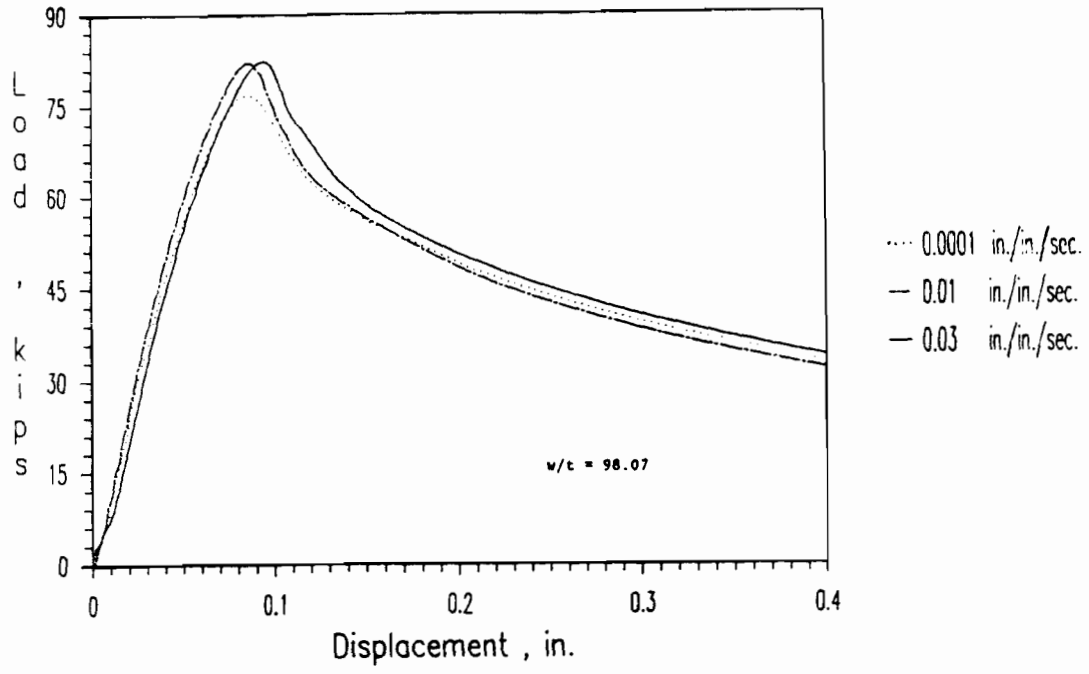

Figure 3.36 Load-Displacement Curves for Stub Column Specimens (50XF) 1D1AX, 1D2AX, and 1D3AX

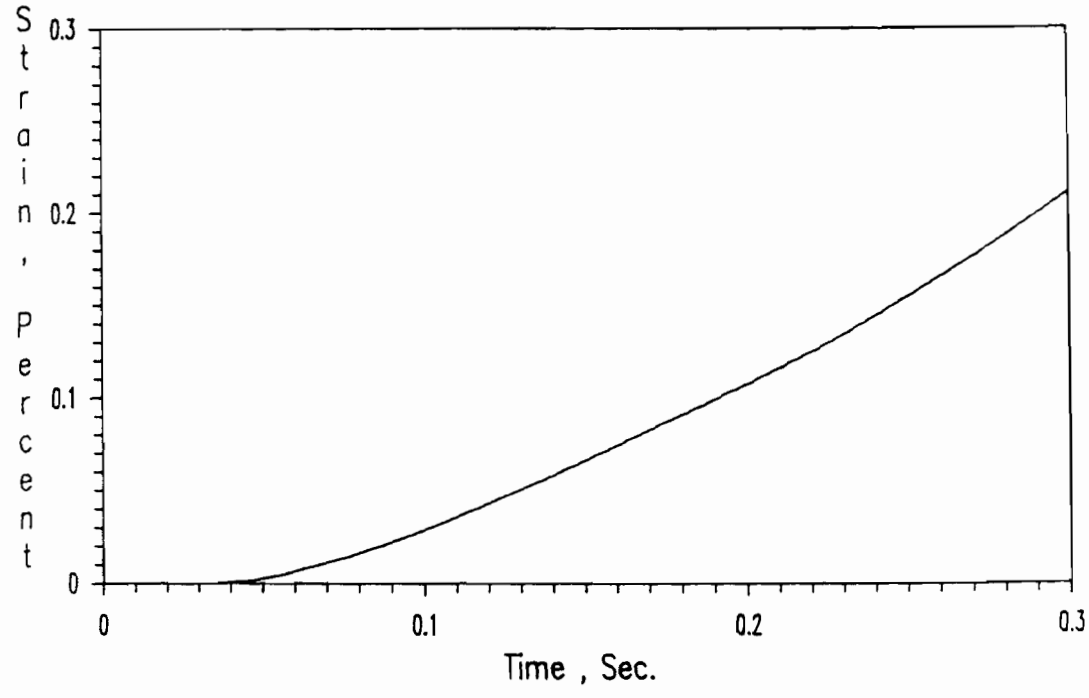

Figure 3.37 Typical Plot of Strain-Time Relationship for Stub Columns with Stiffened Elements Under Intermediate Strain Rate (Spec. 1B2BX)

35XF sheet steel were tested since May 1990 to study the strength of unstiffened elements with the w/t value of 44.57. In addition, a total of 26 stub column test specimens fabricated from 50XF sheet steel were tested to study the local buckling and postbuckling strength of unstiffened elements with w/t ratios ranging from 8.29 to 35.37. The strain rates for all tests ranged from 10^{-5} to 10^{-1} in./in./sec.. Tables 3.47 and 3.48 give the lengths and dimensions of stub column specimens fabricated from 35XF and 50XF sheet steels, respectively.

In order to investigate the behavior and strength of unstiffened compression elements, the web of all channel sections was designed to be fully effective, while the length of all members was designed to be longer than three times the largest dimension of the cross section and less than 20 times the least radius of gyration as recommended in Reference 96 and Part VII of the 1986 AISI Cold Formed Steel Design Specification[66].

As shown in Figure 3.38, PC-7 epoxy adhesive material was used to assemble two channel sections back to back to form an I-shaped stub column specimen. Before two sections were bonded together, the surfaces of webs were paper sanded and cleaned with methyl alcohol and water. In order to maintain a uniform epoxy thickness, 0.002"-diameter wires were placed between the webs of two channel sections. Two channel sections were clamped together by using C-clamps. The test specimens were cured in the room-temperature condition and C-clamps were released after 24 hours. Same as the box-shaped specimens, all I-shaped specimens were milled to make both ends of stub column flat and parallel.

b. Strain Measurements. Fourteen foil strain gages were mounted at midheight of stub column specimens. Four paired strain gages (No. 1-2,

5-6, 7-8, and 11-12) were placed along the tips of unstiffened flanges for the purpose of determining the local buckling load. By using the modified strain reversal method, the critical local buckling load was obtained from load-strain relationships of these paired strain gages. In addition, four strain gages (No. 3, 4, 9, and 10) were placed along the supported edges of unstiffened flanges to measure the maximum edge strains. The paired strain gages (No. 13 and 14) were placed along the centerline of the web to monitor any premature failure of the web. All strain gages on the specimen were used to check the alignment. Figure 3.39 shows the arrangement of strain gages.

c. Instrumentation and Test Procedure. To obtain the necessary background information, all specimens were loaded to failure. The instrumentation and test procedure used for this phase of study are the same as those used in the tests of stub columns for the study of stiffened elements. For all tests, the maximum load ranges of 50 or 100 kips and the maximum stroke ranges of 0.5 or 1.0 inches were selected in the function generator of the test machine. During the test, the applied loads, the actuator displacement, the strains of fourteen strain gages, and the test time were recorded. The strain rates for all tests ranged from 10^{-5} to 10^{-1} in./in./sec..

d. Test Results. Based on the load-strain diagram obtained from the paired strain gages attached back to back along the centerline of the web, it can be seen that no local buckling occurred in the web prior to the attainment of the maximum load. There is no evidence that failure of the bonding material occured before the test specimen reached its ultimate load. The failure mode of the stub column varies with the

Table 3.47

Dimensions of Stub Columns with Unstiffened Flanges
Fabricated from 35XF Sheet Steel
(35XF Sheet Steel)

Specimen	BC (in.)	D (in.)	w/t	Gross Area ($in.^2$)	L (in.)	$(P_u)_{test}$ (kips)
2A1A	1.000	2.000	8.93	0.6220	7.90	25.26
2A1B	1.010	2.018	9.04	0.6285	7.97	25.35
2A2A	1.000	2.040	8.93	0.6288	7.95	26.04
2A2B	1.015	2.002	9.10	0.6275	7.94	27.70
2A3A	1.000	2.040	8.93	0.6288	7.98	31.41
2A3B	1.003	2.014	8.96	0.6254	7.94	29.41
2B1A	1.375	3.025	13.34	0.9238	9.95	34.20
2B1B	1.381	2.981	13.41	0.9184	9.97	34.20
2B2A	1.380	2.987	13.40	0.9190	9.96	36.30
2B2B	1.378	3.007	13.37	0.9217	9.94	37.52
2B3A	1.375	3.020	13.34	0.9229	10.01	41.67
2B3B	1.382	3.006	13.42	0.9229	9.99	42.70
2C0A	2.000	3.000	20.69	1.1320	14.00	36.30
2C1A	2.014	2.976	20.85	1.1327	14.00	37.23
2C1B	2.006	3.018	20.76	1.1371	13.94	37.66
2C2A	2.024	2.967	20.97	1.1346	14.09	41.28
2C2B	2.010	3.015	20.81	1.1380	13.95	41.52
2C3A	2.020	2.970	20.93	1.1337	14.06	47.92
2C3B	2.015	2.977	20.87	1.1332	13.91	46.16
2D1A	4.032	3.302	44.60	1.8743	23.92	41.72
2D1B	4.024	3.311	44.50	1.8731	23.94	41.04
2D2A	4.034	3.278	44.62	1.8709	23.92	46.31
2D2B	4.031	3.289	44.59	1.8717	23.93	44.94
2D3A	4.025	3.241	44.51	1.8615	23.90	48.66
2D3B	4.032	3.301	44.60	1.8741	23.92	49.39

Note : * For symbols BC and D, see Figure 3.38.

* The nominal thickness of the stub column specimens fabricated from 35XF sheet steel is 0.085 inch.

Table 3.48

Dimensions of Stub Columns with Unstiffened Flanges
Fabricated from 50XF Sheet Steel
(50XF Sheet Steel)

Specimen	BC (in.)	D (in.)	w/t	Gross Area ($in.^2$)	L (in.)	$(P_u)_{test}$ (kips)
2A1AX	0.881	1.949	8.41	0.5218	6.97	28.04
2A1BX	0.879	1.958	8.38	0.5225	6.98	28.16
2A2AX	0.880	1.956	8.40	0.5228	6.98	29.02
2A2BX	0.879	1.956	8.38	0.5224	6.97	29.43
2A3AX	0.872	1.975	8.29	0.5232	6.99	30.75
2A3BX	0.877	1.962	8.36	0.5226	6.96	30.95
2B1AX	1.133	2.961	11.68	0.7553	8.99	39.72
2B1BX	1.127	2.992	11.60	0.7582	8.94	39.18
2B1CX	1.129	2.994	11.63	0.7593	8.99	39.47
2B2AX	1.125	2.999	11.58	0.7589	8.97	42.60
2B2BX	1.122	3.024	11.54	0.7616	9.00	42.55
2B2CX	1.121	2.987	11.53	0.7558	8.98	41.77
2B3AX	1.131	2.986	11.65	0.7586	9.00	45.07
2B3BX	1.119	2.994	11.50	0.7563	8.97	45.94
2C1AX	1.992	3.043	22.84	1.0327	14.94	43.62
2C1BX	1.984	3.064	22.73	1.0333	14.96	43.97
2C2AX	1.987	3.047	22.77	1.0316	14.94	46.70
2C2BX	1.986	3.057	22.76	1.0329	14.95	46.26
2C3AX	1.983	3.041	22.72	1.0295	14.97	47.34
2C3BX	1.988	3.055	22.79	1.0333	14.94	46.85
2D1AX	2.957	2.717	35.37	1.2796	17.94	44.06
2D1BX	2.954	2.717	35.33	1.2786	17.94	44.50
2D2AX	2.948	2.719	35.26	1.2772	17.94	46.75
2D2BX	2.945	2.722	35.21	1.2767	17.94	47.58
2D3AX	2.951	2.715	35.29	1.2774	17.94	49.39
2D3BX	2.940	2.725	35.15	1.2754	17.94	48.95

Note : * For symbols BC and D, see Figure 3.38.

* The nominal thickness of the stub column specimens fabricated from 50XF sheet steel is 0.077 inch.

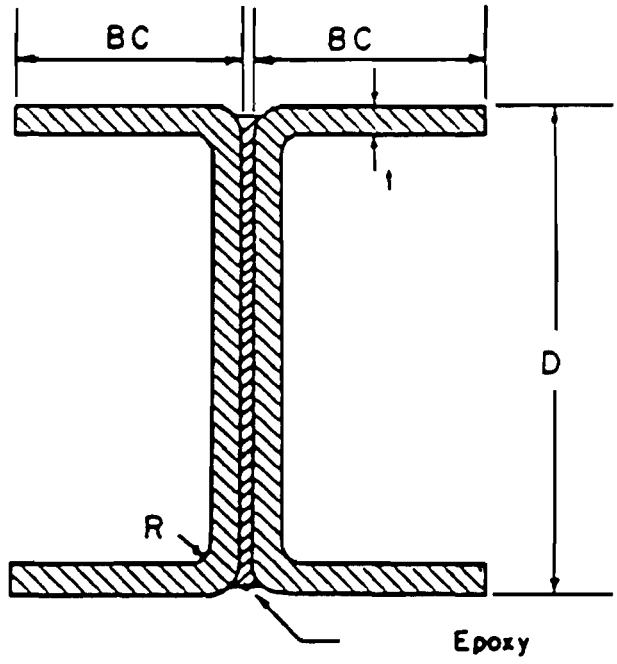

Figure 3.38 Cross Section of I-shaped Stub Columns Used for the Study of Unstiffened Elements

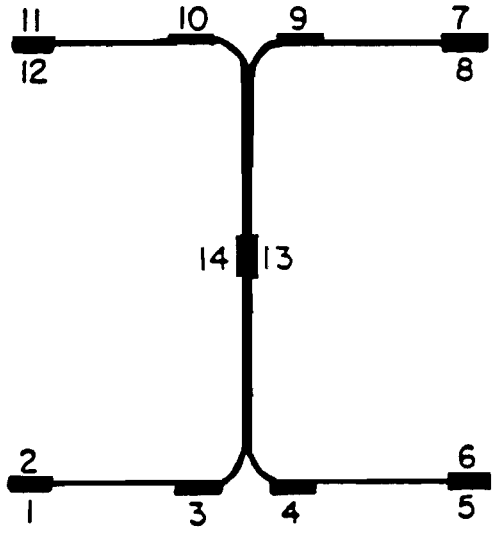

Figure 3.39 Locations of Strain Gages at Midheight of I-Shaped Stub Columns

width-to-thickness ratio of unstiffened elements. Same as the stub columns with stiffened elements, no local buckling occurred in the unstiffened flanges of the specimens with small w/t ratios (case A of Group II for using 35XF and 50XF sheet steels). For specimens with medium w/t ratios, (i.e., case B of Group II for using 35XF and 50XF sheet steels), the unstiffened flanges buckled locally in the inelastic range. The local buckling occurred in the elastic range for the specimens with large w/t ratios (cases C and D of Group II for using 35XF and 50XF sheet steels). Typical load-strain relationship for the specimens with large w/t ratios is shown in Figure 3.40.

Figure 3.41 shows the local buckling mode developed in the stub column specimen with large w/t ratios. Four typical load-displacement relationships are shown in Figures 3.42 to 3.45 for I-shaped stub columns fabricated from 35XF sheet steel and tested under different strain rates. The average w/t ratio of unstiffened elements and the strain rates used in the tests are indicated in each figure. Similarly, Figures 3.46 to 3.49 show four typical load-displacement curves for I-shaped stub columns fabricated from 50XF sheet steel. The value of strain rate for each test was determined from the strain-time relationship. A typical strain-time diagram is shown in Figure 3.50. The tested ultimate loads are presented in Tables 3.47 and 3.48 for the I-shaped stub columns fabricated from 35XF and 50XF sheet steels, respectively.

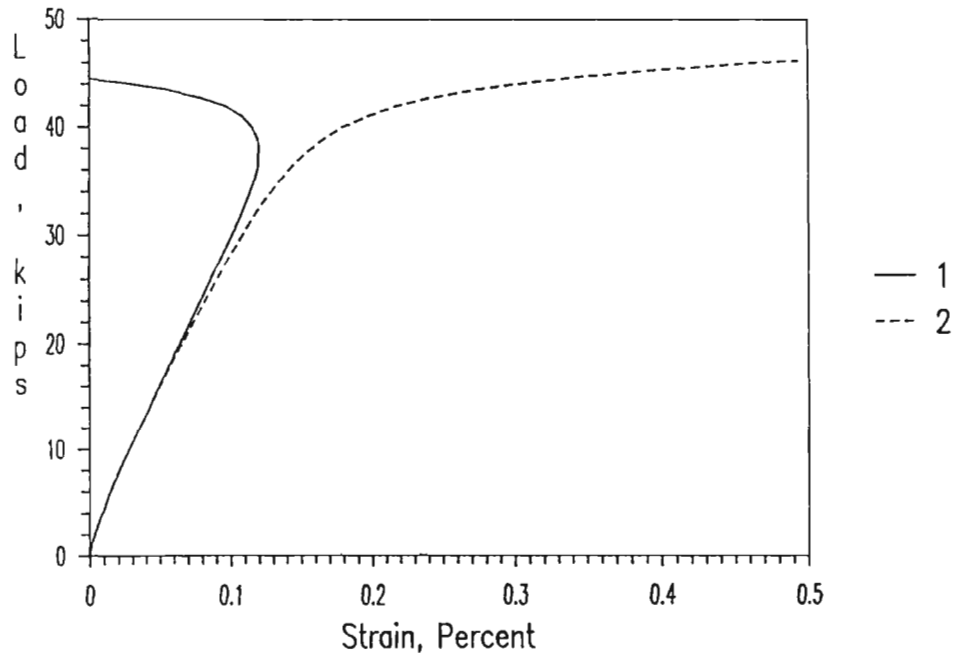

Figure 3.40 Load-Strain Curves of Strain Gages # 1 and 2 Installed at the Tips of Unstiffened Elements (Spec. 2C2BX)

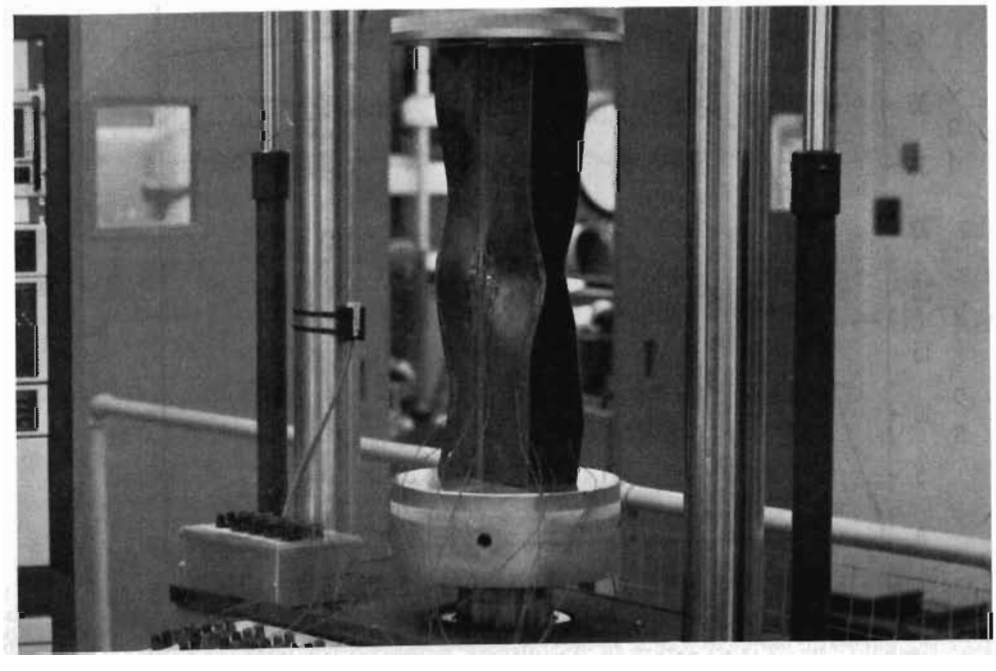

Figure 3.41 Typical Failure of Stub Columns with Large w/t Ratios

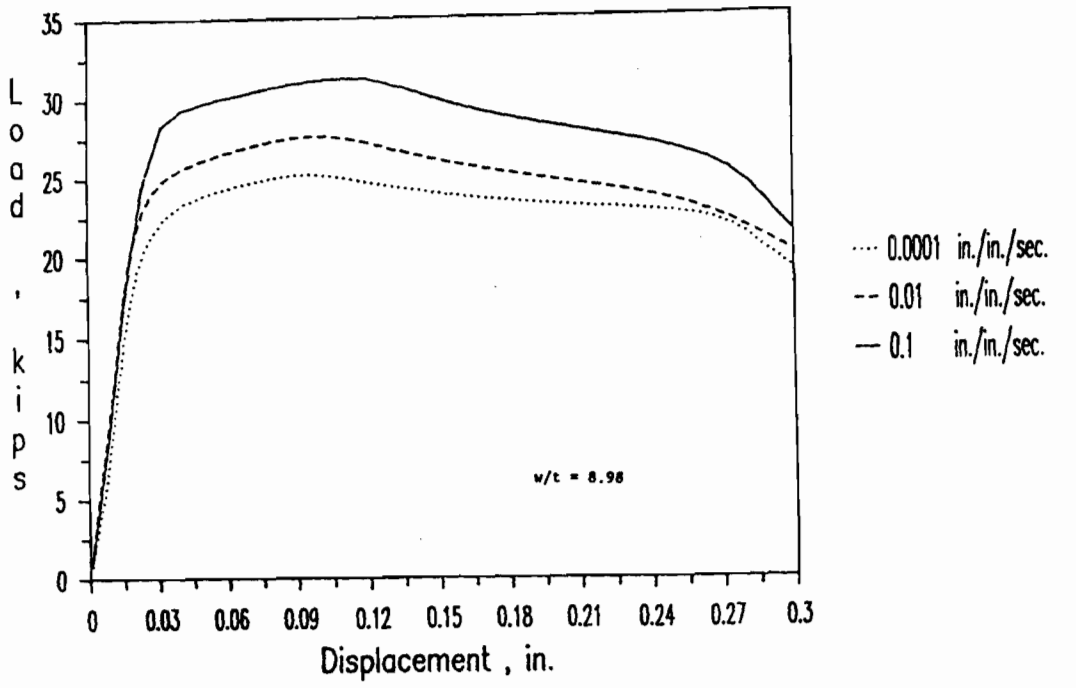

Figure 3.42 Load-Displacement Curves for Stub Column Specimens (35XF) 2A1A, 2A2A, and 2A3A

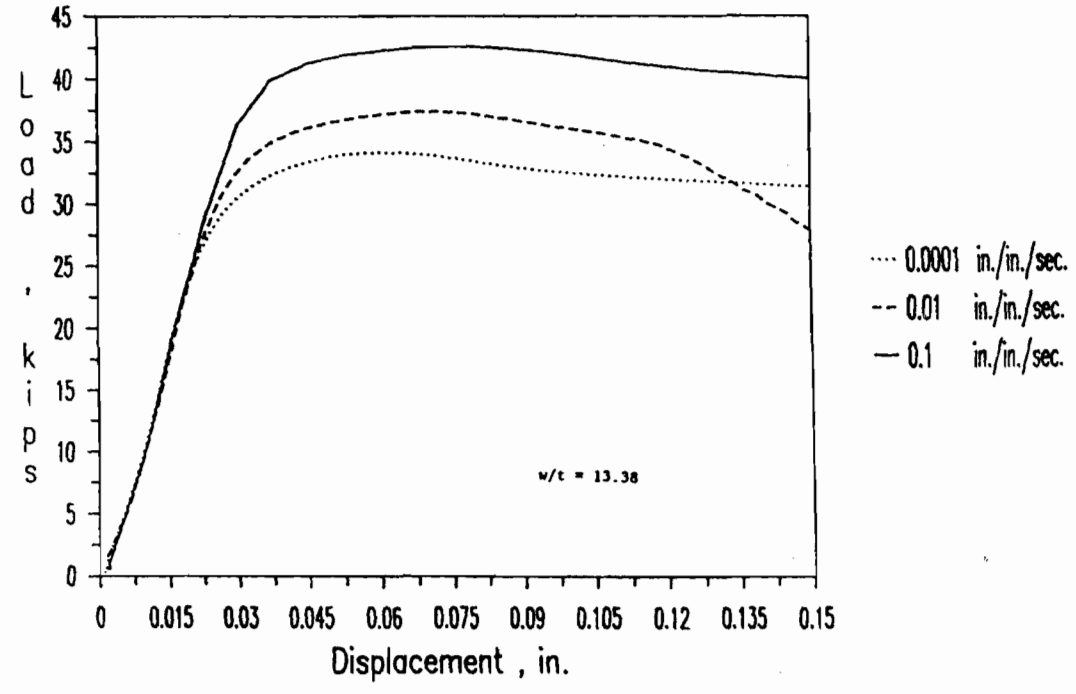

Figure 3.43 Load-Displacement Curves for Stub Column Specimens (35XF) 2B1A, 2B2A, and 2B3A

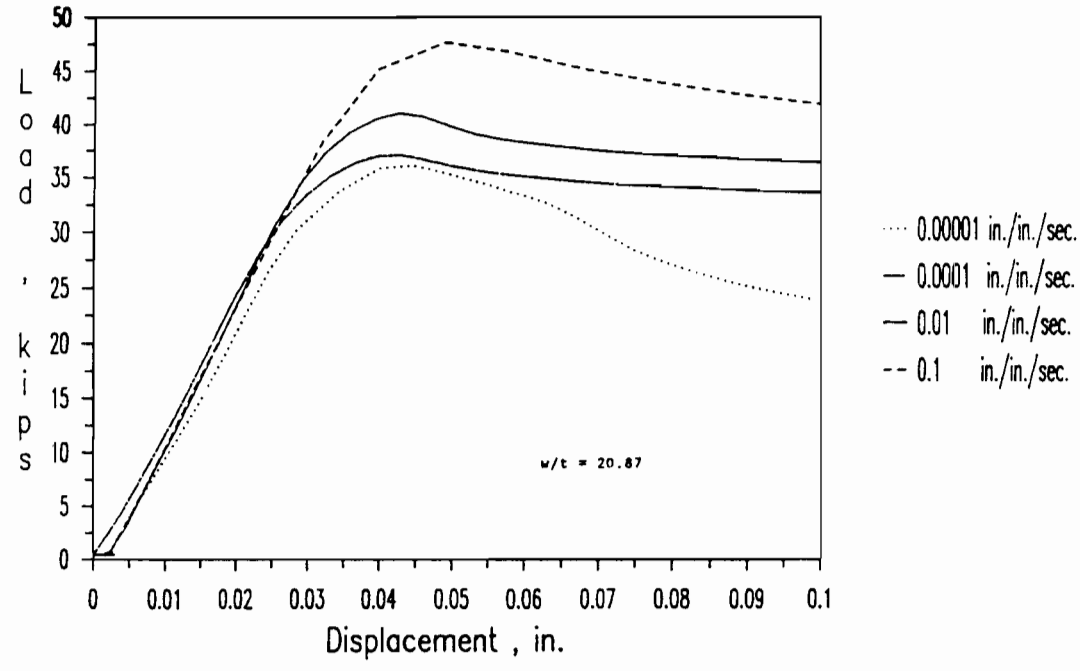

Figure 3.44 Load-Displacement Curves for Stub Column Specimens (35XF) 2C1A, 2C2A, and 2C3A

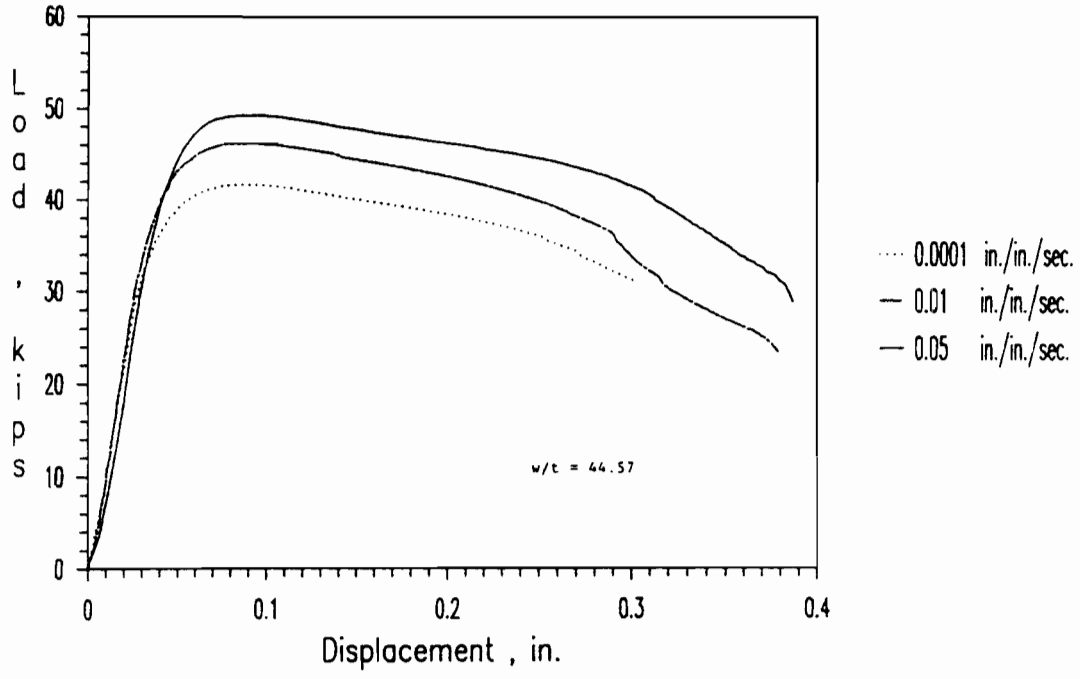

Figure 3.45 Load-Displacement Curves for Stub Column Specimens (35XF) 2D1A, 2D2A, and 2D3A

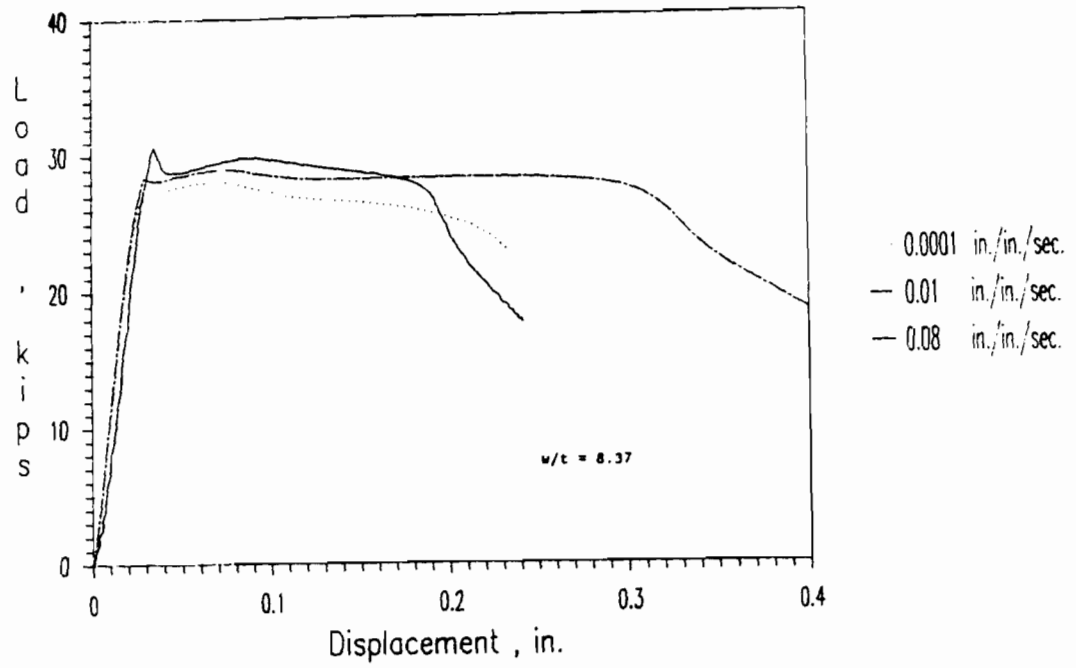

Figure 3.46 Load-Displacement Curves for Stub Column Specimens (50XF) 2A1AX, 2A2AX, and 2A3AX

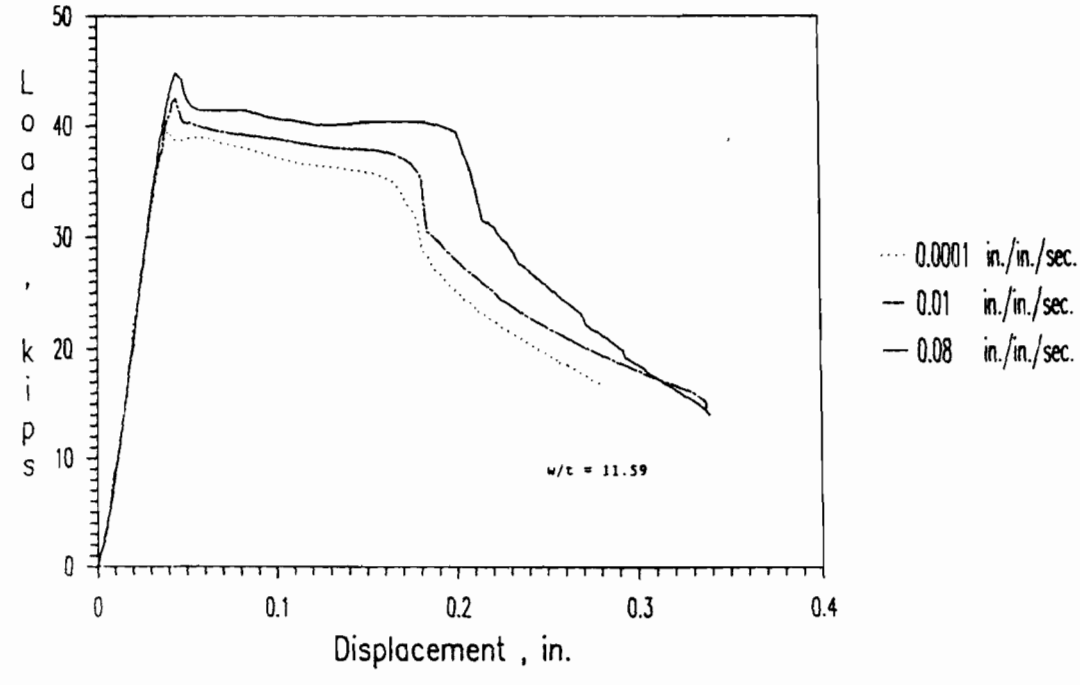

Figure 3.47 Load-Displacement Curves for Stub Column Specimens (50XF) 2B1AX, 2B2AX, and 2B3AX

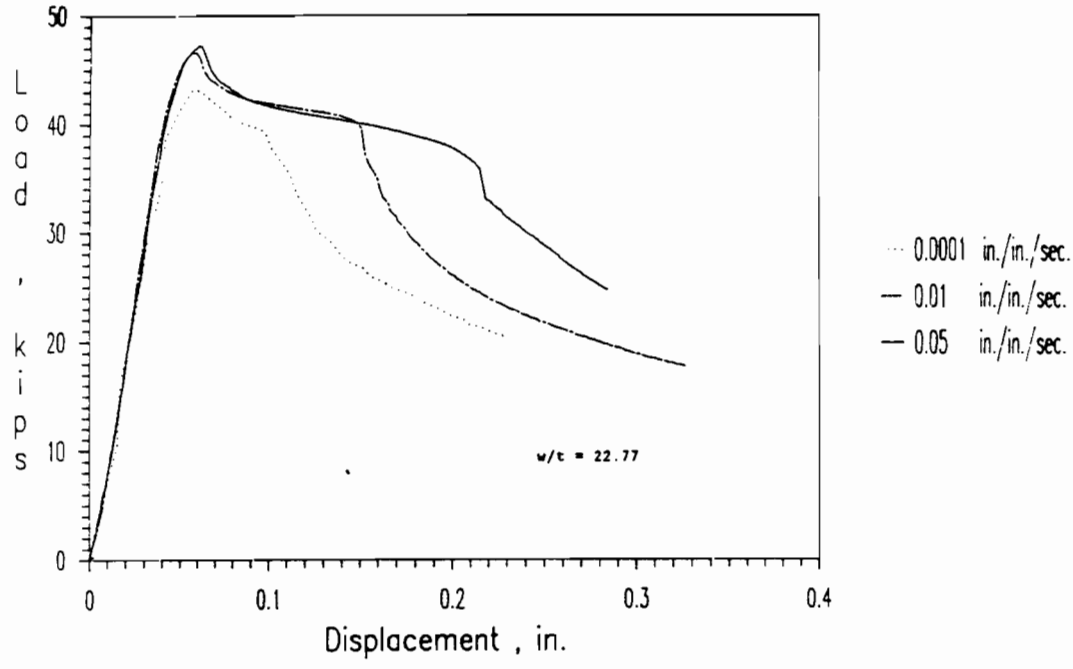

Figure 3.48 Load-Displacement Curves for Stub Column Specimens (50XF) 2C1AX, 2C2AX, and 2C3AX

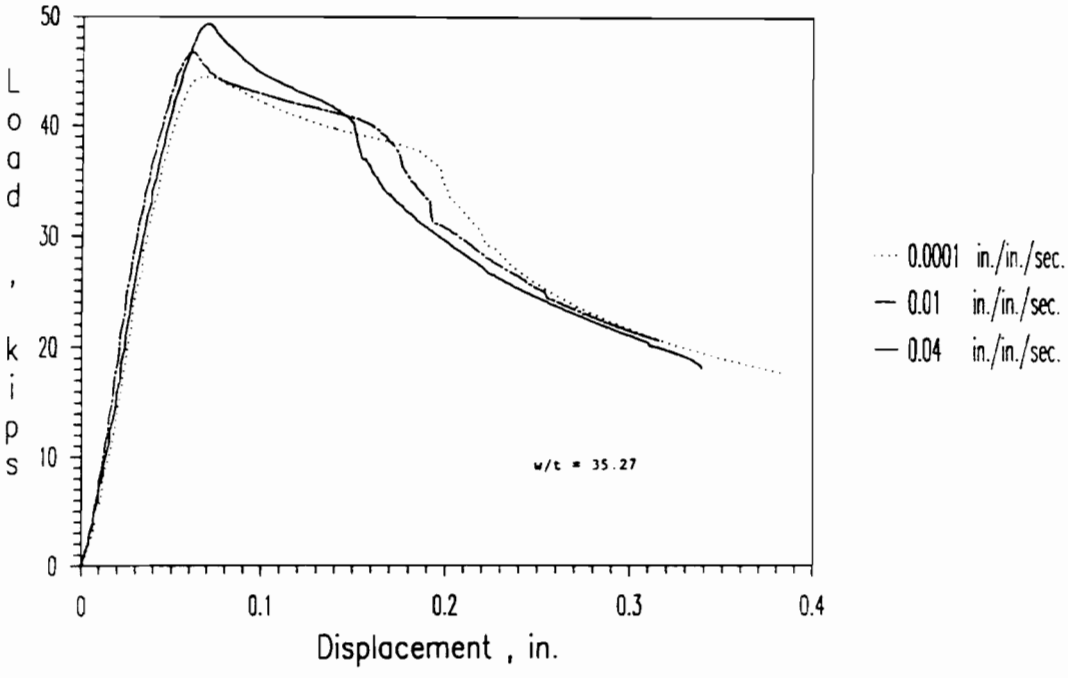

Figure 3.49 Load-Displacement Curves for Stub Column Specimens (50XF) 2D1AX, 2D2AX, and 2D3AX

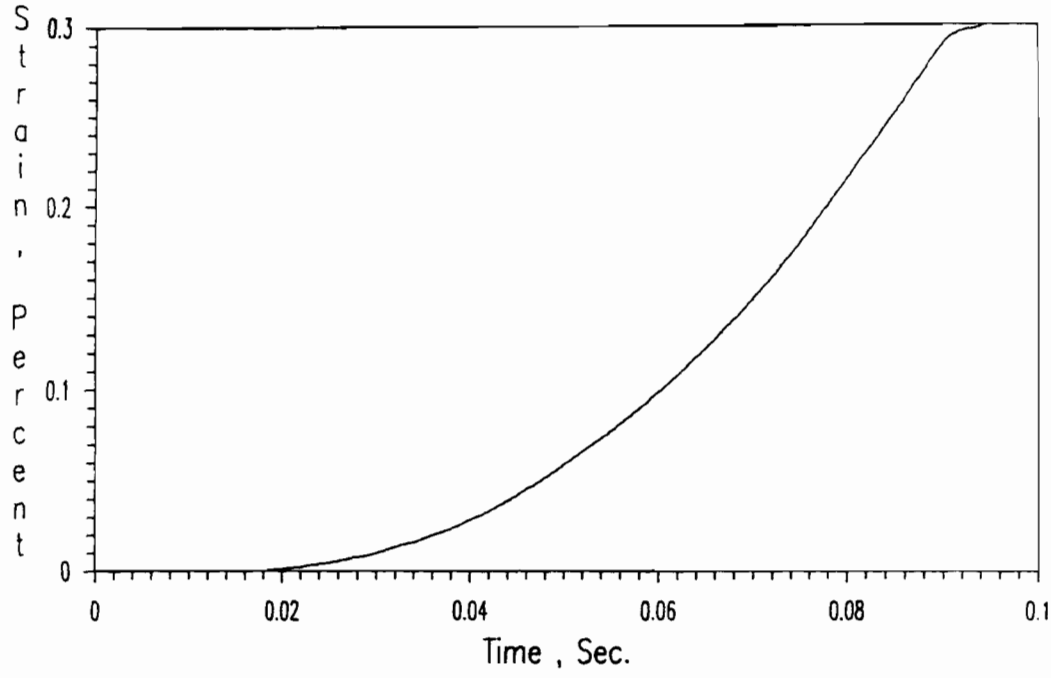

Figure 3.50 Typical Plot of Strain-Time Relationship for Stub Columns with Stiffened Elements (Spec. 2A3AX)

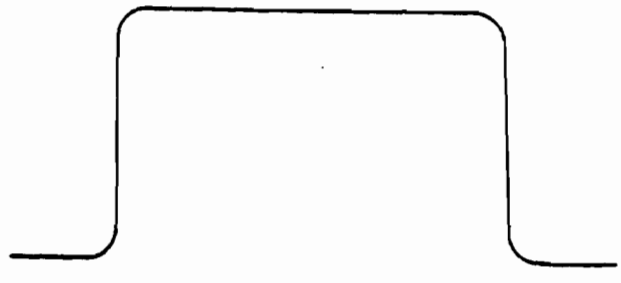

Figure 3.51 Configuration of Beam Test Specimens for Members with a Stiffened Compression Flange

D. BEAM SPECIMENS

The objective of this experimental investigation was to study whether the available effective design formulas using dynamic material properties can be adequately used for the design of structural members subjected to dynamic loads.

The materials used in this phase of the study were 35XF and 50XF sheet steels with nominal yield strengths equal to 35 ksi and 50 ksi, respectively. A total of 15 hat-shaped beams were fabricated from each of the 35XF and 50XF sheet steels. These specimens were tested to study the strength of stiffened elements. For the strength of unstiffened elements, 15 channel beams were fabricated from each of the 35XF and 50XF sheet steels. All these specimens were cold-formed to shape by Holloway Machine Company in Springfield, Missouri.

The configurations of beam specimens having stiffened and unstiffened elements are shown in Figures 3.51 and 3.52, respectively. The designation of test specimens is presented in Table 3.49. Tables 3.50 to 3.53 show the specimen number, test speed, strain rate, w/t ratio, and the overall length of each individual test specimen. The strain rates used in the tests varied from 10^{-5} to 10^{-2} in./in./sec.. A total of 60 beam specimens were tested and are discussed in this section.

1. Material Properties The sheet steels used to fabricate beam specimens were 35XF and 50XF. The average values of the mechanical properties of these two types of sheet steel tested under different strain rate were listed in Tables 3.43 and 3.44.

Table 3.49

Designation of Beam Specimens Used in This Study

1st Digit	1st Letter	2nd Digit	2nd Letter
Section Type (Group)	w/t Ratio (Case)	Strain-Rate (in./in./sec.)	Test No.
3- Hat-Shaped Section for Beam Test	A- Small Ratio	0- 0.00001	A- 1st Test
	B- Medium Ratio	1- 0.0001	B- 2nd Test
4- Channel Section for Beam Test	C- Large Ratio	2- 0.01	

Note: The fifth character (X) in the designation of test specimens represents the specimen fabricated from 50XF sheet steel.

Table 3.50

Number of Performed Beam Tests
Hat Sections Having Stiffened Compression Flanges
(35XF Sheet Steel)

Spec.	Test Speed (in./min.)	Strain Rate (in./in./sec.)	w/t	Full Length (in.)	No. of Tests Performed
3A0A	0.023	0.00001	29.15	47.0	1
3A1A	0.23	0.0001	30.00	47.0	1
3A1B	0.23	0.0001	29.85	47.0	1
3A2A	23.0	0.01	29.05	47.0	1
3A2B	23.0	0.01	30.17	47.0	1
3B0A	0.038	0.00001	55.91	77.0	1
3B1A	0.38	0.0001	55.11	77.0	1
3B1B	0.38	0.0001	55.91	77.0	1
3B2A	38.0	0.01	55.82	77.0	1
3B2B	38.0	0.01	55.97	77.0	1
3C0A	0.15	0.00001	76.17	95.0	1
3C1A	1.50	0.0001	76.64	95.0	1
3C1B	1.50	0.0001	76.57	95.0	1
3C2A	150.0	0.01	76.62	95.0	1
3C2B	150.0	0.01	76.03	95.0	1

Table 3.51

Number of Performed Beam Tests
Hat Sections Having Stiffened Compression Flanges
(50XF Sheet Steel)

Spec.	Test Speed (in./min.)	Strain Rate (in./in./sec.)	w/t	Full Length (in.)	No. of Tests Performed
3A0AX	0.12	0.00001	26.28	41.0	1
3A1AX	1.20	0.0001	26.82	41.0	1
3A1BX	1.20	0.0001	26.79	41.0	1
3A2AX	120.0	0.01	26.82	41.0	1
3A2BX	120.0	0.01	26.71	41.0	1
3B0AX	0.20	0.00001	46.07	61.0	1
3B1AX	2.00	0.0001	46.10	61.0	1
3B1BX	2.00	0.0001	46.11	61.0	1
3B2AX	200.0	0.01	46.16	61.0	1
3B2BX	200.0	0.01	45.99	61.0	1
3C0AX	0.24	0.00001	66.08	71.0	1
3C1AX	2.40	0.0001	65.31	71.0	1
3C1BX	2.40	0.0001	66.07	71.0	1
3C2AX	240.0	0.01	66.08	71.0	1
3C2BX	240.0	0.01	65.31	71.0	1

Table 3.52

Number of Performed Beam Tests
Channel Sections Having Unstiffened Compression Flanges
(35XF Sheet Steel)

Spec.	Test Speed (in./min.)	Strain Rate (in./in./sec.)	w/t	Full Length (in.)	No. of Tests Performed
4A0A	0.043	0.00001	9.28	41.0	1
4A1A	0.43	0.0001	9.16	41.0	1
4A1B	0.43	0.0001	9.16	41.0	1
4A2A	43.0	0.01	9.22	41.0	1
4A2B	43.0	0.01	9.03	41.0	1
4B0A	0.045	0.00001	15.13	47.0	1
4B1A	0.45	0.0001	15.16	47.0	1
4B1B	0.45	0.0001	14.93	47.0	1
4B2A	45.0	0.01	15.04	47.0	1
4B2B	45.0	0.01	15.16	47.0	1
4C0A	0.082	0.00001	20.93	69.0	1
4C1A	0.82	0.0001	20.99	69.0	1
4C1B	0.82	0.0001	20.93	69.0	1
4C2A	82.0	0.01	20.99	69.0	1
4C2B	82.0	0.01	20.93	69.0	1

Table 3.53

Number of Performed Beam Tests
Channel Sections Having Unstiffened Compression Flanges
(50XF Sheet Steel)

Spec.	Test Speed (in./min.)	Strain Rate (in./in./sec.)	w/t	Full Length (in.)	No. of Tests Performed
4A0AX	0.075	0.00001	8.83	35.0	1
4A1AX	0.75	0.0001	8.78	35.0	1
4A1BX	0.75	0.0001	8.84	35.0	1
4A2AX	75.0	0.01	8.83	35.0	1
4A2BX	75.0	0.01	8.85	35.0	1
4B0AX	0.12	0.00001	15.28	45.0	1
4B1AX	1.20	0.0001	15.31	45.0	1
4B1BX	1.20	0.0001	15.31	45.0	1
4B2AX	120.0	0.01	15.39	45.0	1
4B2BX	120.0	0.01	15.35	45.0	1
4C0AX	0.17	0.00001	20.48	63.0	1
4C1AX	1.70	0.0001	20.48	63.0	1
4C1BX	1.70	0.0001	20.50	63.0	1
4C2AX	170.0	0.01	20.57	63.0	1
4C2BX	170.0	0.01	20.54	63.0	1

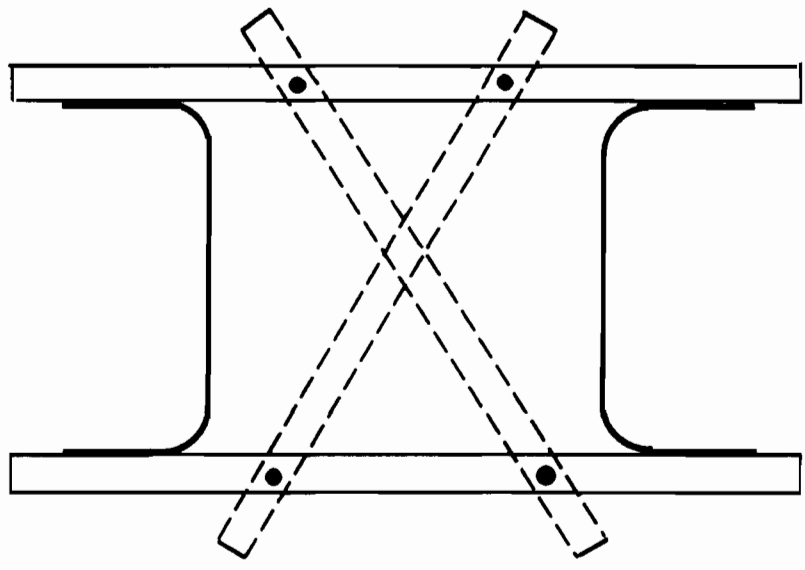

Figure 3.52 Configuration of Beam Test Specimens for Members with Unstiffened Compression Flanges

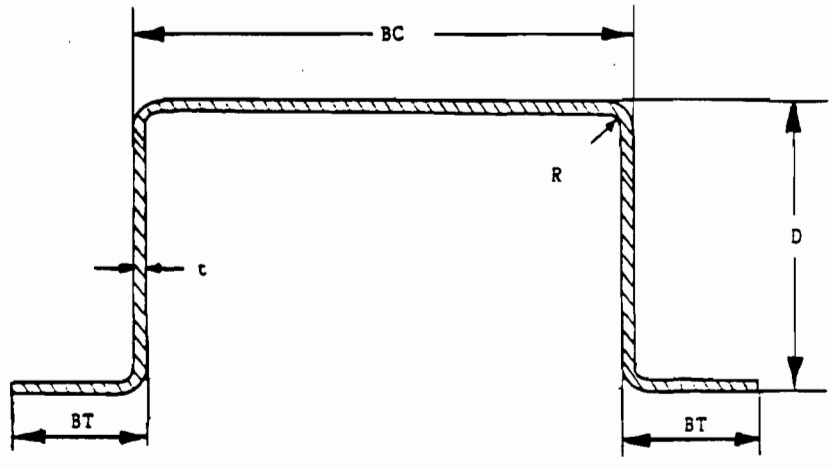

Figure 3.53 Hat Sections Used for Beam Tests

Based on the material test results, empirical equations used to predict material properties are presented in Section IV. The yield strength, tensile strength, and proportional limit were used to evaluate the strength of structural members.

2. Beam Tests for Stiffened Elements.

a. Specimens. Beam tests were used to study the local buckling and postbuckling strengths of compression elements. In order to investigate the behavior and strength of stiffened compression elements, the webs of hat-shaped beam specimens were designed to be fully effective without web crippling according to the AISI Specification[66]. The lengths of beam specimens were designed to be long enough to prevent shear lag effects.

Prior to April 1990, a total of 15 hat-shaped beam specimens fabricated from 35XF sheet steel were tested and reported in the Thirteenth Progress Report[16]. These specimens have stiffened elements with w/t ratios ranging from 29.05 to 76.64. Since March 1991, a total of 15 hat-shaped beam specimens were fabricated from 50XF sheet steel and tested to study the local buckling and postbuckling strengths of stiffened elements with w/t ratios ranging from 26.28 to 66.08. Tables 3.54 and 3.55 give the span lengths and dimensions of beam test specimens fabricated from 35XF and 50XF sheet steels, respectively. Figure 3.53 shows the hat-shaped beam specimens used for beam tests.

As shown in Figure 3.54, T-sections were used in the tests at loading points (one-eighth of span length) to prevent web crippling failure. Six 1/4-in. dia., high strength bolts were used to connected each T-section to each web of beam specimens. Three aluminum bars were connected to the

tension flanges at midspan and quarter points to prevent hat section from opening. Additional aluminum bars were placed close to the bearing plates at both ends of beam specimens.

b. Strain Measurements. Twelve (12) foil strain gages were mounted on each individual hat-shaped beam specimen. The arrangements of strain gages are shown in Figure 3.55. Three paired strain gages (No. 1-2, 3-4, and 9-10) were mounted along the longitudinal centerline of compression flange. The paired strain gages (No. 3-4) were placed at midspan of beam specimens. The other two paired strain gages (No. 1-2 and 9-10) were placed at a distance equal to the overall width of the stiffened compression flange on each side of the midspan of specimens. The load-strain diagrams obtained from these three paired strain gages were used to determine the local buckling load by means of the modified strain reversal method, which is discussed in Reference 97.

Strain gages (No. 5 and 6) placed along both edges of stiffened compression flange were used to measure edge strains for determining the strain rate used in the test. Strain gages (No. 7 and 8) placed on the top of webs were used to study the distribution of compressive stress in the web. Strain gages (No. 11 and 12) placed along the edges of tension flanges were used to determine the yield moment of specimen and to study the shift of the neutral axis during the test.

c. Instrumentation and Test Procedure. All beam tests were performed by using the same 880 Material Test System described in previous sections. For all tests, the maximum load range of 20 kips and the maximum stroke ranges of 2.5 and 1.0 inches were selected for the function generator of the test machine. The ramp time was programmed to have a

Table 3.54

Dimensions of Beam Specimens with Stiffened Flanges
(35XF Sheet Steel)

Spec.	BC (in.)	D (in.)	BT (in.)	t (in.)	w/t	Span Length (in.)
3A0A	2.960	1.510	1.010	0.085	29.15	43.00
3A1A	3.033	1.462	1.012	0.085	30.00	43.00
3A1B	3.020	1.477	1.017	0.085	29.85	43.00
3A2A	2.952	1.515	1.020	0.085	29.05	43.00
3A2B	3.047	1.470	1.012	0.085	30.17	43.00
3B0A	5.235	2.445	1.235	0.085	55.91	73.00
3B1A	5.167	2.460	1.255	0.085	55.11	73.00
3B1B	5.235	2.435	1.230	0.085	55.91	73.00
3B2A	5.227	2.435	1.220	0.085	55.82	73.00
3B2B	5.240	2.440	1.232	0.085	55.97	73.00
3C0A	6.957	2.926	1.490	0.085	76.17	91.00
3C1A	6.997	2.947	1.483	0.085	76.64	91.00
3C1B	6.991	2.954	1.481	0.085	76.57	91.00
3C2A	6.995	2.934	1.483	0.085	76.62	91.00
3C2B	6.945	2.945	1.485	0.085	76.03	91.00

Table 3.55

Dimensions of Beam Specimens with Stiffened Flanges
(50XF Sheet Steel)

Spec.	BC (in.)	D (in.)	BT (in.)	t (in.)	w/t	Span Length (in.)
3A0AX	2.490	1.250	0.769	0.077	26.28	37.0
3A1AX	2.532	1.256	0.757	0.077	26.82	37.0
3A1BX	2.529	1.263	0.757	0.077	26.79	37.0
3A2AX	2.532	1.258	0.757	0.077	26.82	37.0
3A2BX	2.523	1.242	0.767	0.077	26.71	37.0
3B0AX	4.014	1.999	1.006	0.077	46.07	57.0
3B1AX	4.016	1.989	1.028	0.077	46.10	57.0
3B1BX	4.017	1.994	1.028	0.077	46.11	57.0
3B2AX	4.021	1.990	1.036	0.077	46.16	57.0
3B2BX	4.008	1.996	1.029	0.077	45.99	57.0
3C0AX	5.555	2.505	1.260	0.077	66.08	67.0
3C1AX	5.495	2.508	1.275	0.077	65.31	67.0
3C1BX	5.554	2.498	1.258	0.077	66.07	67.0
3C2AX	5.555	2.465	1.295	0.077	66.08	67.0
3C2BX	5.495	2.503	1.258	0.077	65.31	67.0

Note : * For symbols of dimensions, see Figure 3.53.

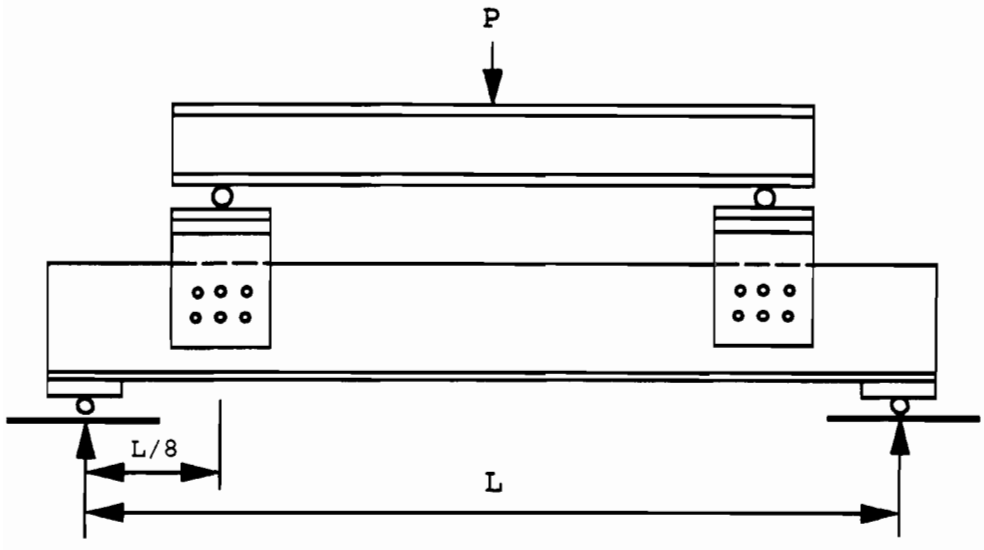

(Test Setup)

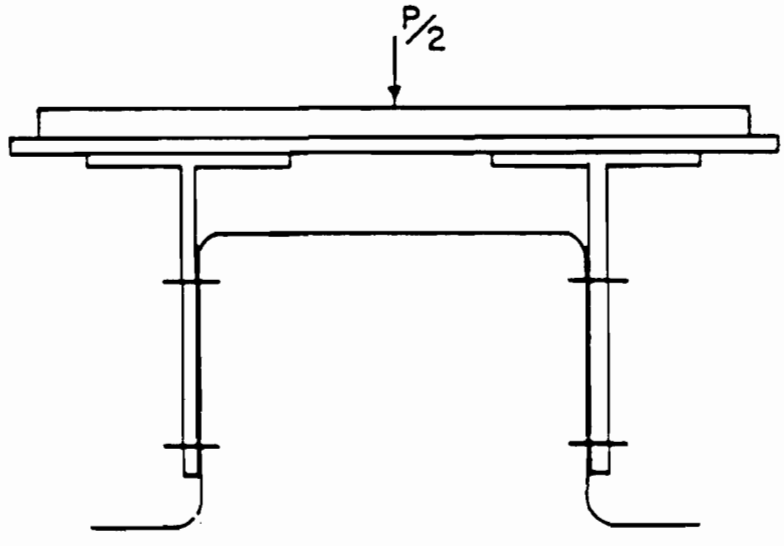

(Detail at Loading Points)

Figure 3.54 Test Setup for Beams with a Stiffened Flange

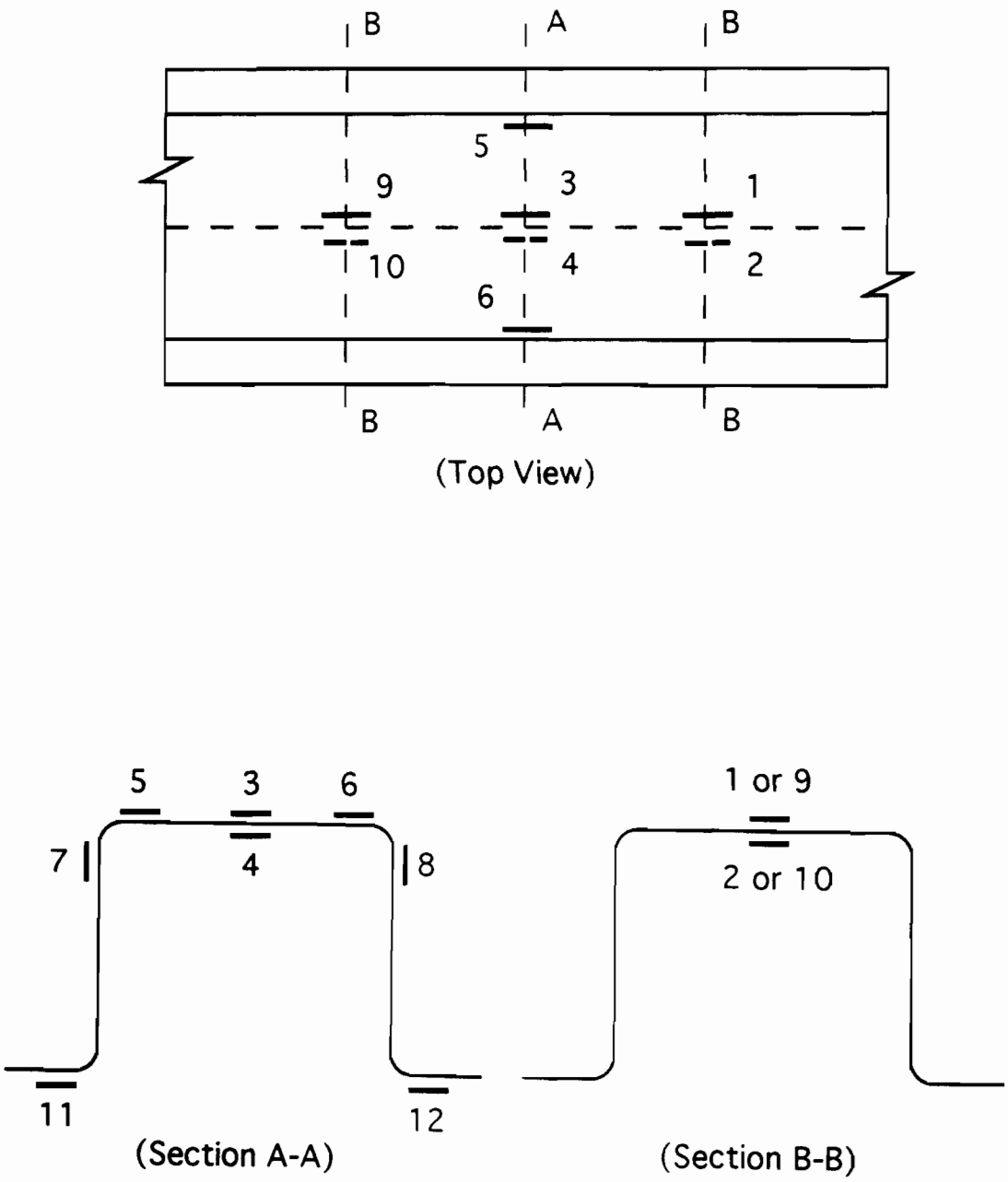

Figure 3.55 Locations of Strain Gages on Hat Sections

constant speed in accordance with the calculated strain rate for each beam specimen.

Figure 3.56 shows the test setup for beam specimens. The beam was simply supported and the load was applied from the lower compression platen to the specimen. The tension flanges at both ends of the beam specimens are clamped to 4-inch wide bearing plates. Two wooden blocks were placed between beam webs at both ends of beam specimens. Two LVDT (Linear Variable Differential Transformer) were used at midspan to measure the beam deflections and to check any rotation of beam specimens during the test. The applied load, actuator displacement, strains from 12 strain gage outputs, and the deflections from two LVDT outputs were recorded and stored in the CAMAC memory. After the data were acquired, it was downloaded to the Data General MV-10000 Computer for analysis purpose.

d. Test Results. The failure mode of the beam specimens varies with the width-to-thickness ratio of the stiffened compression flange. The local buckling load was detected based on the load-strain diagram obtained from the paired strain gages attached back to back along the longitudinal centerline of the stiffened flange. As shown in Figure 3.57, no local buckling occured in specimens with small w/t ratios. The local buckling occured in the elastic range for the specimens having large w/t ratios. After local buckling occurred in the test specimen, the stresses in the compression flange redistributed across the flange until edge stresses reached to the maximum. A typical local buckling pattern of the stiffened compression flange during the test is shown in Figure 3.58. For the

specimen with a large w/t ratio, the typical load-strain relationship is shown in Figure 3.59.

Two typical load-displacement relationships are shown in Figures 3.60 to 3.61 for beam specimens fabricated from 35XF sheet steel and tested under different strain rates. The average w/t ratios of compression flanges and the strain rates used in the tests are indicated in each figure. Similarly, Figures 3.62 to 3.64 show typical load-displacement diagrams for hat-shaped beam specimens fabricated from 50XF sheet steel. Figure 3.65 shows the positions of the neutral axis determined from strain gage readings of a compact section (Specimen 3A0A). It can be seen that the neutral axis remained the same position as long as the stress in the cross section was in the elastic range. The neutral axis shifted away from the bottom flange when the tensile strain in the bottom flange of the hat-shaped beam exceeded its yield strain. The load-deflection diagram can be obtained from the LVDT readouts. As expected, beam deflection increased linearly corresponding to the applied load in the early stage of tests. The nonlinear load-defection relationship was noted when (1) local buckling occured in the compression flange (specimens with medium or large w/t ratios) or (2) yield point reached in the tension flange (specimens with small w/t ratios). A constant speed was applied to the test specimen during the test. Similar to load-deflection relationship, the strain rate could not be retained constant when the specimen attained the aforementioned conditions. Therefore, the value of strain rate was defined by a linear portion of the slope of the strain-time curve. A typical strain-time diagram is

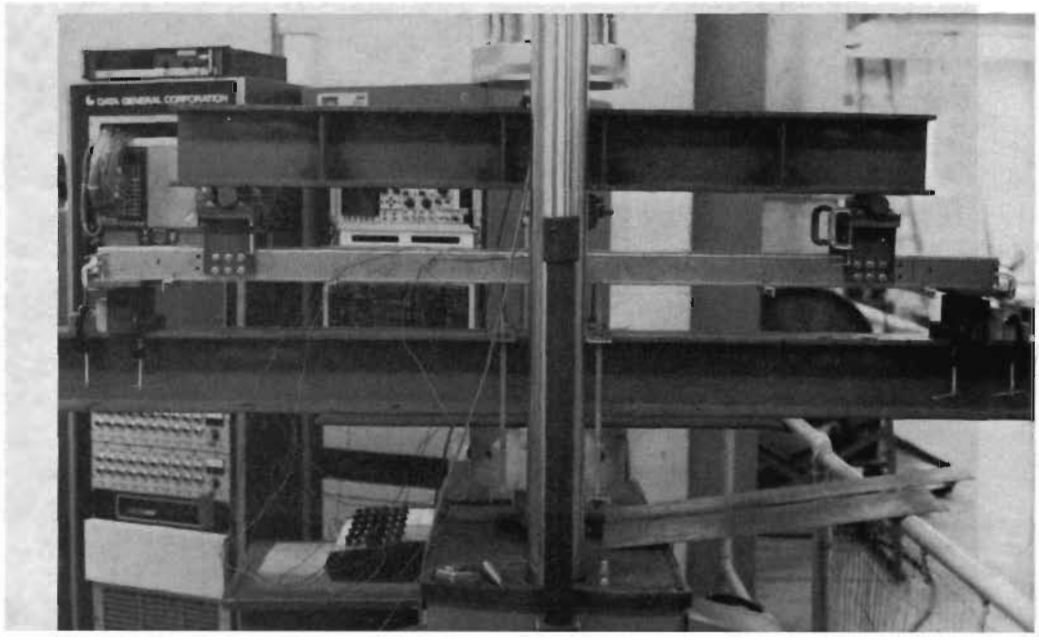

Figure 3.56 Photograph of Test Setup for Hat-Shaped Beam Specimens

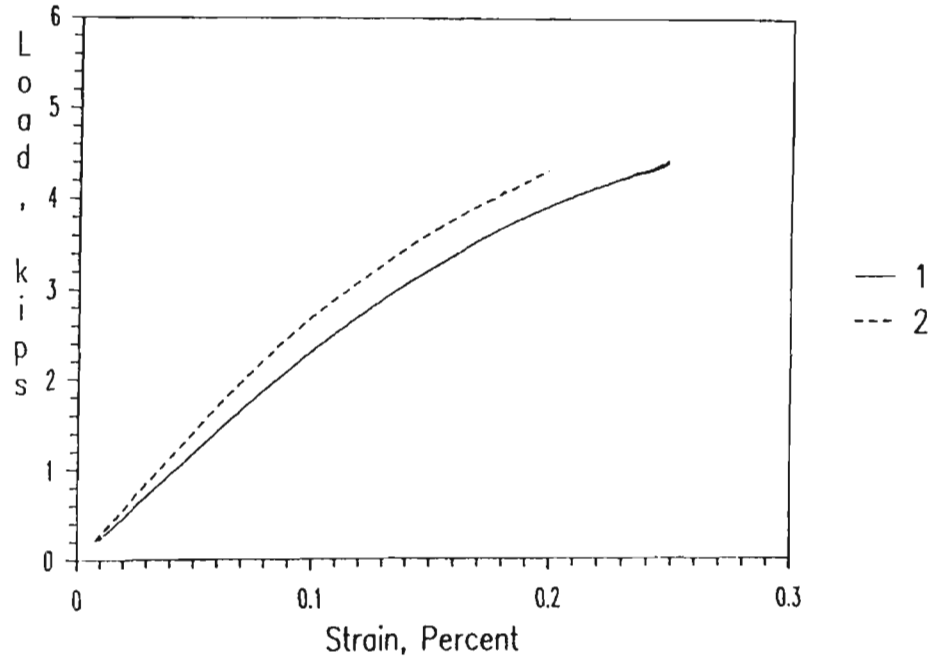

Figure 3.57 Load-Strain Curves of Strain Gages # 1 and 2 Installed at the Center of the Stiffened Flange (Spec. 3A1BX)

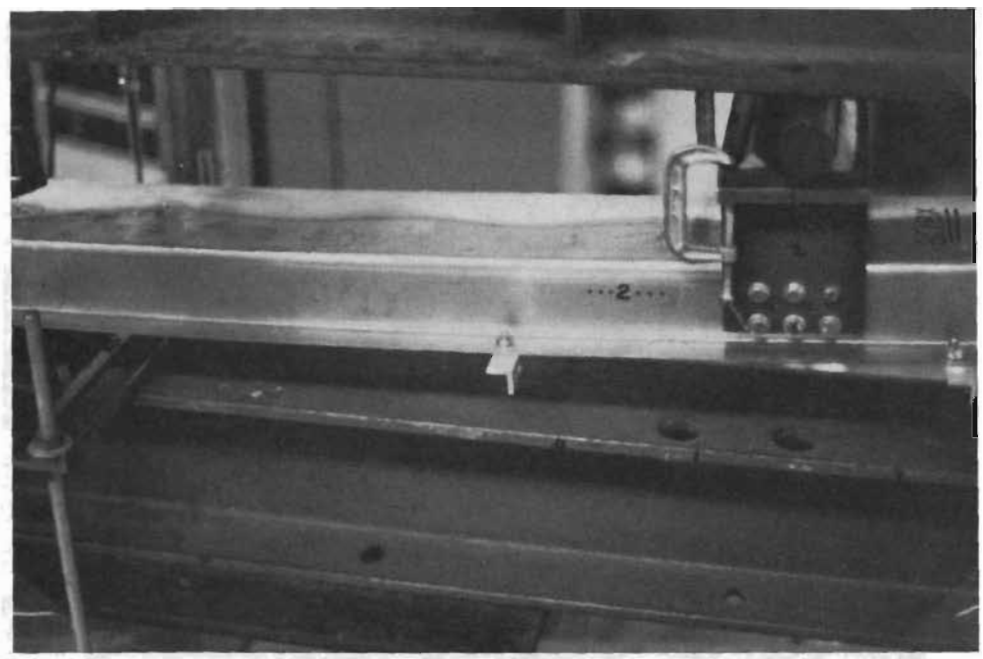

Figure 3.58 Development of Stiffened Flange Buckling Waves During a Medium Speed Test

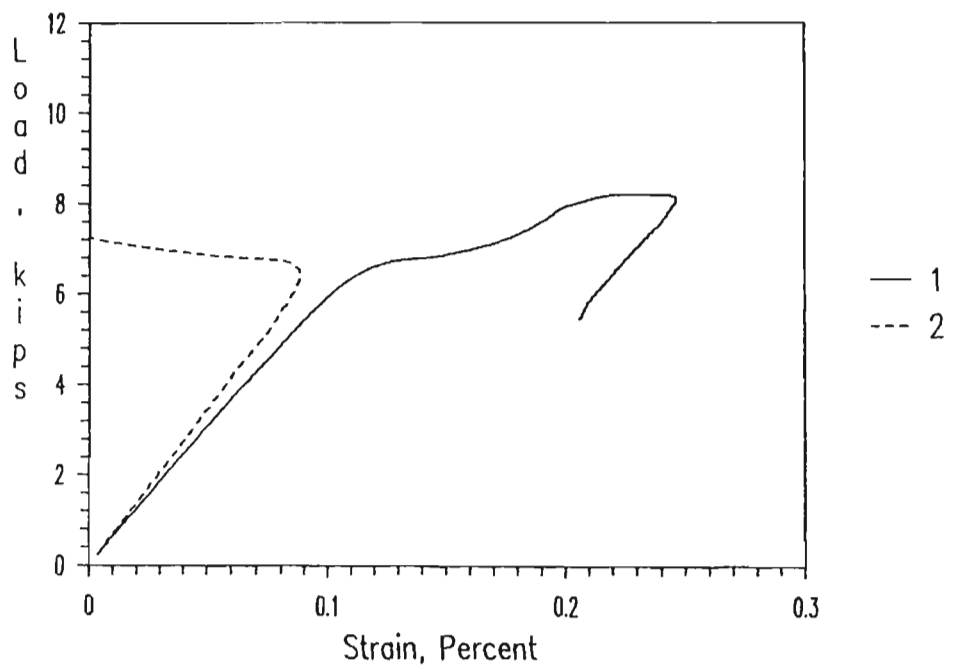

Figure 3.59 Load-Strain Curves of Strain Gages # 1 and 2 Installed at the Center of the Stiffened Flange (Spec. 3C1BX)

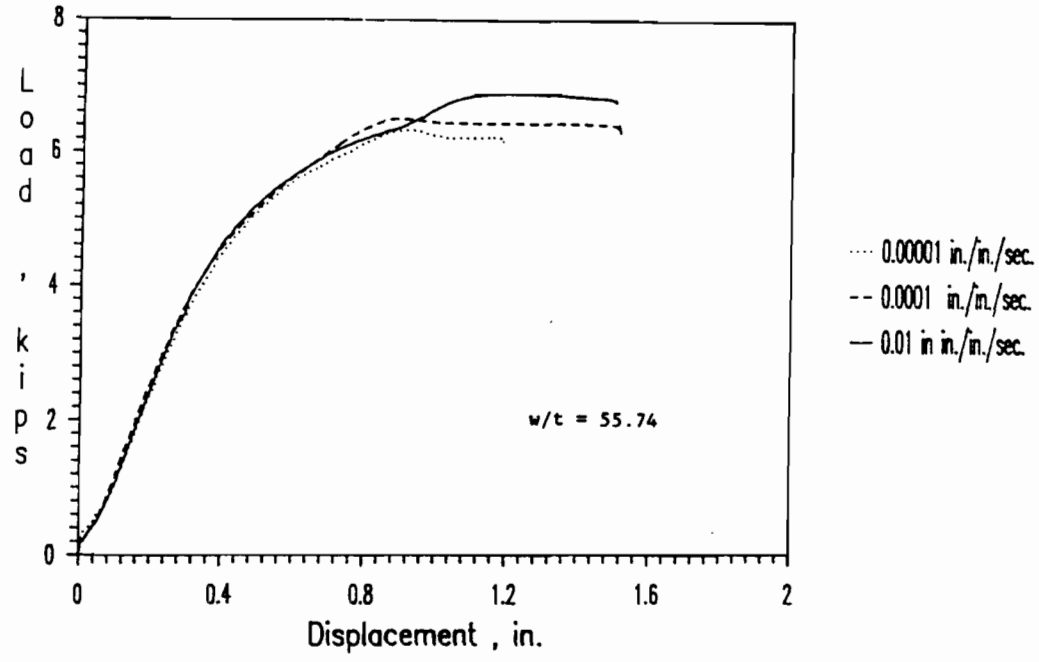

Figure 3.60 Load-Displacement Curves for Hat-Shaped Beam Specimens 3B0A, 3B1A, and 3B2A

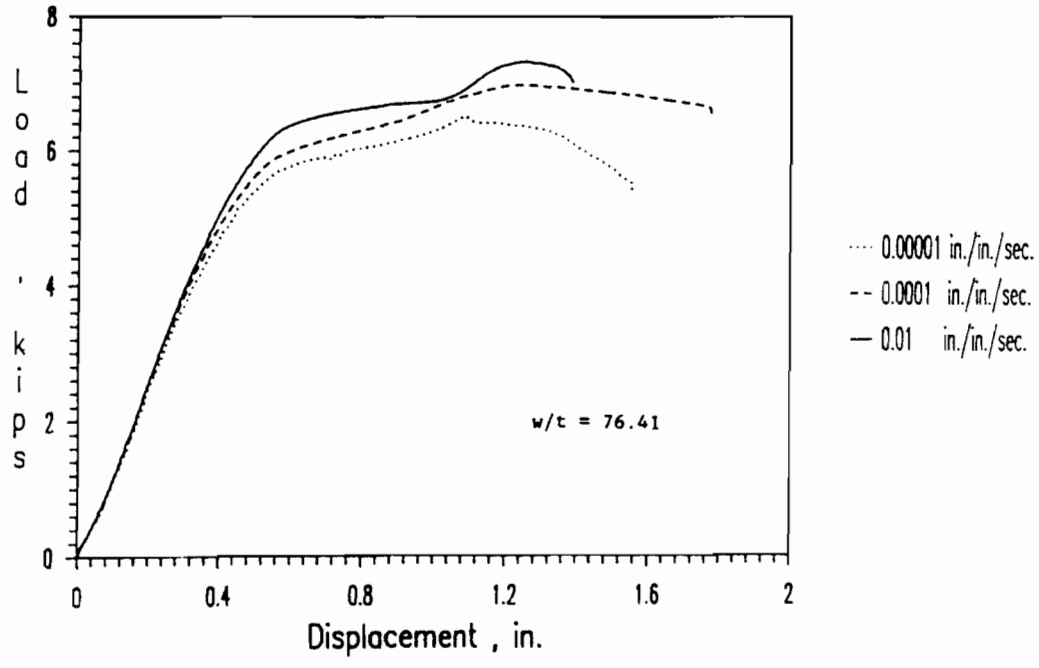

Figure 3.61 Load-Displacement Curves for Hat-Shaped Beam Specimens 3C0A, 3C1A, and 3C2A

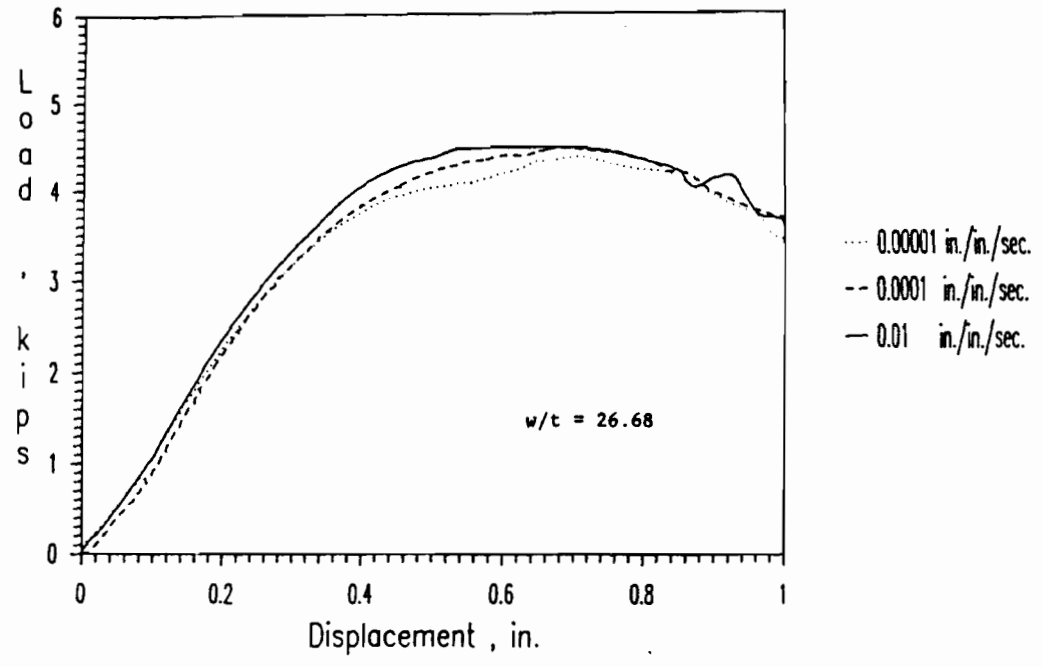

Figure 3.62 Load-Displacement Curves for Hat-Shaped Beam Specimens 3A0AX, 3A1AX, and 3A2AX

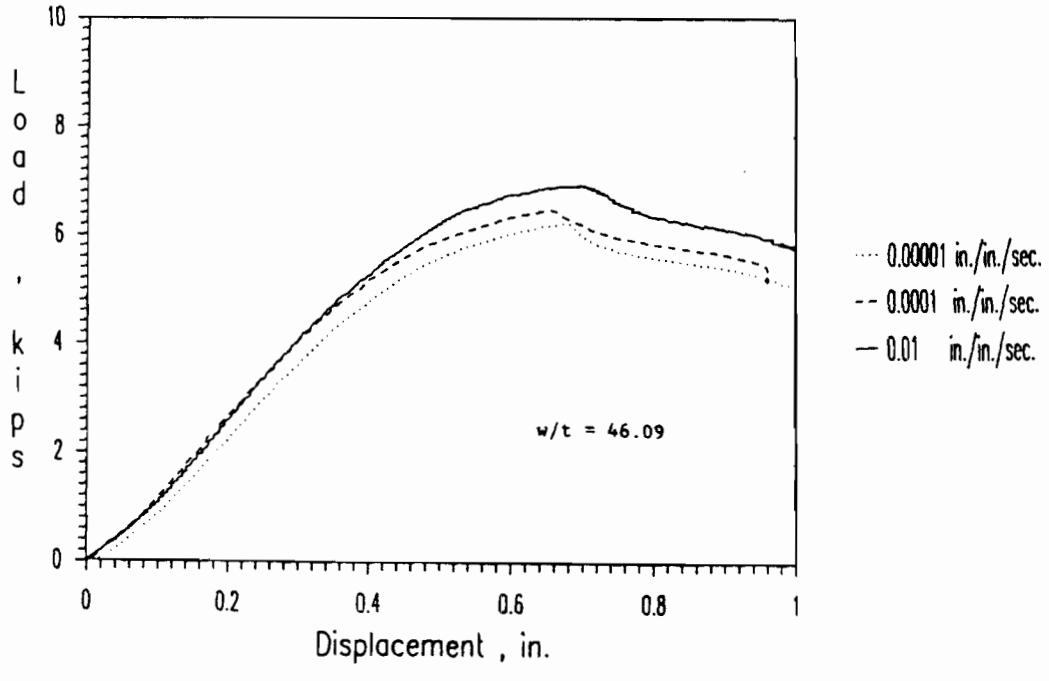

Figure 3.63 Load-Displacement Curves for Hat-Shaped Beam Specimens 3B0AX, 3B1AX, and 3B2BX

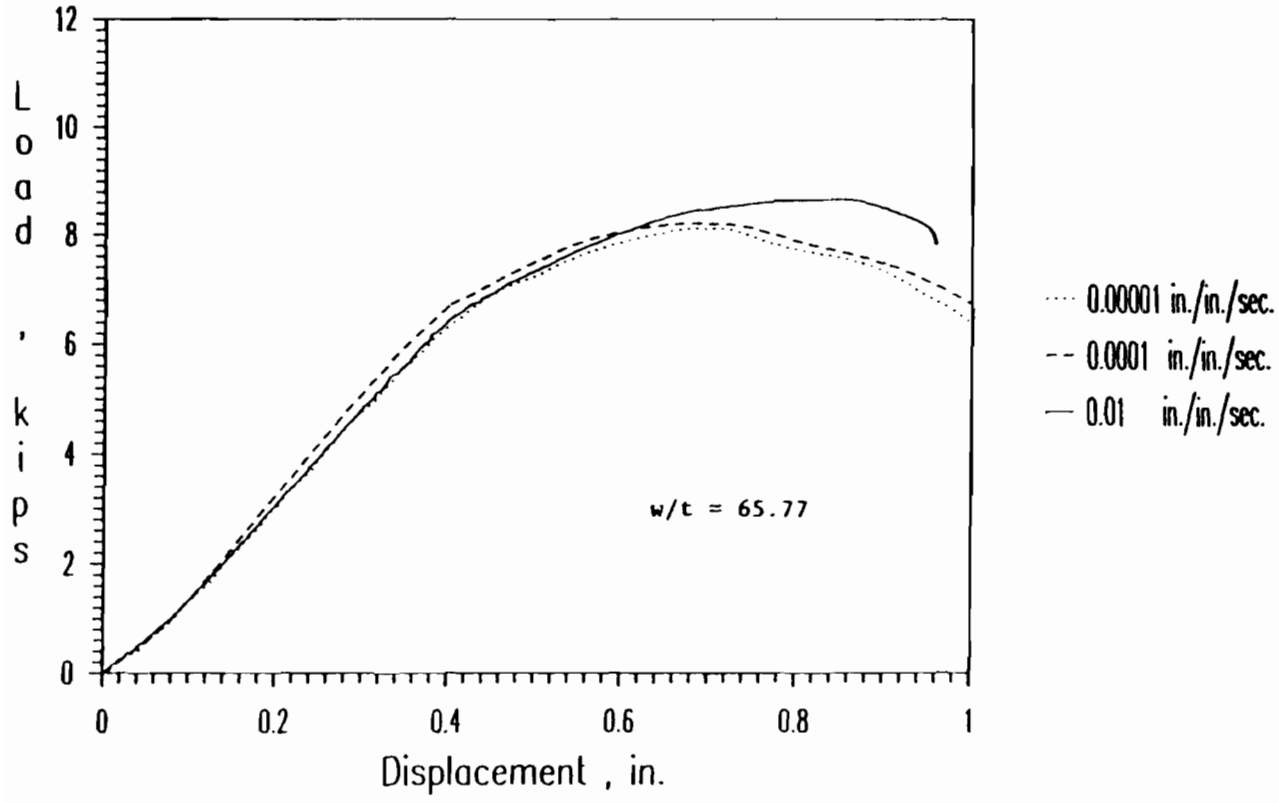

Figure 3.64 Load-Displacement Curves for Hat-Shaped Beam Specimens 3C0AX, 3C1BX, and 3C2AX

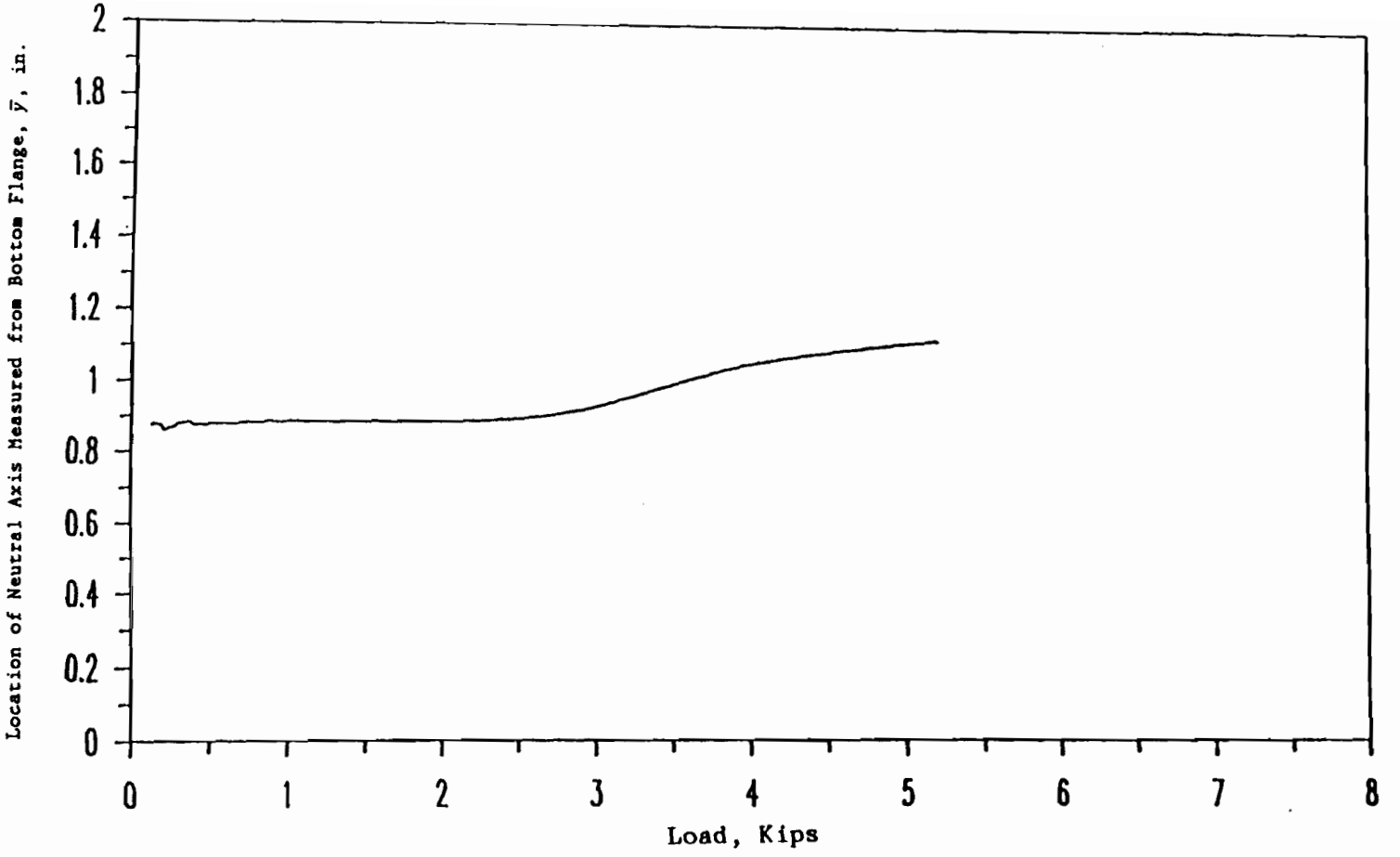

Figure 3.65 Typical Plot of Load vs. Location of Neutral Axis for a Beam with a Stiffened Flange (Spec. 3A0A)

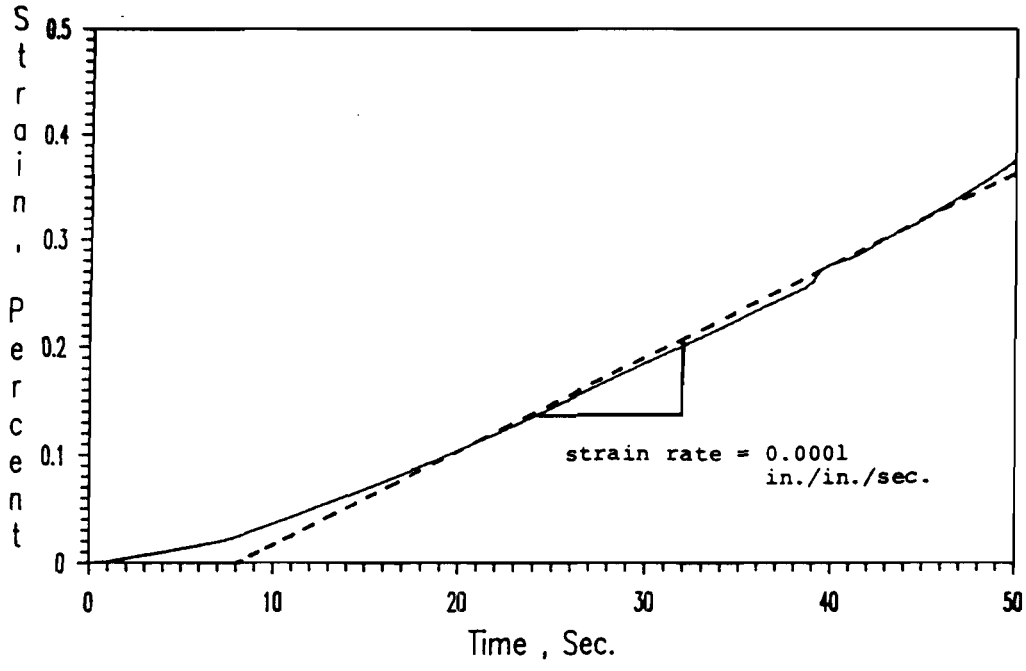

Figure 3.66 Typical Plot of Strain-Time Relationship for a Hat-Shaped Beam Specimen Under a Strain Rate of 10^{-4} in./in./sec. (Spec. 3A1AX)

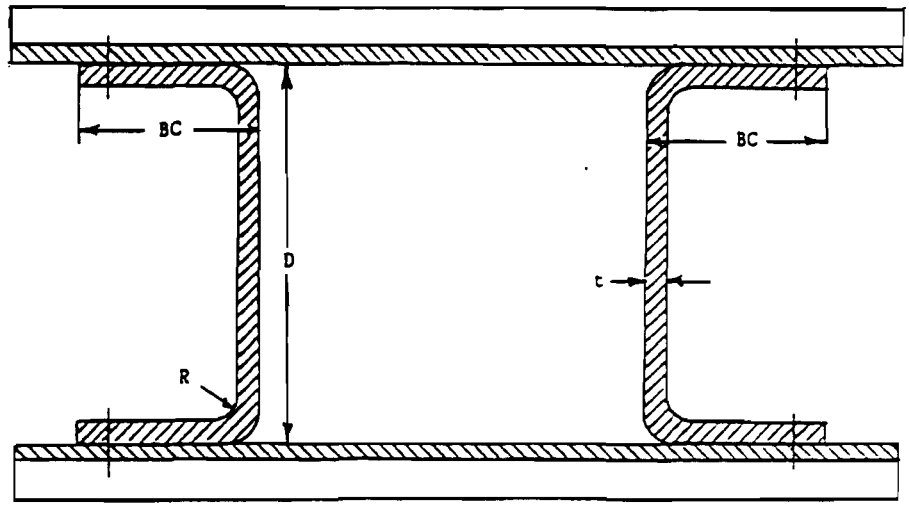

Figure 3.67 Cross Sections of Channel Beams Used for the Study of Unstiffened Elements

shown in Figure 3.66. The tested critical load , yield load, and ultimate load for each beam specimen are presented in Section IV.

3. Beam Tests for Unstiffened Elements.

a. Specimens. In this phase of experimental investigation, beam specimens using channel sections made of 35XF and 50XF sheet steels were tested to study the local buckling and postbuckling strengths of unstiffened elements affected by strain rate. The webs of channel sections were designed to be fully effective without web crippling in accordance with the AISI Specification[66]. Figure 3.67 shows the cross section of beam test specimen. To prevent each channel specimen from lateral buckling, aluminum bars were used to connect two channel sections together to form the beam specimen. In order to reduce the influence of hole on the area of cross section, small-size, high strength bolts were used in the fabrication of beam specimens.

A total of 15 beam test specimens fabricated from 35XF sheet steel were tested and reported in the Thirteenth Progress Report[16]. These specimens had unstiffened compression flanges with w/t ratios from 9.03 to 20.99. In addition, 15 beam specimens were fabricated from 50XF sheet steel and tested to study the local buckling and postbuckling strengths of unstiffened elements with w/t ratios ranging from 8.78 to 20.57 since March 1991. Tables 3.56 and 3.57 give the span lengths and dimensions of all beam specimens fabricated from 35XF and 50XF sheet steels, respectively.

b. Strain Measurements. Eight (8) foil strain gages were placed at midspan of each specimen. Two paired strain gages (No. 1-2 and 5-6)

were mounted along the tips of unstiffened compression flanges for the purpose of determining the local buckling load. By using the modified strain reversal method, the critical local buckling load was obtained from load-strain relationships of these paired strain gages. Two strain gages (No. 3 and 4) were mounted on the supported edges of unstiffened compression flanges to measure the edge strains for determining the strain rate used for the test. The edge stresses of unstiffened compression flanges can be determined from these strain readings using the stress-strain diagram. Strain gages (No. 7 and 8) mounted along the edges of tension flanges were used to determine the yield load of the specimen and to study the shift of the neutral axis during the test. The locations of strain gages placed on beam specimens are shown in Figure 3.68.

c. Instrumentation and Test Procedure. The test setup for the beam specimens using channel sections is illustrated in Figure 3.69. The instrumentation and the test procedure used for this phase of study are the same as that used for the hat-shaped beam tests described in Section C, except that two 4-in. wide bearing plates were placed on the top of compression flanges at the location of one-eighth span length (loading points) from end supports. The tension flanges at both ends of the beam specimens are clamped to 4-in. wide bearing plates, and two wooden blocks were placed between the webs of two channel sections at each end of beam specimens. Same as hat-shaped beam specimens, two LVDT were used to measure the beam deflections and to monitor any rotation of beam specimens during the test.

Load range 3 with a maximum load equal to 20 kips and stroke range 3 with a maximum displacement equal to 1.0 in. were selected for the

Table 3.56

Dimensions of Beam Specimens with Unstiffened Flanges
(35XF Sheet Steel)

Spec.	BC (in.)	D (in.)	t (in.)	w/t	Span Length (in.)
4A0A	1.030	2.020	0.085	9.28	37.00
4A1A	1.020	2.007	0.085	9.16	37.00
4A1B	1.020	2.025	0.085	9.16	37.00
4A2A	1.025	2.012	0.085	9.22	37.00
4A2B	1.009	2.020	0.085	9.03	37.00
4B0A	1.527	2.517	0.085	15.13	43.00
4B1A	1.530	2.510	0.085	15.16	43.00
4B1B	1.510	2.530	0.085	14.93	43.00
4B2A	1.520	2.520	0.085	15.04	43.00
4B2B	1.530	2.510	0.085	15.16	43.00
4C0A	2.020	3.020	0.085	20.93	65.00
4C1B	2.025	3.010	0.085	20.99	65.00
4C1C	2.020	3.010	0.085	20.93	65.00
4C2A	2.025	3.030	0.085	20.99	65.00
4C2B	2.020	3.020	0.085	20.93	65.00

Table 3.57

Dimensions of Beam Specimens with Unstiffened Flanges
(50XF Sheet Steel)

Spec.	BC (in.)	D (in.)	t (in.)	w/t	Span Length (in.)
4A0AX	0.913	1.999	0.077	8.83	31.0
4A1AX	0.909	2.008	0.077	8.78	31.0
4A1BX	0.914	2.001	0.077	8.84	31.0
4A2AX	0.913	2.005	0.077	8.83	31.0
4A2BX	0.915	1.995	0.077	8.85	31.0
4B0AX	1.410	2.267	0.077	15.28	41.0
4B1AX	1.412	2.279	0.077	15.31	41.0
4B1BX	1.412	2.289	0.077	15.31	41.0
4B2AX	1.418	2.263	0.077	15.39	41.0
4B2BX	1.415	2.273	0.077	15.35	41.0
4C0AX	1.810	2.756	0.077	20.48	59.0
4C1AX	1.810	2.763	0.077	20.48	59.0
4C1BX	1.812	2.755	0.077	20.50	59.0
4C2AX	1.817	2.756	0.077	20.57	59.0
4C2BX	1.815	2.760	0.077	20.54	59.0

Note : * For symbols of dimensions, see Figure 3.66.

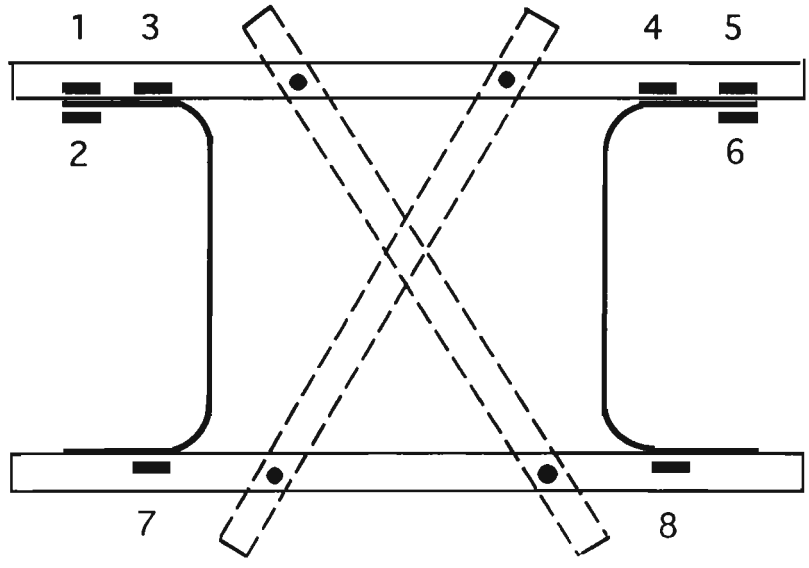

Figure 3.68 Locations of Strain Gages at Midspan Section of Channel Beams

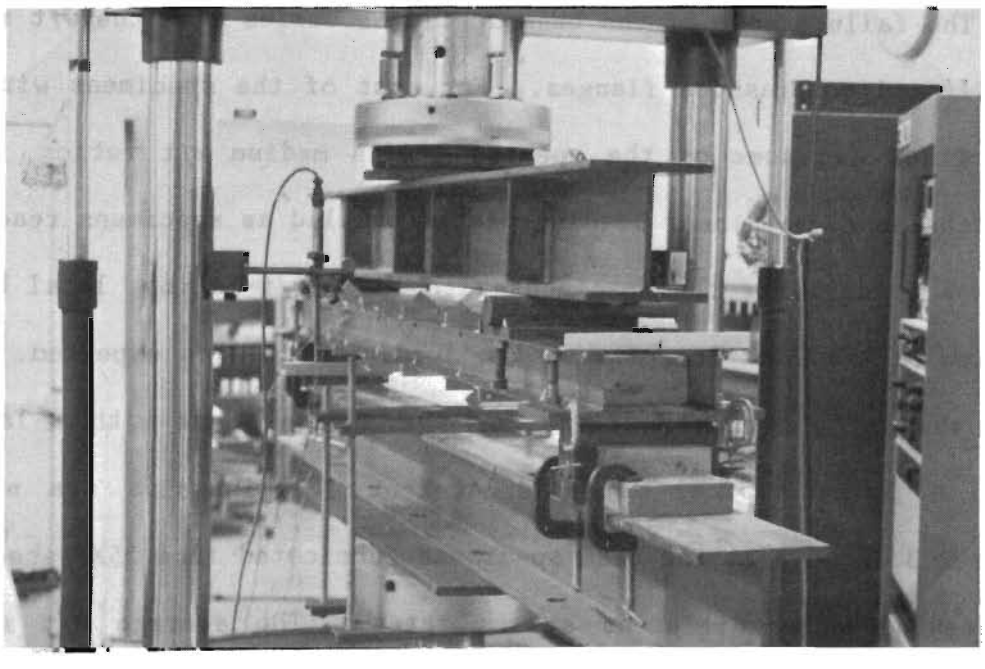

Figure 3.69 Photograph of Test Setup for Channel Beam Specimens

function generator of the 880 MTS test machine. To achieve a constant-speed test, the ramp time was programmed in accordance with the calculated strain rate for each beam specimen. The strain rates for all tests ranged from 10^{-5} to 10^{-2} in./in./sec..

d. Test Results. Similar to the beam tests for the study of stiffened compression elements, no local buckling occured in the unstiffened compression flanges of the specimens with small w/t ratios. For specimens fabricated from 35XF sheet steel with medium w/t ratios, the unstiffened flanges buckled locally in the inelastic range. The local buckling occured in the elastic range for specimens fabricated from 35XF sheet steel with large w/t ratios and specimens fabricated from 50XF sheet steel with medium and large w/t ratios. Typical load-strain relationships for the specimens with large w/t ratios is shown in Figure 3.70.

The failure mode of the beam specimens varies with the w/t ratio of unstiffened compression flanges. For most of the specimens with small w/t ratios and some of the specimens with medium w/t ratios, the top compression flanges near loading plates buckled as specimens reached the maximum loads. For the specimens with large w/t ratios, local buckling occured at the location between two loading points as expected. Figure 3.71 shows the typical failure for the channel beam with a large w/t ratio. Three typical load-displacement relationships are shown in Figures 3.72 to 3.74 for beam specimens fabricated from 35XF sheet steel and tested under different strain rates. The average w/t ratio of unstiffened compression elements and strain rates used in the tests are indicated in each figure. Similarly, Figures 3.75 to 3.77 show three typical load-displacement curves for beam specimens fabricated from 50XF

sheet steel. A typical strain-time curve for the medium strain rate is shown in Figure 3.78. The tested critical load and yield load for each beam specimen are presented and evaluated in Section IV.

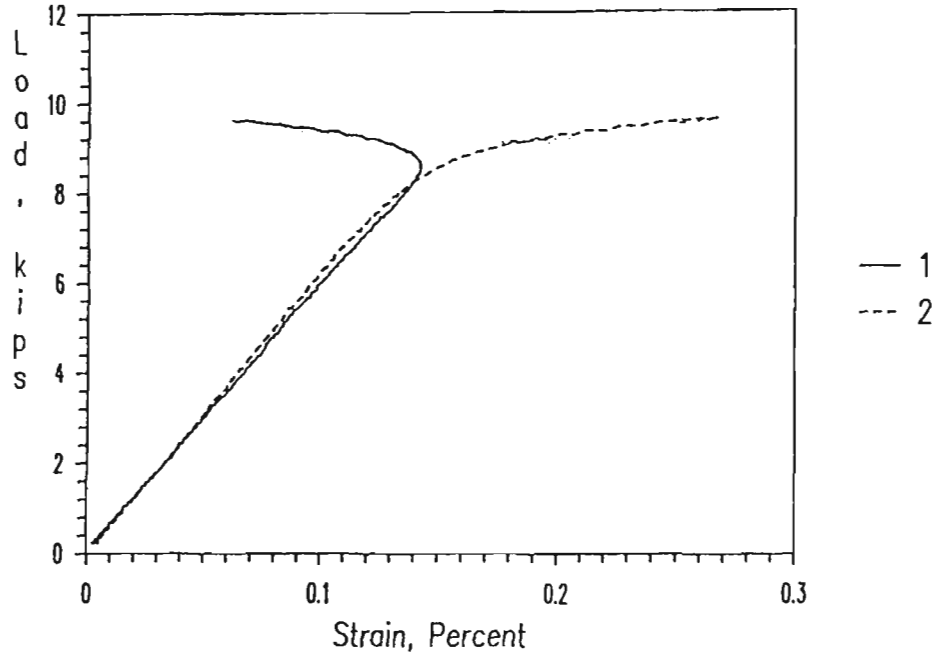

Figure 3.70 Load-Strain Curves of Strain Gages # 1 and 2 Installed at the Center of the Stiffened Flange (Spec. 4C2AX)

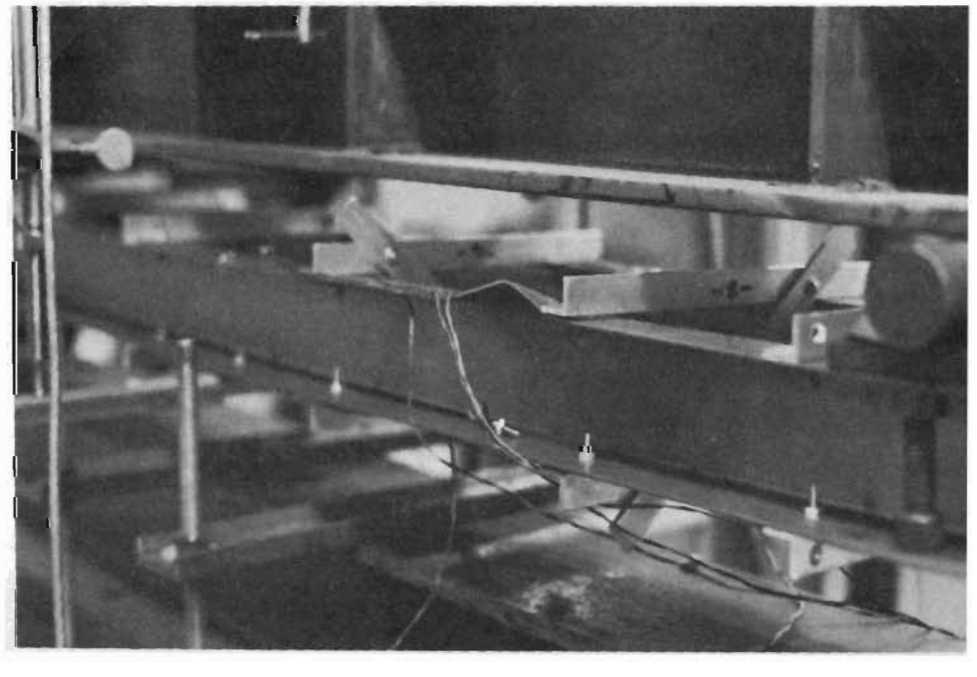

Figure 3.71 Typical Failure of Channel Beam Specimens

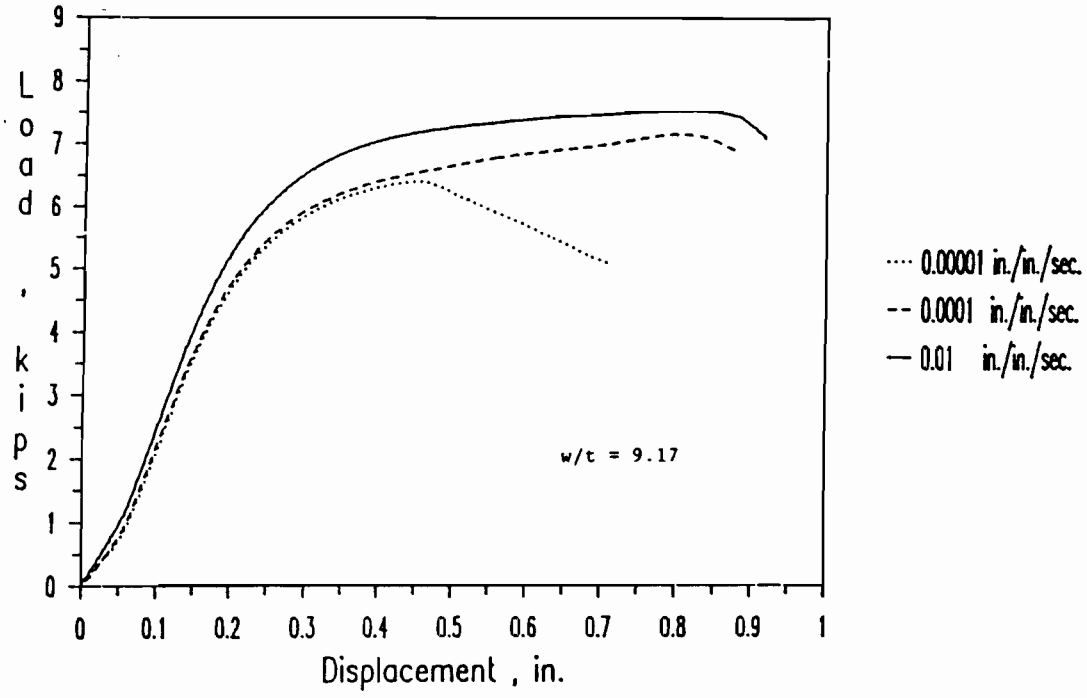

Figure 3.72 Load-Displacement Curves for Channel Beam Specimens 4A0A, 4A1A, and 4A2A

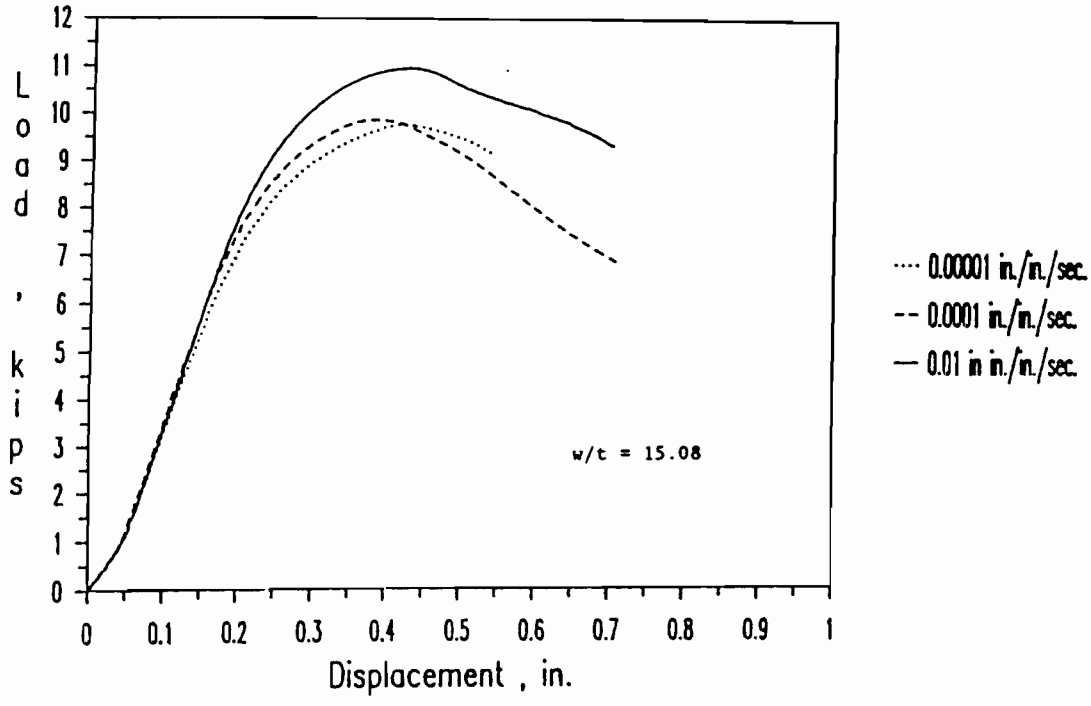

Figure 3.73 Load-Displacement Curves for Channel Beam Specimens 4B0A, 4B1A, and 4B2A

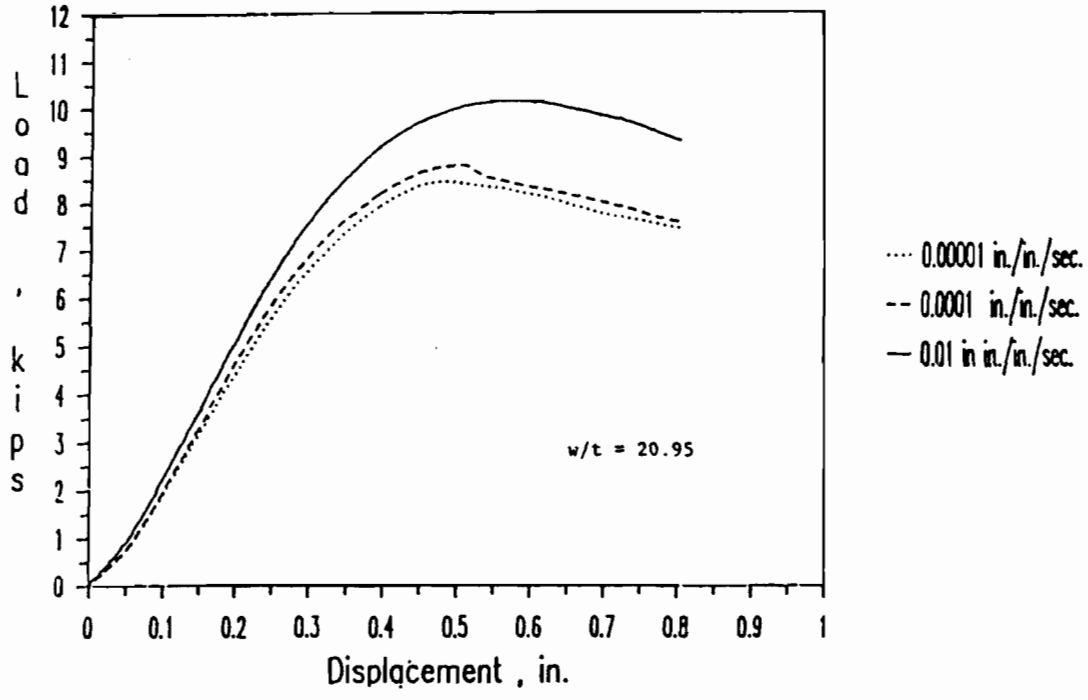

Figure 3.74 Load-Displacement Curves for Channel Beam Specimens 4C0A, 4C1A, and 4C2A

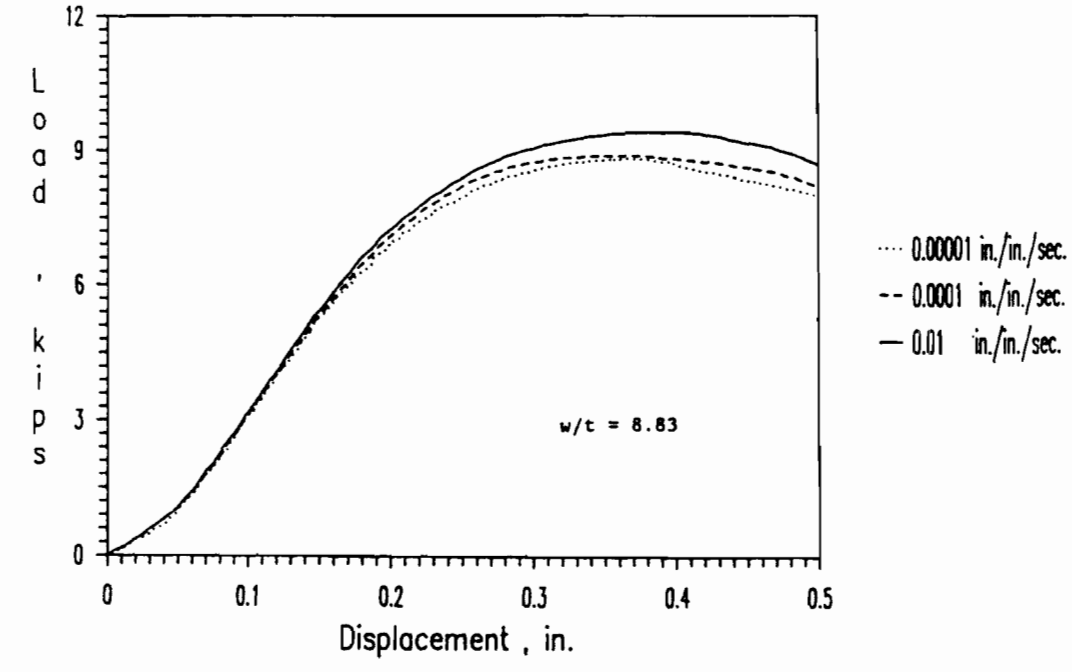

Figure 3.75 Load-Displacement Curves for Channel Beam Specimens 4A0AX, 4A1AX, and 4A2AX

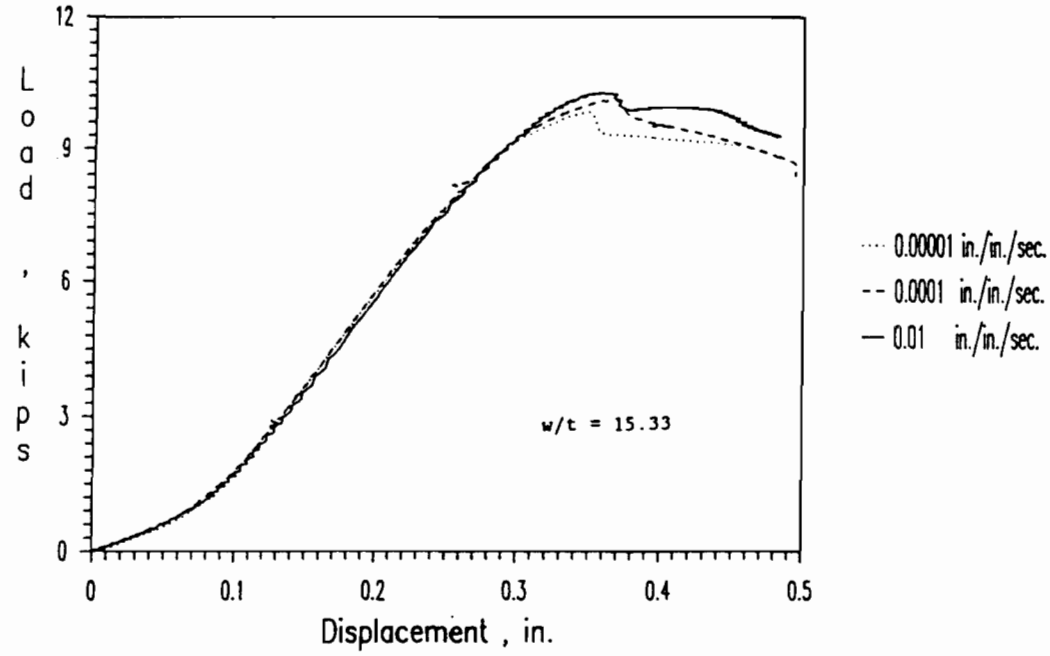

Figure 3.76 Load-Displacement Curves for Channel Beam Specimens 4B0AX, 4B1BX, and 4B2BX

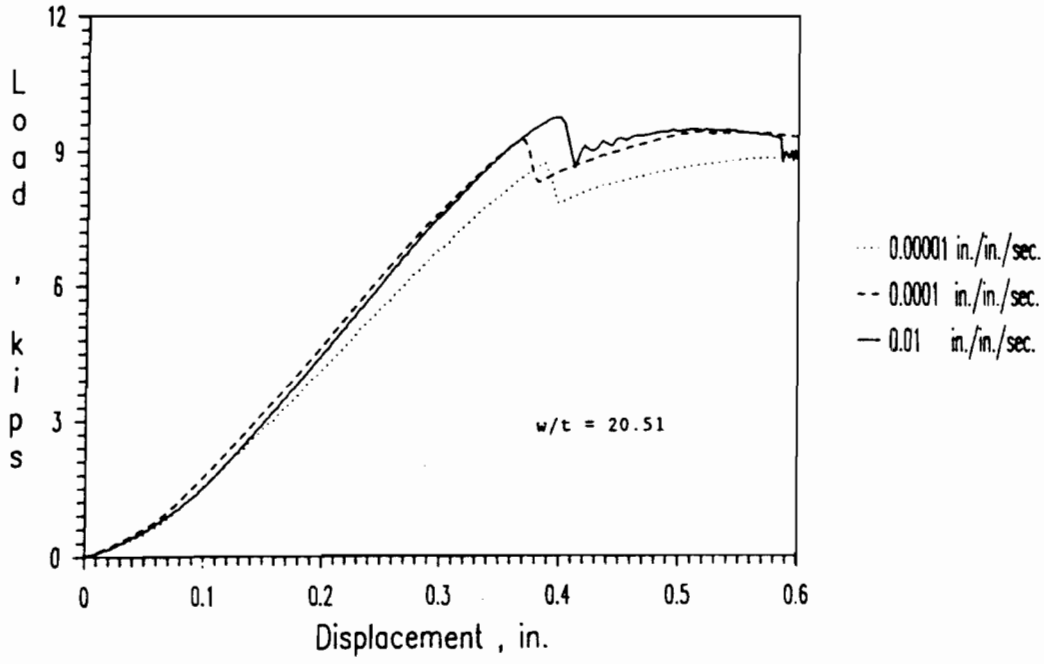

Figure 3.77 Load-Displacement Curves for Channel Beam Specimens 4C0AX, 4C1AX, and 4C2BX

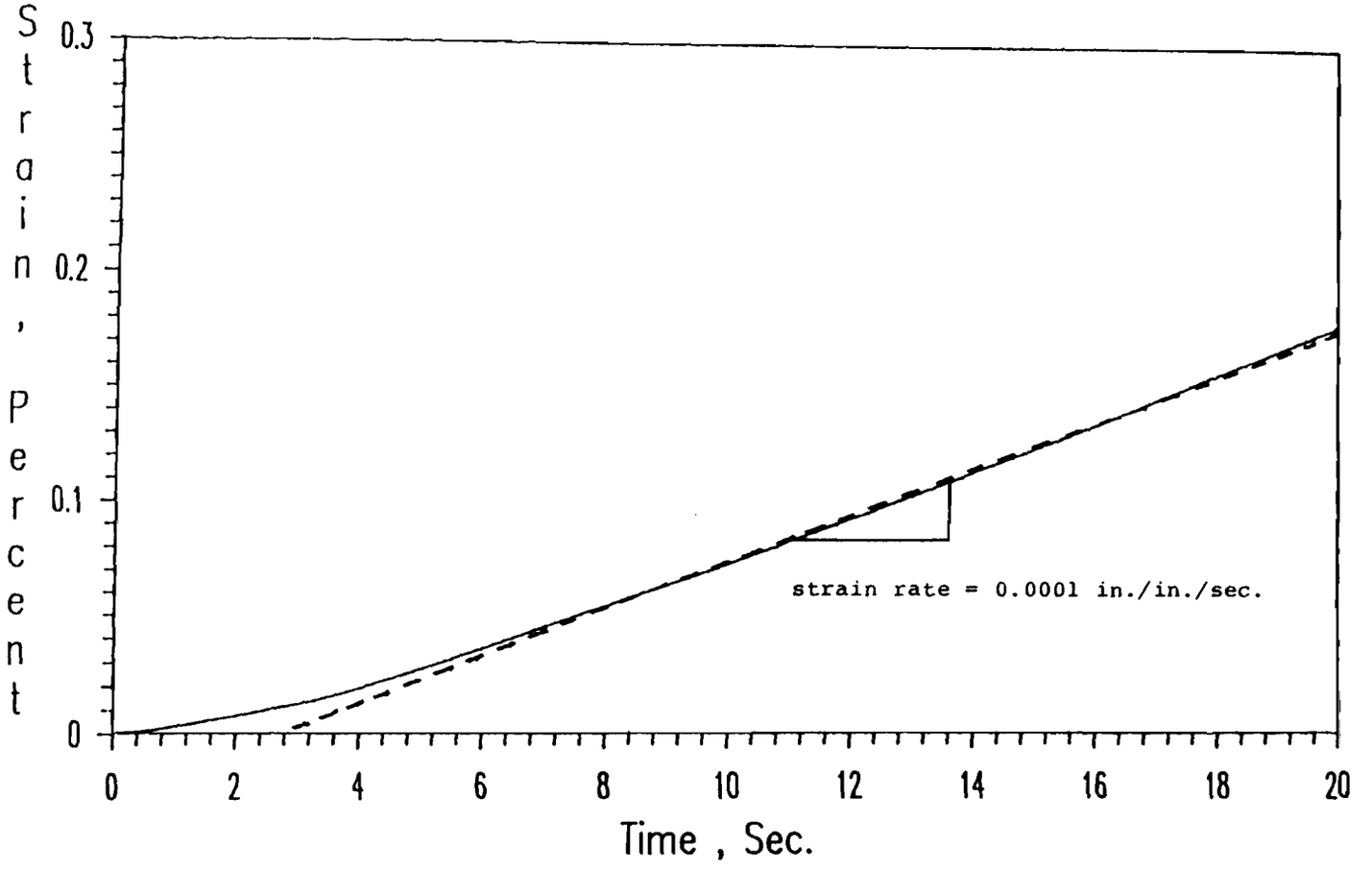

Figure 3.78 Typical Plot of Strain-Time Relationship for a Channel Beam Specimen Under a Strain Rate of 10^{-4} in./in./sec. (Spec. 4C1AX)

IV. EVALUATION OF EXPERIMENTAL DATA

A. GENERAL

The experimental program and tested results for both materials and structural members including stub columns and beams under different strain rates were presented in the Section III. In Section B of this section, the effects of strain rate on the mechanical properties for three selected sheet steels (35XF, 50XF, and 100XF) are discussed. The material properties of 35XF and 50XF sheet steels predicted by the newly developed empirical equations are used in the evaluation of structural member test data.

In Sections C and D of this section, the tested results of stub columns and beams fabricated from 35XF and 50XF sheet steels are evaluated, respectively. These test specimens were used to study the structural strengths of members having stiffened or unstiffened compression elements. Because the material properties and stress-strain relationships are influenced by strain rate, comparisons between the experimental results and the failure loads predicted by the current AISI Automotive Steel Design Manual using static and dynamic material properties are made. The purpose of this investigation was to determine the accuracy of the available effective design formulas by using dynamic material properties for the design of structural members subjected to dynamic loads.

B. EVALUATION OF MATERIAL TEST DATA

The materials used in the experimental program included virgin steels tested for tensile and compression and steels with different amounts of cold stretching used only for tensile tests. The tension and compression coupons were tested in both longitudinal and transverse directions under different strain rates. The strain rates varied from 10^{-4} to 1.0 in./in./sec.. In this study, the work was emphasized on the effect of strain rate on the mechanical properties of sheet steels, the strain-rate sensitivity, and the development of empirical equations on the basis of the test results.

1. Mechanical Properties. The test results indicated that mechanical properties are affected by the strain rate and the amount of cold stretching. It was found that most of the mechanical properties increased with increasing strain rate for these three types of sheet steels. The effect of strain rate on proportional limit, yield strength, and ultimate tensile strength are discussed in the subsequent sections.

a. Proportional Limit. From Tables 3.32 through 3.37, it can be seen that the proportional limit of sheet steels tested in compression increased with increasing strain rate. Even though the proportional limit was difficult to obtain from tensile tests, because of limited number of data points recorded by the MTS extensomter in the linear range of the stress-strain curves, the percentage increases in proportional limits for the three sheet steels tested in longitudinal and transverse compression were found to be: 13% and 24% for 35XF sheet steel, 4% and 22% for 50XF sheet steel, and 24% and 9% for 100XF sheet steel when the strain rate increased from 10^{-4} to 10^{-2} in./in./sec..

b. Yield Strength. Similar to the effect of strain rate on proportional limit, the yield strength of sheet steels increased with increasing strain rate. Table 4.1 compares the dynamic tension yield stresses, $(F_y)_d$, determined at the strain rate of 1.0 in.in./sec. with the static tension yield stresses, $(F_y)_s$, determined at the strain rate of 10^{-4} in./in./sec.. Similarly, Table 4.2 shows the comparison between dynamic yield stresses and static yield stresses in compression. It can be seen from these tables that the values of $(F_y)_d/(F_y)_s$ ratio in longitudinal tension or compression are similar to the those in transverse tension or compression for each virgin sheet steel. However, for 35XF sheet steel tested in compression the values of $(F_y)_d/(F_y)_s$ ratio in transverse direction is larger than that in the longitudinal direction. The effect of the strain rate on yield strength decreases as the static yield stress and/or the amount of cold stretching of sheet steel increases.

It was noted that the percentage increases in proportional limit obtained from the compression tests are larger than the percentage increases in yield stress when the strain rate was increased from 10^{-4} to 1.0 in./in./sec.. Previous study[98] indicated that the increase in yield strength due to cold work is caused mainly by strain hardening and strain aging. However, in the present investigation no significant increase in yield strength was observed due to the strain aging effect.

c. Ultimate Tensile Strength. Comparisons between dynamic ultimate tensile strength to static ultimate tensile strength are also shown in Table 4.1. Similar to the effect of strain rate on yield strength, the

Table 4.1

Ratios of Dynamic to Static Mechanical Properties
for Three Sheet Steels

Type of Sheet Steel	$(F_y)_d/(F_y)_s$	$(F_u)_d/(F_u)_s$	$(\text{Elong.})_d/(\text{Elong.})_s$
100XF-LT-Virgin	1.04	1.04	---
100XF-TT-Virgin	1.04	1.04	1.3
50XF-LT-Virgin	1.10	1.08	0.8
50XF-LT-2%, Non-Aged	1.11	1.10	1.0
50XF-LT-8%, Non-Aged	1.08	1.10	0.85
50XF-LT-2%, Aged	1.07	1.08	0.99
50XF-LT-8%, Aged	1.04	1.07	----
50XF-TT-Virgin	1.10	1.09	1.04
50XF-TT-2%, Non-Aged	1.15	1.09	1.06
50XF-TT-8%, Non-Aged	1.06	1.08	0.85
50XF-TT-2%, Aged	1.07	1.11	0.80
50XF-TT-8%, Aged	1.05	1.09	0.92
35XF-LT-Virgin	1.29	1.15	1.05
35XF-LT-2%, Non-Aged	1.20	1.15	1.04
35XF-LT-8%, Non-Aged	1.14	1.16	1.18
35XF-LT-2%, Aged	1.19	1.14	1.14
35XF-LT-8%, Aged	1.16	1.18	0.96
35XF-TT-Virgin	1.29	1.13	0.98
35XF-TT-2%, Non-Aged	1.22	1.17	1.04
35XF-TT-8%, Non-Aged	1.15	1.18	1.08
35XF-TT-2%, Aged	1.15	1.14	1.09
35XF-TT-8%, Aged	1.12	1.17	1.05

Notes :

$(F_y)_d$ = dynamic yield stress for the strain rate of 1.0 in./in./sec.

$(F_y)_s$ = static yield stress for the strain rate of 10^{-4} in./in./sec.

$(F_u)_d$ = dynamic ultimate stress for the strain rate of 1.0 in./in./sec.

$(F_u)_s$ = static ultimate stress for the strain rate of 10^{-4} in./in./sec.

Table 4.2

Ratios of Dynamic to Static Compressive Yield Stresses for Three Sheet Steels

Type of Sheet Steel	$(F_y)_d/(F_y)_s$
100XF-LC	1.07
100XF-TC	1.07
50XF-LC	1.10
50XF-TC	1.09
35XF-LC	1.24
35XF-TC	1.33

Notes :

$(F_y)_d$ = dynamic yield stress for the strain rate of 1.0 in./in./sec.

$(F_y)_s$ = static yield stress for the strain rate of 10^{-4} in./in./sec.

ultimate tensile strengths of sheet steels increased with increasing strain rate. It was also noted that the amount of increase in ultimate tensile strength due to the increase in strain rate are approximately the same for both longitudinal and transverse tension. The increases in ultimate tensile strengths for the three materials studied in tension were found to be: 13% to 18% for 35XF sheet steel, 7% to 11% for 50XF sheet steel, and 4% for 100XF sheet steel when the strain rate were increased from 10^{-4} to 1.0 in./in./sec.. The ultimate compressive strengths could not be obtained because the buckling of the unsupported lengths at each end of the compression coupon limited the obtainable range of the stress-strain relationships to approximately 1.8 percent.

2. Strain Rate Sensitivity. The flow stress depends on strain (ε) and strain rate ($\dot{\varepsilon}$):

$$\sigma = \sigma(\varepsilon, \dot{\varepsilon}) \tag{4.1}$$

From Equation 2.12, it is recognized that the stress can be obtained by applying the material constant and strain-rate sensitivity to strain rate. As mentioned in literature survey, the strain-rate sensitivity of metals can be calculated from Equation 2.14 as follows:

$$m = \frac{\ln(\sigma_2/\sigma_1)}{\ln(\dot{\varepsilon}_2/\dot{\varepsilon}_1)} \tag{2.14}$$

On the basis of Equation 2.14, the values of the strain-rate sensitivity for 35XF, 50XF, and 100XF sheet steels in tension and compression were computed and listed in Tables 4.3 and 4.4, respectively. In these two tables, the values of m_1 were calculated for the yield

strengths corresponding to the strain rates of 10^{-4} and 10^{-2} in./in./sec., the values of m_2 were calculated for the yield strengths corresponding to the strain rates of 10^{-2} and 1.0 in./in./sec., and the values of m_3 were calculated for the yield strengths corresponding to the strain rates of 10^{-4} and 1.0 in./in./sec.. From these two tables, it can be seen that, in general, the strain-rate sensitivity "m" in tension and compression increases as the strain rate increases. The strain-rate sensitivity decreases progressively as the static yield strength level increases. It was also observed from Table 4.3 that the strain-rate sensitivity decreases as the amount of cold stretching increases.

3. Prediction of Yield Strength for High Strain Rate. A second degree polynominal form (Equation 4.2) was developed for prediction of the yield strength and ultimate tensile strength by using the least square method. The range of strain rate used to calculate the polynominal was from 10^{-4} to 1.0 in./in./sec..

$$Y = A + BX + CX^2 \qquad (4.2)$$

where Y = yield stress

X = log($\dot{\varepsilon}$)

A, B, and C = constants

Figures 4.1 through 4.6 show the test data of tension yield stresses and the predictions calculated from these test data for three sheet steels (35XF, 50XF, and 100XF) in the virgin condition and tested in the longitudinal and transverse directions under different strain rates. Similar plots for the sheet steels tested in compression are shown from

Figures 4.7 through 4.12. The data plotted in these figures are in terms of yield stress versus logarithmic strain rate. The polynominals used for drawing the curve in each plot are shown at the up-left corner of each figure.

Figures 4.13 through 4.16 show the test data of tensile ultimate stresses and the polynominals for 35XF and 50XF sheet steels in the virgin condition and tested in the longitudinal and transverse directions. The plots for the tension yield strength and the tensile ultimate strength of the three materials tested with different amounts of cold stretching were included in Reference 15.

C. EVALUATION OF STUB COLUMN TEST DATA

The width-to-thickness ratio of stiffened and unstiffened elements controls the failure mode of the stub column. To study the behavior of stiffened and unstiffened compression elements, two types of stub column specimens were fabricated from two sheet steels (35XF and 50XF sheet steels) and tested under different strain rates. Comparisons between the test results and the predicted values are presented in this section.

1. Stub Column Tests for the Study of Stiffened Elements.

Box-shaped stub columns fabricated from 35XF and 50XF sheet steels were tested for studying the postbuckling strength of stiffened elements. All stub column specimens were tested under uniform compressive load. The compressive yield stress obtained from material tests was used for calculating the critical local buckling load (P_{cr}) and the ultimate load (P_u) of stub columns. Comparisons were also made between the calculated

Table 4.3

Values of Strain Rate Sensitivities m for Three Sheet Steels Based on the Changes of the Yield Stresses at Different Strain Rates (Tensile Coupon Tests)

Type of Sheet Steel	m_1	m_2	m_3
100XF-LT-Virgin	0.003	0.005	0.004
100XF-TT-Virgin	0.003	0.006	0.004
50XF-LT-Virgin	0.009	0.013	0.011
50XF-LT-2%, Non-Aged	0.009	0.014	0.011
50XF-LT-8%, Non-Aged	0.009	0.009	0.009
50XF-LT-2%, Aged	0.005	0.009	0.007
50XF-LT-8%, Aged	0.000	0.008	0.004
50XF-TT-Virgin	0.011	0.009	0.010
50XF-TT-2%, Non-Aged	-----	-----	0.016
50XF-TT-8%, Non-Aged	-----	-----	0.006
50XF-TT-2%, Aged	-----	-----	0.008
50XF-TT-8%, Aged	-----	-----	0.005
35XF-LT-Virgin	0.022	0.033	0.027
35XF-LT-2%, Non-Aged	0.015	0.023	0.019
35XF-LT-8%, Non-Aged	0.013	0.016	0.014
35XF-LT-2%, Aged	0.008	0.029	0.019
35XF-LT-8%, Aged	0.014	0.018	0.016
35XF-TT-Virgin	0.018	0.037	0.028
35XF-TT-2%, Non-Aged	-----	-----	0.021
35XF-TT-8%, Non-Aged	-----	-----	0.015
35XF-TT-2%, Aged	-----	-----	0.016
35XF-TT-8%, Aged	-----	-----	0.013

Notes:

m_1 = strain rate sensitivity based on the changes of yield stress between strain rates of 0.0001 and 0.01 in./in./sec.

m_2 = strain rate sensitivity based on the changes of yield stress between strain rates of 0.01 and 1.0 in./in./sec.

m_3 = strain rate sensitivity based on the changes of yield stress between strain rates of 0.0001 and 1.0 in./in./sec.

Table 4.4

Values of Strain Rate Sensitivities m for Three Sheet Steels Based on the Changes of the Yield Stresses at Different Strain Rates (Compressive Coupon Tests)

Type of Sheet Steel	m_1	m_2
100XF-LC	0.008	0.007
100XF-TC	0.004	0.009
50XF-LC	0.012	0.009
50XF-TC	0.010	0.008
35XF-LC	0.015	0.031
35XF-TC	0.025	0.037

Notes:

m_1= strain rate sensitivity based on the changes of yield stress between strain rates of 0.0001 in./in./sec. and 0.01 in./in./sec.

m_2= strain rate sensitivity based on the changes of yield stress between strain rates of 0.01 in./in./sec. and 1.0 in./in./sec.

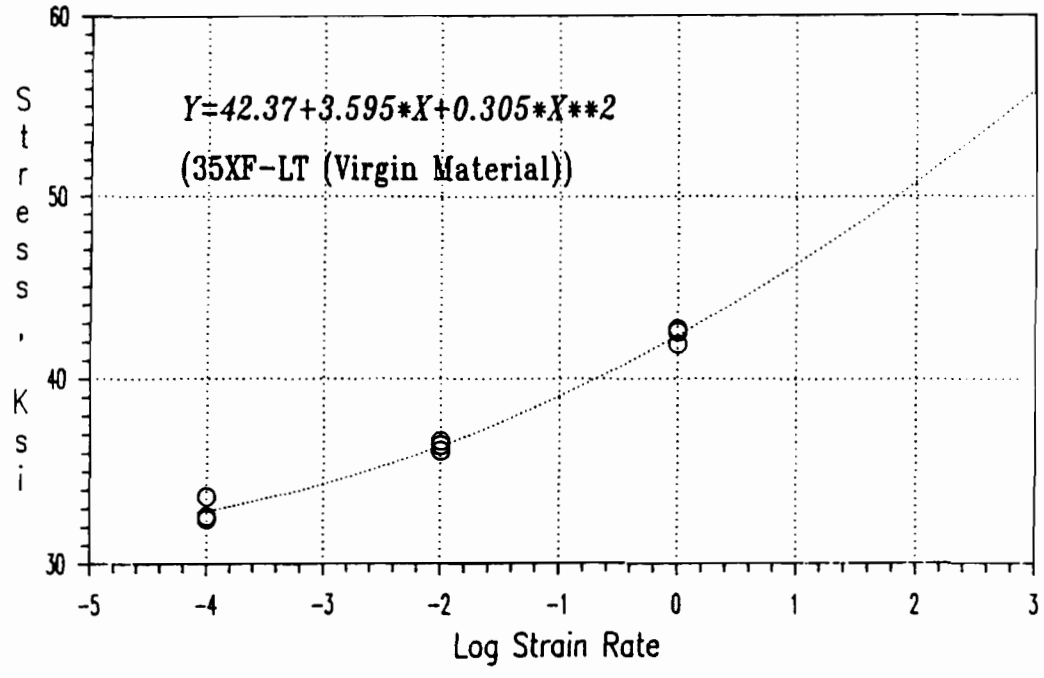

Figure 4.1 Tensile Yield Stress vs. Logarithmic Strain-Rate Curve for 35XF-LT (Virgin Material)

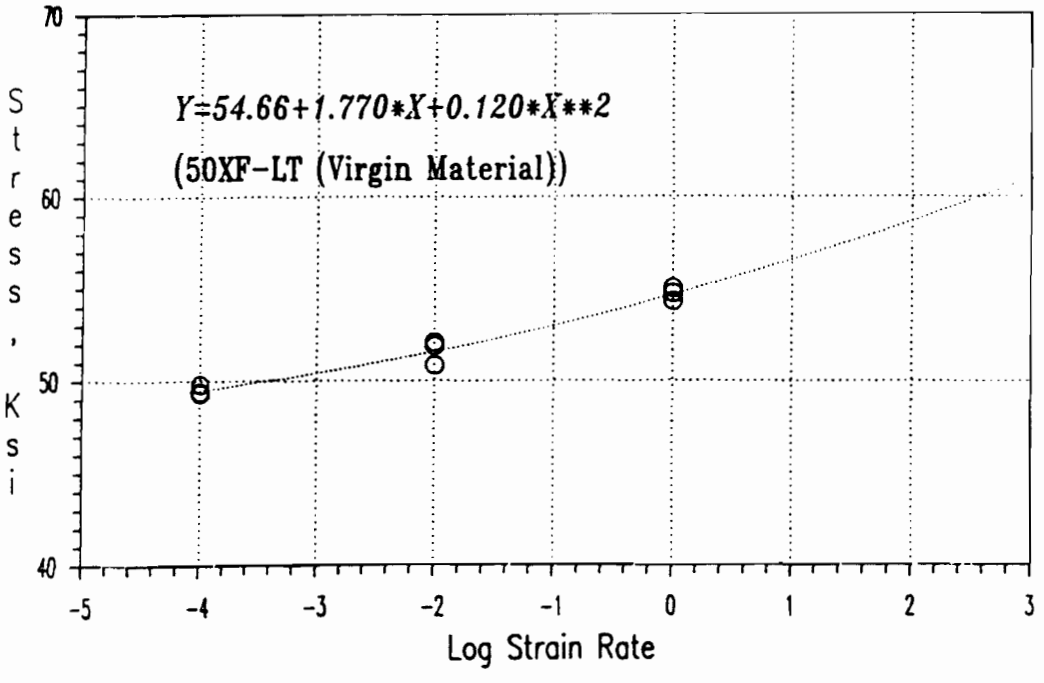

Figure 4.2 Tensile Yield Stress vs. Logarithmic Strain-Rate Curve for 50XF-LT (Virgin Material)

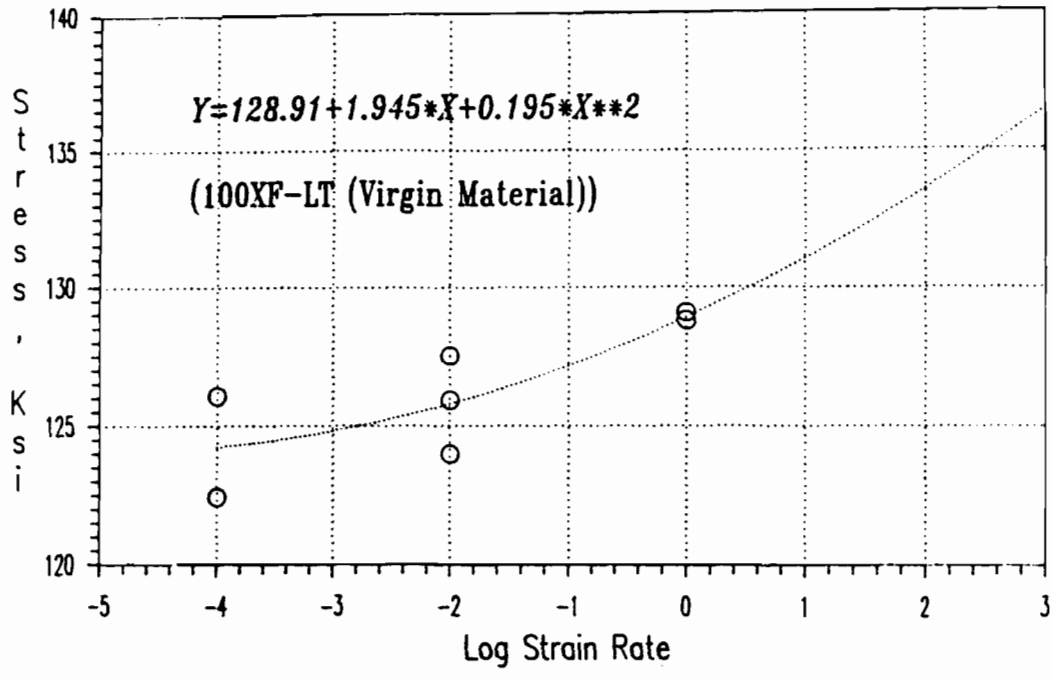

Figure 4.3 Tensile Yield Stress vs. Logarithmic Strain-Rate Curve for 100XF-LT (Virgin Material)

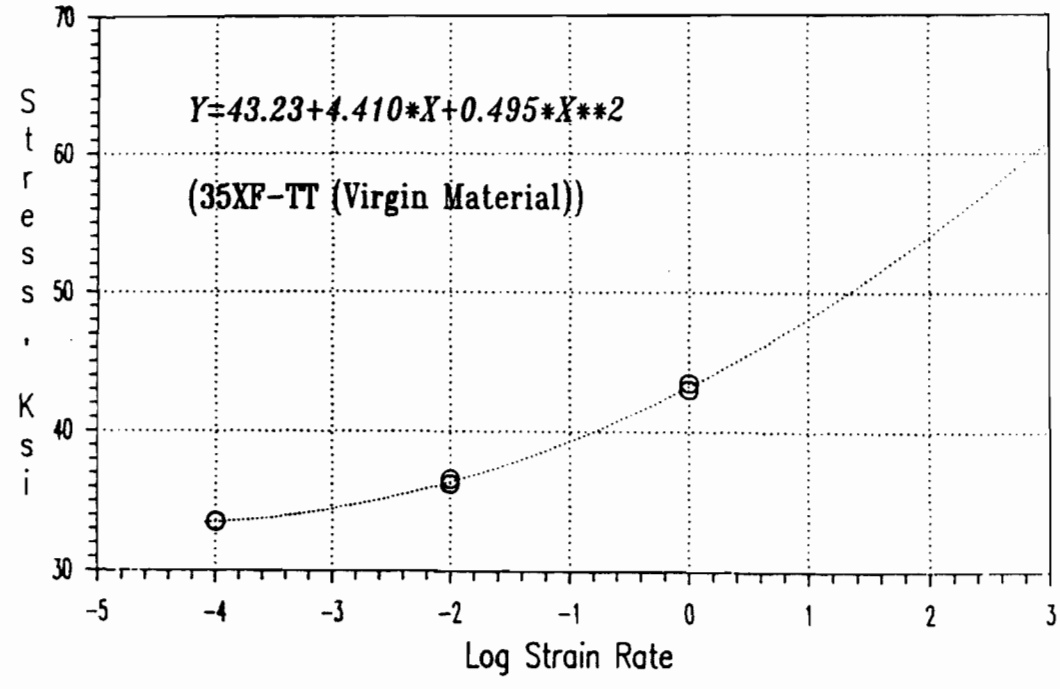

Figure 4.4 Tensile Yield Stress vs. Logarithmic Strain-Rate Curve for 35XF-TT (Virgin Material)

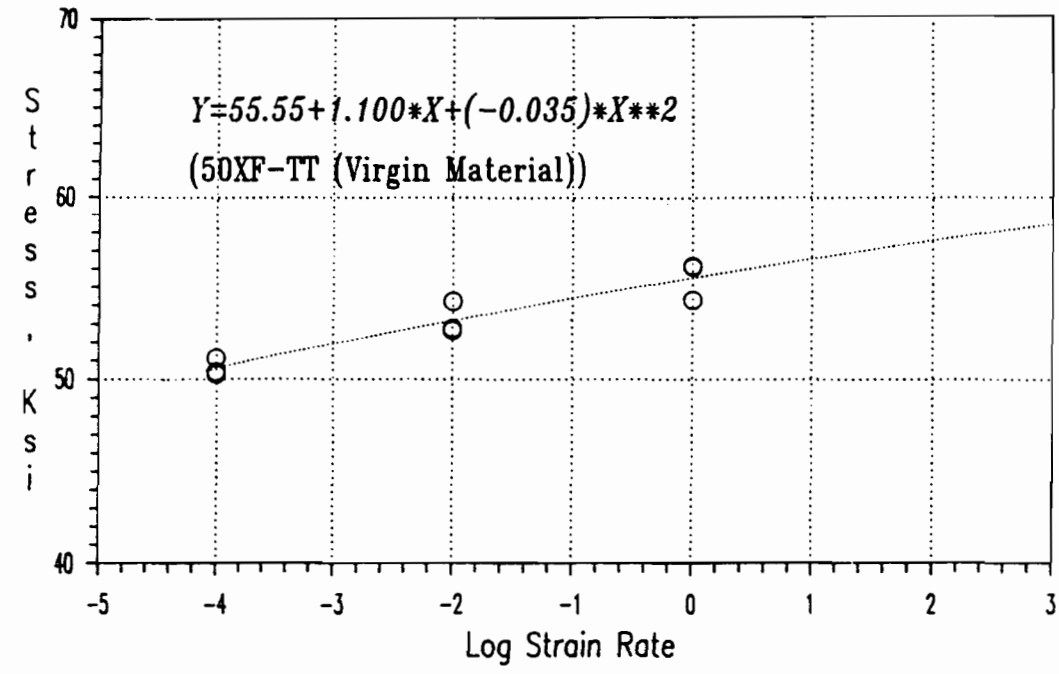

Figure 4.5 Tensile Yield Stress vs. Logarithmic Strain-Rate Curve for 50XF-TT (Virgin Material)

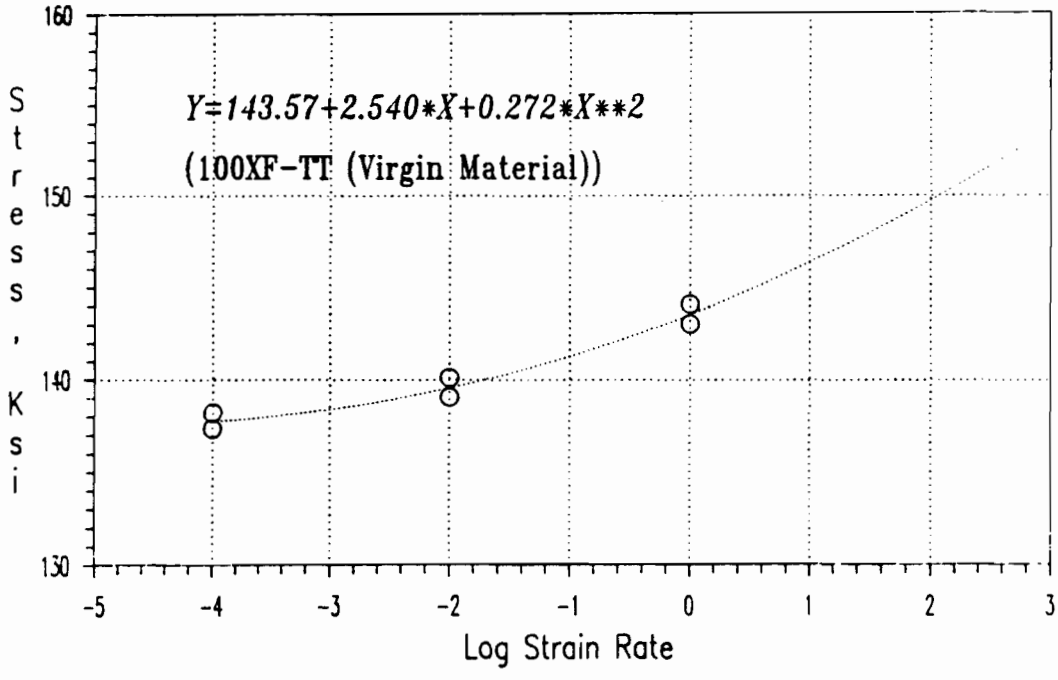

Figure 4.6 Tensile Yield Stress vs. Logarithmic Strain-Rate Curve for 100XF-TT (Virgin Material)

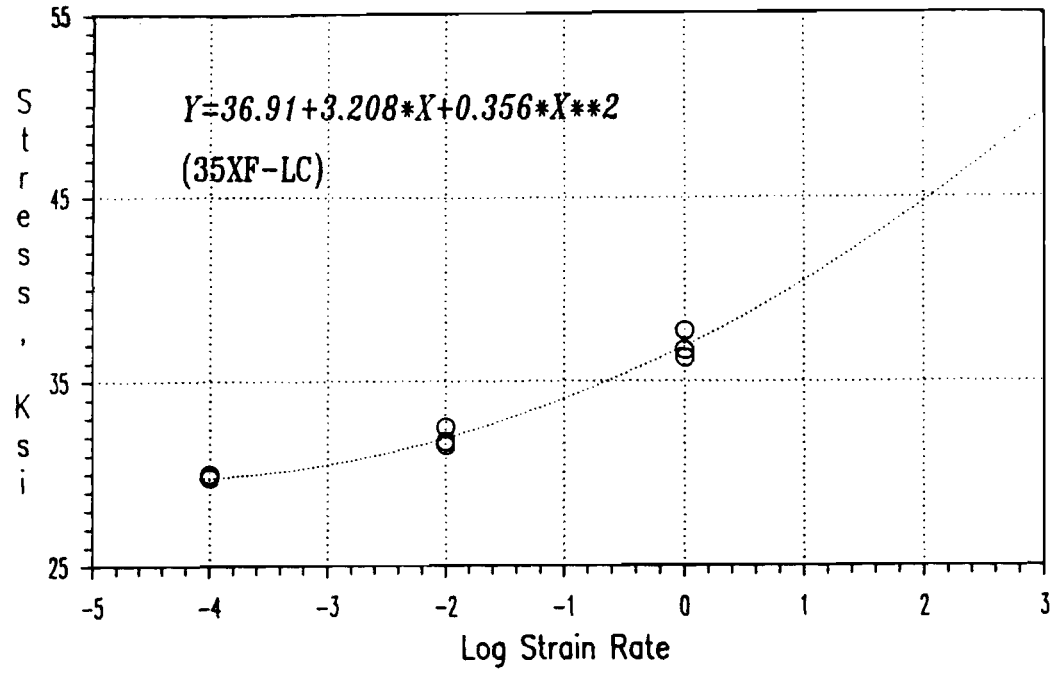

Figure 4.7 Compressive Yield Stress vs. Logarithmic Strain-Rate Curve for 35XF-LC (Virgin Material)

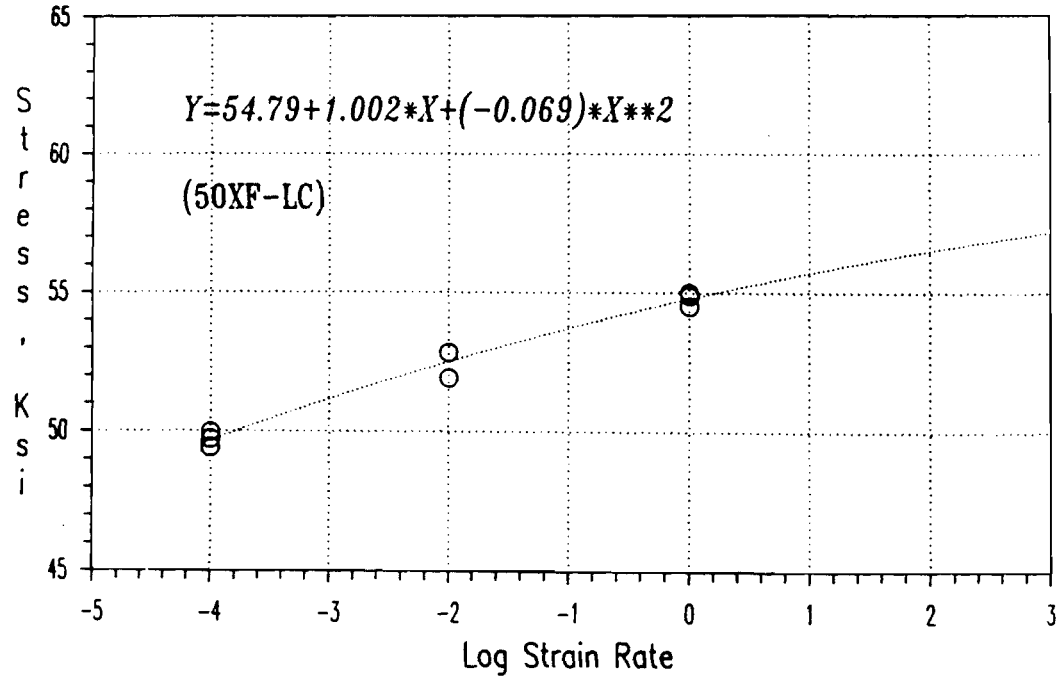

Figure 4.8 Compressive Yield Stress vs. Logarithmic Strain-Rate Curve for 50XF-LC (Virgin Material)

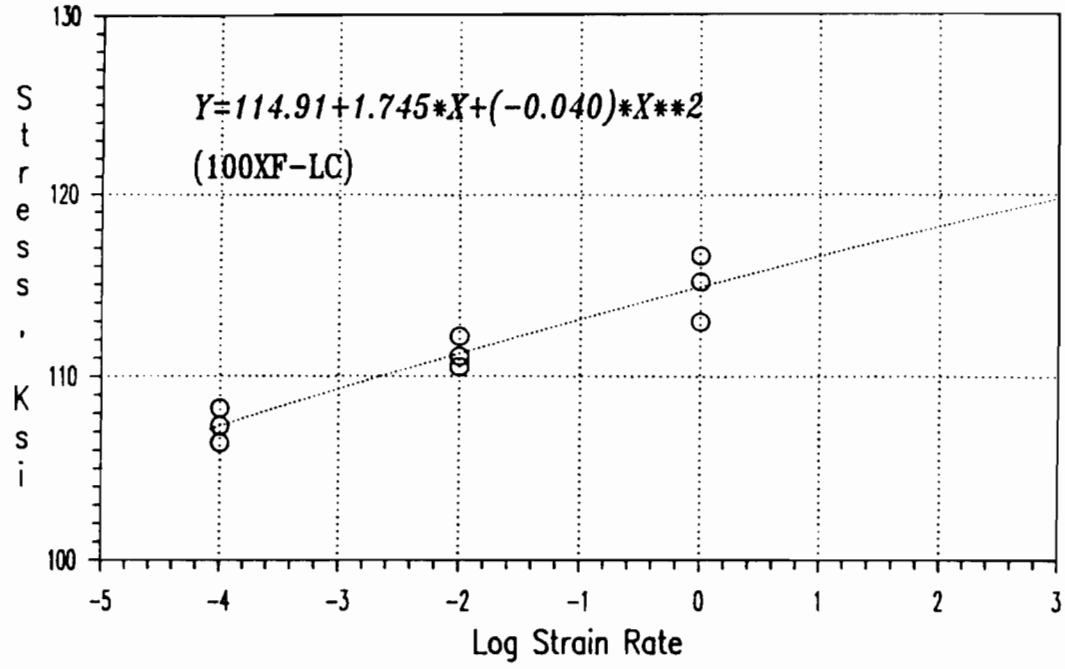

Figure 4.9 Compressive Yield Stress vs. Logarithmic Strain-Rate Curve for 100XF-LC (Virgin Material)

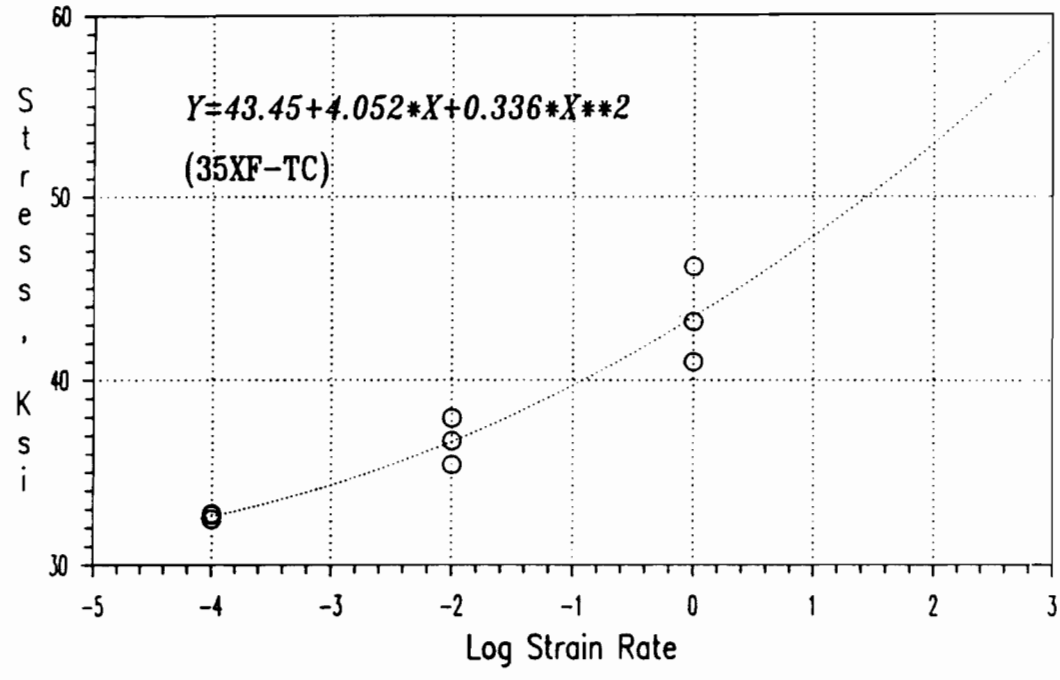

Figure 4.10 Compressive Yield Stress vs. Logarithmic Strain-Rate Curve for 35XF-TC (Virgin Material)

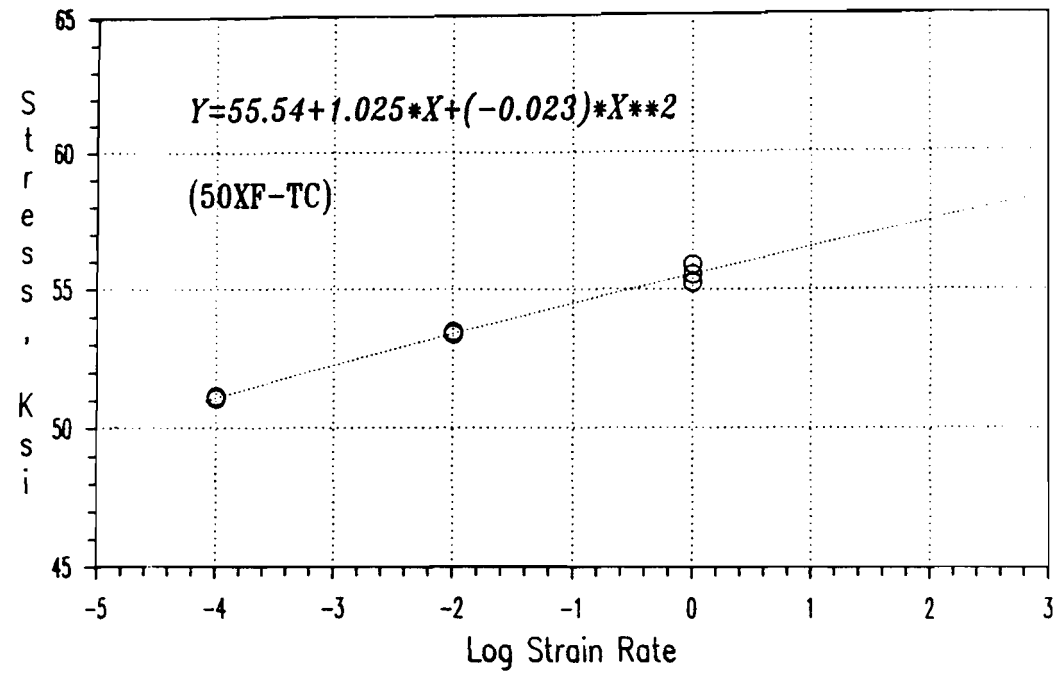

Figure 4.11 Compressive Yield Stress vs. Logarithmic Strain-Rate Curve for 50XF-TC (Virgin Material)

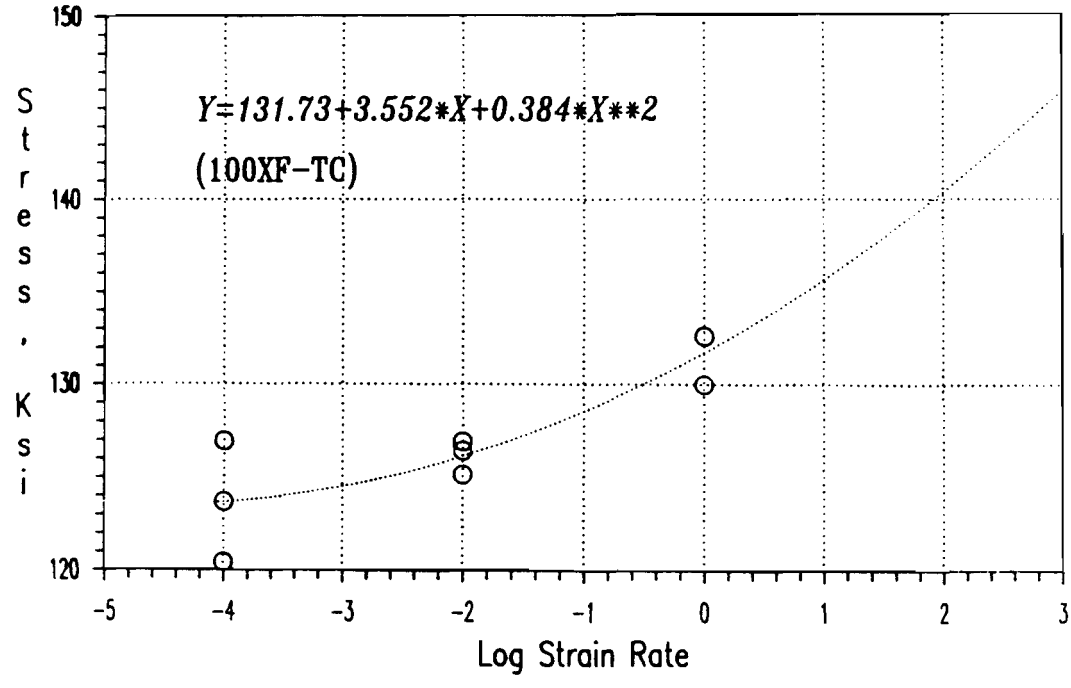

Figure 4.12 Compressive Yield Stress vs. Logarithmic Strain-Rate Curve for 100XF-TC (Virgin Material)

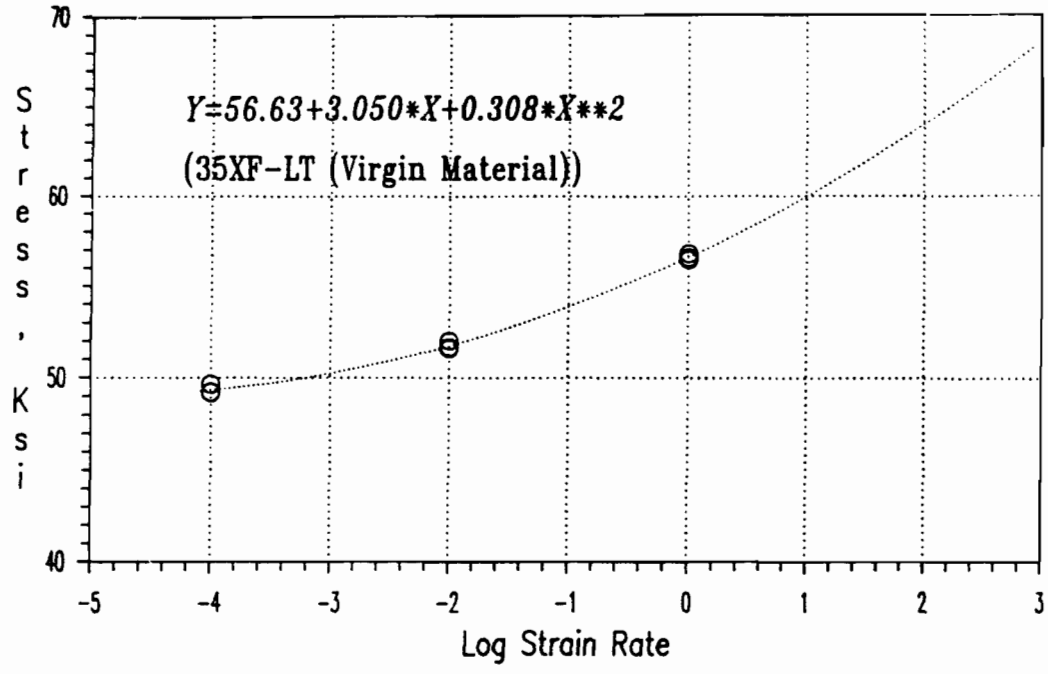

Figure 4.13 Tensile Ultimate Stress vs Logarithmic Strain-Rate Curve for 35XF-LT (Virgin Material)

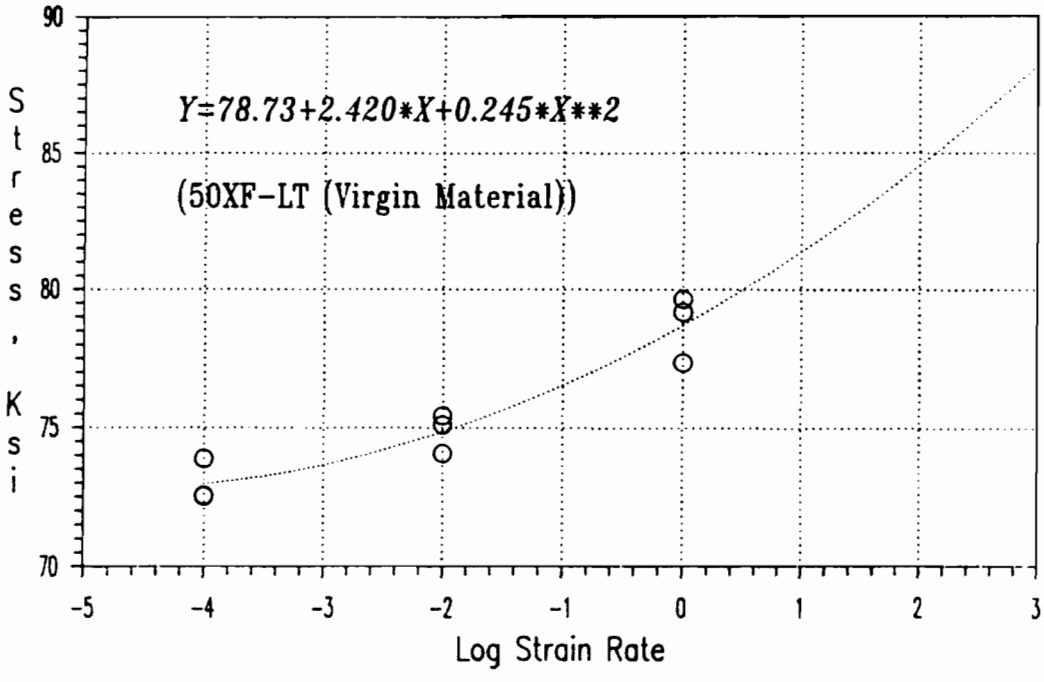

Figure 4.14 Tensile Ultimate Stress vs Logarithmic Strain-Rate Curve for 50XF-LT (Virgin Material)

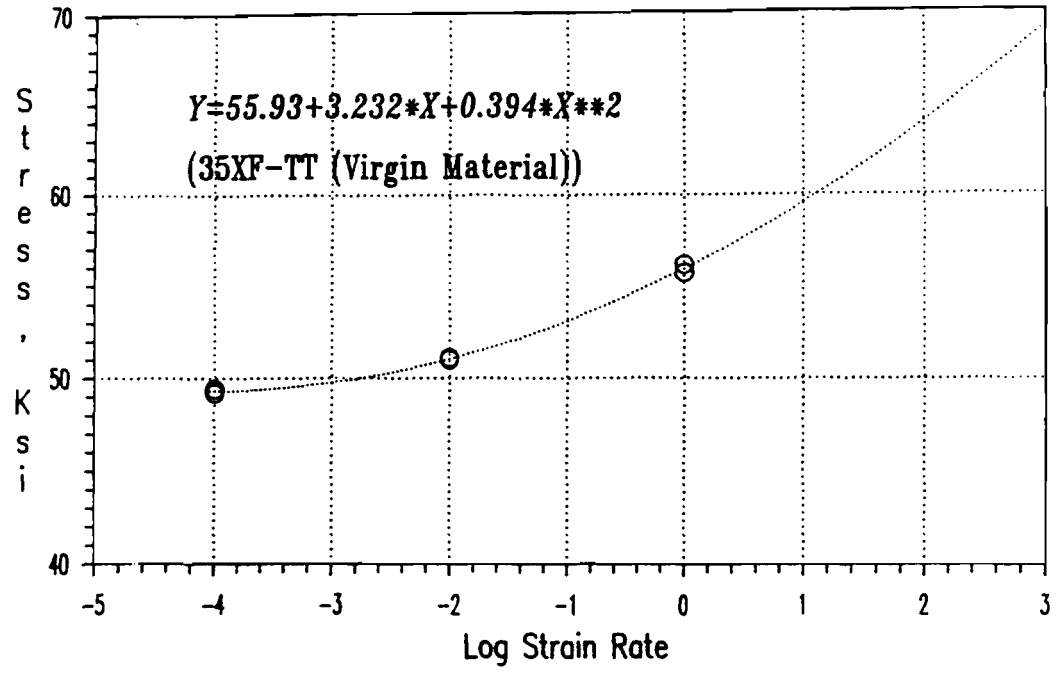

Figure 4.15 Tensile Ultimate Stress vs Logarithmic Strain-Rate Curve for 35XF-TT (Virgin Material)

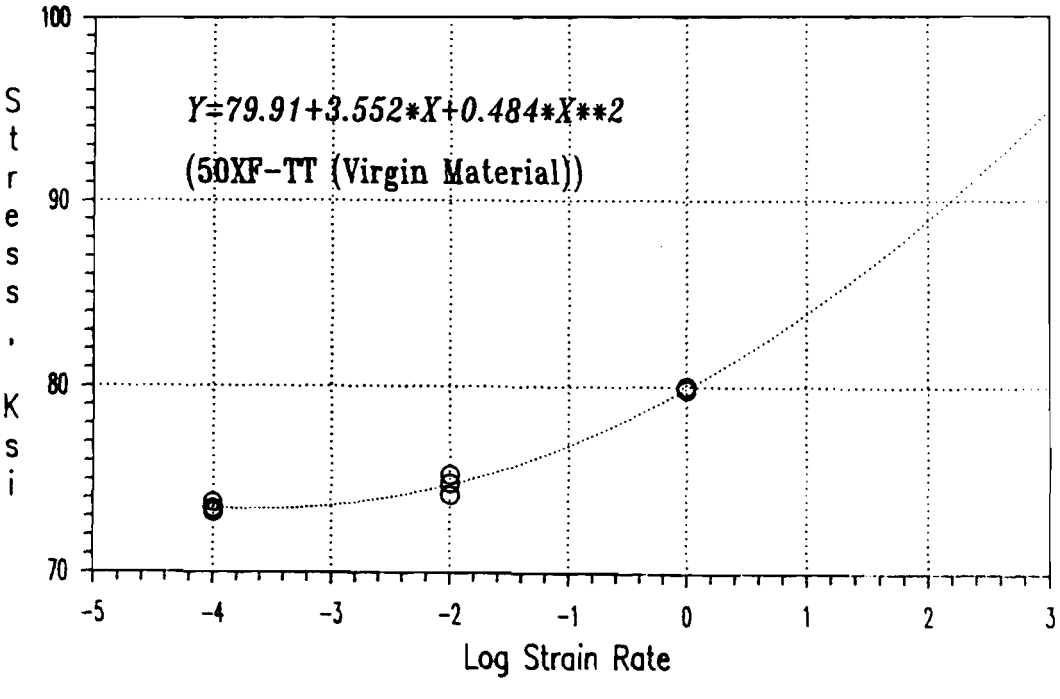

Figure 4.16 Tensile Ultimate Stress vs Logarithmic Strain-Rate Curve for 50XF-TT (Virgin Material)

ultimate loads based on the applicable tensile yield stresses and the tested ultimate loads.

a. Critical Local Buckling Load. The compression element of stub column specimens may buckle locally in the elastic or inelastic range, depending on the w/t ratio of the compression element. The elastic critical local buckling stress, $(f_{cr})_E$, of stiffened elements subjected to a uniform compressive load can be calculated by using Equation 2.22 which is derived from Bryan's differential equation (Equation 2.17) based on small deflection.

$$(f_{cr})_E = \frac{k\pi^2 E}{12(1-\mu^2)(w/t)^2} \quad . \tag{2.22}$$

where E = modulus of elasticity

μ = Poisson's ratio = 0.3 for steel

k = buckling coefficient

t = thickness of element

w = width of element

When the elastic critical buckling stress exceeds the proportional limit, the compression element buckles in the inelastic range. Therefore, the concept of tangent modulus[99] can be applied to calculate the inelastic buckling stress, $(f_{cr})_I$, by using Equation 4.3.

$$(f_{cr})_I = F_y - \frac{F_{pr}(F_y - F_{pr})}{(f_{cr})_E} \tag{4.3}$$

where F_y = compressive yield stress of steel

F_{pr} = proportional limit of steel

$(f_{cr})_E$ = elastic critical local buckling stress

The critical local buckling load of a stub column can be predicted by using Equation 4.4. The buckling coefficient used to compute the critical buckling stress, f_{cr}, ($(f_{cr})_E$ or $(f_{cr})_I$) in Equation 4.4 is equal to 4.0 for stiffened compression elements supported along both longitudinal edges. Consequently, the critical buckling load is

$$P_{cr} = A_g f_{cr} \tag{4.4}$$

where f_{cr} = critical buckling stress

A_g = gross cross-sectional area of the stub column

The predicted critical local buckling loads determined from Equation 4.4 and the critical local buckling loads obtained from the test results are presented in Tables 4.5 and 4.6 for 35XF and 50XF sheet steels, respectively. The values listed in column (1) of Tables 4.5 and 4.6 are the average values of the tested critical local buckling stresses of stiffened compression flanges of stub columns. The predicted critical local buckling loads shown in column (2) of Tables 4.5 and 4.6 were calculated on the basis of dynamic material properties.

The tested critical local buckling loads listed in column (3) of Tables 4.5 and 4.6 were determined from load-strain relationships by using the modified strain reversal method. The load-strain relationships indicated that no local buckling occurred in the specimens with small and medium w/t ratios for both sheet steels. The comparisons of computed and tested local critical buckling loads are listed in column (4) of Tables 4.5 and 4.6. The mean values of $(P_{cr})_{test}/(P_{cr})_{comp}$ ratios for 35XF and

Table 4.5

Comparison of Computed and Tested Critical Buckling Loads
Stub Columns with Stiffened Flanges (Based on k=4.0)
(35XF Sheet Steel)

Specimen	f_{cr} (ksi) (1)	$(P_{cr})_{comp}$ (kips) (2)	$(P_{cr})_{test}$ (kips) (3)	(3)/(2) (4)
1A1A	28.35	34.19	N/A	N/A
1A1B	28.32	34.15	N/A	N/A
1A2A	30.30	36.39	N/A	N/A
1A2B	30.28	36.52	N/A	N/A
1A3A	32.16	38.62	N/A	N/A
1A3B	32.15	38.61	N/A	N/A
1B1A	26.79	41.46	N/A	N/A
1B1B	26.75	41.41	N/A	N/A
1B2A	28.55	44.00	N/A	N/A
1B2B	28.51	44.08	N/A	N/A
1B3A	30.22	46.73	N/A	N/A
1B3B	30.20	46.63	N/A	N/A
1C1A	24.25	46.72	50.56	1.082
1C1B	24.20	46.66	50.90	1.091
1C2A	25.83	49.60	58.09	1.171
1C2B	25.63	49.51	55.94	1.130
1C3A	26.88	51.99	66.15	1.272
1C3B	26.81	51.83	65.51	1.264
1D1A	10.52	29.68	22.96	0.774
1D1B	10.59	29.87	22.37	0.749
1D2A	10.56	29.75	22.23	0.747
1D2B	10.53	29.69	27.80	0.936
1D3A	10.49	29.57	30.29	1.024
1D3B	10.51	29.63	33.17	1.119
Mean				1.030
Standard Deviation				0.189

Table 4.6

Comparison of Computed and Tested Critical Buckling Loads
Stub Columns with Stiffened Flanges (Based on k=4.0)
(50XF Sheet Steel)

Specimen	f_{cr} (ksi) (1)	$(P_{cr})_{comp}$ (kips) (2)	$(P_{cr})_{test}$ (kips) (3)	(3)/(2) (4)
1A1AX	47.58	55.05	N/A	N/A
1A1BX	47.54	55.39	N/A	N/A
1A2AX	50.00	57.92	N/A	N/A
1A2BX	50.05	57.99	N/A	N/A
1A3AX	50.70	58.84	N/A	N/A
1A3BX	50.74	58.92	N/A	N/A
1B1AX	44.74	58.38	N/A	N/A
1B1BX	44.89	58.41	N/A	N/A
1B2AX	46.94	61.00	N/A	N/A
1B2BX	46.79	61.07	65.27	1.069
1B3AX	47.19	61.55	N/A	N/A
1B3BX	47.25	61.66	N/A	N/A
1C1AX	38.31	57.94	46.12	0.796
1C1BX	37.40	56.94	45.92	0.806
1C2AX	37.88	58.02	47.39	0.817
1C2BX	39.10	58.99	52.51	0.890
1C3AX	39.95	59.96	50.07	0.835
1C3BX	38.11	57.82	52.76	0.912
1D1AX	11.11	25.64	21.98	0.857
1D2AX	11.06	25.53	28.04	1.098
1D3AX	11.11	25.67	21.59	0.841
1D3BX	11.08	25.65	22.47	0.876
Mean				0.891
Standard Deviation				0.102

50XF sheet steels are 1.030 and 0.891 with standard deviations of 0.189 and 0.102, respectively. It seems that the predicted buckling loads for box-shaped stub columns fabricated from 50XF sheet steel are less conservative than the stub columns fabricated from 35XF sheet steel. It was also observed from Tables 4.5 and 4.6 that the ratio of $(P_{cr})_{test}/(P_{cr})_{comp}$ increases with increasing strain rate for stub columns with relatively large w/t ratios, except for the stub columns with extra large w/t ratios for 50XF sheet steel.

b. Ultimate Axial Load. It is assumed that a stub column reaches its ultimate load when the maximum edge stress in the stiffened flanges reaches the yield stress of steel. The ultimate load can be calculated from the effective cross-sectional area of the stub column and the compressive yield stress of steel as expressed in Equation 4.5. The concept of effective width formula[1] (Equation 2.39) can be used to compute the effective cross-sectional area.

$$P_u = A_e f_y \tag{4.5}$$

where A_e = effective cross-sectional area of the stub column

F_y = static or dynamic yield stress of steel

The predicted ultimate loads computed from Equation 4.5 and the ultimate loads obtained from tests are presented in Tables 4.7(a) and 4.7(b) for 35XF sheet steel. Tables 4.8(a) and 4.8(b) present the similar values for 50XF sheet steel. The computed ultimate loads listed in column (5) of Tables 4.7(a) and 4.8(a) are based on the static compressive yield stress, while the values listed in column (5) of Tables 4.7(b) and 4.8(b) are based on the dynamic compressive yield stress corresponding to the

strain rate used in the test. The tested ultimate loads are listed in column (6) of Tables 4.7 and 4.8. Comparisons of the computed loads based on the static yield stress and the tested ultimate loads are listed in column (7) of Tables 4.7(a) and 4.8(a). The mean values of $(P_u)_{test}/(P_u)_{comp}$ ratios for the box-shaped sections made of 35XF and 50XF sheet steels are 1.222 and 1.020 with standard deviations of 0.149 and 0.061, respectively. Comparisons of the computed loads based on the dynamic yield stress and the tested ultimate loads are listed in column (7) of Tables 4.7(b) and 4.8(b). The mean values and standard deviations of $(P_u)_{test}/(P_u)_{comp}$ ratios are (1.148, 0.105) for using 35XF sheet steel and (0.981, 0.044) for using 50XF sheet steel.

For the purpose of comparison, Figures 4.17 and 4.18 show graphically the effect of strain rate on the ratios of the tested ultimate load to the computed ultimate load obtained from Tables 4.7(a) and 4.7(b), respectively. Similarly, Figures 4.19 and 4.20 show the strain rates vs. the ratios of the tested ultimate load to the computed ultimate load obtained from Tables 4.8(a) and 4.8(b). Tables 4.9 and 4.10 list average failure loads obtained from Tables 4.7 and 4.8, respectively. Each value given in Tables 4.9 and 4.10 and each point shown in Figures 4.17 through 4.20 is the average of two values obtained from similar tests, except for the stub columns with extra large w/t ratios using 50XF sheet steel.

By comparing the mean values and standard deviations of $(P_u)_{test}/(P_u)_{comp}$ ratios listed in Tables 4.7(a) and 4.8(a) with those listed in Tables 4.7(b) and 4.8(b), it can be seen that the computed ultimate loads using dynamic yield stresses are better than the computed ultimate loads using static yield stress. Similar to the results of

Table 4.7

Comparison of Computed and Tested Failure Loads Based on the Effective Width Formulas in the 1991 AISI Automotive Steel Design Manual for Stub Columns with Stiffened Flanges (35XF Sheet Steel)

(a) Based on Static Compressive Yield Stress

Spec.	Strain Rate (in./in./sec.)	w/t	$(F_y)_c$ (ksi)	A_e ($in.^2$)	$(P_u)_{comp}$ (kips)	$(P_u)_{test}$ (kips)	(6)/(5)
	(1)	(2)	(3)	(4)	(5)	(6)	(7)
1A1A	0.0001	27.15	29.83	1.2060	35.97	46.12	1.28
1A1B	0.0001	27.39	29.83	1.2058	35.97	44.89	1.25
1A2A	0.01	26.92	29.83	1.2007	35.82	50.02	1.40
1A2B	0.01	27.06	29.83	1.2014	35.82	49.29	1.38
1A3A	0.10	27.31	29.83	1.2009	35.82	53.54	1.49
1A3B	0.10	27.40	29.83	1.2009	35.82	54.37	1.52
1B1A	0.0001	38.93	29.83	1.5477	46.17	49.19	1.06
1B1B	0.0001	39.17	29.83	1.5480	46.18	53.54	1.16
1B2A	0.01	38.86	29.83	1.5412	45.97	56.28	1.22
1B2B	0.01	39.10	29.83	1.5463	46.13	57.01	1.23
1B3A	0.10	38.86	29.83	1.5463	46.13	64.78	1.40
1B3B	0.10	38.96	29.83	1.5440	46.06	60.87	1.32
1C1A	0.0001	52.69	29.83	1.8135	54.10	56.76	1.05
1C1B	0.0001	52.96	29.83	1.8122	54.06	56.52	1.05
1C2A	0.01	52.20	29.83	1.8122	54.06	61.02	1.13
1C2B	0.01	53.06	29.83	1.8147	54.13	64.58	1.19
1C3A	0.10	53.15	29.83	1.8164	54.18	73.96	1.36
1C3B	0.10	53.39	29.83	1.8130	54.08	69.27	1.28
1D1A	0.0001	100.68	29.83	2.1169	63.15	63.85	1.01
1D1B	0.0001	100.35	29.83	2.1210	63.27	63.90	1.01
1D2A	0.01	100.49	29.83	2.1157	63.11	70.35	1.11
1D2B	0.01	100.62	29.83	2.1158	63.12	69.22	1.10
1D3A	0.05	100.85	29.83	2.1141	63.06	74.06	1.17
1D3B	0.05	100.72	29.83	2.1139	63.06	72.45	1.15
Mean							1.222
Standard Deviation							0.149

Table 4.7 (Cont'd)

(b) Based on Dynamic Compressive Yield Stress

Spec.	Strain Rate (in./in./sec.) (1)	w/t (2)	$(F_y)_c$ (ksi) (3)	A_e ($in.^2$) (4)	$(P_u)_{comp}$ (kips) (5)	$(P_u)_{test}$ (kips) (6)	(6)/(5) (7)
1A1A	0.0001	27.15	29.83	1.2060	35.97	46.12	1.28
1A1B	0.0001	27.39	29.83	1.2058	35.97	44.89	1.25
1A2A	0.01	26.92	31.92	1.2007	38.33	50.02	1.30
1A2B	0.01	27.06	31.92	1.2014	38.35	49.29	1.29
1A3A	0.10	27.31	34.06	1.2009	40.90	53.54	1.31
1A3B	0.10	27.40	34.06	1.2009	40.90	54.37	1.33
1B1A	0.0001	38.93	29.83	1.5477	46.17	49.19	1.06
1B1B	0.0001	39.17	29.83	1.5480	46.18	53.54	1.16
1B2A	0.01	38.86	31.92	1.5412	49.20	56.28	1.14
1B2B	0.01	39.10	31.92	1.5449	49.31	57.01	1.16
1B3A	0.10	38.86	34.06	1.5372	52.36	64.78	1.24
1B3B	0.10	38.96	34.06	1.5340	52.25	60.87	1.16
1C1A	0.0001	52.69	29.83	1.8135	54.10	56.76	1.05
1C1B	0.0001	52.96	29.83	1.8122	54.06	56.52	1.05
1C2A	0.01	52.20	31.92	1.7977	57.38	61.02	1.06
1C2B	0.01	53.06	31.92	1.8000	57.46	64.58	1.12
1C3A	0.10	53.15	34.06	1.7875	60.88	73.96	1.21
1C3B	0.10	53.39	34.06	1.7840	60.76	69.27	1.14
1D1A	0.0001	100.68	29.83	2.1169	63.15	63.85	1.01
1D1B	0.0001	100.35	29.83	2.1210	63.27	63.90	1.01
1D2A	0.01	100.49	31.92	2.0943	66.85	70.35	1.05
1D2B	0.01	100.62	31.92	2.0945	66.86	69.22	1.04
1D3A	0.05	100.85	33.34	2.0792	69.32	74.06	1.07
1D3B	0.05	100.72	33.34	2.0791	69.32	72.45	1.05
Mean							1.148
Standard Deviation							0.105

Table 4.8

Comparison of Computed and Tested Failure Loads Based on the Effective Width Formulas in the 1991 AISI Automotive Steel Design Manual for Stub Columns with Stiffened Flanges (50XF Sheet Steel)

(a) Based on Static Compressive Yield Stress

Spec.	Strain Rate (in./in./sec.) (1)	w/t (2)	$(F_y)_c$ (ksi) (3)	A_e ($in.^2$) (4)	$(P_u)_{comp}$ (kips) (5)	$(P_u)_{test}$ (kips) (6)	(6)/(5) (7)
1A1AX	0.0001	22.89	49.68	1.1569	57.47	57.89	1.01
1A1BX	0.0001	23.15	49.68	1.1652	57.89	57.65	1.00
1A2AX	0.01	23.15	49.68	1.1584	57.55	59.82	1.02
1A2BX	0.01	22.94	49.68	1.1587	57.56	60.23	1.05
1A3AX	0.05	23.10	49.68	1.1605	57.66	63.95	1.11
1A3BX	0.05	22.92	49.68	1.1612	57.69	62.04	1.08
1B1AX	0.0001	35.49	49.68	1.2783	63.50	62.19	0.98
1B1BX	0.0001	34.59	49.68	1.2785	63.51	61.75	0.97
1B2AX	0.01	34.50	49.68	1.2774	63.46	68.88	1.09
1B2BX	0.01	34.96	49.68	1.2798	63.57	67.86	1.07
1B3AX	0.04	34.97	49.68	1.2790	63.54	71.42	1.12
1B3BX	0.04	34.79	49.68	1.2809	63.64	71.52	1.12
1C1AX	0.0001	52.76	49.68	1.3299	66.07	60.09	0.91
1C1BX	0.0001	53.40	49.68	1.3336	66.25	60.67	0.92
1C2AX	0.01	53.06	49.68	1.3323	66.19	64.00	0.97
1C2BX	0.01	52.23	49.68	1.3316	66.15	66.44	1.00
1C3AX	0.04	51.67	49.68	1.3292	66.03	66.54	1.01
1C3BX	0.04	52.90	49.68	1.3336	66.25	69.47	1.05
1D1AX	0.0001	97.99	49.68	1.6385	81.40	76.94	0.95
1D2AX	0.01	98.21	49.68	1.6371	81.33	82.22	1.01
1D3AX	0.03	98.01	49.68	1.6416	81.56	82.46	1.01
1D3BX	0.03	98.07	49.68	1.6423	81.59	80.85	0.99
Mean							1.020
Standard Deviation							0.061

Table 4.8 (Cont'd)

(b) Based on Dynamic Compressive Yield Stress

Spec.	Strain Rate (in./in./sec.) (1)	w/t (2)	$(F_y)_c$ (ksi) (3)	A_e ($in.^2$) (4)	$(P_u)_{comp}$ (kips) (5)	$(P_u)_{test}$ (kips) (6)	(6)/(5) (7)
1A1AX	0.0001	22.89	49.68	1.1569	57.47	57.89	1.01
1A1BX	0.0001	23.15	49.68	1.1652	57.89	57.65	1.00
1A2AX	0.01	23.15	52.51	1.1584	60.83	59.82	0.98
1A2BX	0.01	22.94	52.51	1.1587	60.84	60.23	0.99
1A3AX	0.05	23.10	53.37	1.1605	61.94	63.95	1.03
1A3BX	0.05	22.92	53.37	1.1612	61.97	62.04	1.00
1B1AX	0.0001	35.49	49.68	1.2783	63.50	62.19	0.98
1B1BX	0.0001	34.59	49.68	1.2785	63.51	61.75	0.97
1B2AX	0.01	34.50	52.51	1.2712	66.75	68.88	1.03
1B2BX	0.01	34.96	52.51	1.2736	66.87	67.86	1.01
1B3AX	0.04	34.97	53.25	1.2710	67.68	71.42	1.06
1B3BX	0.04	34.79	53.25	1.2730	67.79	71.52	1.06
1C1AX	0.0001	52.76	49.68	1.3299	66.07	60.09	0.91
1C1BX	0.0001	53.40	49.68	1.3336	66.25	60.67	0.92
1C2AX	0.01	53.06	52.51	1.3323	69.74	64.00	0.92
1C2BX	0.01	52.23	52.51	1.3223	69.44	66.44	0.96
1C3AX	0.04	51.67	53.25	1.3182	70.17	66.54	0.95
1C3BX	0.04	52.90	53.25	1.3219	70.39	69.47	0.99
1D1AX	0.0001	97.99	49.68	1.6388	81.40	76.94	0.95
1D2AX	0.01	98.21	52.51	1.6254	85.34	82.22	0.96
1D3AX	0.03	98.01	53.10	1.6273	86.41	82.46	0.95
1D3BX	0.03	98.07	53.10	1.6279	86.44	80.85	0.94
Mean							0.981
Standard Deviation							0.044

Table 4.9

Average Tested Failure Loads for Stub Column Specimens with Stiffened Flanges (35XF Sheet Steel)

Strain Rate in./in./sec.	w/t			
	27.21	38.98	52.91	100.62
0.0001	45.51	51.37	56.64	63.88
0.01	49.66	56.65	62.80	69.79
0.05				73.26
0.1	53.96	62.83	71.62	

Table 4.10

Average Tested Failure Loads for Stub Column Specimens with Stiffened Flanges (50XF Sheet Steel)

Strain Rate in./in./sec.	w/t			
	23.03	34.88	52.67	98.07
0.0001	57.77	61.97	60.37	76.94
0.01	60.03	68.37	65.22	82.22
0.03				82.46
0.04		71.47	68.01	
0.05	63.00			

Note: The tested value of Specimen 1D3BX is not iincluded in this table.

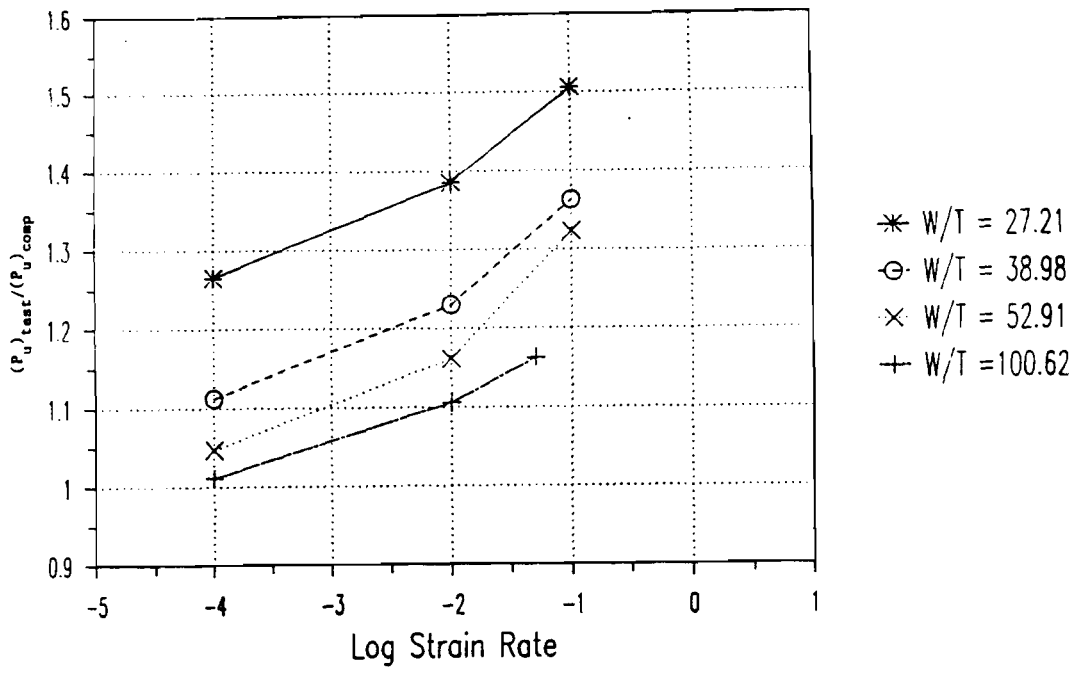

Figure 4.17 Ratios of Tested Ultimate Loads to Computed Ultimate Loads (Based on Static Yield Stress) vs. Logarithmic Strain Rate for Box-Shaped Stub Columns (35XF Sheet Steel)

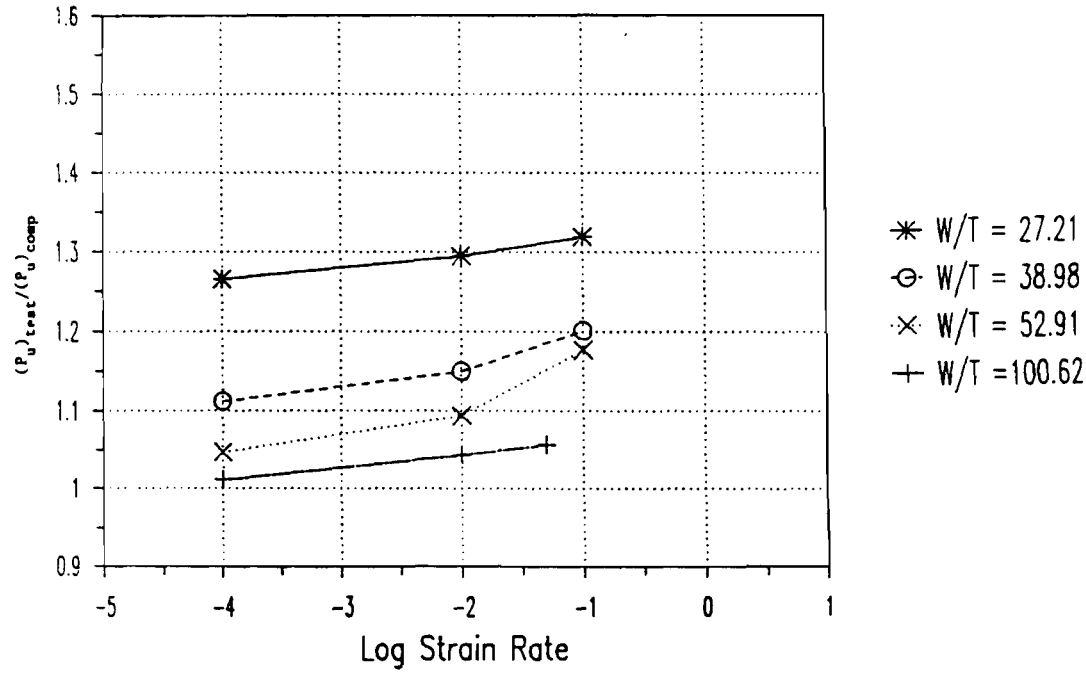

Figure 4.18 Ratios of Tested Ultimate Loads to Computed Ultimate Loads (Based on Dynamic Yield Stresses) vs. Logarithmic Strain Rate for Box-Shaped Stub Columns (35XF Sheet Steel)

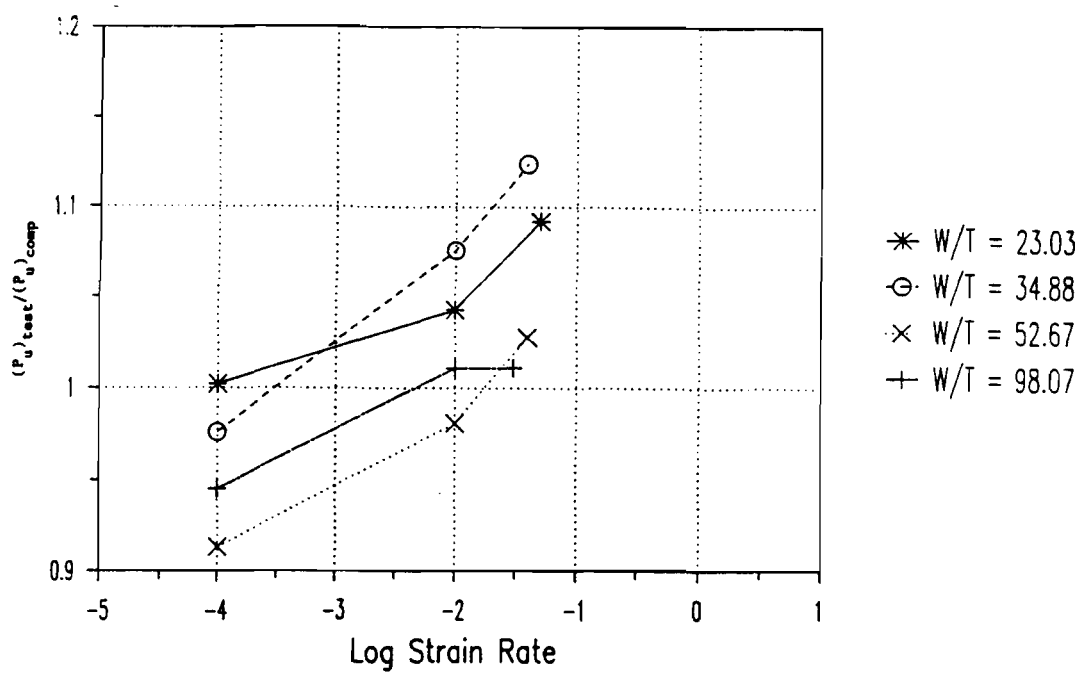

Figure 4.19 Ratios of Tested Ultimate Loads to Computed Ultimate Loads (Based on Static Yield Stress) vs. Logarithmic Strain Rate for Box-Shaped Stub Columns (50XF Sheet Steel)

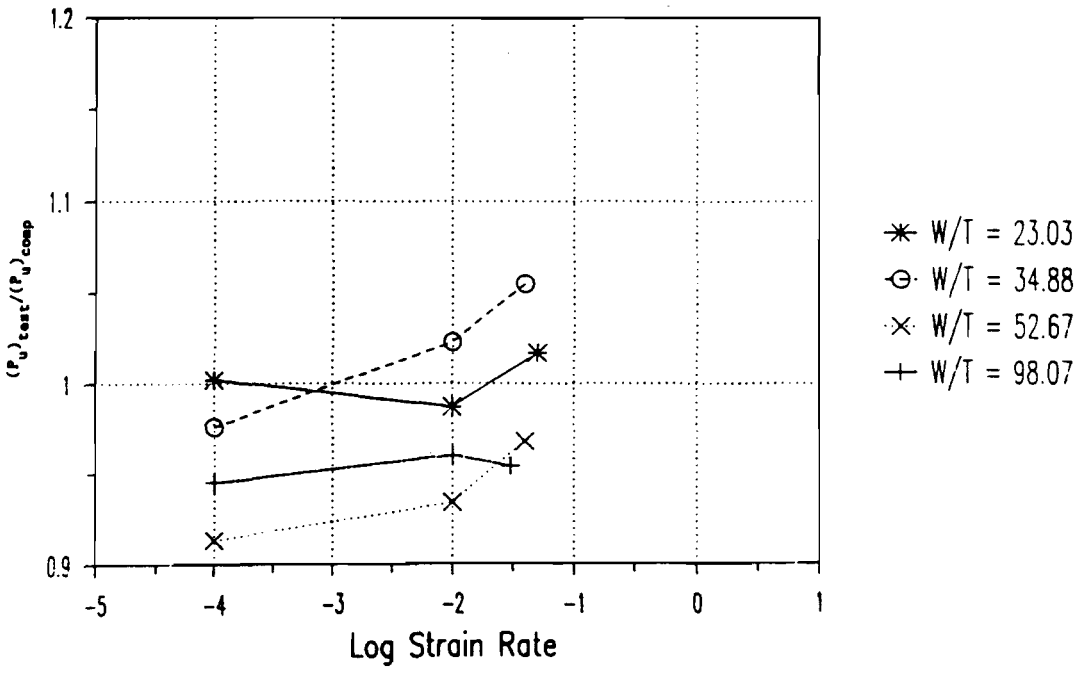

Figure 4.20 Ratios of Tested Ultimate Loads to Computed Ultimate Loads (Based on Dynamic Yield Stresses) vs. Logarithmic Strain Rate for Box-Shaped Stub Columns (50XF Sheet Steel)

critical local buckling loads listed in Tables 4.5 and 4.6, all predicted ultimate loads are lower than the tested ultimate loads for using 35XF sheet steel. However for using 50XF sheet steel, some predicted ultimate loads are higher than the tested ultimate loads. The predicted ultimate loads for box-shaped stub columns fabricated from 50XF sheet steel are found to be less conservative than the stub columns fabricated from 35XF sheet steel. It is also noted from Tables 4.9 and 4.10 that the tested ultimate load increases with strain rate for specimens having the same w/t ratios.

It is well known that cold-forming operation increases the yield stress and tensile strength of the steel particularly in the corners of cross sections. In order to consider the effect of cold-work on the axial strength of the stub columns, comparisons between the tested ultimate loads and the predicted ultimate loads based on applicable tensile yield stresses are presented in the following paragraphs.

According to the AISI Cold-Formed Steel Design Specification[66], the load-carrying capacity of a compact section (i.e. $\rho = 1$) including the cold work of forming can be determined by substituting F_{ya} for F_y, where F_{ya} is the average yield stress of the full section, and can be computed as follows:

$$F_{ya} = C(F_y)_c + (1-C)F_{yf} \tag{4.6}$$

where

F_{ya} = average tensile yield stress of steel.

C = ratio of the total corner cross-sectional area to the total cross-sectional area of the full section.

F_{yf} = weighted average tensile yield stress of flat portions.

$(F_y)_c = B_c F_{yv}/(R/t)^m$, tensile yield stress of corners. (4.7)

$B_c = 3.69(F_{uv}/F_{yv}) - 0.819(F_{uv}/F_{yv})^2 - 1.79$ (4.8)

$m = 0.192(F_{uv}/F_{yv}) - 0.068$ (4.9)

R = inside bend radius.

F_{yv} = tensile yield stress of virgin steel.

F_{uv} = ultimate tensile strength of virgin steel.

The above equations are applicable when $F_{uv}/F_{yv} > 1.2$, $R/t < 7$, and minimum included angle $< 120°$

The predicted ultimate loads based on the applicable tensile yield stresses and the tested ultimate loads are presented in Table 4.11 for box-shaped stub columns fabricated from 35XF sheet steel. Table 4.12 presents the similar data for box-shaped stub columns fabricated from 50XF sheet steel. The ultimate loads for the box-shaped stub columns with small w/t ratios (w/t<27.40 in Table 4.11(b) and w/t<23.15 in Table 12(b)) were computed by considering the cold work effect.

The computed ultimate loads based on the static and dynamic yield stresses are listed in columns (3) and (4) of Tables 4.11(a) and 4.12(a), respectively. By comparing the mean values and standard deviations of $(P_u)_{test}/(P_u)_{comp}$ ratios listed in columns 6 and 7 of Tables 4.11(a) 4.12(a), it can be seen that the computed ultimate loads using dynamic yield stresses are better than that using static yield stress for 35XF steel. The predicted ultimate loads for box-shaped stub columns fabricated from 50XF sheet steel were found to be slightly less

Table 4.11

Comparison of Computed and Tested Failure Loads Based on the Effective Width Formulas in the 1991 AISI Automotive Steel Design Manual for Stub Columns with Stiffened Flanges (35XF Sheet Steel)

(a) Based on Tensile Yield Stress (without Considering Cold-Work of Forming)

Spec.	Strain Rate	w/t	$(P_u)_{comp}$, kips Based on		$(P_u)_{test}$	(5)/(3)	(5)/(4)
	in./in./sec.		$(F_y)_s$	$(F_y)_d$	kips		
	(1)	(2)	(3)	(4)	(5)	(6)	(7)
1A1A	0.0001	27.15	39.64	39.64	46.12	1.16	1.16
1A1B	0.0001	27.39	39.63	39.63	44.89	1.13	1.13
1A2A	0.01	26.92	39.48	43.71	50.02	1.27	1.14
1A2B	0.01	27.06	39.49	43.73	49.29	1.25	1.15
1A3A	0.10	27.31	39.47	46.93	53.54	1.36	1.14
1A3B	0.10	27.40	39.47	46.93	54.37	1.38	1.16
1B1A	0.0001	38.93	50.73	50.73	49.19	0.97	0.97
1B1B	0.0001	39.17	50.68	50.68	53.54	1.06	1.06
1B2A	0.01	38.86	50.53	55.41	56.28	1.11	1.02
1B2B	0.01	39.10	50.64	55.52	57.01	1.13	1.03
1B3A	0.10	38.86	50.70	59.26	64.78	1.28	1.09
1B3B	0.10	38.96	50.60	59.13	60.87	1.20	1.03
1C1A	0.0001	52.69	58.92	58.92	56.76	0.96	0.96
1C1B	0.0001	52.96	58.88	58.88	56.52	0.96	0.96
1C2A	0.01	52.20	58.88	64.42	61.02	1.04	0.95
1C2B	0.01	53.06	58.96	64.48	64.58	1.10	1.00
1C3A	0.10	53.15	59.01	68.70	73.96	1.25	1.08
1C3B	0.10	53.39	58.89	68.56	69.27	1.18	1.01
1D1A	0.0001	100.68	68.58	68.58	63.85	0.93	0.93
1D1B	0.0001	100.35	68.72	68.72	63.90	0.93	0.93
1D2A	0.01	100.49	68.54	74.46	70.35	1.03	0.94
1D2B	0.01	100.62	68.55	74.78	69.22	1.01	0.93
1D3A	0.05	100.85	68.49	77.88	74.06	1.08	0.95
1D3B	0.05	100.72	68.48	77.87	72.45	1.06	0.93
Mean						1.118	1.027
Standard Deviation						0.132	0.085

Note : The sectional properties used for calculating the computed ultimate loads are listed in Appendix B (Table 1).

Table 4.11 (Cont'd)

(b) Based on Tensile Yield Stress
(with Considering Cold-Work of Forming)

(i) Based on Static Tensile Yield Stress

Spec.	Strain Rate (in./in./sec.)	w/t	$(F_y)_t$ (ksi)	A_e ($in.^2$)	$(P_u)_{comp}$ (kips)	$(P_u)_{test}$ (kips)	(6)/(5)
	(1)	(2)	(3)	(4)	(5)	(6)	(7)
1A1A	0.0001	27.15	36.72	1.2060	44.28	46.12	1.04
1A1B	0.0001	27.39	36.72	1.2058	44.28	44.89	1.01
1A2A	0.01	26.92	36.73	1.2007	44.11	50.02	1.13
1A2B	0.01	27.06	36.73	1.2014	44.13	49.29	1.12
1A3A	0.10	27.31	36.73	1.2009	44.11	53.54	1.21
1A3B	0.10	27.40	36.73	1.2009	44.11	54.37	1.23
Mean							1.123
Standard Deviation							0.088

(ii) Based on Dynamic Tensile Yield Stress

Spec.	Strain Rate (in./in./sec.)	w/t	$(F_y)_t$ (ksi)	A_e ($in.^2$)	$(P_u)_{comp}$ (kips)	$(P_u)_{test}$ (kips)	(6)/(5)
	(1)	(2)	(3)	(4)	(5)	(6)	(7)
1A1A	0.0001	27.15	36.72	1.2060	44.28	46.12	1.04
1A1B	0.0001	27.39	36.72	1.2058	44.28	44.89	1.01
1A2A	0.01	26.92	40.19	1.2007	48.26	50.02	1.04
1A2B	0.01	27.06	40.19	1.2014	48.29	49.29	1.02
1A3A	0.10	27.31	42.84	1.2009	51.45	53.54	1.04
1A3B	0.10	27.40	42.84	1.2009	51.45	54.37	1.06
Mean							1.035
Standard Deviation							0.018

Table 4.12

Comparison of Computed and Tested Failure Loads Based on the Effective Width Formulas in the 1991 AISI Automotive Steel Design Manual for Stub Columns with Stiffened Flanges (50XF Sheet Steel)

(a) Based on Tensile Yield Stress (without Considering Cold-Work of Forming)

Spec.	Strain Rate in./in./sec. (1)	w/t (2)	$(P_u)_{comp}$, kips Based on $(F_y)_s$ (3)	$(P_u)_{comp}$, kips Based on $(F_y)_d$ (4)	$(P_u)_{test}$ kips (5)	(5)/(3) (6)	(5)/(4) (7)
1A1AX	0.0001	22.89	57.27	57.27	57.89	1.01	1.01
1A1BX	0.0001	23.15	57.68	57.68	57.65	1.00	1.00
1A2AX	0.01	23.15	57.34	59.77	59.82	1.04	1.00
1A2BX	0.01	22.94	57.36	59.79	60.23	1.05	1.01
1A3AX	0.05	23.10	57.44	61.00	63.95	1.11	1.05
1A3BX	0.05	22.92	57.48	61.03	62.04	1.08	1.02
1B1AX	0.0001	35.49	63.29	63.29	62.19	0.98	0.98
1B1BX	0.0001	34.59	63.30	63.30	61.75	0.98	0.98
1B2AX	0.01	34.50	63.25	65.69	68.88	1.09	1.05
1B2BX	0.01	34.96	63.37	65.81	67.86	1.07	1.03
1B3AX	0.04	34.97	63.33	66.72	71.42	1.13	1.07
1B3BX	0.04	34.79	63.43	66.82	71.52	1.13	1.07
1C1AX	0.0001	52.76	65.86	65.86	60.09	0.91	0.91
1C1BX	0.0001	53.40	66.04	66.04	60.67	0.92	0.92
1C2AX	0.01	53.06	65.98	68.42	64.00	0.97	0.94
1C2BX	0.01	52.23	65.94	68.30	66.44	1.01	0.97
1C3AX	0.04	51.67	65.82	69.21	66.54	1.01	0.96
1C3BX	0.04	52.90	66.04	69.43	69.47	1.05	1.00
1D1AX	0.0001	97.99	81.15	81.15	76.94	0.95	0.95
1D2AX	0.01	98.21	81.08	84.05	82.22	1.01	0.98
1D3AX	0.03	98.01	81.30	85.20	82.46	1.01	0.97
1D3BX	0.03	98.07	81.33	85.23	80.85	0.99	0.95
Mean						1.023	0.992
Standard Deviation						0.062	0.045

Note : The sectional properties used for calculating the computed ultimate loads are listed in Appendix B (Table 2).

Table 4.12 (Cont'd)

(b) Based on Tensile Yield Stress
(with Considering Cold-Work of Forming)

(i) Based on Static Tensile Yield Stress

Spec.	Strain Rate (in./in./sec.)	w/t	$(F_y)_t$ (ksi)	A_e ($in.^2$)	$(P_u)_{comp}$ (kips)	$(P_u)_{test}$ (kips)	(6)/(5)
	(1)	(2)	(3)	(4)	(5)	(6)	(7)
1A1AX	0.0001	22.89	54.38	1.1569	62.91	57.89	0.92
1A1BX	0.0001	23.15	54.35	1.1652	63.32	57.65	0.91
1A2AX	0.01	23.15	54.38	1.1584	62.99	59.82	0.95
1A2BX	0.01	22.94	54.38	1.1587	63.00	60.23	0.96
1A3AX	0.05	23.10	54.37	1.1605	63.10	63.95	1.01
1A3BX	0.05	22.92	54.36	1.1612	63.13	62.04	0.98
Mean							0.955
Standard Deviation							0.037

(ii) Based on Dynamic Tensile Yield Stress

Spec.	Strain Rate (in./in./sec.)	w/t	$(F_y)_t$ (ksi)	A_e ($in.^2$)	$(P_u)_{comp}$ (kips)	$(P_u)_{test}$ (kips)	(6)/(5)
	(1)	(2)	(3)	(4)	(5)	(6)	(7)
1A1AX	0.0001	22.89	54.38	1.1569	62.91	57.89	0.92
1A1BX	0.0001	23.15	54.35	1.1652	63.32	57.65	0.91
1A2AX	0.01	23.15	56.51	1.1584	65.49	59.82	0.91
1A2BX	0.01	22.94	56.51	1.1587	65.48	60.23	0.92
1A3AX	0.05	23.10	57.51	1.1605	66.74	63.95	0.96
1A3BX	0.05	22.92	57.51	1.1612	66.77	62.04	0.93
Mean							0.925
Standard Deviation							0.019

conservative than those fabricated from 35XF sheet steel. By comparing Tables 4.7(a) and 4.7(b) to Table 4.11(a), it was noted that the ultimate loads calculated based on tensile yield stresses are better than those calculated on the basis of compressive yield stresses for the stub columns fabricated from 35XF sheet steel.

By comparing the $(P_u)_{test}/(P_u)_{comp}$ ratios of compact sections listed in Tables 4.11(a) and 4.11(b), it can be seen that a better prediction of the ultimate loads of compact sections can be obtained by considering the cold-work effect for the box-shaped stub columns fabricated from 35XF sheet steel. However, the percentage increases in the $(P_u)_{test}/(P_u)_{comp}$ ratios of compact sections given in Table 4.11(a) are similar to the ratios of compact sections presented in Table 4.11(b). Similar results were found in Tables 4.12(a) and 4.12(b) for box-shaped stub columns fabricated from 50XF sheet steel. It seems that the percentage increases in $(P_u)_{comp}$ values after considering the cold-forming operation in dynamic cases are similar to those in static cases. For the box-shaped stub columns fabricated from 50XF sheet steel, the computed ultimate loads can not be improved by considering the cold-work effect.

2. Stub Column Tests for the Study of Unstiffened Elements. I-shaped stub columns fabricated from 35XF and 50XF sheet steels were tested for studying the postbuckling strength of unstiffened elements. As mentioned in Section III, the length of specimen was designed to prevent overall column buckling failure, and the stiffened webs of channel sections used to form I-shaped specimens were designed to be fully effective. All stub column specimens were tested under a uniform compressive load. The compressive yield stresses obtained from material

tests were used for the evaluation of all stub column specimens in this section. Again, the tensile yield stresses were also used to calculate the predicted ultimate loads in order to consider the cold-work effect on the compact sections.

a. Critical Local Buckling Load. Similar to stiffened elements, unstiffened elements of stub columns may buckle locally in the elastic or inelastic range, depending on the w/t ratio of the compression element. Equations 2.22 and 4.3 can be applied to calculate the elastic critical local buckling stress ($(f_{cr})_E$) and the inelastic critical local buckling stress ($(f_{cr})_I$) of unstiffened elements subjected to a uniform compressive load. A "k" value of 0.43 was used for buckling coefficient in Equation 4.4 for the calculation of critical local buckling stress (f_{cr}). The critical local buckling loads of stub columns can be predicted by using Equation 4.4.

The computed and tested critical local buckling loads of stub column specimens are given in Tables 4.13 and 4.14 for 35XF and 50XF sheet steels, respectively. The computed critical local buckling loads listed in Tables 4.13 and 4.14 were calculated on the basis of the dynamic material properties. The values given in column (1) of Tables 4.13 and 4.14 are the average values of four critical local buckling stresses of unstiffened compression flanges of stub columns.

The tested critical local buckling loads listed in column (3) of Tables 4.13 and 4.14 were determined from the load-strain relationships by using the modified strain reversal method. It was noted that no local buckling occurred in the specimens with small and medium w/t ratios for both sheet steels. Column (4) of Tables 4.13 and 4.14 show the

Table 4.13

Comparison of Computed and Tested Critical Buckling Loads
Stub Columns with Unstiffened Flanges (Based on k=0.43)
(35XF Sheet Steel)

Specimen	$(f_{cr})_{comp}$ (ksi) (1)	$(P_{cr})_{comp}$ (kips) (2)	$(P_{cr})_{test}$ (kips) (3)	(3)/(2) (4)
2A1A	28.34	17.63	N/A	N/A
2A1B	28.30	17.79	N/A	N/A
2A2A	30.26	19.03	N/A	N/A
2A2B	30.20	18.95	N/A	N/A
2A3A	32.17	20.23	N/A	N/A
2A3B	32.16	20.11	N/A	N/A
2B1A	26.50	24.48	N/A	N/A
2B1B	26.47	24.31	N/A	N/A
2B2A	28.19	25.91	N/A	N/A
2B2B	28.21	26.00	N/A	N/A
2B3A	29.85	27.55	N/A	N/A
2B3B	29.80	27.50	N/A	N/A
2C0A	21.81	24.69	35.42	1.434
2C1A	21.71	24.59	36.44	1.482
2C1B	21.78	24.77	36.44	1.471
2C2A	22.78	25.85	40.40	1.563
2C2B	22.92	26.08	40.35	1.547
2C3A	23.70	26.87	46.95	1.747
2C3B	23.76	26.92	44.38	1.648
2D1A	5.764	10.80	20.27	1.877
2D1B	5.789	10.84	21.84	2.015
2D2A	5.758	10.77	17.05	1.583
2D2B	5.767	10.80	22.86	2.117
2D3A	5.786	10.77	21.40	1.987
2D3B	5.764	10.80	15.39	1.425
Mean				1.684
Standard Deviation				0.240

Table 4.14

Comparison of Computed and Tested Critical Buckling Loads
Stub Columns with Unstiffened Flanges (Based on k=0.43)
(50XF Sheet Steel)

Specimen	$(f_{cr})_{comp}$ (ksi) (1)	$(P_{cr})_{comp}$ (kips) (2)	$(P_{cr})_{test}$ (kips) (3)	(3)/(2) (4)
2A1AX	46.86	24.45	N/A	N/A
2A1BX	47.00	24.56	N/A	N/A
2A2AX	49.43	25.84	N/A	N/A
2A2BX	49.44	25.83	N/A	N/A
2A3AX	50.34	26.34	N/A	N/A
2A3BX	50.31	26.29	N/A	N/A
2B1AX	44.60	33.69	N/A	N/A
2B1BX	44.63	33.84	N/A	N/A
2B1CX	43.76	33.23	N/A	N/A
2B2AX	46.67	35.42	N/A	N/A
2B2BX	46.72	35.58	N/A	N/A
2B2CX	46.00	34.77	N/A	N/A
2B3AX	47.18	35.79	N/A	N/A
2B3BX	47.34	35.80	N/A	N/A
2C1AX	21.79	22.69	33.51	1.48
2C1BX	22.19	22.93	36.82	1.61
2C2AX	22.11	22.81	37.42	1.64
2C2BX	22.13	22.86	33.07	1.45
2C3AX	22.20	22.86	29.26	1.28
2C3BX	22.07	22.81	22.37	0.98
2D1AX	9.16	11.72	23.21	1.98
2D1BX	9.18	11.74	21.51	1.83
2D2AX	9.22	11.78	22.56	1.92
2D2BX	9.24	11.80	22.62	1.92
2D3AX	9.21	11.76	22.57	1.92
2D3BX	9.28	11.84	11.92	1.01
Mean				1.585
Standard Deviation				0.354

comparisons between the computed and tested critical local buckling loads. The mean values of $(P_{cr})_{test}/(P_{cr})_{comp}$ ratios for using 35XF and 50XF sheet steels are 1.684 and 1.585 with standard deviations of 0.240 and 0.354, respectively. These large mean values indicate that for most test specimens, initial local buckling did not occur at the location of strain gages. In addition, the actual buckling coefficient "k" could be greater than the value of 0.43 used in Equation 4.4.

b. Ultimate Axial Load. It is assumed that a stub column reaches its ultimate load when the maximum edge stress in the unstiffened flanges reaches the yield stress of steel. The ultimate load-carrying capacities (P_u) of stub columns can be predicted from Equation 4.5. The effective width formula given in Equation 2.39 can be applied for the calculation of the effective cross-sectional area to be used in Equation 4.5.

The predicated ultimate loads computed from Equation 4.5 and the ultimate loads obtained from tests are presented in Tables 4.15(a) and 4.15(b) for using 35XF sheet steel. Tables 4.16(a) and 4.16(b) present the similar values for using 50XF sheet steel. The computed ultimate loads based on the static compressive yield stresses are given in column (5) of Tables 4.15(a) and 4.16(a), while the computed ultimate loads based on the dynamic compressive yield stresses are given in Tables 4.15(b) and 4.16(b). The values listed in column (6) of Tables 4.15 and 4.16 are ultimate loads obtained from tests. Comparisons of the computed ultimate loads based on the static yield stress and the tested ultimate loads are listed in column (7) of Tables 4.15(a) and 4.16(a). The mean values of $(P_u)_{test}/(P_u)_{comp}$ ratios for using 35XF and 50XF sheet steels are 1.410 and 1.162 with standard deviations of 0.132 and 0.064, respectively. The

values listed in column (7) of Tables 4.15(b) and 4.16(b) are the comparisons between the computed ultimate loads based on the dynamic yield stresses and the tested ultimate loads. The mean values and standard deviations of $(P_u)_{test}/(P_u)_{comp}$ ratios are (1.330, 0.067) for using 35XF sheet steel and (1.121, 0.044) for using 50XF sheet steel.

For the purpose of comparison, Figures 4.21 and 4.22 show graphically the effect of strain rate on the ratios of the tested ultimate load to the computed ultimate load obtained from Tables 4.15(a) and 4.15(b), respectively. Similarly, Figures 4.23 and 4.24 show the strain rates vs. the ratios of the tested ultimate load to the computed ultimate load obtained from Tables 4.16(a) and 4.16(b). Tables 4.17 and 4.18 list average failure loads obtained from Tables 4.15 and 4.16, respectively. Each value given in Tables 4.17 and 4.18 and each point shown in Figures 4.21 through 4.24 is the average of two values obtained from similar tests, except for the stub columns with extra large w/t ratios using 50XF sheet steel.

From Tables 4.15 and 4.16, it can be seen that the computed ultimate loads using the dynamic yield stresses are better than the computed ultimate loads using the static yield stresses. Similar to the results for studying box-shaped stub columns, the predicted ultimate loads for I-shaped stub columns fabricated from 50XF sheet steel are less conservative than the stub columns fabricated from 35XF sheet steel. Tables 4.17 and 4.18 indicate that the tested ultimate load increases with strain rate for the specimens having the same w/t ratio.

Comparisons between the tested ultimate loads and the predicted values based on tensile yield stresses are presented in Table 4.19 for

Table 4.15

Comparison of Computed and Tested Failure Loads Based on the Effective Width Formulas in the 1991 AISI Automotive Steel Design Manual for Stub Columns with Unstiffened Flanges (35XF Sheet Steel)

(a) Based on Static Compressive Yield Stress

Spec.	Strain Rate (in./in./sec.)	w/t	$(F_y)_c$ (ksi)	A_e (in.^{2})	$(P_u)_{comp}$ (kips)	$(P_u)_{test}$ (kips)	(6)/(5)
	(1)	(2)	(3)	(4)	(5)	(6)	(7)
2A1A	0.0001	8.93	29.83	.6220	18.55	25.26	1.36
2A1B	0.0001	9.04	29.83	.6285	18.75	25.35	1.35
2A2A	0.01	8.93	29.83	.6288	18.76	26.04	1.39
2A2B	0.01	9.10	29.83	.6275	18.72	27.70	1.48
2A3A	0.10	8.93	29.83	.6288	18.76	31.41	1.67
2A3B	0.10	8.96	29.83	.6254	18.65	29.41	1.58
2B1A	0.0001	13.34	29.83	.9216	27.49	34.20	1.24
2B1B	0.0001	13.41	29.83	.9151	27.30	34.20	1.25
2B2A	0.01	13.40	29.83	.9160	27.32	36.30	1.33
2B2B	0.01	13.37	29.83	.9191	27.42	37.52	1.37
2B3A	0.10	13.34	29.83	.9208	27.47	41.67	1.52
2B3B	0.10	13.42	29.83	.9195	27.43	42.70	1.56
2C0A	0.00001	20.69	29.83	.9825	29.31	36.30	1.24
2C1A	0.0001	20.85	29.83	.9793	29.21	37.23	1.27
2C1B	0.0001	20.76	29.83	.9860	29.41	37.66	1.28
2C2A	0.01	20.97	29.83	.9785	29.19	41.28	1.41
2C2B	0.01	20.81	29.83	.9857	29.40	41.52	1.41
2C3A	0.10	20.93	29.83	.9787	29.19	47.92	1.64
2C3B	0.10	20.87	29.83	.9796	29.22	46.16	1.58
2D1A	0.0001	44.60	29.83	1.0971	32.73	41.72	1.27
2D1B	0.0001	44.50	29.83	1.0985	32.77	41.04	1.25
2D2A	0.01	44.62	29.83	1.0931	32.61	46.31	1.42
2D2B	0.01	44.59	29.83	1.0949	32.66	44.94	1.38
2D3A	0.05	44.51	29.83	1.0867	32.41	48.66	1.50
2D3B	0.05	44.60	29.83	1.0970	32.72	49.39	1.51
Mean							1.410
Standard Deviation							0.132

Table 4.15 (Cont'd)

(b) Based on Dynamic Compressive Yield Stress

Spec.	Strain Rate (in./in./sec.) (1)	w/t (2)	$(F_y)_c$ (ksi) (3)	A_e ($in.^2$) (4)	$(P_u)_{comp}$ (kips) (5)	$(P_u)_{test}$ (kips) (6)	(6)/(5) (7)
2A1A	0.0001	8.93	29.83	.6220	18.55	25.26	1.36
2A1B	0.0001	9.04	29.83	.6285	18.75	25.35	1.35
2A2A	0.01	8.93	31.92	.6288	20.07	26.04	1.30
2A2B	0.01	9.10	31.92	.6275	20.03	27.70	1.38
2A3A	0.10	8.93	34.06	.6288	21.42	31.41	1.47
2A3B	0.10	8.96	34.06	.6254	21.30	29.41	1.38
2B1A	0.0001	13.34	29.83	.9216	27.49	34.20	1.24
2B1B	0.0001	13.41	29.83	.9151	27.30	34.20	1.25
2B2A	0.01	13.40	31.92	.9091	29.02	36.30	1.25
2B2B	0.01	13.37	31.92	.9122	29.12	37.52	1.29
2B3A	0.10	13.34	34.06	.9069	30.89	41.67	1.35
2B3B	0.10	13.42	34.06	.9049	30.82	42.70	1.38
2C0A	0.00001	20.69	29.77	.9828	29.26	36.30	1.24
2C1A	0.0001	20.85	29.83	.9793	29.21	37.23	1.27
2C1B	0.0001	20.76	29.83	.9859	29.41	37.66	1.28
2C2A	0.01	20.97	31.92	.9672	30.87	41.28	1.34
2C2B	0.01	20.81	31.92	.9745	31.11	41.52	1.33
2C3A	0.10	20.93	34.06	.9587	32.65	47.92	1.47
2C3B	0.10	20.87	34.06	.9637	32.82	46.16	1.41
2D1A	0.0001	44.60	29.83	1.0971	32.73	41.72	1.27
2D1B	0.0001	44.50	29.83	1.0985	32.77	41.04	1.25
2D2A	0.01	44.62	31.92	1.0778	34.40	46.31	1.35
2D2B	0.01	44.59	31.92	1.0796	34.46	44.94	1.30
2D3A	0.05	44.51	33.34	1.0618	35.40	48.66	1.37
2D3B	0.05	44.60	33.34	1.0721	35.74	49.39	1.38
Mean							1.330
Standard Deviation							0.067

Table 4.16

Comparison of Computed and Tested Failure Loads Based on the Effective Width Formulas in the 1991 AISI Automotive Steel Design Manual for Stub Columns with Unstiffened Flanges (50XF Sheet Steel)

(a) Based on Static Compressive Yield Stress

Spec.	Strain Rate (in./in./sec.)	w/t	$(F_y)_c$ (ksi)	A_e ($in.^2$)	$(P_u)_{comp}$ (kips)	$(P_u)_{test}$ (kips)	(6)/(5)
	(1)	(2)	(3)	(4)	(5)	(6)	(7)
2A1AX	0.0001	8.41	49.68	.5220	25.92	28.04	1.08
2A1BX	0.0001	8.38	49.68	.5227	25.96	28.16	1.09
2A2AX	0.01	8.40	49.68	.5228	25.98	29.02	1.12
2A2BX	0.01	8.38	49.68	.5224	25.95	29.43	1.13
2A3AX	0.08	8.29	49.68	.5232	25.99	30.75	1.18
2A3BX	0.08	8.36	49.68	.5227	25.96	30.95	1.19
2B1AX	0.0001	11.68	49.68	.7354	36.54	39.72	1.09
2B1BX	0.0001	11.60	49.68	.7395	36.74	39.18	1.07
2B1CX	0.00001	11.63	49.68	.7402	36.77	39.47	1.07
2B2AX	0.01	11.58	49.68	.7405	36.79	42.60	1.16
2B2BX	0.01	11.54	49.68	.7438	36.95	42.55	1.15
2B2CX	0.001	11.53	49.68	.7382	36.67	41.77	1.14
2B3AX	0.08	11.65	49.68	.7391	36.72	45.07	1.23
2B3BX	0.08	11.50	49.68	.7391	36.72	44.94	1.22
2C1AX	0.0001	22.84	49.68	.7985	39.67	43.62	1.10
2C1BX	0.0001	22.73	49.68	.8015	39.82	43.97	1.10
2C2AX	0.01	22.77	49.68	.7989	39.69	46.70	1.18
2C2BX	0.01	22.76	49.68	.8004	39.77	46.26	1.16
2C3AX	0.05	22.72	49.68	.7979	39.64	47.34	1.19
2C3BX	0.05	22.79	49.68	.8002	39.75	46.85	1.18
2D1AX	0.0001	35.37	49.68	.7669	38.10	44.06	1.16
2D1BX	0.0001	35.33	49.68	.7668	38.10	44.50	1.17
2D2AX	0.01	35.26	49.68	.7672	38.11	46.75	1.23
2D2BX	0.01	35.21	49.68	.7676	38.14	47.58	1.25
2D3AX	0.04	35.29	49.68	.7666	38.09	49.39	1.30
2D3BX	0.04	35.15	49.68	.7679	38.15	48.95	1.28
Mean							1.162
Standard Deviation							0.064

Table 4.16 (Cont'd)

(b) Based on Dynamic Compressive Yield Stress

Spec.	Strain Rate (in./in./sec.) (1)	w/t (2)	$(F_y)_c$ (ksi) (3)	A_e ($in.^2$) (4)	$(P_u)_{comp}$ (kips) (5)	$(P_u)_{test}$ (kips) (6)	(6)/(5) (7)
2A1AX	0.0001	8.41	49.68	.5220	25.92	28.04	1.08
2A1BX	0.0001	8.38	49.68	.5227	25.96	28.16	1.09
2A2AX	0.01	8.40	52.51	.5228	27.45	29.02	1.06
2A2BX	0.01	8.38	52.51	.5224	27.43	29.43	1.07
2A3AX	0.08	8.29	53.61	.5232	28.05	30.75	1.10
2A3BX	0.08	8.36	53.61	.5227	28.02	30.95	1.10
2B1AX	0.0001	11.68	49.68	.7354	36.54	39.72	1.09
2B1BX	0.0001	11.60	49.68	.7397	36.74	39.18	1.07
2B1CX	0.00001	11.63	48.06	.7415	35.69	39.47	1.10
2B2AX	0.01	11.58	52.51	.7363	38.66	42.60	1.10
2B2BX	0.01	11.54	52.51	.7399	38.84	42.55	1.10
2B2CX	0.001	11.53	51.16	.7347	37.65	41.77	1.11
2B3AX	0.08	11.65	53.61	.7333	39.31	45.07	1.15
2B3BX	0.08	11.50	53.61	.7333	39.31	44.94	1.14
2C1AX	0.0001	22.84	49.68	.7991	39.67	43.62	1.10
2C1BX	0.0001	22.73	49.68	.8015	39.82	43.97	1.10
2C2AX	0.01	22.77	52.51	.7919	41.58	46.70	1.12
2C2BX	0.01	22.76	52.51	.7936	41.66	46.26	1.11
2C3AX	0.05	22.72	53.37	.7891	42.10	47.34	1.12
2C3BX	0.05	22.79	53.37	.7909	42.23	46.85	1.11
2D1AX	0.0001	35.37	49.68	.7669	38.10	44.06	1.16
2D1BX	0.0001	35.33	49.68	.7668	38.10	44.50	1.17
2D2AX	0.01	35.26	52.51	.7592	39.87	46.75	1.17
2D2BX	0.01	35.21	52.51	.7596	39.89	47.58	1.19
2D3AX	0.04	35.29	53.25	.7566	40.29	49.39	1.23
2D3BX	0.04	35.15	53.25	.7576	40.36	48.95	1.21
Mean							1.121
Standard Deviation							0.044

Table 4.17

Average Tested Failure Loads for Stub Column Specimens with Unstiffened Flanges (35XF Sheet Steel)

Strain Rate in./in./sec.	w/t			
	8.98	13.38	20.87	44.57
0.0001	25.31	34.20	37.50	41.38
0.01	26.87	36.91	41.40	45.63
0.05				49.03
0.1	30.41	42.19	47.04	

Table 4.18

Average Tested Failure Loads for Stub Column Specimens with Unstiffened Flanges (50XF Sheet Steel)

Strain Rate in./in./sec.	w/t			
	8.37	11.59	22.77	35.27
0.0001	28.10	39.45	43.80	44.28
0.01	29.23	42.58	46.48	47.17
0.04				49.17
0.05			47.10	
0.08	30.85	45.01		

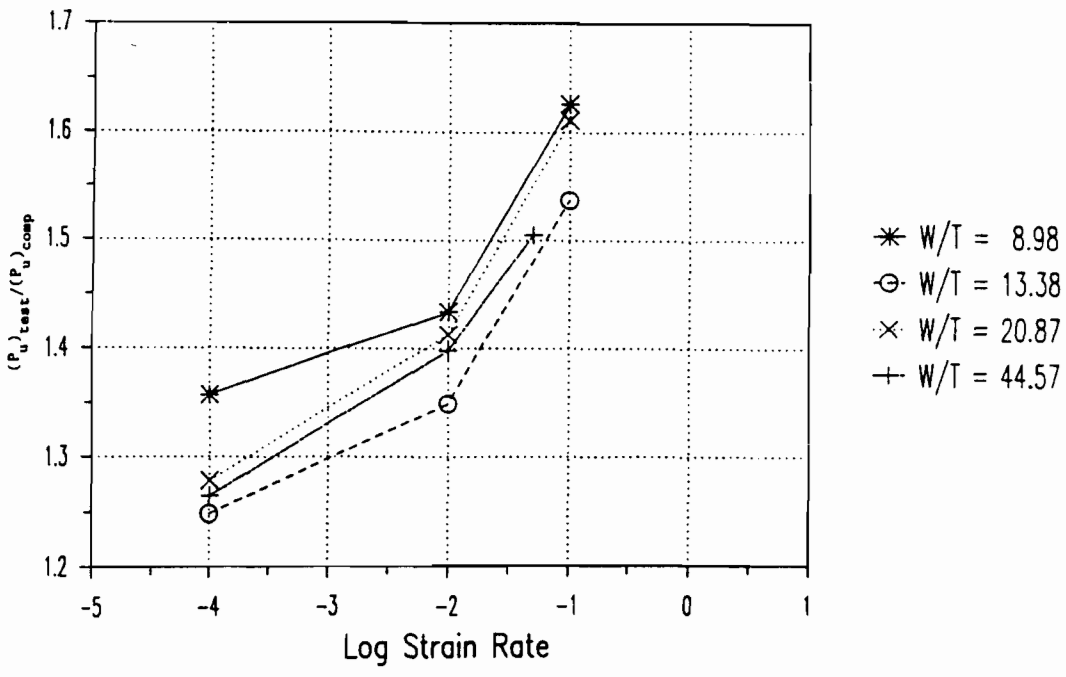

Figure 4.21 Ratios of Tested Ultimate Loads to Computed Ultimate Loads (Based on Static Yield Stress) vs. Logarithmic Strain Rate for I-Shaped Stub Columns (35XF Sheet Steel)

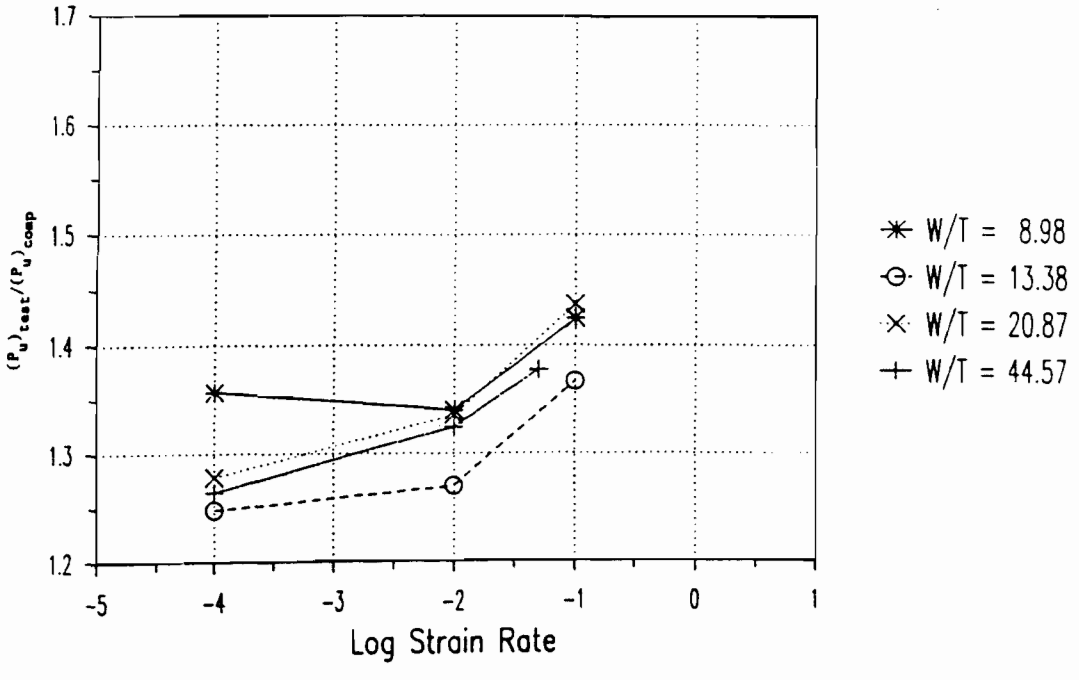

Figure 4.22 Ratios of Tested Ultimate Loads to Computed Ultimate Loads (Based on Dynamic Yield Stresses) vs. Logarithmic Strain Rate for I-Shaped Stub Columns (35XF Sheet Steel)

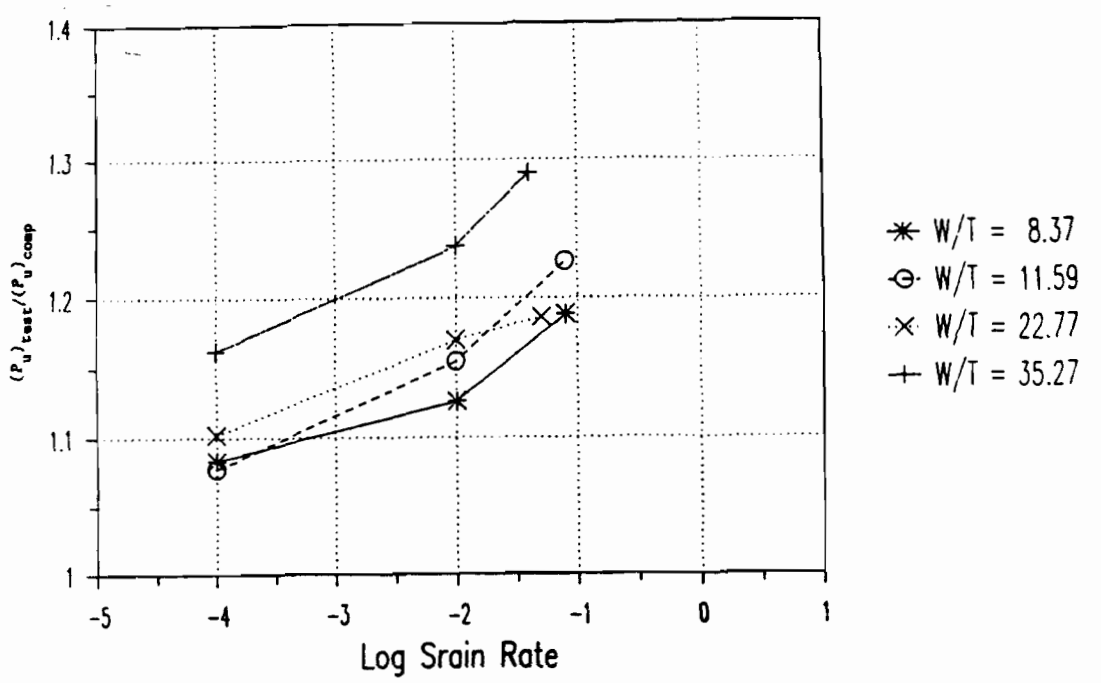

Figure 4.23 Ratios of Tested Ultimate Loads to Computed Ultimate Loads (Based on Static Yield Stress) vs. Logarithmic Strain Rate for I-Shaped Stub Columns (50XF Sheet Steel)

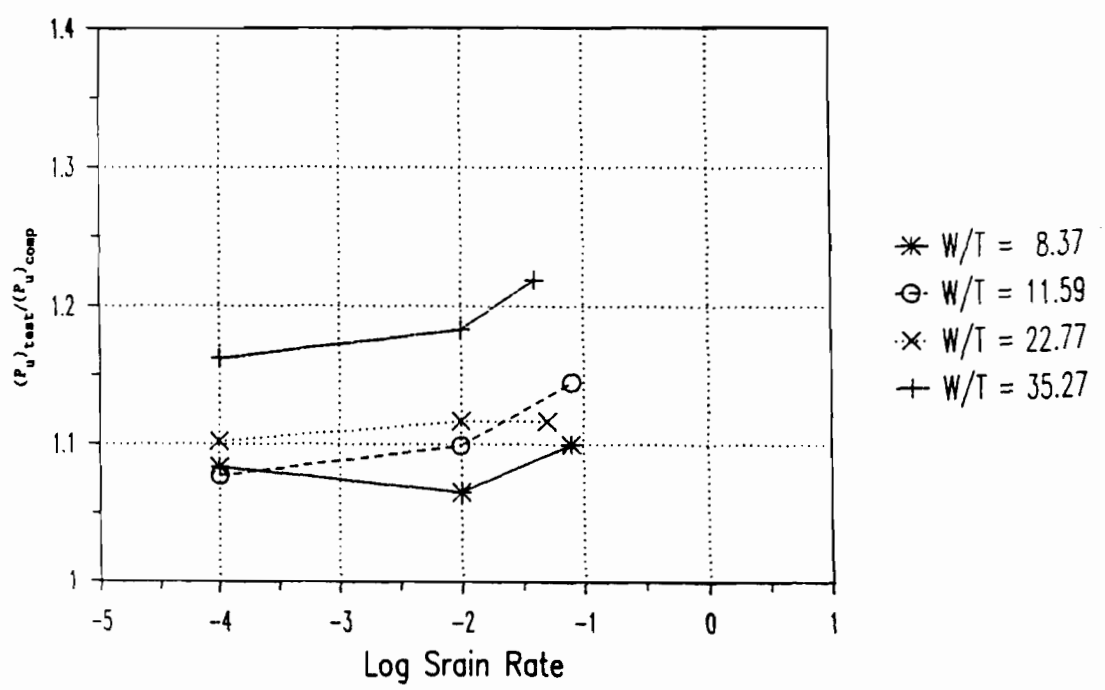

Figure 4.24 Ratios of Tested Ultimate Loads to Computed Ultimate Loads (Based on Dynamic Yield Stresses) vs. Logarithmic Strain Rate for I-Shaped Stub Columns (50XF Sheet Steel)

Table 4.19

Comparison of Computed and Tested Failure Loads Based on the Effective Width Formulas in the 1991 AISI Automotive Steel Design Manual for Stub Columns with Unstiffened Flanges (35XF Sheet Steel)

(a) Based on Tensile Yield Stress (without Considering Cold-Work of Forming)

Spec.	Strain Rate in./in./sec. (1)	w/t (2)	$(P_u)_{comp}$, kips Based on $(F_y)_s$ (3)	$(F_y)_d$ (4)	$(P_u)_{test}$ kips (5)	(5)/(3) (6)	(5)/(4) (7)
2A1A	0.0001	8.93	20.45	20.45	25.26	1.24	1.24
2A1B	0.0001	9.04	20.67	20.67	25.35	1.23	1.23
2A2A	0.01	8.93	20.67	22.89	26.04	1.26	1.14
2A2B	0.01	9.10	20.63	22.84	27.70	1.34	1.21
2A3A	0.10	8.93	20.67	24.58	31.41	1.52	1.28
2A3B	0.10	8.96	20.56	24.44	29.41	1.43	1.20
2B1A	0.0001	13.34	29.97	29.97	34.20	1.14	1.14
2B1B	0.0001	13.41	29.75	29.75	34.20	1.15	1.15
2B2A	0.01	13.40	29.78	32.59	36.30	1.22	1.11
2B2B	0.01	13.37	29.88	32.70	37.52	1.26	1.15
2B3A	0.10	13.34	29.94	34.88	41.67	1.39	1.19
2B3B	0.10	13.42	29.90	34.82	42.70	1.43	1.23
2C0A	0.00001	20.69	31.77	31.09	36.30	1.14	1.17
2C1A	0.0001	20.85	31.67	31.67	37.23	1.18	1.18
2C1B	0.0001	20.76	31.88	31.88	37.66	1.18	1.18
2C2A	0.01	20.97	31.63	34.43	41.28	1.31	1.20
2C2B	0.01	20.81	31.88	34.70	41.52	1.30	1.20
2C3A	0.10	20.93	31.64	36.53	47.92	1.51	1.31
2C3B	0.10	20.87	31.67	36.57	46.16	1.46	1.26
2D1A	0.0001	44.60	35.35	35.35	41.72	1.18	1.18
2D1B	0.0001	44.50	35.39	35.39	41.04	1.16	1.16
2D2A	0.01	44.62	35.21	38.19	46.31	1.32	1.21
2D2B	0.01	44.59	35.27	38.26	44.94	1.27	1.17
2D3A	0.05	44.51	35.00	39.46	48.66	1.39	1.23
2D3B	0.05	44.60	35.34	39.85	49.39	1.40	1.24
Mean						1.296	1.198
Standard Deviation						0.118	0.047

Note : The sectional properties used for calculating the computed ultimate loads are listed in Appendix B (Table 3).

Table 4.19 (Cont'd)

(b) Based on Tensile Yield Stress
(with Considering Cold-Work of Forming)

(i) Based on Static Tensile Yield Stress

Spec.	Strain Rate (in./in./sec.)	w/t	$(F_y)_t$ (ksi)	A_e ($in.^2$)	$(P_u)_{comp}$ (kips)	$(P_u)_{test}$ (kips)	(6)/(5)
	(1)	(2)	(3)	(4)	(5)	(6)	(7)
2A1A	0.0001	8.93	36.60	0.6220	22.77	25.26	1.11
2A1B	0.0001	9.04	36.56	0.6285	22.98	25.35	1.10
2A2A	0.01	8.93	36.56	0.6288	22.99	26.04	1.13
2A2B	0.01	9.10	36.57	0.6275	22.95	27.70	1.21
2A3A	0.10	8.93	36.56	0.6288	22.99	31.41	1.37
2A3B	0.10	8.96	36.58	0.6254	22.88	29.41	1.29
Mean							1.202
Standard Deviation							0.110

(ii) Based on Dynamic Tensile Yield Stress

Spec.	Strain Rate (in./in./sec.)	w/t	$(F_y)_t$ (ksi)	A_e ($in.^2$)	$(P_u)_{comp}$ (kips)	$(P_u)_{test}$ (kips)	(6)/(5)
	(1)	(2)	(3)	(4)	(5)	(6)	(7)
2A1A	0.0001	8.93	36.60	0.6220	22.77	25.26	1.11
2A1B	0.0001	9.04	36.56	0.6285	22.98	25.35	1.10
2A2A	0.01	8.93	40.02	0.6288	25.17	26.04	1.03
2A2B	0.01	9.10	40.03	0.6275	25.12	27.70	1.10
2A3A	0.10	8.93	42.67	0.6288	26.83	31.41	1.17
2A3B	0.10	8.96	42.67	0.6254	26.70	29.41	1.10
Mean							1.102
Standard Deviation							0.044

Table 4.20

Comparison of Computed and Tested Failure Loads Based on the Effective Width Formulas in the 1991 AISI Automotive Steel Design Manual for Stub Columns with Unstiffened Flanges (50XF Sheet Steel)

(a) Based on Tensile Yield Stress (without Considering Cold-Work of Forming)

Spec.	Strain Rate in./in./sec. (1)	w/t (2)	$(P_u)_{comp}$, kips Based on $(F_y)_s$ (3)	$(F_y)_d$ (4)	$(P_u)_{test}$ kips (5)	(5)/(3) (6)	(5)/(4) (7)
2A1AX	0.0001	8.41	25.84	25.84	28.04	1.09	1.09
2A1BX	0.0001	8.38	25.87	25.87	28.16	1.09	1.09
2A2AX	0.01	8.40	25.88	26.98	29.02	1.12	1.08
2A2BX	0.01	8.38	25.86	26.96	29.43	1.14	1.09
2A3AX	0.08	8.29	25.90	27.66	30.75	1.19	1.11
2A3BX	0.08	8.36	25.87	27.63	30.95	1.20	1.12
2B1AX	0.0001	11.68	36.42	36.42	39.72	1.09	1.09
2B1BX	0.0001	11.60	36.63	36.63	39.18	1.07	1.07
2B1CX	0.00001	11.63	36.65	36.19	39.47	1.08	1.09
2B2AX	0.01	11.58	36.67	38.06	42.60	1.16	1.12
2B2BX	0.01	11.54	36.84	38.24	42.55	1.15	1.11
2B2CX	0.001	11.53	36.55	37.17	41.77	1.14	1.12
2B3AX	0.08	11.65	36.60	38.82	45.07	1.23	1.16
2B3BX	0.08	11.50	36.59	38.82	44.94	1.23	1.16
2C1AX	0.0001	22.84	39.55	39.55	43.62	1.10	1.10
2C1BX	0.0001	22.73	39.70	39.70	43.97	1.11	1.11
2C2AX	0.01	22.77	39.57	40.98	46.70	1.18	1.14
2C2BX	0.01	22.76	39.65	41.06	46.26	1.17	1.13
2C3AX	0.05	22.72	39.52	41.56	47.34	1.20	1.14
2C3BX	0.05	22.79	39.63	41.69	46.85	1.18	1.12
2D1AX	0.0001	35.37	37.99	37.99	44.06	1.16	1.16
2D1BX	0.0001	35.33	37.99	37.99	44.50	1.17	1.17
2D2AX	0.01	35.26	38.00	39.30	46.75	1.23	1.19
2D2BX	0.01	35.21	38.02	39.32	47.58	1.25	1.21
2D3AX	0.04	35.29	37.97	39.78	49.39	1.30	1.24
2D3BX	0.04	35.15	38.04	39.85	48.95	1.29	1.23
Mean						1.166	1.132
Standard Deviation						0.064	0.046

Note : The sectional properties used for calculating the computed ultimate loads are listed in Appendix B (Table 4).

Table 4.20 (Cont'd)

(b) Based on Tensile Yield Stress
(with Considering Cold-Work of Forming)

(i) Based on Static Tensile Yield Stress

Spec.	Strain Rate (in./in./sec.)	w/t	$(F_y)_t$ (ksi)	A_e ($in.^2$)	$(P_u)_{comp}$ (kips)	$(P_u)_{test}$ (kips)	(6)/(5)
	(1)	(2)	(3)	(4)	(5)	(6)	(7)
2A1AX	0.0001	8.41	54.91	0.5220	28.66	28.04	1.00
2A1BX	0.0001	8.38	54.90	0.5227	28.70	28.16	0.98
2A2AX	0.01	8.40	54.90	0.5228	28.70	29.02	1.01
2A2BX	0.01	8.38	54.90	0.5224	28.69	29.43	1.03
2A3AX	0.08	8.29	54.90	0.5232	28.72	30.75	1.07
2A3BX	0.08	8.36	54.90	0.5227	28.70	30.95	1.08
Mean							1.028
Standard Deviation							0.040

(ii) Based on Dynamic Tensile Yield Stress

Spec.	Strain Rate (in./in./sec.)	w/t	$(F_y)_t$ (ksi)	A_e ($in.^2$)	$(P_u)_{comp}$ (kips)	$(P_u)_{test}$ (kips)	(6)/(5)
	(1)	(2)	(3)	(4)	(5)	(6)	(7)
2A1AX	0.0001	8.41	54.91	0.5220	28.66	28.04	1.00
2A1BX	0.0001	8.38	54.90	0.5227	28.70	28.16	0.98
2A2AX	0.01	8.40	57.04	0.5228	29.82	29.02	0.97
2A2BX	0.01	8.38	57.04	0.5224	29.80	29.43	0.99
2A3AX	0.08	8.29	58.37	0.5232	30.54	30.75	1.01
2A3BX	0.08	8.36	58.37	0.5227	30.52	30.95	1.01
Mean							0.993
Standard Deviation							0.016

35XF sheet steel and in Table 4.20 for 50XF sheet steel, in which the cold work effect was considered in the computations of ultimate loads for the I-shaped stub columns with w/t ratios less than 9.1. It can be seen that the computed ultimate loads using the dynamic yield stresses are better than the computed loads using the static yield stress. Similar to the results for studying box-shaped stub columns, the predicted ultimate loads for I-shaped stub columns fabricated from 50XF sheet steel are slightly less conservative than the stub columns fabricated from 35XF sheet steel. Again, it can be seen from Tables 4.19 and 4.20 that a better prediction of the ultimate loads of compact sections can be obtained by considering the cold-work effect for the I-shaped stub columns. Comparing Table 4.15 to Table 4.19, it was observed that the ultimate loads caculated based on tensile yield stresses are better than the those calculated based on compressive yield stresses for the stub columns fabricated from 35XF sheet steel.

D. EVALUATION OF BEAM TEST DATA

Two types of beam specimens were tested to study the stiffened and unstiffened compression elements subjected to dynamic loads. The width-to-thickness ratio of stiffened and unstiffened elements controls the failure mode of the beam. Since the material properties and stress-strain relationships are influenced by strain rate, comparisons between the experimental results and the failure loads predicted by the current AISI Automotive Steel Design Manual[1] using static and dynamic material properties are presented in this section. In order to consider the effect of cold-work on the strength of beams, comparisons were also

made between the test results and the predicted loads for compact sections.

1. Beam Tests for the Study of Stiffened Elements. Hat-shaped beam specimens fabricated from 35XF and 50XF sheet steels were tested for studying the postbuckling strength of stiffened compression elements. All beam specimens were subjected to pure moments between two loading points located at one-eighth of span length from end supports. The weight of test beam specimen and the cross beam placed on the top of the specimen are light enough (approximate 70 lbs.) to be neglected in the evaluation of test results. The compressive yield stress obtained from material tests was used for calculating the critical local buckling moment (M_{cr}) and the tested tensile stress was used to evaluate the yield moment (M_y) and the the ultimate moment (M_u) for all beam specimens.

a. Critical Local Buckling Strength. The compression element of beam specimens may buckle locally in the elastic or inelastic range, depending on the w/t ratio of the compression element. The elastic critical local buckling stress, $(f_{cr})_E$, of stiffened compression elements subjected to a uniform compression can be calculated by using Equation 2.22 which is derived from Bryan's differential equation based on small deflection. If the critical buckling stress exceeds the proportional limit, the compression element buckles in the inelastic range. Therefore, the concept of tangent modulus[99] can be applied to calculate the inelastic buckling stress, $(f_{cr})_I$, by using Equation 4.3.

The critical local buckling moment ($(M_{cr})_{comp}$) of a beam can be predicted by using Equation 4.10. The buckling cofficient used to compute

the critical buckling stress, f_{cr}, ($(f_{cr})_E$ or $(f_{cr})_I$) in Equation 4.10 is equal to 4.0 for stiffened compression elements supported along both longitudinal edges. Consequently, the computed critical local buckling moment can be calculated as follows:

$$(M_{cr})_{comp} = S_{xc} f_{cr} \qquad (4.10)$$

where f_{cr} = critical local buckling stress

S_{xc} = elastic section modulus of the full cross section relative to the compression flange

The tested critical local buckling moments of beam specimens were determined from the product of the bending arm (L/8) and one half of the tested critical local buckling load ($P_{cr}/2$) as follows:

$$(M_{cr})_{test} = \frac{P_{cr} L}{16} \qquad (4.11)$$

where P_{cr} = tested critical local buckling load

L = span length of beam specimen

The computed critical local buckling moments determined from Equation 4.10 and the tested critical moments obtained from Equation 4.11 are presented in Tables 4.21 and 4.22 for 35XF and 50XF sheet steels, respectively. The tested critical local buckling loads ($(P_{cr})_{test}$) listed in column (3) of Tables 4.21 and 4.22 were determined from load-strain relationships by using the modified strain reversal method. The computed local buckling moments listed in column (4) of Tables 4.21 and 4.22 were calculated on the basis of dynamic material properties.

Table 4.21

Comparison of Computed and Tested Critical local Buckling Moments
Beam Specimens with a Stiffened Flange (Based on k=4.0)
(35XF Sheet Steel)

Spec.	S_{xc} ($in.^3$) (1)	f_{cr} (ksi) (2)	$(P_{cr})_{test}$ (kips) (3)	$(M_{cr})_{comp}$ (in.-kips) (4)	$(M_{cr})_{test}$ (in.-kips) (5)	(5)/(4) (6)
3A0A	0.342	28.12	N/A	9.62	N/A	N/A
3A1A	0.335	28.02	N/A	9.39	N/A	N/A
3A1B	0.338	28.04	N/A	9.48	N/A	N/A
3A2A	0.343	30.22	N/A	10.36	N/A	N/A
3A2B	0.338	30.09	N/A	10.17	N/A	N/A
3B0A	1.011	23.55	5.833	23.81	26.61	1.117
3B1A	1.010	23.73	6.214	23.97	28.35	1.183
3B1B	1.005	23.55	5.774	23.67	26.34	1.113
3B2A	1.003	25.66	6.106	25.74	27.86	1.082
3B2B	1.009	25.63	N/A	25.86	N/A	N/A
3C0A	1.615	18.38	5.042	29.68	28.68	0.966
3C1A	1.635	18.16	5.291	29.69	30.10	1.014
3C1B	1.638	18.19	5.217	29.79	29.67	0.996
3C2A	1.626	18.17	5.823	29.54	33.12	1.121
3C2B	1.624	18.45	5.760	29.96	32.76	1.093
Mean						1.076
Standard Deviation						0.066

Note: The dynamic compressive yield stress was used for calculating the critical local buckling moment ($(M_{cr})_{comp}$).

Table 4.22

Comparison of Computed and Tested Critical Local Buckling Moments
Beam Specimens with a Stiffened Flange (Based on k=4.0)
(50XF Sheet Steel)

Spec.	S_{xc} ($in.^3$) (1)	f_{cr} (ksi) (2)	$(P_{cr})_{test}$ (kips) (3)	$(M_{cr})_{comp}$ (in.-kips) (4)	$(M_{cr})_{test}$ (in.-kips) (5)	(5)/(4) (6)
3A0AX	0.206	45.70	N/A	9.41	N/A	N/A
3A1AX	0.209	46.80	N/A	9.80	N/A	N/A
3A1BX	0.211	46.81	N/A	9.86	N/A	N/A
3A2AX	0.210	49.14	N/A	10.31	N/A	N/A
3A2BX	0.206	49.17	N/A	10.14	N/A	N/A
3B0AX	0.570	40.81	5.57	23.25	19.84	0.853
3B1AX	0.568	41.18	5.79	23.40	20.63	0.882
3B1BX	0.570	41.18	6.03	23.48	21.48	0.915
3B2AX	0.570	42.54	5.76	24.24	20.52	0.847
3B2BX	0.570	42.61	6.11	24.29	21.78	0.897
3C0AX	1.002	24.42	6.68	24.47	27.97	1.143
3C1AX	0.996	25.01	6.28	24.92	26.29	1.055
3C1BX	0.998	24.43	6.21	24.39	26.00	1.066
3C2AX	0.987	24.42	6.17	24.10	25.84	1.072
3C2BX	0.992	25.01	6.17	24.81	25.84	1.042
Mean						0.977
Standard Deviation						0.109

Note: The dynamic compressive yield stress was used for calculating the critical local buckling moment ($(M_{cr})_{comp}$).

From load-strain relationships of beam specimens, it can be observed that no local buckling occured in the specimens with small w/t ratios for both sheet steels. The comparisons of computed and tested local critical moments are listed in column (6) of Tables 4.21 and 4.22. The mean values of $(M_{cr})_{test}/(M_{cr})_{comp}$ ratios for specimens fabricated from 35XF and 50XF sheet steels are 1.076 and 0.977 with standard deviations of 0.066 and 0.109, respectively. Similar to the results of stub-column tests, it seems that the computed buckling moments for hat-shaped beams fabricated from 50XF sheet steel are slightly less conservative than the beams fabricated from 35XF sheet steel. It was noted that the number of half sine waves developed in the stiffened compression flanges of the specimens having large w/t ratios is the same for all tests regardless of the strain rate used for the test.

b. Nominal Flexural Strength. According to the AISI Specification[66], two methods can be used to calculate the nominal strength of beams. One is based on the initiation of yielding using the effective section and the other is based on the inelastic reserve capacity. Same as that used in the analysis of stub columns, the effective design formulas (Equation 2.39) can be used to calculate the effective section properties. For the stiffened compression element, when the ratio of w/t exceeds the value of $((w/t)_{lim})$ (Equation 2.46) the effective width design formulas can be used to compute the effective width of stiffened elements.

i) Yield flexural strength. Based on the initiation of yielding in the effective section, the computed yield moment $((M_y)_{comp})$ of a beam can be calculated by using the following equation:

$$(M_y)_{comp} = F_y S_e \qquad (4.12)$$

where F_y = static or dynamic yield stress of steel

S_e = elastic section modulus of effective section

The computed yield moment was determined on the basis of the effective design width formulas (Equations 3.9) with the extreme compression and/or tension stress at yield point (F_y). The tested yield moments of beam specimens were determined from the product of bending arm (L/8) and one half of the yield load ($P_y/2$) as follows:

$$(M_y)_{test} = \frac{P_y L}{16} \qquad (4.13)$$

The tested yield load (P_y) shown above was determined from the load-strain relationship for each individual specimen. Tables 4.23(a) and 4.23(b) compare the computed and tested yield moments for 35XF sheet steel. Similarly, Tables 4.24(a) and 4.24(b) present the values for 50XF sheet steel. The computed yield moments listed in column (4) of Tables 4.23(a) and 4.24(a) are based on the static tensile yield stresses, while the values listed in column (4) of Tables 4.23(b) and 4.24(b) are based on the dynamic tensile stresses corresponding to the strain rate used in the test. The tested yield moments are listed in Column (5) of Tables 4.23 and 4.24.

Comparisons of the computed yield moments based on the static yield stresses and the tested yield moments are listed in column (6) of Tables 4.23(a) and 4.24(a). The mean values of $(M_y)_{test}/(M_y)_{comp}$ ratios for the hat-spaped sections made of 35XF and 50XF sheet steels are 1.321 and 1.057

with standard deviations of 0.148 and 0.126, respectively. Comparsions of the computed yield moments based on the dynamic yield stresses and the tested yield moments are listed in column (6) of Tables 4.23(b) and 4.24(b). The mean values and standard deviations of $(M_y)_{test}/(M_y)_{comp}$ ratios are (1.237 and 0.102) for 35XF sheet steel and (1.028 and 0.117) for 50XF sheet steel.

As expected, the ratios of tested to computed yield moments listed in Tables 4.23(a) and 4.24(a) are larger than those listed in Tables 4.23(b) and 4.24(b), because the latter tables take into account the effect of strain rate on yield stress. It is noted that all computed yield moments are lower than the tested yield moments for using 35XF sheet steel. However, for using 50XF sheet steel, some computed yield moments are higher than the tested yield moments. It is also noted from those tables that the tested yield moment increases with strain rate for specimens having the same w/t ratios.

In order to consider the effect of cold-work on the bending strength of the beam, comparisons were made between the tested and computed yield moments for compact beam specimens with small w/t ratios. According to the AISI Cold-Formed Steel Design Specification[66], the strength of a compact section (i.e. $\rho = 1$) including the cold-work of forming may be determined by substituting F_{ya} (average tensile yield stress of the beam flange) for F_y. The formula used for calculating F_{ya} for the beam section is the same as that for the stub column. However, the value of C used in Equation 4.6 is defined as the ratio of the total corner cross-sectional area of the controlling flange to the full cross-sectional area of the controlling flange.

Table 4.23

Comparison of Computed and Tested Yield Moments
Beam Specimens with a Stiffened Flange
(35XF Sheet Steel)

(a) Based on Static Tensile Yield Stress

Spec.	S_e ($in.^3$) (1)	F_y (ksi) (2)	$(P_y)_{test}$ (kips) (3)	$(M_y)_{comp}$ (in.-kips) (4)	$(M_y)_{test}$ (in.-kips) (5)	(5)/(4) (6)
3A0A	0.268	32.02	3.773	8.58	10.14	1.182
3A1A	0.258	32.02	3.936	8.25	10.58	1.282
3A1B	0.262	32.02	4.137	8.39	11.12	1.325
3A2A	0.271	32.02	4.799	8.68	12.90	1.486
3A2B	0.260	32.02	4.844	8.32	13.02	1.565
3B0A	0.635	32.02	5.824	20.32	26.57	1.307
3B1A	0.646	32.02	4.894	20.69	22.33	1.079
3B1B	0.629	32.02	5.668	20.15	25.86	1.283
3B2A	0.626	32.02	6.511	20.04	29.71	1.482
3B2B	0.632	32.02	7.130	20.23	32.53	1.608
3C0A	0.924	32.02	6.038	29.58	34.34	1.161
3C1A	0.930	32.02	6.825	29.79	38.82	1.303
3C1B	0.932	32.02	6.112	29.86	34.76	1.164
3C2A	0.925	32.02	6.873	29.61	39.09	1.320
3C2B	0.930	32.02	6.684	29.78	38.01	1.276
Mean						1.321
Standard Deviation						0.148

(Considering Cold-Work of Forming)

3A0A	0.268	38.42	3.773	10.30	10.14	0.984
3A1A	0.258	38.40	3.936	9.90	10.58	1.069
3A1B	0.262	38.38	4.137	10.06	11.12	1.105
3A2A	0.271	38.36	4.799	10.40	12.90	1.240
3A2B	0.260	38.40	4.844	9.98	13.02	1.305
Mean(with consideration of cold-work)						1.141
Standard Deviation(with consideration of cold-work)						0.130
Mean(without consideration of cold-work)						1.368
Standard Deviation(without consideration of cold-work)						0.155

Table 4.23 (Cont'd)

(b) Based on Dynamic Tensile Yield Stress

Spec.	S_e ($in.^3$) (1)	F_y (ksi) (2)	$(P_y)_{test}$ (kips) (3)	$(M_y)_{comp}$ (in.-kips) (4)	$(M_y)_{test}$ (in.-kips) (5)	(5)/(4) (6)
3A0A	0.268	32.02	3.773	8.58	10.14	1.182
3A1A	0.258	32.87	3.936	8.46	10.58	1.251
3A1B	0.262	32.87	4.137	8.62	11.12	1.290
3A2A	0.271	36.40	4.799	9.87	12.90	1.307
3A2B	0.260	36.40	4.844	9.45	13.02	1.378
3B0A	0.635	32.02	5.824	20.32	26.57	1.307
3B1A	0.645	32.87	4.894	21.21	22.33	1.053
3B1B	0.629	32.87	5.668	20.66	25.86	1.252
3B2A	0.623	36.40	6.511	22.66	29.71	1.311
3B2B	0.628	36.40	7.130	22.87	32.53	1.422
3C0A	0.924	32.02	6.038	29.58	34.34	1.161
3C1A	0.929	32.87	6.825	30.53	38.82	1.271
3C1B	0.931	32.87	6.112	30.61	34.76	1.135
3C2A	0.917	36.40	6.873	34.33	39.09	1.139
3C2B	0.922	36.40	6.684	34.52	38.01	1.101
Mean						1.237
Standard Deviation						0.102

(Considering Cold-Work of Forming)

3A0A	0.268	38.42	3.773	10.30	10.14	0.984
3A1A	0.258	39.17	3.936	10.09	10.58	1.049
3A1B	0.262	39.14	4.137	10.26	11.12	1.084
3A2A	0.271	42.54	4.799	11.54	12.90	1.118
3A2B	0.260	42.59	4.844	11.06	13.02	1.177
Mean(with consideration of cold-work)						1.082
Standard Deviation(with consideration of cold-work)						0.072
Mean(without consideration of cold-work)						1.282
Standard Deviation(without consideration of cold-work)						0.072

Table 4.24

Comparison of Computed and Tested Yield Moments
Beam Specimens with a Stiffened Flange
(50XF Sheet Steel)

(a) Based on Static Tensile Yield Stress

Spec.	S_e ($in.^3$) (1)	F_y (ksi) (2)	$(P_y)_{test}$ (kips) (3)	$(M_y)_{comp}$ (in.-kips) (4)	$(M_y)_{test}$ (in.-kips) (5)	(5)/(4) (6)
3A0AX	0.152	48.81	2.90	7.40	6.71	0.907
3A1AX	0.151	48.81	3.21	7.38	7.42	1.005
3A1BX	0.152	48.81	3.02	7.44	6.98	0.938
3A2AX	0.152	48.81	3.22	7.40	7.45	1.007
3A2BX	0.150	48.81	3.34	7.33	7.72	1.053
3B0AX	0.371	48.81	5.80	18.10	20.66	1.141
3B1AX	0.374	48.81	5.86	18.23	20.88	1.145
3B1BX	0.375	48.81	6.33	18.29	22.58	1.234
3B2AX	0.376	48.81	6.41	18.34	22.84	1.245
3B2BX	0.376	48.81	6.72	18.33	23.94	1.306
3C0AX	0.591	48.81	6.38	28.84	26.72	0.926
3C1AX	0.596	48.81	6.79	29.09	28.42	0.977
3C1BX	0.588	48.81	6.80	28.70	28.45	0.991
3C2AX	0.588	48.81	6.82	28.72	28.54	0.994
3C2BX	0.589	48.81	6.72	28.77	28.14	0.978
Mean						1.057
Standard Deviation						0.126

Table 4.24 (Cont'd)

(b) Based on Dynamic Tensile Yield Stress

Spec.	S_e ($in.^3$) (1)	F_y (ksi) (2)	$(P_y)_{test}$ (kips) (3)	$(M_y)_{comp}$ (in.-kips) (4)	$(M_y)_{test}$ (in.-kips) (5)	(5)/(4) (6)
3A0AX	0.152	48.81	2.90	7.40	6.71	0.907
3A1AX	0.151	49.50	3.21	7.48	7.42	0.992
3A1BX	0.152	49.50	3.02	7.54	6.98	0.926
3A2AX	0.152	51.60	3.22	7.81	7.45	0.954
3A2BX	0.150	51.60	3.34	7.75	7.72	0.996
3B0AX	0.371	48.81	5.80	18.10	20.66	1.141
3B1AX	0.373	49.50	5.86	18.48	20.88	1.130
3B1BX	0.375	49.50	6.33	18.54	22.58	1.218
3B2AX	0.375	51.60	6.41	19.34	22.84	1.181
3B2BX	0.375	51.60	6.72	19.33	23.94	1.238
3C0AX	0.591	48.81	6.38	28.84	26.72	0.926
3C1AX	0.595	49.50	6.79	29.48	28.42	0.964
3C1BX	0.587	49.50	6.80	29.08	28.45	0.978
3C2AX	0.586	51.60	6.82	30.26	28.54	0.943
3C2BX	0.587	51.60	6.72	30.31	28.14	0.928
Mean						1.028
Standard Deviation						0.117

The computed yield moments for Specimen series 3A by considering cold-work of forming and the tested yield moments are presented in the lower portions of Tables 4.23(a) and 4.23(b) for hat-shaped beam specimens fabricated from 35XF sheet steel. The mean values and standard deviations are based on 5 beam specimens. These two tables indicate the improvements of computed yield moments when cold-work of forming was considered. However, from Tables 4.24(a) and 4.24(b), it was found that the computed ultimate loads by considering cold-work of forming is not conservative for the box-shaped stub columns fabricated from 50XF sheet steel. In consideration of the cold-work of forming for beams fabricated from 50XF sheet steel, the values of C used to calculate the average tensile yield stresses of the beam flanges are much larger than the values calculated for the stub columns. As a result, the $(M_y)_{test}/(M_y)_{comp}$ ratios of compact sections are lower than 1.0 as shown in Table 4.24(b). Therefore, the effect of cold-work of forming was not considered for the computed yield moments for the beam specimens fabricated from 50XF sheet steel.

ii) Inelastic reserve capacity. The inelastic reserve capacity of flexural members, which allows partial yielding of a cross section, is recognized in the current AISI Automotive Steel Design Manual[1]. It can be used to predict the ultimate moments of flexural members provided that such members satisfy the specific requirements. The ultimate strengths of hat sections or track sections with yielded tension flanges may be calculated on the basis of inelastic reserve capacity. According to the AISI Specification[66], the inelastic flexural reserve capacity may be used when the following conditions are met:

(1) The member is not subject to twisting or to lateral, torsional, or torsional-flexural buckling.

(2) The effect of cold forming is not included in determining the yield point F_y.

(3) The ratio of the depth of the compressed portion of the web to its thickness does not exceed λ_1(Equation 4.17).

(4) The shear force does not exceed $0.35F_y$ times the web area (hxt).

(5) The angle between any web and the vertical does not exceed 30 degrees.

Figure 4.25 shows the stress distribution in sections with yielded tension flanges at ultimate moment. The inelastic stress distribution in the cross section depends on the maximum strain in the compression flange. The following equations can be used to compute the values of y_c, y_t, y_p, and y_{tp} shown in Figure 4.25 and the ultimate moment, M_u. For the purpose of simplicity, midline dimensions were used in the calculations[24].

$$y_c = \frac{b_t - b_c + 2d}{4} \qquad (4.14a)$$

$$y_t = d - y_c \qquad (4.14b)$$

$$y_p = \frac{y_c}{C_y} \qquad (4.14c)$$

$$y_{cp} = y_c - y_p \qquad (4.14d)$$

$$y_{tp} = y_t - y_p \qquad (4.14e)$$

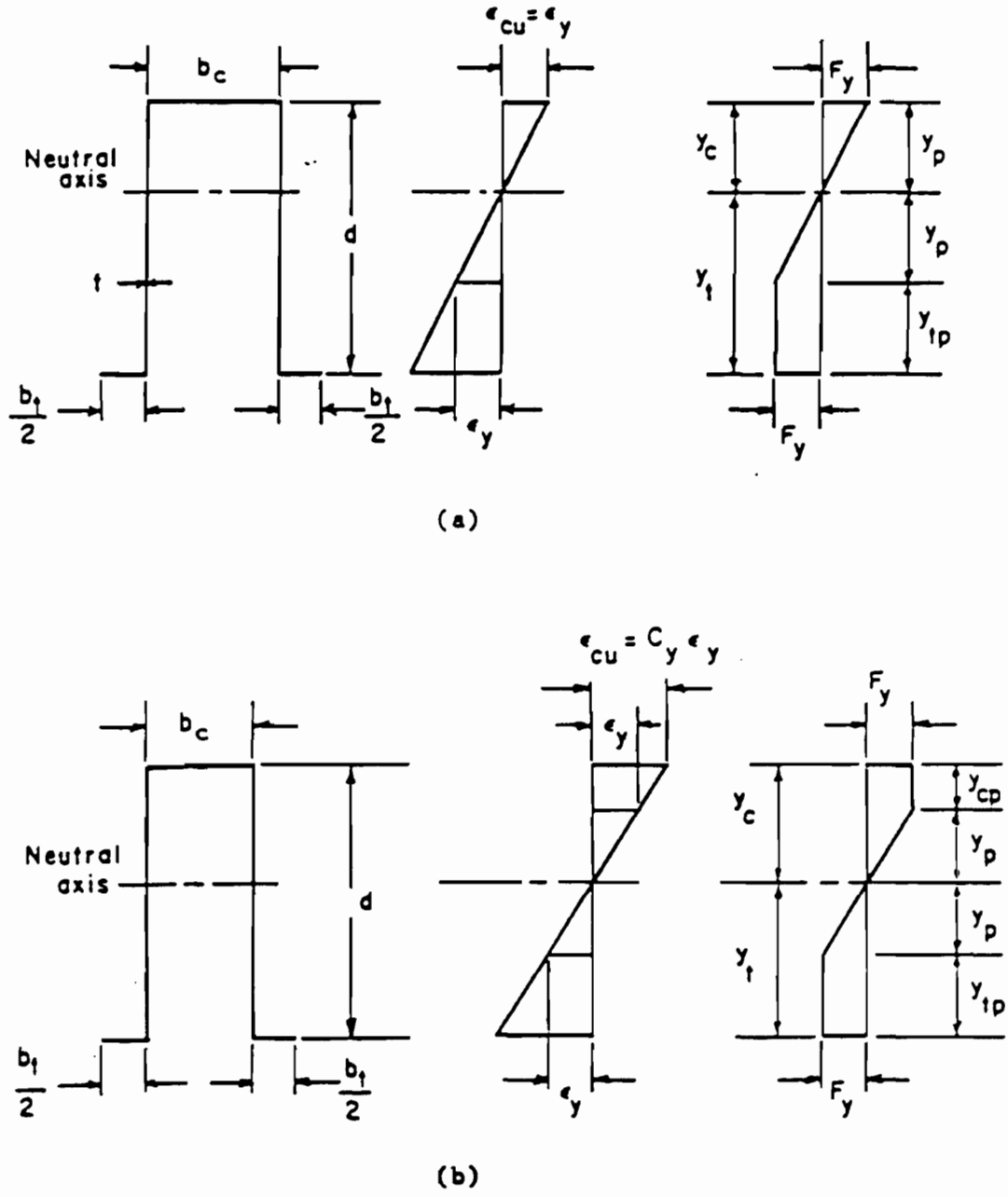

Figure 4.25 Stress Distribution in Sections with Yielded Tension Flanges at Ultimate Moments[12]

$$M_u = F_y t\left[b_c y_c + 2y_{cp}(y_p + \frac{y_{cp}}{2}) + \frac{4}{3}(y_p)^2 + 2y_{tp}(y_p + \frac{y_{tp}}{2}) + b_t y_t \right] \qquad (4.15)$$

where b_c = effective width of the compression flange

b_t = total width of the tension flange

d = depth of the section

t = thickness of the section

C_y = compression strain factor for stiffened compression elements without intermediate stiffeners, which can be determined as follows:

$$C_y = 3 \qquad \text{for} \quad w/t \le \lambda_1 \qquad (4.16a)$$

$$C_y = 3 - 2(\frac{w/t - \lambda_1}{\lambda_2 - \lambda_1}) \qquad \text{for} \quad \lambda_1 < w/t < \lambda_2 \qquad (4.16b)$$

$$C_y = 1 \qquad \text{for} \quad w/t \ge \lambda_2 \qquad (4.16c)$$

where $$\lambda_1 = \frac{1.11}{\sqrt{F_y/E}} \qquad (4.17)$$

$$\lambda_2 = \frac{1.28}{\sqrt{F_y/E}} \qquad (4.18)$$

According to the AISI Automotive Steel Design Manual[1], The computed ultimate moments obtained from Equation 4.15 should not exceed the limit of $1.25\ S_e F_y$. The tested ultimate moments of beam specimens were determined from the product of bending arm (L/8) and one half of the ultimate load ($P_u/2$) as follows:

$$(M_u)_{test} = \frac{P_u L}{16} \qquad (4.19)$$

Tables 4.25(a) and 4.25(b) present the computed ultimate moments computed from Equation 4.15 and the tested ultimate moments obtained from the tests for 35XF sheet steel. Tables 4.26(a) and 4.26(b) present the similar values for 50XF sheet steel. Similar to Tables 4.23 and 4.24, Tables 4.25(a) and 4.26(a) use static tensile stresses while Tables 4.25(b) and 4.26(b) use dynamic yield stresses corresponding to the strain rate used in the test. The tested ultimate loads are listed in column (3) of Tables of 4.25 and 4.26. Comparsions of the computed ultimate moments based on the static yield stresses and the tested ultimate moments are listed in Column (6) of Tables 4.25(a) and 4.26(a). The mean value of $(M_u)_{test}/(M_u)_{comp}$ ratios for hat-shaped sections made of 35XF and 50XF sheet steels are 1.270 and 1.063 with standard deviations of 0.198 and 0.075, respectively. Comparisons between the computed ultimate moments based on the dynamic yield stresses and the tested ultimate moments are listed in column (6) of Tables of 4.25(b) and 4.26(b). The mean values and standard deviations of $(M_u)_{test}/(M_u)_{comp}$ ratios are (1.191 and 0.169) for using 35XF sheet steel and (1.036 and 0.063) for using 50XF sheet steel.

It is noted from column (6) of these tables that the ratio of the tested ultimate moment to the computed ultimate moment decreases with increasing w/t ratio. Figure 4.26 shows graphically a typical moment-displacement diagram for the beam specimen. The computed critical moment($(M_{cr})_{comp}$), yield moment($(M_y)_{comp}$), and ultimate moment($(M_u)_{comp}$) are marked in this figure for the purpose of comparison. It can be seen

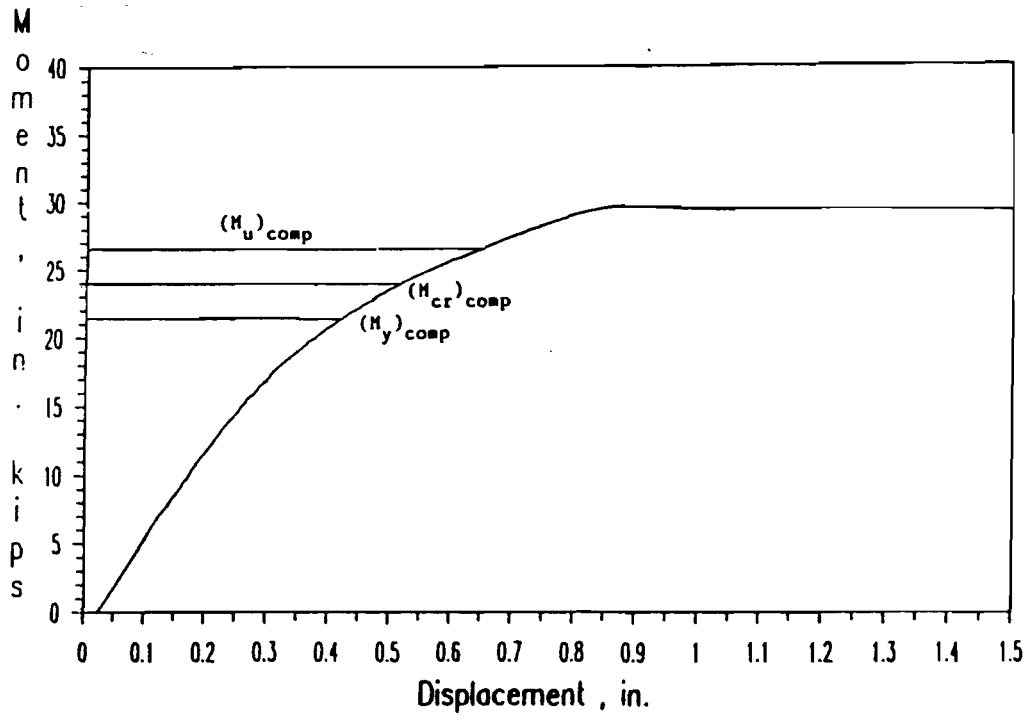

Figure 4.26 Moment-Displacement Curve for Hat-Shaped Beam Specimens (Spec. 3B1A)

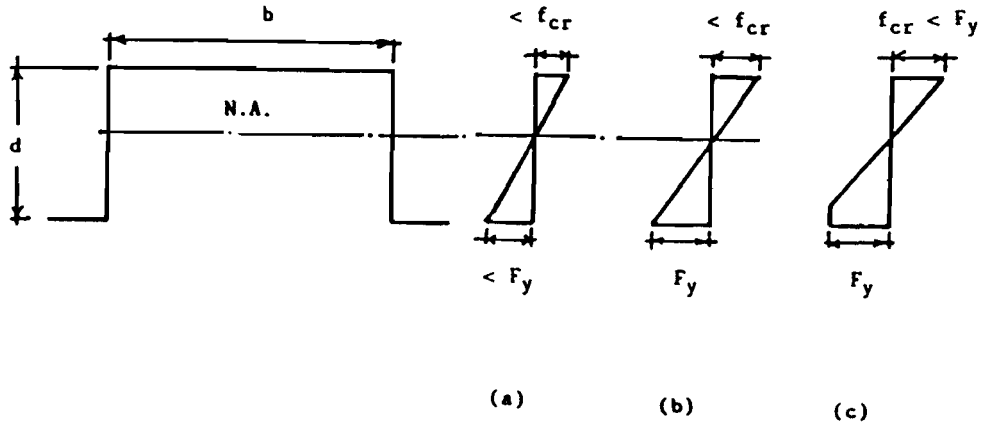

Figure 4.27 Stress Distribution in Hat Sections

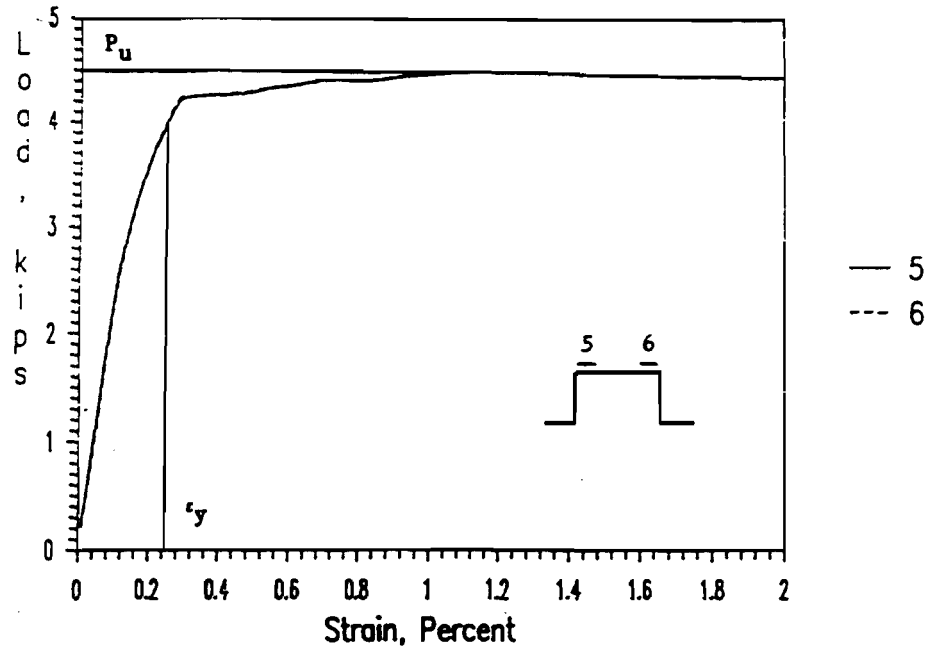

(a) Compressive Strain

(b) Tensile Strain

Figure 4.28 Load-Strain Curves for a Hat-Shaped Beam Specimen Using 50XF Sheet Steel (3A1AX)

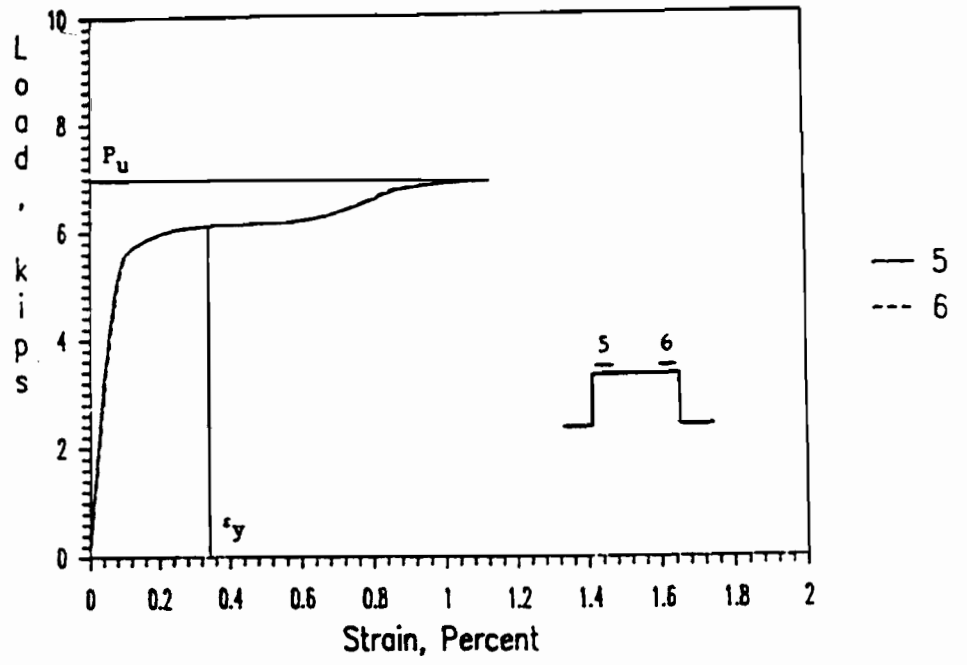

(a) Compressive Strain

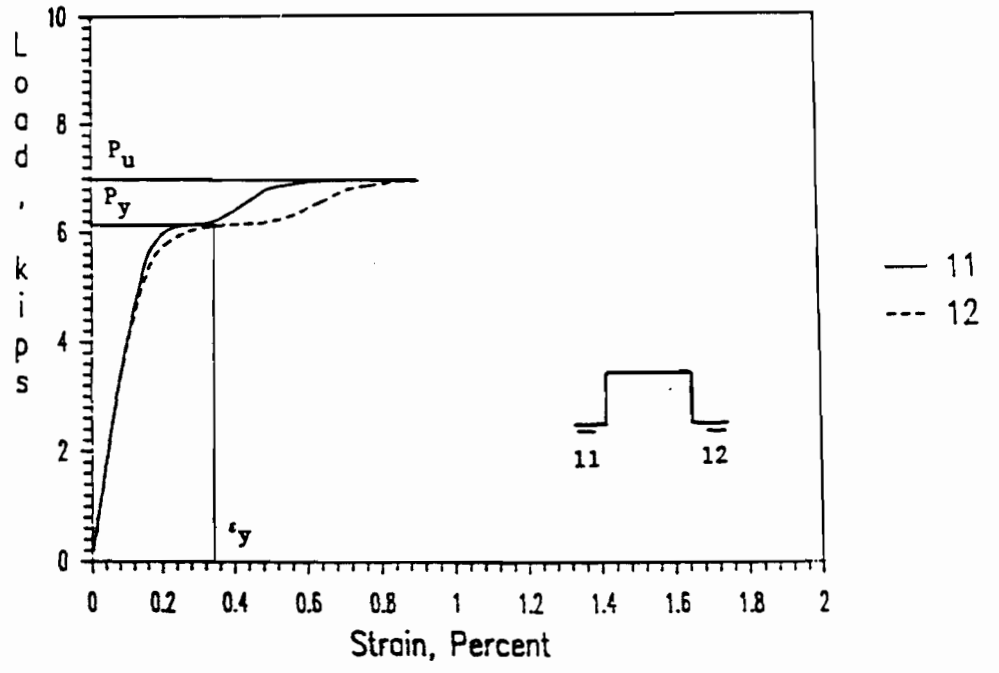

(b) Tensile Strain

Figure 4.29 Load-Strain Curves for a Hat-Shaped Beam Specimen Using 35XF Sheet Steel (3C1B)

from Figure 4.26 that for Specimen 3B1A the critical buckling moment is greater than the yield moment. This is because the stress in the compression flange at the initiation of yielding in the tension flange is less than the critical local buckling stress as shown in Figure 4.27(b). The critical local buckling moment was calculated according to the stress distribution shown in Figure 4.27(c) and assuming that the strain diagram is linear.

Figure 4.28 shows the load-strain diagrams of a hat-shaped beam specimen 3A1AX using 50XF sheet steel. The curves shown in Figure 4.28(a) are drawn from the readings of paired strain gages (5 and 6) mounted on the compression flange of the beam. The readings of the paired strain gages (11 and 12) mounted on the tension flanges of the beam are shown in Figure 4.28(b). It can be seen that the bottom flanges of the hat-shaped beam reached the yield point first, because the neutral axis is close to the top flange. By comparing Figure 4.28 with the results obtained from the material tests as shown in Figures 3.8 and 3.17, It is noted that the strains of the beam specimen remained in the plastic range as the beam specimen reached its maximum capacity. Figure 4.29 shows the similar plots for the specimen 3C1B using 35XF sheet steel.

Figures 4.30 and 4.31 show graphically the effect of strain rate on the ratio of the tested ultimate moment to the computed ultimate moment obtained from Tables 4.24(a) and 4.24(b), respectively. Similarly, Figures 4.32 and 4.33 show the strain rates vs. the ratios of the tested ultimate moment to the computed ultimate moment obtained from Tables 4.25(a) and 4.25(b). Tables 4.27 and 4.28 list the average tested ultimate moments for beam specimens with stiffened flanges using 35XF and

Table 4.25(a)

Comparison of Computed and Tested Failure Moments Based on the Effective width Formulas in the 1991 AISI Automotive Steel Design Manual for Beam Specimens with a Stiffened Flange (35XF Sheet Steel)

(a) Based on Static Tensile Yield Stress

Spec.	Strain Rate in./in./sec. (1)	F_y (ksi) (2)	$(P_u)_{test}$ (kips) (3)	$(M_u)_{comp}$ (in.-kips) (4)	$(M_u)_{test}$ (in.-kips) (5)	(5)/(4) (6)
3A0A	0.00001	32.02	5.69	10.73	15.29	1.425
3A1A	0.0001	32.02	5.43	10.33	14.59	1.412
3A1B	0.0001	32.02	5.72	10.49	15.37	1.465
3A2A	0.01	32.02	6.31	10.85	16.96	1.563
3A2B	0.01	32.02	6.39	10.41	17.17	1.649
3B0A	0.00001	32.02	6.38	25.41	29.11	1.146
3B1A	0.0001	32.02	6.54	25.86	29.84	1.154
3B1B	0.0001	32.02	6.49	25.17	29.61	1.176
3B2A	0.01	32.02	6.97	25.05	31.80	1.269
3B2B	0.01	32.02	7.63	25.29	34.81	1.376
3C0A	0.00001	32.02	6.53	36.98	37.14	1.004
3C1A	0.0001	32.02	6.99	37.22	39.75	1.068
3C1B	0.0001	32.02	6.96	37.30	39.58	1.061
3C2A	0.01	32.02	7.45	37.02	42.37	1.144
3C2B	0.01	32.02	7.42	37.22	42.20	1.134
Mean						1.270
Standard Deviation						0.198

Note : The cold-work of forming was not considered for the Specimen 3A because the inelastic reserve capacity was used for the calculation of ultimate moments.

Table 4.25 (Cont'd)

(b) Based on Dynamic Tensile Yield Stress

Spec.	Strain Rate in./in./sec. (1)	F_y (ksi) (2)	$(P_u)_{test}$ (kips) (3)	$(M_u)_{comp}$ (in.-kips) (4)	$(M_u)_{test}$ (in.-kips) (5)	(5)/(4) (6)
3A0A	0.00001	32.02	5.69	10.73	15.29	1.425
3A1A	0.0001	32.87	5.43	10.57	14.59	1.380
3A1B	0.0001	32.87	5.72	10.77	15.37	1.427
3A2A	0.01	36.40	6.31	12.34	16.96	1.374
3A2B	0.01	36.40	6.39	11.81	17.17	1.454
3B0A	0.00001	32.02	6.38	25.40	29.11	1.146
3B1A	0.0001	32.87	6.54	26.51	29.84	1.126
3B1B	0.0001	32.87	6.49	25.82	29.61	1.147
3B2A	0.01	36.40	6.97	28.32	31.80	1.123
3B2B	0.01	36.40	7.63	28.59	34.81	1.217
3C0A	0.00001	32.02	6.53	36.97	37.14	1.004
3C1A	0.0001	32.87	6.99	38.16	39.75	1.042
3C1B	0.0001	32.87	6.96	38.26	39.58	1.034
3C2A	0.01	36.40	7.45	42.91	42.37	0.987
3C2B	0.01	36.40	7.42	43.15	42.20	0.978
Mean						1.191
Standard Deviation						0.169

Note : The cold-work of forming was not considered for the Specimen 3A because the inelastic reserve capacity was used for the calculation of ultimate moments.

Table 4.26

Comparison of Computed and Tested Failure Moments Based on the Effective width Formulas in the 1991 AISI Automotive Steel Design Manual for Beam Specimens with a Stiffened Flange (50XF Sheet Steel)

(a) Based on Static Tensile Yield Stress

Spec.	Strain Rate in./in./sec. (1)	F_y (ksi) (2)	$(P_u)_{test}$ (kips) (3)	$(M_u)_{comp}$ (in.-kips) (4)	$(M_u)_{test}$ (in.-kips) (5)	(5)/(4) (6)
3A0AX	0.00001	48.81	4.42	9.25	10.22	1.105
3A1AX	0.0001	48.81	4.51	9.22	10.44	1.132
3A1BX	0.0001	48.81	4.44	9.29	10.26	1.104
3A2AX	0.01	48.81	4.56	9.24	10.55	1.142
3A2BX	0.01	48.81	4.93	9.16	11.41	1.246
3B0AX	0.00001	48.81	6.25	22.62	22.28	0.985
3B1AX	0.0001	48.81	6.50	22.79	23.15	1.016
3B1BX	0.0001	48.81	6.67	22.87	23.76	1.039
3B2AX	0.01	48.81	6.69	22.92	23.84	1.040
3B2BX	0.01	48.81	6.98	22.91	24.87	1.086
3C0AX	0.00001	48.81	8.16	34.62	34.16	0.987
3C1AX	0.0001	48.81	8.04	34.69	33.67	0.971
3C1BX	0.0001	48.81	8.25	34.49	34.53	1.001
3C2AX	0.01	48.81	8.72	34.10	36.54	1.072
3C2BX	0.01	48.81	8.43	34.52	35.31	1.023
Mean						1.063
Standard Deviation						0.075

Note : The cold-work of forming was not considered for the Specimen 3A because the inelastic reserve capacity was used for the calculation of ultimate moments.

Table 4.26 (Cont'd)

(b) Based on Dynamic Tensile Yield Stress

Spec.	Strain Rate in./in./sec. (1)	F_y (ksi) (2)	$(P_u)_{test}$ (kips) (3)	$(M_u)_{comp}$ (in.-kips) (4)	$(M_u)_{test}$ (in.-kips) (5)	(5)/(4) (6)
3A0AX	0.00001	48.81	4.42	9.25	10.22	1.105
3A1AX	0.0001	49.50	4.51	9.35	10.44	1.117
3A1BX	0.0001	49.50	4.44	9.43	10.26	1.088
3A2AX	0.01	51.60	4.56	9.77	10.55	1.080
3A2BX	0.01	51.60	4.93	9.69	11.41	1.178
3B0AX	0.00001	48.81	6.25	22.62	22.28	0.985
3B1AX	0.0001	49.50	6.50	23.10	23.15	1.002
3B1BX	0.0001	49.50	6.67	23.18	23.76	1.025
3B2AX	0.01	51.60	6.69	24.17	23.84	0.986
3B2BX	0.01	51.60	6.98	24.16	24.87	1.029
3C0AX	0.00001	48.81	8.16	34.62	34.16	0.987
3C1AX	0.0001	49.50	8.04	35.06	33.67	0.960
3C1BX	0.0001	49.50	8.25	34.86	34.53	0.991
3C2AX	0.01	51.60	8.72	35.56	36.54	1.028
3C2BX	0.01	51.60	8.43	36.01	35.31	0.981
Mean						1.036
Standard Deviation						0.063

Note : The cold-work of forming was not considered for the Specimen 3A because the inelastic reserve capacity was used for the calculation of ultimate moments.

Table 4.27

Average Tested Failure Moments for Beam Specimens with a Stiffened Flange (35XF Sheet Steel)

Strain Rate in./in./sec.	w/t		
	29.64	55.74	76.41
0.00001	15.29	29.11	37.14
0.0001	15.37	29.73	39.67
0.01	17.07	33.31	42.29

Note: The tested value of Specimen 3A1A is not included in this table.

Table 4.28

Average Tested Failure Moments for Beam Specimens with a Stiffened Flange (50XF Sheet Steel)

Strain Rate in./in./sec.	w/t		
	26.68	46.09	65.77
0.00001	10.22	22.28	34.16
0.0001	10.35	23.46	34.10
0.01	10.98	24.36	35.93

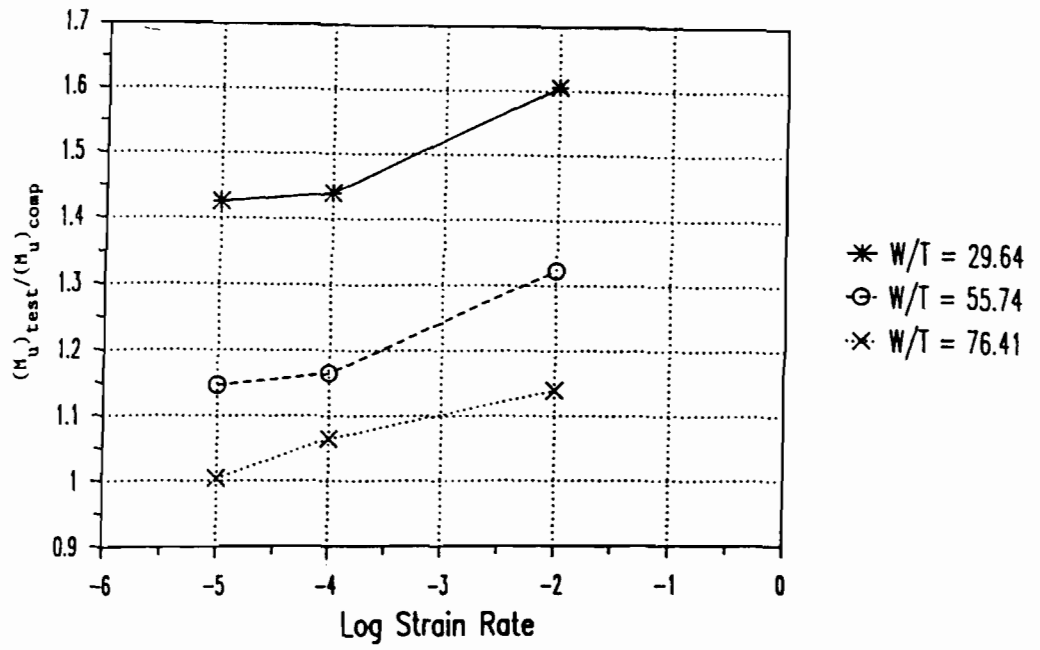

Figure 4.30 Ratios of Tested Failure Moments to Computed Failure Moments (Based on Static Yield Stress) vs. Logarithmic Strain Rate for Hat-Shaped Beams (35XF Sheet Steel)

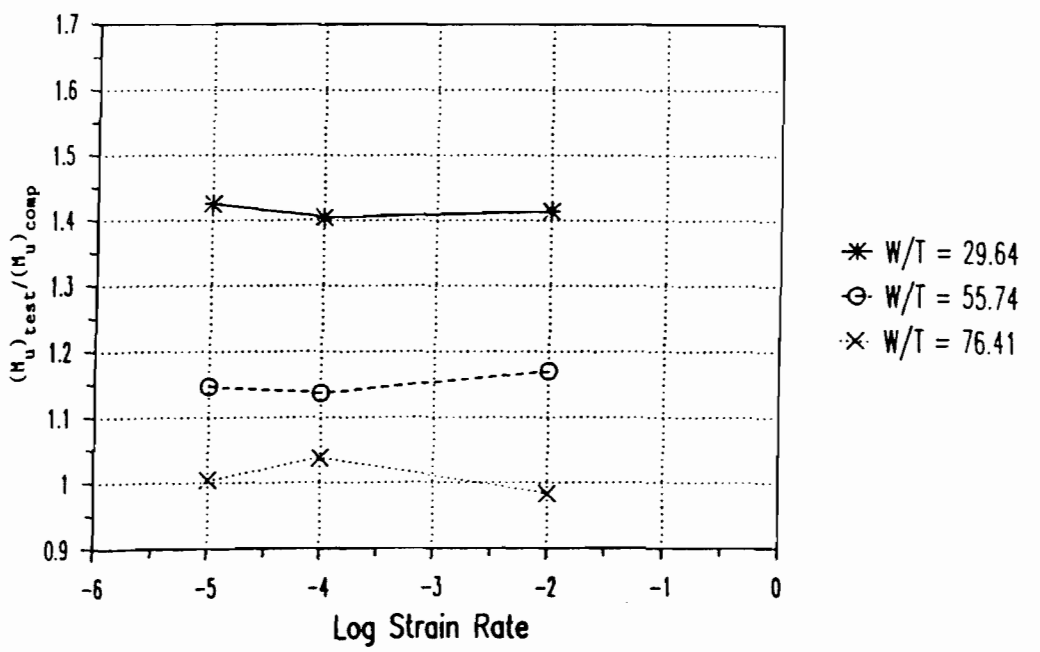

Figure 4.31 Ratios of Tested Failure Moments to Computed Failure Moments (Based on Dynamic Yield Stress) vs. Logarithmic Strain Rate for Hat-Shaped Beams (35XF Sheet Steel)

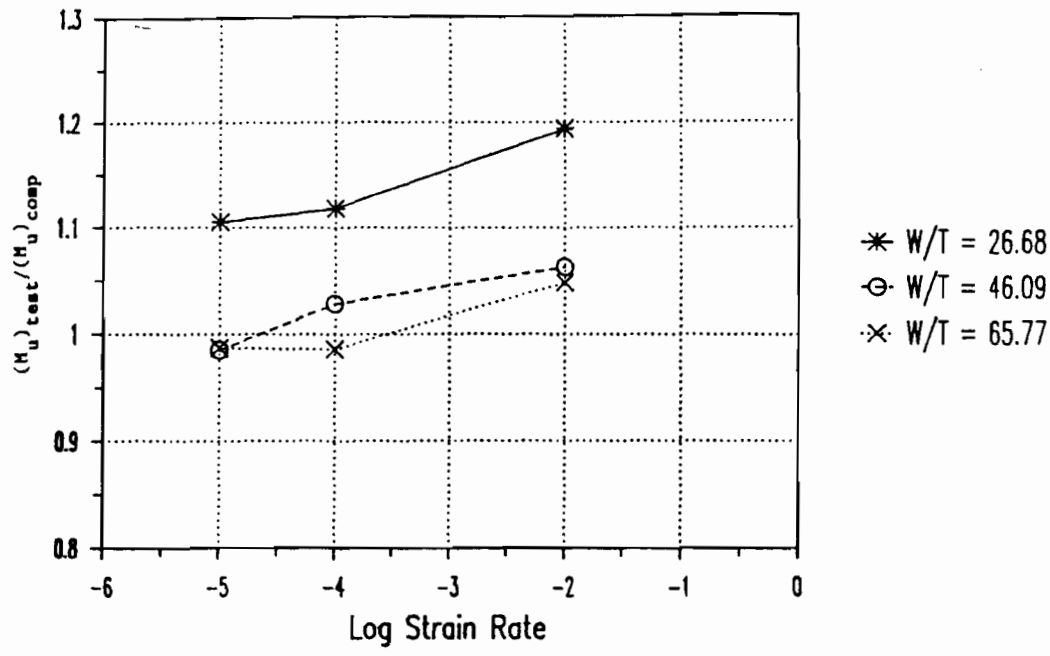

Figure 4.32 Ratios of Tested Failure Moments to Computed Failure Moments (Based on Static Yield Stress) vs. Logarithmic Strain Rate for Hat-Shaped Beams (50XF Sheet Steel)

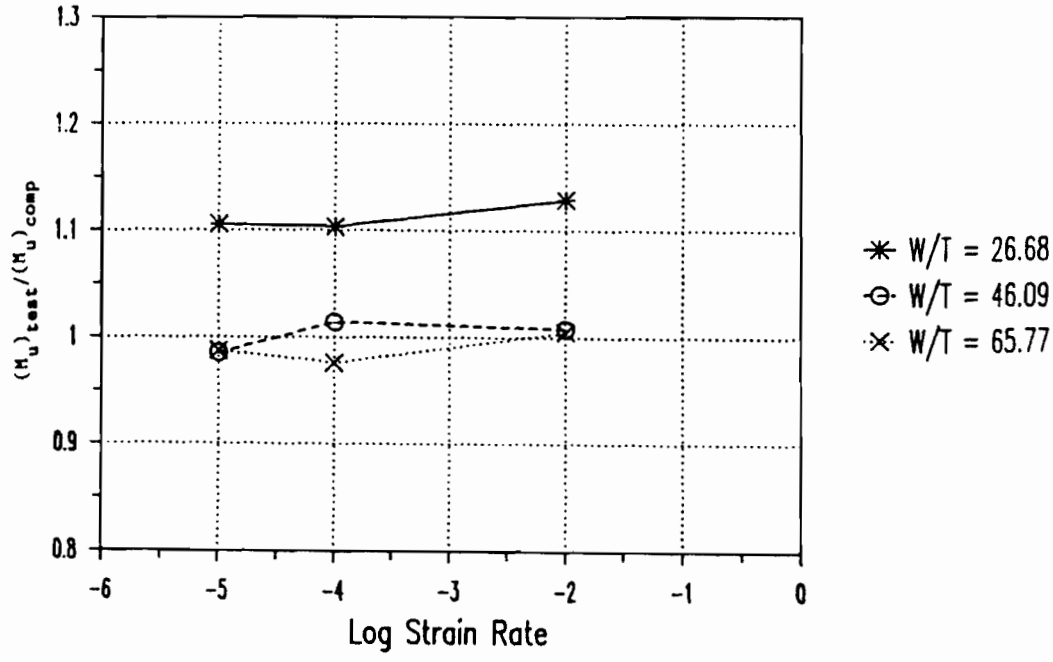

Figure 4.33 Ratios of Tested Failure Moments to Computed Failure Moments (Based on Dynamic Yield Stress) vs. Logarithmic Strain Rate for Hat-Shaped Beams (50XF Sheet Steel)

50XF sheet steels, respectively. Each value given in Tables 4.27 and 4.28 and each point shown in Figures 4.30 through 4.33 is the average of two values obtained from two similar tests.

By comparing the mean values and standard deviations of $(M_u)_{test}/(M_u)_{comp}$ ratios listed in Tables 4.25(a) and 4.25(b) for 35XF sheet steel, it can be seen that the computed ultimate moments using dynamic yield stresses are better than the computed values using static stresses. It is also noted from the same tables that the discrepancies between the tested and computed ultimate moments are excessive particularly for Specimen series 3A. This is because the effect of cold-work was neglected in the calculation of ultimate moments and that the computed ultimate moment were restricted by AISI limit of $1.25S_eF_y$.

Similar to the results of stub-column specimens for studying stiffened elements, computed ultimate moments are lower than the tested ultimate moments for all beams fabricated from 35XF sheet steel. However, for the 50XF sheet steel, the computed ultimate moments are higher than the tested ultimate moments for some beams. Therefore, the prediction of ultimate moments for hat-shaped beams fabricated from 50XF sheet steel were found to be less conservative than the beams fabricated from 35XF sheet steel. Tables 4.27 and 4.28 show that the tested ultimate moment increases with strain rate for specimens having the same w/t ratios.

2. Beam Tests for the Study of Unstiffened Elements. Beam specimens using channel sections fabricated from 35XF and 50XF sheet steels were tested for studying the postbuckling strength of unstiffened elements. All beam specimens were subjected to pure moments between two loading

points located at one-eighth span length from end supports. As mentioned in Section III, the webs of specimens were designed to be fully effective. Lateral-torsional buckling of channel beams was prevented by using lateral supports provided by aluminum angles connected to the top and bottom flanges. The weights of test beam and the cross beam placed on the top of the specimen (approximate 70 lbs.) are small as compared to the ultimate loads and were neglected in the evaluation of test results. The compressive yield stress obtained from material tests was used for calculating the critical local buckling load (P_{cr}) and the tensile stress was used to evaluate the yield moment (M_y) for all specimens.

a. Critical Local Buckling Strength. Like stiffened elements, unstiffened elements of beams may buckle locally in the elastic or inelastic range, depending on the w/t ratio of the compression element. The critical local buckling stress (f_{cr}) can be computed by using Equation 2.22 or Equation 4.3 for the unstiffened element subjected to a uniform compressive stress. The value of buckling coefficient (k) used to calculate the critical buckling stress is 0.43 in this phase of study. The critical local buckling moment ($(M_{cr})_{comp}$) can be predicted by using Equation 4.4.

The computed and tested critical local buckling moments of beam specimens are given in Tables 4.29 and 4.30 for 35XF and 50XF sheet steels, respectively. The tested critical local buckling loads listed in column (3) of Tables 4.29 and 4.30 were determined from load-strain diagrams by using the modified strain reversal method. The computed critical local buckling moments listed in these tables were calculated on the basis of the dynamic material properties. The values given in

Table 4.29

Comparison of Computed and Tested Critical Local Buckling Moments
Beam Specimens with Unstiffened Flanges (Based on k=0.43)
(35XF Sheet Steel)

Spec.	S_{xc} ($in.^3$) (1)	f_{cr} (ksi) (2)	$(P_{cr})_{test}$ (kips) (3)	$(M_{cr})_{comp}$ (in.-kips) (4)	$(M_{cr})_{test}$ (in.-kips) (5)	(5)/(4) (6)
4A0A	0.384	28.22	N/A	10.84	N/A	N/A
4A1A	0.377	28.26	N/A	10.65	N/A	N/A
4A1B	0.382	28.26	N/A	10.79	N/A	N/A
4A2A	0.380	30.15	N/A	11.46	N/A	N/A
4A2B	0.377	30.23	N/A	11.40	N/A	N/A
4B0A	0.719	25.55	N/A	18.37	N/A	N/A
4B1A	0.717	25.53	N/A	18.30	N/A	N/A
4B1B	0.717	25.66	N/A	18.40	N/A	N/A
4B2A	0.717	27.22	N/A	19.52	N/A	N/A
4B2B	0.717	27.14	N/A	19.46	N/A	N/A
4C0A	1.153	21.64	8.22	24.95	33.39	1.338
4C1A	1.150	21.60	8.15	24.84	33.11	1.333
4C1B	1.148	21.64	8.63	24.84	35.06	1.411
4C2A	1.160	22.77	9.56	26.41	38.84	1.471
4C2B	1.153	22.82	9.52	26.31	38.67	1.470
Mean						1.405
Standard Deviation						0.060

Note: The dynamic compressive yield stress was used for calculating the critical local buckling moment ($(M_{cr})_{comp}$).

Table 4.30

Comparison of Computed and Tested Critical Local Buckling Moments
Beam Specimens with Unstiffened Flanges (Based on k=0.43)
(50XF Sheet Steel)

Spec.	S_{xc} ($in.^3$) (1)	f_{cr} (ksi) (2)	$(P_{cr})_{test}$ (kips) (3)	$(M_{cr})_{comp}$ (in.-kips) (4)	$(M_{cr})_{test}$ (in.-kips) (5)	(5)/(4) (6)
4A0AX	0.314	45.58	N/A	14.33	N/A	N/A
4A1AX	0.315	46.81	N/A	14.75	N/A	N/A
4A1BX	0.315	46.77	N/A	14.74	N/A	N/A
4A2AX	0.316	49.12	N/A	15.50	N/A	N/A
4A2BX	0.314	49.10	N/A	15.42	N/A	N/A
4B0AX	0.537	40.64	9.28	21.81	23.78	1.090
4B1AX	0.541	40.96	9.07	22.16	23.24	1.049
4B1BX	0.544	40.96	9.09	22.29	23.29	1.045
4B2AX	0.538	42.21	9.62	22.71	24.65	1.085
4B2BX	0.540	42.26	10.11	22.82	25.91	1.135
4C0AX	0.854	27.34	7.87	23.35	29.02	1.243
4C1AX	0.857	27.34	9.01	23.43	33.22	1.418
4C1BX	0.855	27.27	8.37	23.31	30.86	1.324
4C2AX	0.857	27.10	8.40	23.22	30.98	1.334
4C2BX	0.858	27.17	8.79	23.30	32.41	1.391
Mean						1.211
Standard Deviation						0.147

Note: The dynamic compressive yield stress was used for calculating the critical local buckling moment ($(M_{cr})_{comp}$).

column (2) of Tables 4.29 and 4.30 are the average values of two critical local buckling stresses of unstiffened compression flanges of beams.

It was noted that no local buckling occured in the specimens with small and medium w/t ratios for 35XF sheet steel, and the specimens with small w/t ratios for 50XF sheet steel. All tested critical buckling moments are greater than the computed critical local buckling moments. This is because a value of 0.43 was used as the buckling coefficient for unstiffened compression flanges ignoring any effect of rotational edge restraint provided by the adjoining webs.

Column (6) of Tables 4.29 and 4.30 show the comparisons between the computed and tested critical local buckling moments. The mean values of $(M_{cr})_{test}/(M_{cr})_{comp}$ ratios for using 35XF and 50XF sheet steels are 1.405 and 1.211 with standard deviations of 0.060 and 0.147, respectively. Similar to the results of hat-shaped beam tests, the computed buckling moments for specimens fabricated from 50XF sheet steel are less conservative than specimens fabricated from 35XF sheet steel.

b. Nominal Flexural Strength. Based on the initiation of yielding, a channel beam reaches its nominal section strength when the maximum edge stress in the compression flanges reaches the yield stress of steel. The section strengths of all channel beams can be calculated by using Equation 4.12. The effective width formulas (Equations 2.39) can be applied for the calculation of the elastic section modulus of the effective section to be used in Equation 4.12. A buckling coefficient of 0.43 was used to calculate the effective width of an unstiffened compression element. As mentioned in Section II, when the ratio of w/t exceeds the value of

$((w/t)_{lim})$ the effective width design formulas can be used to compute the effective width of the compression element.

The computed and tested ultimate moments of channel beams fabricated from 35XF sheet steel are given in Tables 4.31(a) and 4.31(b). Tables 4.32(a) and 4.32(b) present similar values for using 50XF sheet steel. The computed ultimate moments based on the static tensile yield stresses are given in column (4) of Tables 4.31(a) and 4.32(a), while the computed ultimate moments based on dynamic tensile yield stresses are given in Tables 4.31(b) and 4.32(b). The computed ultimate moments $((M_y)_{comp})$ listed in these tables were calculated by using Equation 4.12. The tested ultimate moments listed in these tables were determined from the product of bending arm (L/8) and one-half of the tested failure load as given in Equation 4.13. Comparisons of computed ultimate moments based on the static yield stresses and the tested ultimate moments are listed in column (6) of Tables 4.31(a) and 4.32(a) for 35XF and 50XF sheet steels, respectively. The mean values of $(M_u)_{test}/(M_y)_{comp}$ ratios listed in Tables 4.31(a) and 4.32(a) are 1.299 and 1.121 with standard deviations of 0.096 and 0.040, respectively. The values listed in column (6) of Tables 4.31(b) and 4.32(b) are compared between the computed ultimate moments based on the dynamic yield stresses and the tested ultimate moments. The mean values and standard deviations of $(M_u)_{test}/(M_y)_{comp}$ ratios are (1.228, 0.052) for using 35XF sheet steel and (1.094, 0.026) for using 50XF sheet steel.

For the purpose of comparison, Figures 4.34 and 4.35 show graphically the effect of strain rate on the ratio of the tested ultimate moment to the computed ultimate moment obtained from Tables 4.31(a) and 4.31(b).

Table 4.31

Comparison of Computed and Tested Failure Moments Based on the Effective width Formulas in the 1991 AISI Automotive Steel Design Manual for Beam Specimens with Unstiffened Flanges (35XF Sheet Steel)

(a) Based on Static Tensile Yield Stress

Spec.	Strain Rate in./in./sec. (1)	F_y (ksi) (2)	$(P_u)_{test}$ (kips) (3)	$(M_y)_{comp}$ (in.-kips) (4)	$(M_u)_{test}$ (in.-kips) (5)	(5)/(4) (6)
4A0A	0.00001	32.02	6.41	12.29	14.82	1.206
4A1A	0.0001	32.02	7.15	12.08	16.53	1.369
4A1B	0.0001	32.02	7.18	12.23	16.60	1.357
4A2A	0.01	32.02	7.53	12.17	17.41	1.430
4A2B	0.01	32.02	7.63	12.07	17.64	1.461
4B0A	0.00001	32.02	9.77	21.73	26.26	1.208
4B1A	0.0001	32.02	10.12	21.67	27.20	1.255
4B1B	0.0001	32.02	9.87	21.78	26.52	1.218
4B2A	0.01	32.02	10.97	21.73	29.48	1.357
4B2B	0.01	32.02	10.98	21.67	29.51	1.361
4C0A	0.00001	32.02	8.49	30.47	34.49	1.132
4C1A	0.0001	32.02	8.83	30.35	35.87	1.182
4C1B	0.0001	32.02	9.15	30.33	37.17	1.225
4C2A	0.01	32.02	10.23	30.62	41.56	1.357
4C2B	0.01	32.02	10.22	30.47	41.52	1.363
Mean						1.299
Standard Deviation						0.096

(Considering Cold-Work of Forming)

4A0A	0.00001	38.30	6.41	14.70	14.82	1.008
4A1A	0.0001	38.36	7.15	14.47	16.53	1.142
4A1B	0.0001	38.36	7.18	14.65	16.60	1.133
4A2A	0.01	38.33	7.53	14.57	17.41	1.195
4A2B	0.01	38.42	7.63	14.49	17.64	1.217
Mean(with consideration of cold-work)						1.139
Standard Deviation(with consideration of cold-work)						0.081
Mean(without consideration of cold-work)						1.365
Standard Deviation(without consideration of cold-work)						0.098

Note : $(M_y)_{comp}=(M_u)_{comp}$

Table 4.31 (Cont'd)

(b) Based on Dynamic Tensile Yield Stress

Spec.	Strain Rate in./in./sec. (1)	F_y (ksi) (2)	$(P_u)_{test}$ (kips) (3)	$(M_y)_{comp}$ (in.-kips) (4)	$(M_u)_{test}$ (in.-kips) (5)	(5)/(4) (6)
4A0A	0.00001	32.02	6.41	12.29	14.82	1.206
4A1A	0.0001	32.87	7.15	12.40	16.53	1.333
4A1B	0.0001	32.87	7.18	12.55	16.60	1.322
4A2A	0.01	36.40	7.53	13.83	17.41	1.259
4A2B	0.01	36.40	7.63	13.73	17.64	1.285
4B0A	0.00001	32.02	9.77	21.73	26.26	1.208
4B1A	0.0001	32.87	10.12	22.14	27.20	1.228
4B1B	0.0001	32.87	9.87	22.26	26.52	1.191
4B2A	0.01	36.40	10.97	24.14	29.48	1.221
4B2B	0.01	36.40	10.98	24.07	29.51	1.226
4C0A	0.00001	32.02	8.49	30.47	34.49	1.132
4C1A	0.0001	32.87	8.83	30.99	35.87	1.157
4C1B	0.0001	32.87	9.15	30.97	37.17	1.200
4C2A	0.01	36.40	10.23	33.89	41.56	1.226
4C2B	0.01	36.40	10.22	33.72	41.52	1.231
Mean						1.228
Standard Deviation						0.052

(Considering Cold-Work of Forming)

4A0A	0.00001	38.30	6.41	14.70	14.82	1.008
4A1A	0.0001	39.13	7.15	14.76	16.53	1.120
4A1B	0.0001	39.13	7.18	14.94	16.60	1.111
4A2A	0.01	42.51	7.53	16.16	17.41	1.077
4A2B	0.01	42.60	7.63	16.07	17.64	1.098
Mean(with consideration of cold-work)						1.083
Standard Deviation(with consideration of cold-work)						0.045
Mean(without consideration of cold-work)						1.281
Standard Deviation(without consideration of cold-work)						0.051

Note : $(M_y)_{comp}=(M_u)_{comp}$

Table 4.32

Comparison of Computed and Tested Failure Moments Based on the Effective width Formulas in the 1991 AISI Automotive Steel Design Manual for Beam Specimens with Unstiffened Flanges (50XF Sheet Steel)

(a) Based on Static Tensile Yield Stress

Spec.	Strain Rate in./in./sec. (1)	F_y (ksi) (2)	$(P_u)_{test}$ (kips) (3)	$(M_y)_{comp}$ (in.-kips) (4)	$(M_u)_{test}$ (in.-kips) (5)	(5)/(4) (6)
4A0AX	0.00001	48.81	8.84	15.34	17.13	1.117
4A1AX	0.0001	48.81	8.92	15.38	17.27	1.123
4A1BX	0.0001	48.81	8.75	15.38	16.94	1.101
4A2AX	0.01	48.81	9.45	15.41	18.31	1.189
4A2BX	0.01	48.81	9.36	15.33	18.13	1.183
4B0AX	0.00001	48.81	9.87	22.78	25.29	1.110
4B1AX	0.0001	48.81	10.01	22.95	25.66	1.118
4B1BX	0.0001	48.81	10.16	23.09	26.04	1.128
4B2AX	0.01	48.81	10.28	22.77	26.35	1.157
4B2BX	0.01	48.81	10.31	22.89	26.41	1.154
4C0AX	0.00001	48.81	8.94	31.92	32.96	1.033
4C1AX	0.0001	48.81	9.48	32.03	34.95	1.091
4C1BX	0.0001	48.81	9.28	31.92	34.20	1.071
4C2AX	0.01	48.81	9.67	31.95	35.67	1.116
4C2BX	0.01	48.81	9.77	32.01	36.03	1.126
Mean						1.121
Standard Deviation						0.040

(Considering Cold-Work of Forming)

4A0AX	0.00001	58.20	8.84	18.29	17.13	0.937
4A1AX	0.0001	58.24	8.92	18.35	17.27	0.941
4A1BX	0.0001	58.19	8.75	18.33	16.94	0.924
4A2AX	0.01	58.20	9.45	18.37	18.31	0.997
4A2BX	0.01	58.18	9.36	18.27	18.13	0.992
Mean(with consideration of cold-work)						0.958
Standard Deviation(with consideration of cold-work)						0.034
Mean(without consideration of cold-work)						1.143
Standard Deviation(without consideration of cold-work)						0.040

Note : $(M_y)_{comp}=(M_u)_{comp}$

Table 4.32 (Cont'd)

(b) Based on Dynamic Tensile Yield Stress

Spec.	Strain Rate in./in./sec. (1)	F_y (ksi) (2)	$(P_u)_{test}$ (kips) (3)	$(M_y)_{comp}$ (in.-kips) (4)	$(M_u)_{test}$ (in.-kips) (5)	(5)/(4) (6)
4A0AX	0.00001	48.81	8.84	15.34	17.13	1.117
4A1AX	0.0001	49.50	8.92	15.60	17.27	1.107
4A1BX	0.0001	49.50	8.75	15.60	16.94	1.086
4A2AX	0.01	51.60	9.45	16.29	18.31	1.124
4A2BX	0.01	51.60	9.36	16.20	18.13	1.119
4B0AX	0.00001	48.81	9.87	22.78	25.29	1.110
4B1AX	0.0001	49.50	10.01	23.21	25.66	1.106
4B1BX	0.0001	49.50	10.16	23.35	26.04	1.115
4B2AX	0.01	51.60	10.28	23.81	26.35	1.107
4B2BX	0.01	51.60	10.31	23.94	26.41	1.103
4C0AX	0.00001	48.81	8.94	31.92	32.96	1.033
4C1AX	0.0001	49.50	9.48	32.39	34.95	1.079
4C1BX	0.0001	49.50	9.28	32.27	34.20	1.060
4C2AX	0.01	51.60	9.67	33.40	35.67	1.068
4C2BX	0.01	51.60	9.77	33.45	36.03	1.077
Mean						1.094
Standard Deviation						0.026

(Considering Cold-Work of Forming)

4A0AX	0.00001	58.20	8.84	18.29	17.13	0.937
4A1AX	0.0001	58.84	8.92	18.55	17.27	0.931
4A1BX	0.0001	58.80	8.75	18.52	16.94	0.915
4A2AX	0.01	60.97	9.45	19.24	18.31	0.952
4A2BX	0.01	60.95	9.36	19.14	18.13	0.947
Mean(with consideration of cold-work)						0.936
Standard Deviation(with consideration of cold-work)						0.015
Mean(without consideration of cold-work)						1.111
Standard Deviation(without consideration of cold-work)						0.015

Note : $(M_y)_{comp}=(M_u)_{comp}$

Table 4.33

Average Tested Failure Moments for Beam Specimens with Unstiffened Flanges (35XF Sheet Steel)

Strain Rate in./in./sec.	w/t		
	9.17	15.08	20.95
0.00001	14.82	26.26	34.49
0.0001	16.57	26.86	36.52
0.01	17.53	29.49	41.54

Table 4.34

Average Tested Failure Moments for Beam Specimens with Unstiffened Flanges (50XF Sheet Steel)

Strain Rate in./in./sec.	w/t		
	8.83	15.33	20.51
0.00001	17.13	25.29	32.96
0.0001	17.11	25.85	34.58
0.01	18.22	26.38	35.85

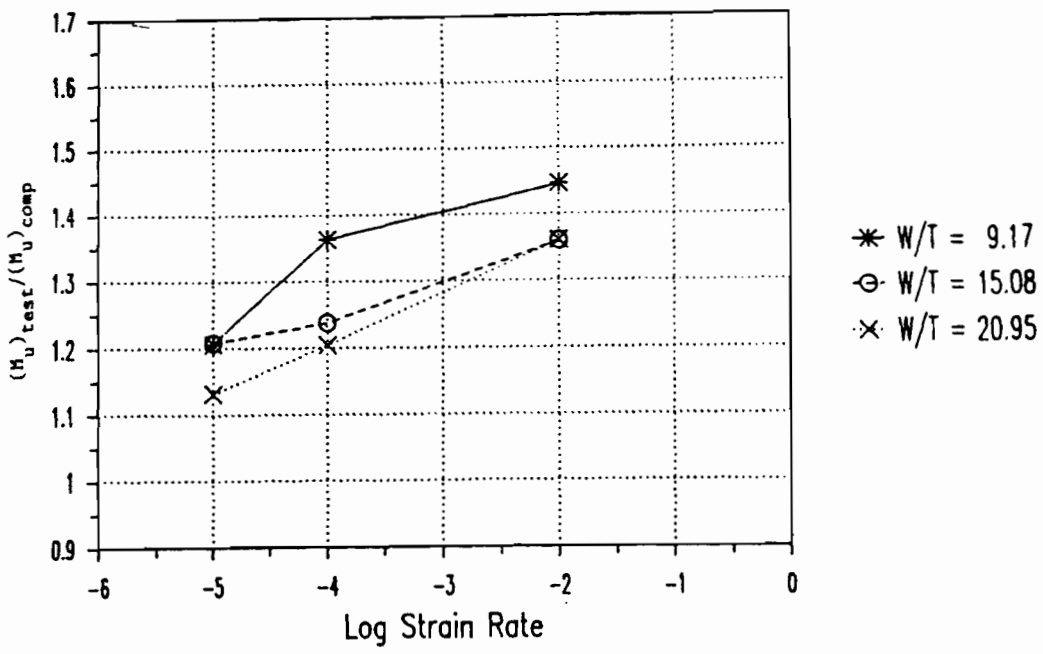

Figure 4.34 Ratios of Tested Failure Moments to Computed Failure Moments (Based on Static Yield Stress) vs. Logarithmic Strain Rate for Channel Beams (35XF Sheet Steel)

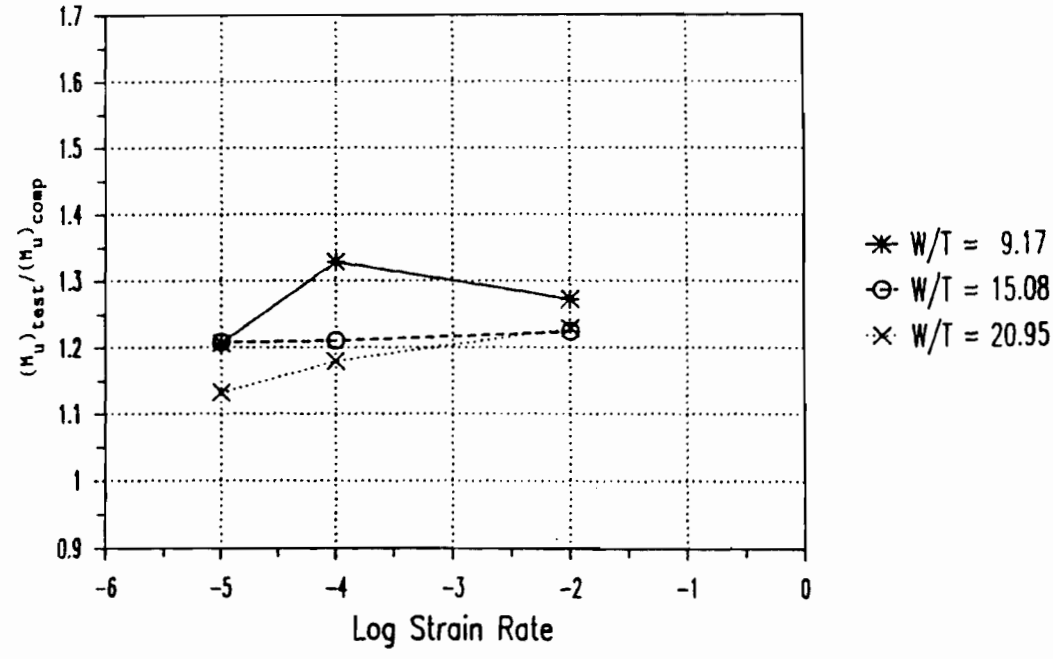

Figure 4.35 Ratios of Tested Failure Moments to Computed Failure Moments (Based on Dynamic Yield Stress) vs. Logarithmic Strain Rate for Channel Beams (35XF Sheet Steel)

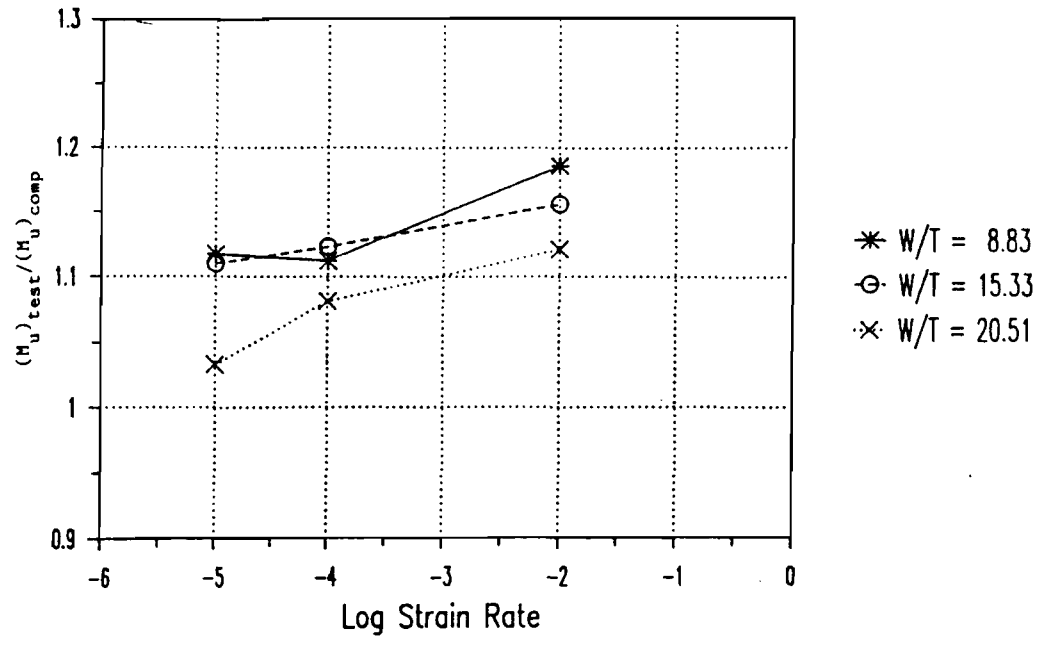

Figure 4.36 Ratios of Tested Failure Moments to Computed Failure Moments (Based on Static Yield Stress) vs. Logarithmic Strain Rate for Channel Beams (50XF Sheet Steel)

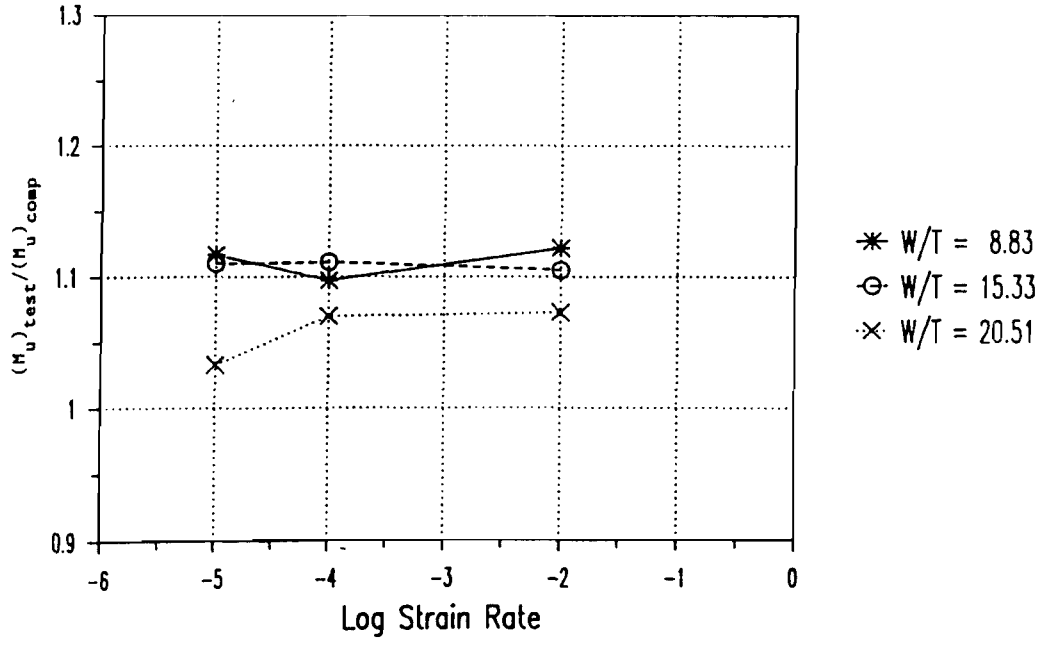

Figure 4.37 Ratios of Tested Failure Moments to Computed Failure Moments (Based on Dynamic Yield Stress) vs. Logarithmic Strain Rate for Channel Beams (50XF Sheet Steel)

Similarly, Figures 4.36 and 4.37 show the strain rates vs. the ratios of the tested ultimate moment to the computed ultimate moment obtained from Tables 4.32(a) and 4.32(b). The horizontal axis represents logarithmic strain rate while the vertical axis represents the ratio of the tested ultimate moment to the computed ultimate moment. The tests performed at strain rate of 10^{-4} in./in./sec. are considered to be the static loading conditions. Tables 4.33 and 4.34 list average failure moments for beam specimens using 35XF and 50XF sheet steels, respectively. Each value listed in Tables 4.33 and 4.34 and each point shown in Figures 4.34 through 4.37 is the average of two values obtained from similar tests.

For the specimens with small w/t ratios (Specimen series 4A), the computed ultimate moments considering cold-work of forming and the tested ultimate moments are presented in the lower portions of Tables 4.31(a) and 4.31(b) for channel beams fabricated from 35XF sheet steel. The lower portions of Tables 4.32(a) and 4.32(b) present the similar data for beam specimens fabricated from 50XF sheet steel. The mean values and standard deviations listed in the lower portions of Tables 4.31 and 4.32 are based on 5 beam specimens. It can be seen that the computed yield moments can be improved by considering cold-work of forming.

From Tables 4.31 and 4.32, it can be seen that the computed ultimate moments using the dynamic yield stresses are better than the computed ultimate moments using the static yield stresses. A better prediction of ultimate moments can be obtained by considering the cold work effect for specimens with small w/t ratios. Similar to the results for studying hat-shaped beams, the computed ultimate moments for channel beams fabricated from 50XF sheet steel are less conservative than the beams

fabricated from 35XF sheet steel. It is observed from Tables 4.33 and 4.34 that the tested ultimate moment increases with strain rate for specimens having the same w/t ratios.

3. Deflection of Beam Specimens. The deflection (d) of beam specimen (Figure 4.38) was measured by placing two LVDTs (Linear Variable Differential Transformer) at midspan. The measured deflection under service moment, which was considered to be 60% of the computed yield moment, was obtained from the moment-deflection relationship. The computed deflection ($(d)_{comp}$) was calculated by using the following theoretical deflection equation:

$$(d)_{comp} = \frac{9M_s L^2}{128EI_e} \qquad (4.20)$$

where E = modulus of elasticity

I_e = effective moment of inertia under service moment

L = span length of beam

M_s = service moment

For studying the hat-shaped beam specimens, Equations 2.43 and 2.44 (Procedure II) listed in Section II were used to calculate the effective moment of inertia, while Procedure I was used to calculate the effective moment of inertia for channel beam specimens.

Tables 4.35 and 4.36 compare the deflections calculated from Equation 4.20 and the tested deflections measured from the LVDT readings under service moments for hat-shaped beam specimens fabricated from 35XF and 50XF sheet steels, respectively. Similarly, Tables 4.37 and 4.38 show

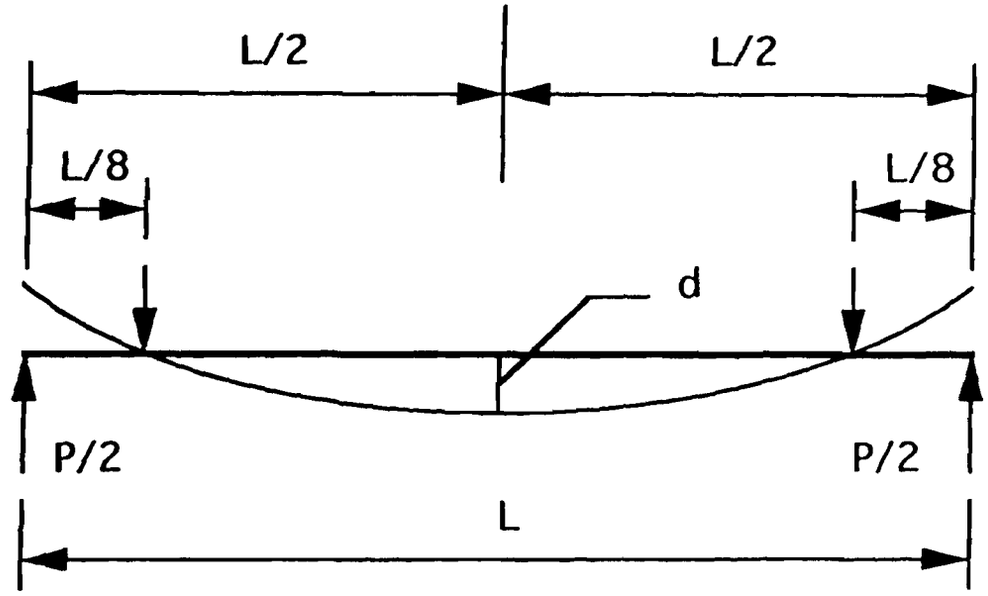

Figure 4.38 Schematic Diagram for a Beam Specimen Showing Midspan Deflection

Table 4.35

Deflections under Service Moments Based on Effective Sections for Hat-Beam Specimens with a Stiffened Flange (35XF Sheet Steel)

Spec.	$(M_s)_{test}$ (kips-in.) (1)	$(d)_{test}$ (in.) (2)	$(d)_{comp}$ (in.) (3)	(2)/(3) (4)
3B1A	12.73	0.1213	0.1658	0.732
3B1B	12.40	0.1319	0.1661	0.794
3B2A	13.60	0.1350	0.1830	0.738
3B2B	13.72	0.1396	0.1827	0.764
3C0A	17.75	0.1518	0.2003	0.758
3C1A	18.32	0.1974	0.2037	0.969
3C1B	18.37	0.2002	0.2033	0.985
3C2A	20.60	0.1835	0.2329	0.788
3C2B	20.71	0.1727	0.2325	0.743
Mean				0.808
Standard Deviation				0.093

Table 4.36

Deflections under Service Moments Based on Effective Sections for Hat-Beam Specimens with a Stiffened Flange (50XF Sheet Steel)

Spec.	$(M_s)_{test}$ (kips-in.) (1)	$(d)_{test}$ (in.) (2)	$(d)_{comp}$ (in.) (3)	(2)/(3) (4)
3A0AX	4.44	0.1410	0.1327	1.063
3A1AX	4.49	0.1034	0.1329	0.778
3A1BX	4.52	0.1472	0.1322	1.113
3A2AX	4.69	0.1291	0.1383	0.933
3A2BX	4.65	0.1225	0.1406	0.871
3B0AX	10.86	0.1424	0.1858	0.766
3B1AX	11.09	0.1964	0.1899	1.034
3B1BX	11.12	0.1824	0.1894	0.963
3B2AX	11.60	0.1821	0.1977	0.921
3B2BX	11.60	0.1912	0.1971	0.970
3C0AX	17.30	0.1469	0.1960	0.749
3C1AX	17.67	0.1521	0.1996	0.762
3C1BX	17.45	0.1596	0.1992	0.801
3C2AX	18.16	0.1512	0.2117	0.714
3C2BX	18.17	0.1970	0.2079	0.948
Mean				0.892
Standard Deviation				0.126

Table 4.37

Deflections under Service Moments Based on Effective Sections for Channel Specimens with Unstiffened Flanges (35XF Sheet Steel)

Spec.	$(M_s)_{test}$ (kips-in.) (1)	$(d)_{test}$ (in.) (2)	$(d)_{comp}$ (in.) (3)	(2)/(3) (4)
4A0A	7.37	0.0639	0.0620	1.031
4A1A	7.44	0.0609	0.0641	0.950
4A1B	7.53	0.0715	0.0649	1.102
4A2A	8.30	0.0542	0.0708	0.765
4A2B	8.24	0.0471	0.0706	0.667
4B0A	13.04	0.0511	0.0635	0.805
4B1A	13.28	0.0491	0.0650	0.755
4B1B	13.36	0.0445	0.0649	0.701
4B2A	14.48	0.0588	0.0706	0.833
4B2B	14.44	0.0527	0.0707	0.745
4C0A	18.28	0.0929	0.1097	0.847
4C1A	18.59	0.0924	0.1126	0.821*
4C1B	18.58	0.0630	0.1127	0.559*
4C2A	20.33	0.0992	0.1227	0.808*
4C2B	20.23	0.0639	0.1232	0.519*
Mean				0.833
Standard Deviation				0.121

(*) This value was not considered in the calculation of mean and standard deviation because the LVDT which measured the midspan deflection was not functioning properly during the test.

Table 4.38

Deflections under Service Moments Based on Effective Sections
for Channel Specimens with Unstiffened Flanges
(50XF Sheet Steel)

Spec.	$(M_s)_{test}$ (kips-in.) (1)	$(d)_{test}$ (in.) (2)	$(d)_{comp}$ (in.) (3)	(2)/(3) (4)
4A0AX	9.21	0.0663	0.0671	0.988
4A1AX	9.36	0.0690	0.0678	1.018
4A1BX	9.36	0.0576	0.0680	0.847
4A2AX	9.77	0.0648	0.0707	0.917
4A2BX	9.72	0.0631	0.0711	0.887
4B0AX	13.67	0.0825	0.0914	0.903
4B1AX	13.93	0.0780	0.0920	0.848
4B1BX	14.01	0.0846	0.0916	0.924
4B2AX	14.26	0.0786	0.0960	0.819
4B2BX	14.36	0.0810	0.0957	0.846
4C0AX	19.15	0.1240	0.1465	0.846
4C1AX	19.44	0.1038	0.1480	0.701
4C1BX	19.36	0.1096	0.1483	0.739
4C2AX	20.04	0.1260	0.1541	0.818
4C2BX	20.07	0.1225	0.1539	0.796
Mean				0.860
Standard Deviation				0.084

the comparisons of computed and tested deflections for the channel beam specimens fabricate from 35XF and 50XF sheet steels. The mean values and standard deviations are given in all tables. It is noted that for most cases the measured deflections are less than the computed values. These discrepancies appear to be caused by the setup used in the tests and high speed of loading.

E. FURTHER DISCUSSIONS OF MATERIAL PROPERTIES AND TEST RESULTS OF STUB COLUMNS AND BEAMS

1. General Equations for Predicting Dynamic Yield Stresses. In the material tests, the yield stresses were determined from three selected strain rates, i.e., 10^{-4}, 10^{-2}, and 1.0 in./in./sec.. However, for stub columns and beams, some specimens were tested under different strain rates as compared with those used for material tests. In the calculation of member ultimate strengths, the yield stresses were computed from the second degree polynominal equations derived from the least square method as mentioned in Section B of this section. In order to simplify the design method, it is desirable to have general equations to predict the yield strengths for different sheet steels under various strain rates. A combination of material properties obtained from 5 different sheet steels (25AK, 35XF, 50XF, 50SK, and 100XF) were used to develop these equations. The material properties of 35XF, 50XF, and 100XF sheet steels are listed in Tables 3.17 through 3.22 and 3.32 through 3.37. The material properties of recently tested 25AK and 50SK sheet steels are listed in Tables 5 and 6 of Appendix B. For additional information on 25AK and 50SK sheet steels, see Reference 101. Consequently, the

following general equations were derived to predict the tensile and compressive yield stresses for strain rates ranging from 10^{-4} to 10^{2} in./in./sec.:

$$(F_y)_{pred} = (A\, e^{(B/F_y)} + 1)(F_y)_s \qquad (4.21)$$

$$A = a_1 + b_1 \log(\dot{\varepsilon}) + c_1 \log(\dot{\varepsilon})^2 \qquad (4.22a)$$

$$B = a_2 + b_2 \log(\dot{\varepsilon}) + c_2 \log(\dot{\varepsilon})^2 \qquad (4.22b)$$

For tensile yield stress:

$a_{1t} = 0.0226$ $\qquad$ $a_{2t} = 77.7183$

$b_{1t} = 0.0094$ $\qquad$ $b_{2t} = 0.0693$

$c_{1t} = 0.0011$ $\qquad$ $c_{2t} = -0.5952$

For compressive yield stress:

$a_{1c} = 0.0327$ $\qquad$ $a_{2c} = 64.9205$

$b_{1c} = 0.0035$ $\qquad$ $b_{2c} = 11.1227$

$c_{1c} = 0.0000$ $\qquad$ $c_{2c} = -1.8670$

In Equation 4.21, $(F_y)_s$ is the static yield stress tested under a strain rate of 10^{-4} in./in./sec. and $(F_y)_{pred}$ is the dynamic yield stress for a given strain rate higher than 10^{-4} in./in./sec.. Based on Equations 4.21 and 4.22, Figures 4.39 and 4.40 show graphically the predictions of yield stresses for tension and compression, respectively. In each of these figures, a three dimensional graph is produced for the three variables (static yield stress, logarithmic strain rate, and predicted yield stress). Tables 4.39(a) and 4.39(b) compare the tested and predicted tensile and compressive yield stresses for these five sheet

Table 4.39

Prediction of Dynamic Yield Stresses
(Based on 5 Different Sheet Steels)

(a) Tensile Yield Stress

Strain Rate in./in./sec.	$(F_y)_{test}$ (ksi) (1)	$(F_y)_{pred}$ (ksi) (2)	(1)/(2) (3)
	(25AK Sheet Steel)		
0.0001	24.60		
0.01	27.86	28.89	0.96
0.1	31.72	32.66	0.97
1.0	35.13	37.69	0.93
100.0	45.90*	48.83	0.94
	(35XF Sheet Steel)		
0.0001	32.87		
0.01	36.40	35.53	1.02
0.1	39.08*	37.77	1.03
1.0	42.37	40.77	1.04
100.0	50.78*	47.83	1.06
	(50XF Sheet Steel)		
0.0001	49.50		
0.01	51.60	51.35	1.00
0.1	53.01*	52.86	1.00
1.0	54.66	54.88	1.00
100.0	58.68*	59.92	0.98
	(50SK Sheet Steel)		
0.0001	54.97		
0.01	56.83	56.74	1.00
0.1	58.06	58.16	1.00
1.0	60.73	60.08	1.01
100.0	67.00*	64.91	1.03
	(100XF Sheet Steel)		
0.0001	124.25		
0.01	125.80	126.12	1.00
0.1	127.16*	127.55	1.00
1.0	128.91	129.50	1.00
100.0	133.58*	134.70	0.99
Mean			0.998
Standard Deviation			0.032

Note: The superscript * indicates that the values were computed from polynominal equations listed in Figures 4.1 through 4.3.

Table 4.39 (Cont'd)

(b) Compressive Yield Stress

Strain Rate in./in./sec.	$(F_y)_{test}$ (ksi) (1)	$(F_y)_{pred}$ (ksi) (2)	(1)/(2) (3)
	(25AK Sheet Steel)		
0.0001	21.66		
0.01	24.77	24.49	1.01
0.1	29.80	28.61	1.04
1.0	38.14*	35.85	1.06
100.0	62.06*	55.73	1.11
	(35XF Sheet Steel)		
0.0001	29.83		
0.01	31.92*	32.33	0.99
0.1	34.06*	34.80	0.98
1.0	36.91*	38.43	0.96
100.0	44.75*	46.96	0.95
	(50XF Sheet Steel)		
0.0001	49.68		
0.01	52.51*	52.27	1.00
0.1	53.72*	53.81	1.00
1.0	54.79*	55.68	0.98
100.0	56.52*	59.49	0.95
	(50SK Sheet Steel)		
0.0001	53.35		
0.01	55.91	56.00	1.00
0.1	56.96	57.47	0.99
1.0	59.41*	59.24	1.00
100.0	64.27*	62.78	1.02
	(100XF Sheet Steel)		
0.0001	107.29		
0.01	111.26*	111.12	1.00
0.1	113.13*	112.37	1.01
1.0	114.91*	113.75	1.01
100.0	118.24*	116.24	1.02
Mean			1.004
Standard Deviation			0.037

Note: The superscript * indicates that the values were computed from polynominal equations listed in Figures 4.7 through 4.9.

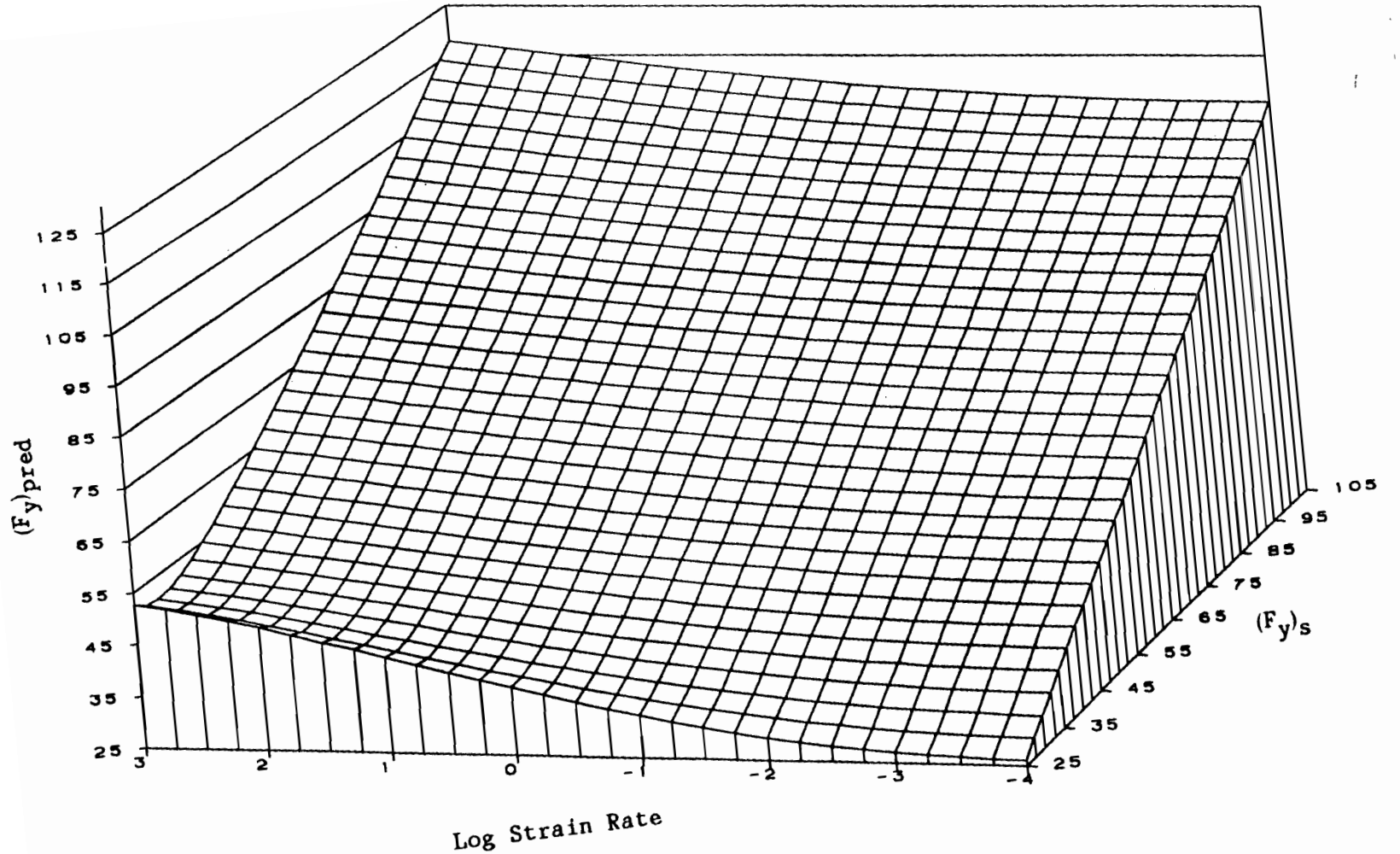

Figure 4.39 Prediction of Tensile Yield Stresses

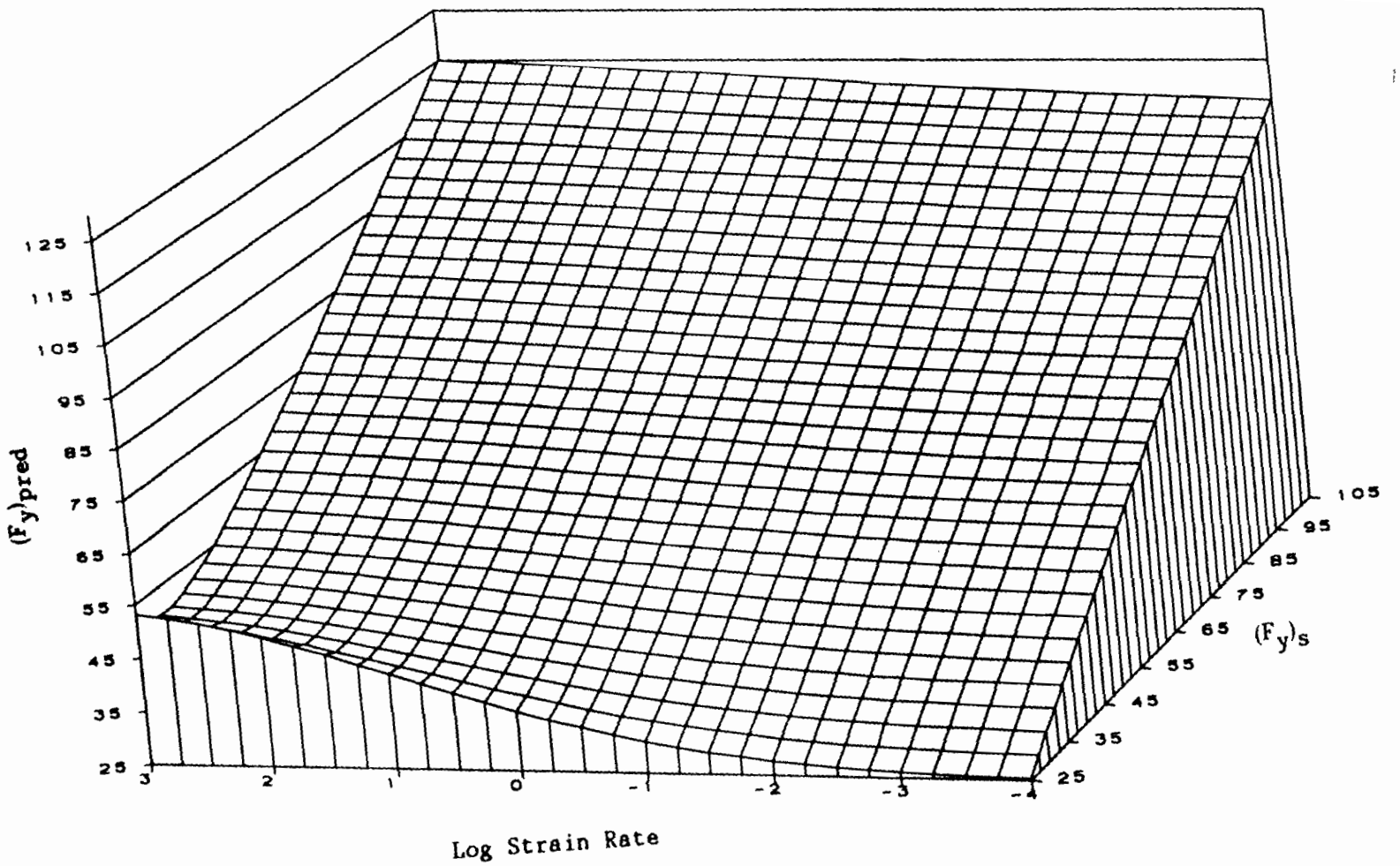

Figure 4.40 Prediction of Compressive Yield Stresses

steels. In both tables, the mean values of $(F_y)_{test}/(F_y)_{pred}$ are approximately 1.0 with standard deviations less than 0.04. Therefore, these equations can provide good predictions for both tensile and compressive yield stresses.

2. Effect of Stress-Strain Relationship on Member Strength. By comparing Table 4.11(b) with Table 4.12(b) and Table 4.19(b) with Table 4.20(b), it was found that the ratios of tested to computed failure loads for compact sections of stub columns fabricated from 35XF sheet steel are larger than those fabricated from 50XF sheet steel. This fact can be explained by the load-strain diagrams shown in Figures 4.41 through 4.44. Figures 4.41 and 4.42 show the load-strain diagrams of box-shaped stub column Specimens 1A1B (35XF) and 1A2AX (50XF), respectively. The curves shown in these figures were drawn from the readings of strain gages mounted on the corner of compression flange of box-shaped stub columns.

From Figure 4.42, it can be seen that the load reached its maximum value when the strain reached the yield strain for the stub column fabricated from 50XF sheet steel. However, for the stub column fabricated from 35XF sheet steel, the maximum strain under ultimate load occured at approximately three times the yield strain as shown in Figure 4.41. This is because the types of stress-strain relationship for these two materials are different. The stress-strain curve for 35XF sheet steel is a gradual-yielding type but it is a sharp-yielding type for 50XF sheet steel. Similar finding was also found for the compact sections of I-shaped stub columns. Figures 4.43 and 4.44 show the load-strain diagrams of I-shaped stub column Specimens 2A1B (35XF) and 2A2AX (50XF), respectively. The curves shown in these figures were drawn from the

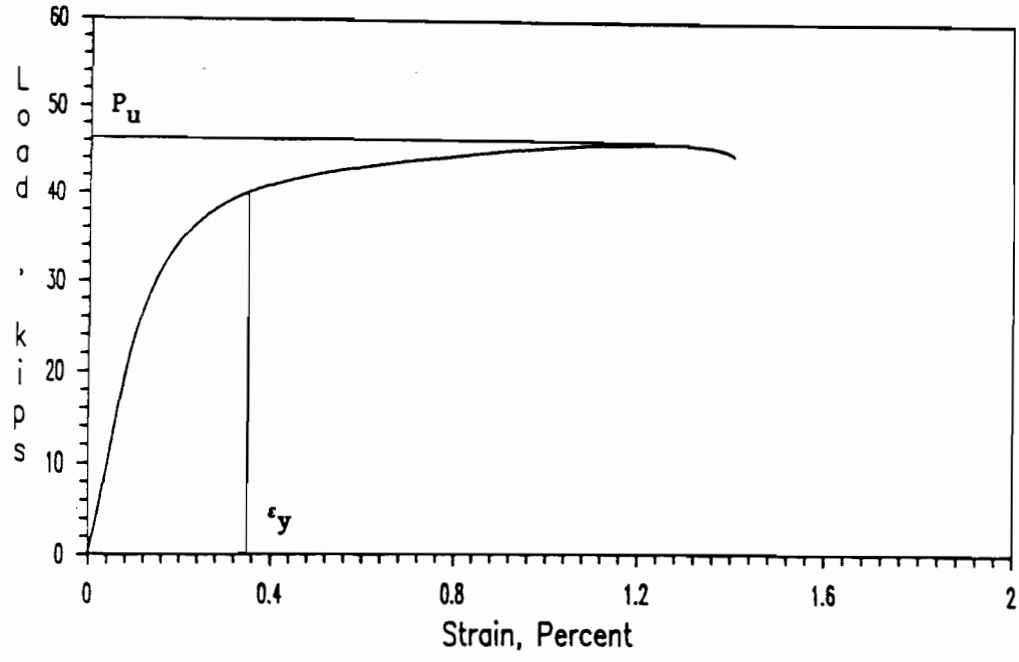

Figure 4.41 Load-Strain Curve of Specimen 1A1B (35XF)

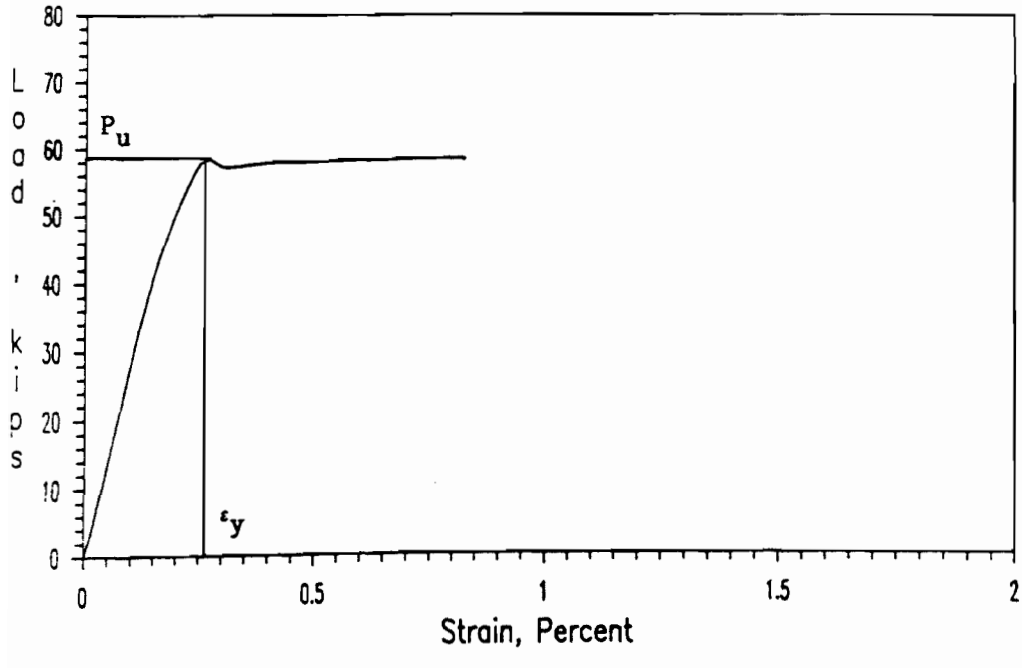

Figure 4.42 Load-Strain Curve of Specimen 1A2AX (50XF)

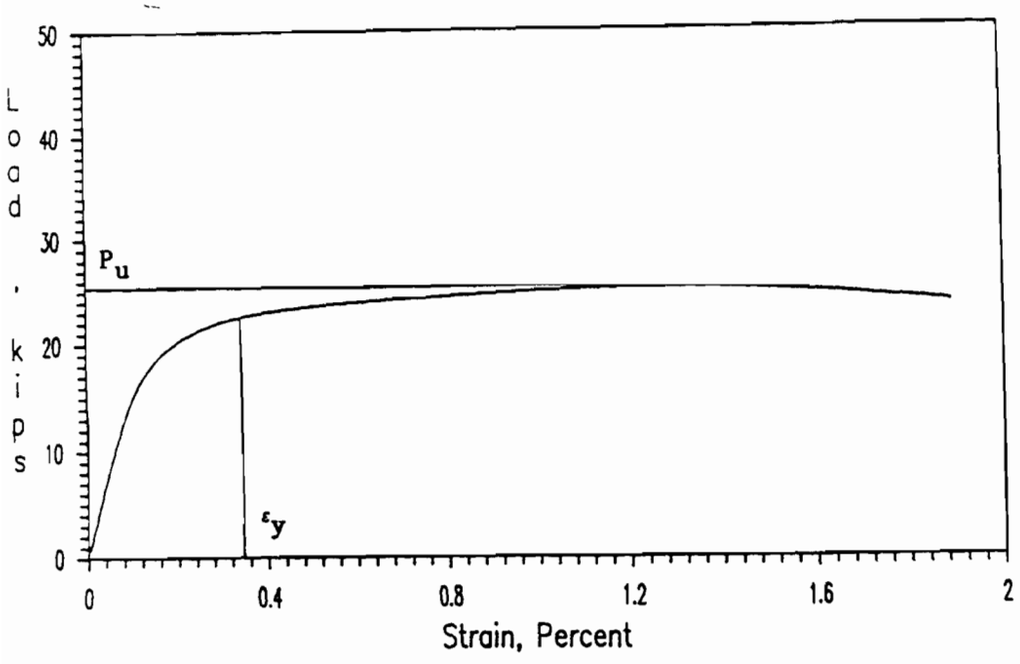

Figure 4.43 Load-Strain Curve of Specimen 2A1B (35XF)

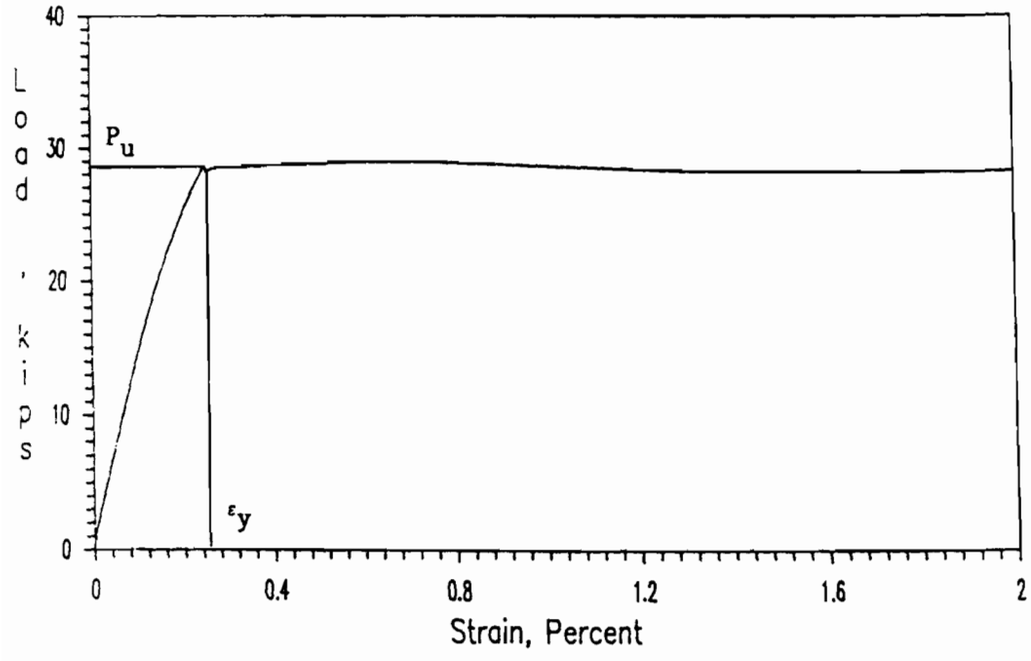

Figure 4.44 Load-Strain Curve of Specimen 2A2AX (50XF)

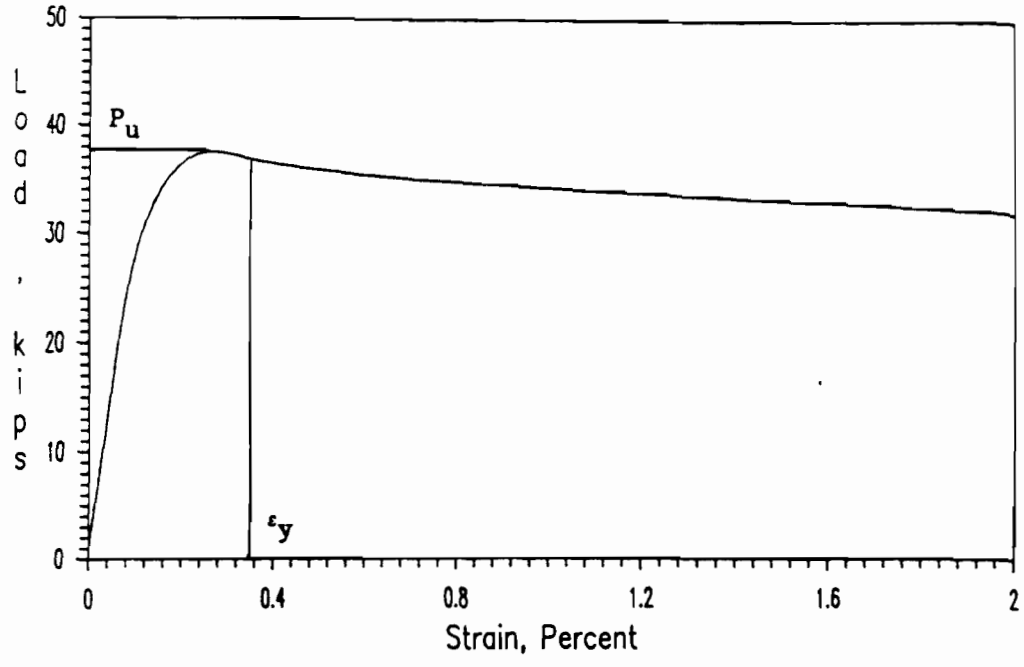

Figure 4.45 Load-Strain Curve of Specimen 2C1B (35XF)

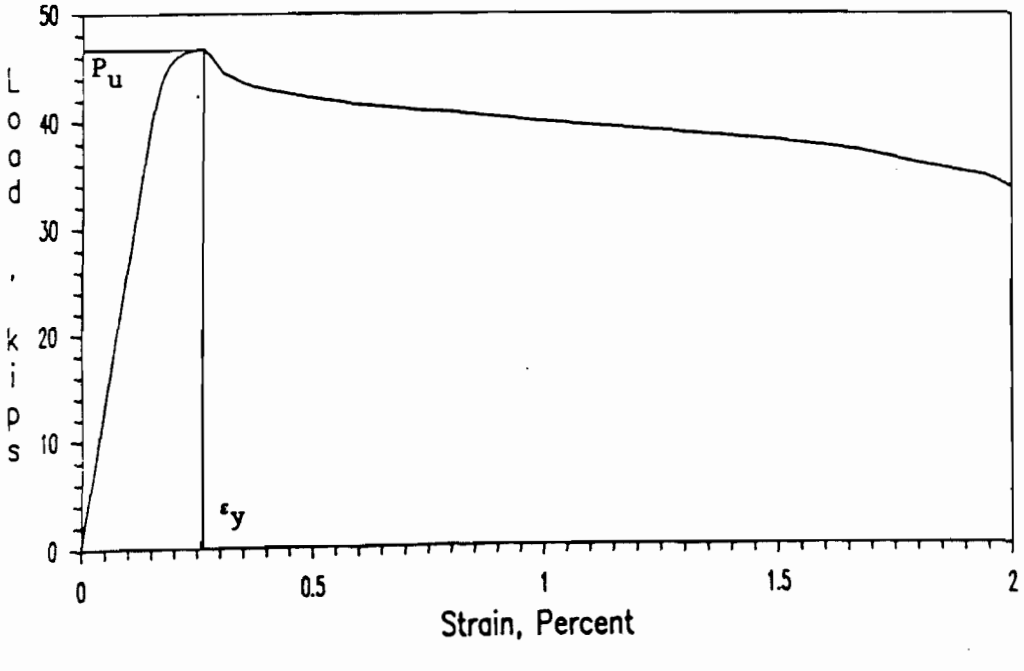

Figure 4.46 Load-Strain Curve of Specimen 2C3BX (50XF)

readings of strain gages mounted on the supported edge of unstiffened flanges of I-shaped stub columns. For the noncompact sections of box-shaped and I-shaped stub columns, the maximum strains under ultimate loads were close to the yield strains for both sheet steels. Figure 4.45 shows the load-strain curve of an I-shaped stub column fabricated from 35XF sheet steel with a flange w/t value of 20.76 (Specimen 2C1B). For I-shaped stub column fabricated from 50XF sheet steel, the load-strain curve is shown in Figure 4.46 (Specimen 2C3BX)

3. Local Buckling Coefficient for Unstiffened Compression Elements. Comparing Table 4.11 with Table 4.19 and Table 4.12 with Table 4.20, it can be seen that the ratios of tested to computed ultimate loads for I-shaped stub columns are much larger than those for box-shaped stub columns. This is possibly due to the use of low buckling coefficients for calculation of the ultimate loads for noncompact I-shaped stub columns with unstiffened flanges, because in the calculation of ultimate loads, a minimum value of 0.43 was used as the buckling coefficient for all unstiffened compression flanges ignoring any effect of rotational edge restraint provided by the adjoining web. It is well known that the buckling coefficient is a function of the aspect ratio (length to width ratio) and the rotational edge restraint factor. For an unstiffened compression element having a high aspect ratio, the value of elastic buckling coefficient (k) varies from 0.425 for the hinged edge condition to 1.277 for the fixed edge condition. In 1952, a series of theoretical formulas were derived by Bleich[99] for calculating the elastic buckling coefficients for stiffened and unstiffened compression elements considering the rotational edge restraint. Assuming the wavelength of

buckling element (λ) to be infinite, the rotational edge restraint of an unstiffened compression flange for I-shaped sections can be calculated as follows:

$$\xi = 2 \frac{t_b^3}{t_r^3} \frac{B_r}{B_b} \frac{1}{1 - 0.106(t_b^2 B_r^2 / t_r^2 B_b^2)} \qquad (4.23)$$

where ξ = rotational edge restraint

B_b = width of bending element

B_r = width of restraining element

t_b = thickness of bending element

t_r = thickness of restraining element

The elastic local buckling coefficient, K^*, can be determined by using Equation 4.24.

$$K^* = p + 2\sqrt{q} \qquad (4.24)$$

where $p = 0.425+0.016/(0.025+\xi)$

$q = 0.061/(0.43+\xi)$

Since the adhesive material (PC-7 epoxy) was used to assemble two channel sections back to back to form an I-shaped specimen, Equation 4.24 can be used to calculate the elastic local buckling coefficient for unstiffened compression flanges. Consequently, the buckling coefficients for Specimen series 2B, 2C, and 2D were computed and are presented in Tables 4.40 and 4.41 for I-shaped sections fabricated from 35XF and 50XF sheet steels, respectively.

In reality, the local buckling coefficient, K, is likely to be lower than the elastic buckling coefficient due to a combination of the

following reasons: (1) nonlinearity of stress-strain relationship near the yield region for the elastic-plastic materials; (2) increase in out-of-plane deformation caused by initial imperfections prior to local buckling; and (3) the consequent partial yielding of elements on the concave side of the waves[64]. In 1979, Kalyanaraman[64] derived a series of empirical equations on the basis of the test results for the determination of the local buckling coefficients of elastic-plastic members with stiffened and unstiffened elements. According to Kalyanaraman, the following equations can be used to calculate the local buckling coefficient of unstiffened elements of I-shaped stub columns under axial compression.

$$K_e = 0.851 + 0.426 \frac{\varepsilon^{0.7} - 1.5}{\varepsilon^{0.7} + 1.5} \tag{4.25a}$$

$$K_p = 0.637 + 0.212 \frac{\varepsilon^{0.74} - 2.04}{\varepsilon^{0.74} + 2.04} \tag{4.25b}$$

In Equations 4.25a and 4.25b, the subscripts e and p represent the elastic and plastic buckling coefficients, respectively. The symbol "ε" used in Equation 4.25 is a rotational edge restraint factor which can be determined by using the following equation:

$$\varepsilon = \frac{B_b}{B_r} \frac{D_r}{D_b} \frac{C_f}{N_b} S''_r \tag{4.26}$$

where B_b = width of bending element

B_r = width of restraining element

C_f = correction factor (Equation 4.27)

D_b = flexural rigidity of the bending element

D_r = flexural rigidity of the restraining element

N_b = number of buckling elements at the junction

S''_r = rotational edge stiffness (Equation 4.28)

$$C_f = 1.0 - \frac{K_b}{K_r}\left(\frac{B_r}{B_b}\right)^2\left(\frac{t_b}{t_r}\right)^2 \qquad (4.27)$$

In Equation 4.27, K_b and K_r are the buckling coefficients of bending and restraining elements corresponding to the hinged edge condition, respectively; while t_b and t_r are thicknesses of the bending and restraining elements, respectively. The ratio of K_b/K_r was taken as 0.106 in the calculation of a correction factor (C_f) for I-shaped stub columns. The rotational edge stiffness is

$$S''_r \cong \sqrt{118.8 + 84.6\left(\frac{B_r}{\lambda}\right)^2} - 8.9 \qquad (4.28)$$

in which λ is the half wavelength of the buckling element. It can be conservatively assumed to be infinite.

The actual buckling coefficient, K, of a compression element can vary between K_e and K_p depending upon the yield stress (σ_y) and the element dimensions. On the basis of the available test results, Kalyanaraman derived the following equations for determining the local buckling coefficient of compression elements.

a. $K = K_e$ if $K_y \geq 1.25K_e$ (4.29a)

b. $K = K_e - (K_e - K_p)\dfrac{1.25K_e - K_y}{1.25K_e - K_p}$ if $1.25K_e \geq K_y \geq K_p$ (4.29b)

c. $K = K_p$ if $K_y \leq K_p$ (4.29c)

where $K_y = \dfrac{\sigma_y 12(1-\mu^2)(B_b/t_b)^2}{\pi^2 E}$ (4.30)

In Equations 4.29 and 4.30, K_y is a hypothetical buckling coefficient that will cause the buckling stress of the element to be its yield stress, σ_y . Therefore, instead of using 0.43, the local buckling coefficient can be determined by using Equation 4.29 to calculate the ultimate loads for noncompact sections of I-shaped stub columns. The local buckling coefficients K_s and K_d calculated from static and dynamic yield stresses are listed in Tables 4.40 and 4.41 for I-shaped stub columns fabricated from 35XF and 50XF sheet steels, respectively. Based on these new values, comparisons between the tested and predicted ultimate loads are presented in Table 4.42 for 35XF sheet steel and in Table 4.43 for 50XF sheet steel. In these two tables, the specimens with an average w/t ratio of 13.38 for 35XF sheet steel and 11.59 for 50XF sheet steel (Specimen series 2B) were considered to be compact sections after using new buckling coefficients to check the effective width formulas. The computed ultimate loads of Specimen series 2A and 2B were calculated by considering cold-work of forming and are presented in Tables 4.42 and 4.43.

Comparing Tables 4.19 with 4.42 and 4.20 with 4.43, it can be seen that the computed ultimate loads can be improved by using the new local buckling coefficients for I-shaped stub columns. From column (7) of Table 4.42, it can be seen that the tested ultimate loads of Specimen series 2A are about 10% higher than the computed ultimate loads even though dynamic yield stresses are used. As mentioned previously for this case,

the strain under ultimate load occured at approximately three times the yield strain as shown in Figure 4.43. For Specimen series 2C, the ratios of tested to computed ultimate loads $((P_u)_{test}/(P_u)_{comp})$ listed in column (7) of Table 4.42 are slightly higher than 1.0. This is because the computed ultimate loads neglected the effect of cold-work of forming. However, the effect of cold-work of forming is insignificant for Specimen series 2D because of large w/t ratios. From Table 4.43, it can be seen that the predicted ultimate loads agree well with tested loads for I-shaped stub columns fabricated from 50XF sheet steel, which is slightly less conservative than those fabricated from 35XF sheet steel.

It should be noted that since the I-shaped stub columns were assembled by using epoxy between channel webs, the local buckling coefficients listed in Tables 4.40 and 4.41 were calculated by considering the web thickness of stub columns to be twice the thickness of steel sheet. In order to investigate the effect of rotational edge restraint provided by the web elements, three additional specimens (Specimen 2B1AA, 2B1BA, and 2B3AA) were fabricated from 35XF sheet steel by means of bolts for the purpose of comparison. The first two specimens were tested under 10^{-4} in./in./sec. and the third specimen was tested under 10^{-1} in./in./sec.. Figure 4.47 shows the test setup for Specimen 2B3AA which was assembled by bolts. The dimensions of all three specimens are listed in Table 4.44(a), and the local buckling coefficients of specimens are listed in Table 4.44(b). Because these stub columns were assembled by bolts, the buckling coefficients of unstiffened flanges as given in Table 4.44(b) were determined by using the sheet steel thickness as the thickness of web element. Consequently, the computed ultimate loads are

Table 4.40

Buckling Coefficients Used to Calculate the Ultimate Loads of Stub Columns with Unstiffened Flanges (35XF Sheet Steel) (Based on Tensile Yield Stress)

Spec.	w/t	K^*	K_e	K_p	K_{ys}	K_{yd}	K_s	K_d
2B1A	13.34	0.928	0.935	0.652	0.303	0.303	0.652	0.652
2B1B	13.41	0.933	0.939	0.654	0.306	0.306	0.654	0.654
2B2A	13.40	0.932	0.938	0.653	0.305	0.338	0.653	0.653
2B2B	13.37	0.930	0.937	0.652	0.304	0.337	0.652	0.652
2B3A	13.34	0.929	0.935	0.652	0.303	0.360	0.652	0.652
2B3B	13.42	0.931	0.937	0.653	0.306	0.364	0.653	0.653
2C0A	20.69	1.007	1.000	0.688	0.654	0.637	0.688	0.688
2C1A	20.85	1.010	1.002	0.689	0.663	0.663	0.689	0.689
2C1B	20.76	1.006	0.999	0.687	0.658	0.658	0.687	0.687
2C2A	20.97	1.011	1.003	0.690	0.670	0.742	0.690	0.719
2C2B	20.81	1.007	1.000	0.688	0.661	0.731	0.688	0.712
2C3A	20.93	1.011	1.003	0.689	0.667	0.793	0.689	0.747
2C3B	20.87	1.010	1.002	0.689	0.664	0.789	0.689	0.745
2D1A	44.60	1.114	1.078	0.733	2.716	2.716	1.078	1.078
2D1B	44.50	1.114	1.078	0.732	2.705	2.705	1.078	1.078
2D2A	44.62	1.116	1.079	0.733	2.719	3.010	1.079	1.079
2D2B	44.59	1.115	1.078	0.733	2.714	3.006	1.078	1.078
2D3A	44.51	1.117	1.080	0.733	2.706	3.146	1.080	1.080
2D3B	44.60	1.114	1.078	0.733	2.716	3.157	1.078	1.078

Note: K^* : elastic buckling coefficient from Eq. 4.24
K_e : elastic buckling coefficient from Eq. 4.25
K_p : plastic buckling coefficient from Eq. 4.25
K_{ys} : yield buckling coefficient from Eq. 4.30 (based on static yield stress)
K_{yd} : yield buckling coefficient from Eq. 4.30 (based on dynamic yield stress)
K_s : buckling coefficient from Eq.4.29 for static condition
K_d : buckling coefficient from Eq.4.29 for dynamic condition

Table 4.41

Buckling Coefficients Used to Calculate the Ultimate Loads of Stub Columns with Unstiffened Flanges (50XF Sheet Steel) (Based on Tensile Yield Stress)

Spec.	w/t	K^*	K_e	K_p	K_{ys}	K_{yd}	K_s	K_d
2B1AX	11.68	0.888	0.900	0.633	0.375	0.375	0.633	0.633
2B1BX	11.60	0.884	0.896	0.631	0.371	0.371	0.631	0.631
2B1CX	11.63	0.885	0.896	0.631	0.372	0.367	0.631	0.631
2B2AX	11.58	0.883	0.895	0.630	0.370	0.385	0.630	0.630
2B2BX	11.54	0.881	0.893	0.629	0.368	0.383	0.629	0.629
2B2CX	11.53	0.884	0.895	0.630	0.367	0.374	0.630	0.630
2B3AX	11.65	0.886	0.897	0.631	0.374	0.400	0.631	0.631
2B3BX	11.50	0.883	0.894	0.630	0.366	0.390	0.630	0.630
2C1AX	22.84	1.003	0.997	0.686	1.195	1.195	0.968	0.968
2C1BX	22.73	1.001	0.995	0.685	1.185	1.185	0.963	0.963
2C2AX	22.77	1.002	0.996	0.686	1.189	1.239	0.965	0.993
2C2BX	22.76	1.002	0.996	0.685	1.188	1.238	0.964	0.992
2C3AX	22.72	1.002	0.996	0.686	1.184	1.257	0.962	0.996
2C3BX	22.79	1.002	0.996	0.685	1.190	1.264	0.965	0.996
2D1AX	35.37	1.095	1.065	0.725	2.667	2.667	1.065	1.065
2D1BX	35.33	1.095	1.065	0.725	2.662	2.662	1.065	1.065
2D2AX	35.26	1.094	1.065	0.725	2.651	2.763	1.065	1.065
2D2BX	35.21	1.094	1.064	0.725	2.645	2.757	1.064	1.064
2D3AX	35.29	1.095	1.065	0.725	2.656	2.813	1.065	1.065
2D3BX	35.15	1.093	1.064	0.724	2.636	2.792	1.064	1.064

Note: K^* : elastic buckling coefficient from Eq. 4.24
K_e : elastic buckling coefficient from Eq. 4.25
K^e_p : plastic buckling coefficient from Eq. 4.25
K^p_{ys} : yield buckling coefficient from Eq. 4.30 (based on static yield stress)
K_{yd} : yield buckling coefficient from Eq. 4.30 (based on dynamic yield stress)
K_s : buckling coefficient from Eq.4.29 for static condition
K^s_d : buckling coefficient from Eq.4.29 for dynamic condition

Table 4.42

Comparison of Computed and Tested Failure Loads
for Stub Columns with Unstiffened Flanges
(35XF Sheet Steel)
(Based on Tensile Yield Stress)

Spec.	Strain Rate in./in./sec. (1)	w/t (2)	$(P_u)_{comp}$, kips Based on $(F_y)_s$ (3)	Based on $(F_y)_d$ (4)	$(P_u)_{test}$ kips (5)	(5)/(3) (6)	(5)/(4) (7)
2A1A	0.0001	8.93	22.77*	22.77*	25.26	1.11	1.11
2A1B	0.0001	9.04	22.98*	22.98*	25.35	1.10	1.10
2A2A	0.01	8.93	22.99*	25.17*	26.04	1.13	1.03
2A2B	0.01	9.10	22.95*	25.12*	27.70	1.21	1.10
2A3A	0.10	8.93	22.99*	26.83*	31.41	1.37	1.17
2A3B	0.10	8.96	22.88*	26.70*	29.41	1.29	1.10
2B1A	0.0001	13.34	32.69*	32.69*	34.20	1.05	1.05
2B1B	0.0001	13.41	32.51*	32.51*	34.20	1.05	1.05
2B2A	0.01	13.40	32.53*	35.73*	36.30	1.12	1.02
2B2B	0.01	13.37	32.62*	35.83*	37.52	1.15	1.05
2B3A	0.10	13.34	32.66*	38.33*	41.67	1.28	1.09
2B3B	0.10	13.42	32.66*	38.33*	42.70	1.31	1.11
2C0A	0.00001	20.69	34.35	33.61	36.30	1.06	1.08
2C1A	0.0001	20.85	34.28	34.28	37.23	1.09	1.09
2C1B	0.0001	20.76	34.47	34.47	37.66	1.09	1.09
2C2A	0.01	20.97	34.26	37.56	41.28	1.20	1.10
2C2B	0.01	20.81	34.47	37.75	41.52	1.20	1.10
2C3A	0.10	20.93	34.26	40.12	47.92	1.40	1.19
2C3B	0.10	20.87	34.28	40.12	46.16	1.35	1.15
2D1A	0.0001	44.60	43.23	43.23	41.72	0.97	0.97
2D1B	0.0001	44.50	43.27	43.27	41.04	0.95	0.95
2D2A	0.01	44.62	43.11	46.63	46.31	1.07	0.99
2D2B	0.01	44.59	43.16	46.69	44.94	1.04	0.96
2D3A	0.05	44.51	42.90	48.17	48.66	1.13	1.01
2D3B	0.05	44.60	43.23	48.55	49.39	1.14	1.02
Mean						1.154	1.067
Standard Deviation						0.121	0.063

Note: 1. The sectional properties used for calculating the computed ultimate loads are listed in Appendix B (Table 7).
2. The superscript * indicates that the value was computed by considering the cold-work of forming.

Table 4.43

Comparison of Computed and Tested Failure Loads
for Stub Columns with Unstiffened Flanges
(50XF Sheet Steel)
(Based on Tensile Yield Stress)

Spec.	Strain Rate in./in./sec. (1)	w/t (2)	$(P_u)_{comp}$, kips Based on $(F_y)_s$ (3)	$(F_y)_d$ (4)	$(P_u)_{test}$ kips (5)	(5)/(3) (6)	(5)/(4) (7)
2A1AX	0.0001	8.41	28.66*	28.66*	28.04	1.00	1.00
2A1BX	0.0001	8.38	28.70*	28.70*	28.16	0.98	0.98
2A2AX	0.01	8.40	28.70*	29.82*	29.02	1.01	0.97
2A2BX	0.01	8.38	28.69*	29.80*	29.43	1.03	0.99
2A3AX	0.08	8.29	28.72*	30.54*	30.75	1.07	1.01
2A3BX	0.08	8.36	28.70*	30.52*	30.95	1.08	1.01
2B1AX	0.0001	11.68	40.22*	40.22*	39.72	0.99	0.99
2B1BX	0.0001	11.60	40.36*	40.36*	39.18	0.97	0.97
2B1CX	0.00001	11.63	40.41*	39.91*	39.47	0.98	0.99
2B2AX	0.01	11.58	40.39*	42.00*	42.60	1.05	1.01
2B2BX	0.01	11.54	40.53*	42.15*	42.55	1.05	1.01
2B2CX	0.001	11.53	40.23*	40.93*	41.77	1.04	1.02
2B3AX	0.08	11.65	40.38*	42.99*	45.07	1.12	1.05
2B3BX	0.08	11.50	40.26*	42.86*	44.94	1.12	1.05
2C1AX	0.0001	22.84	45.21	45.21	43.62	0.96	0.96
2C1BX	0.0001	22.73	45.30	45.30	43.97	0.97	0.97
2C2AX	0.01	22.77	45.20	47.02	46.70	1.04	0.99
2C2BX	0.01	22.76	45.27	47.09	46.26	1.02	0.98
2C3AX	0.05	22.72	45.12	47.71	47.34	1.05	0.99
2C3BX	0.05	22.79	45.27	47.84	46.85	1.03	0.98
2D1AX	0.0001	35.37	45.74	45.74	44.06	0.96	0.96
2D1BX	0.0001	35.33	45.74	45.74	44.50	0.97	0.97
2D2AX	0.01	35.26	45.74	47.26	46.75	1.02	0.99
2D2BX	0.01	35.21	45.76	47.27	47.58	1.04	1.01
2D3AX	0.04	35.29	45.72	47.82	49.39	1.08	1.03
2D3BX	0.04	35.15	45.77	47.88	48.95	1.07	1.02
Mean						1.027	0.996
Standard Deviation						0.047	0.025

Note: 1. The sectional properties used for calculating the computed ultimate loads are listed in Appendix B (Table 8).
2. The superscript * indicates that the value was computed by considering the cold-work of forming.

listed in Table 4.44(c). As expected, the tested ultimate loads for the specimens assembled by bolts were found to be smaller than those assembled by epoxy for the tests conducted under the same strain rate.

For beams with unstiffened compression flanges, similar equations were used to calculate local buckling coefficients. The new local buckling coefficients listed in Tables 4.45 for channel beams fabricated from 35XF and 50XF sheet steels are based on the equations of Bleich and Kalyannaraman. For the use of Kalyanaraman's equations, the value of K_b/K_r was taken to be 0.055 for pure bending condition. In addition, the rotational edge stiffness is computed according to the following equation:

$$S''_r \cong \sqrt{33.4 + 50.7\left(\frac{B_r}{\lambda}\right)^2} - 2.78 \qquad (4.31)$$

Same as the I-shaped stub columns, the half wavelength (λ) was assumed to be infinite for beam specimens. Comparisons between the tested failure moments and the predicted values based on these new buckling coefficients are presented in Table 4.46 for 35XF sheet steel and in Table 4.47 for 50XF sheet steel, in which the computed failure moments listed in columns (3) and (4) are calculated on the basis of local buckling coefficients K_s and K_d, respectively. From Tables 4.31 and 4.46, it can be seen that the computed failure moments can be improved by using the new local buckling coefficients for channel beams fabricated from 35XF sheet steel. The values of $(M_y)_{comp}$ for beam Specimen series 4A and 4C fabricated from 50XF sheet steel (Table 4.47) are slight overestimated. For Specimen series 4B, the ratios of $(M_u)_{test}/(M_y)_{comp}$ listed in column (7) of Tables 4.46 and 4.47 are higher than the ratios for Specimen series 4A and 4C.

Figure 4.47 Photograph of an I-Shaped Stub Column Specimen Assembled by Bolts (Spec. 2B3AA)

Table 4.44
Comparison of Computed and Tested Failure Loads
for Stub Columns with Unstiffened Flanges
(Connecting Two Channel Sections by Bolts)
(35XF Sheet Steel)

(a) Dimensions of Stub Column Specimens

Specimen	BC (in.)	D (in.)	w/t	Gross Area ($in.^2$)	L (in.)	$(P_u)_{test}$ (kips)
2B1AA	1.386	3.023	13.47	0.9272	9.98	32.39
2B1BA	1.367	3.016	13.24	0.9195	9.92	31.56
2B3AA	1.363	3.005	13.20	0.9163	9.95	38.64

(b) Buckling Coefficients

Spec.	w/t	K^*	K_e	K_p	K_{ys}	K_{yd}	K_s	K_d
2B1AA	13.47	0.653	0.660	0.516	0.308	0.308	0.516	0.516
2B1BA	13.24	0.649	0.656	0.514	0.299	0.299	0.514	0.514
2B3AA	13.20	0.649	0.656	0.514	0.298	0.354	0.514	0.514

(c) Comparison of Computed and Tested Failure Loads

Spec.	Strain Rate in./in./sec. (1)	w/t (2)	$(P_u)_{comp}$, kips Based on $(F_y)_s$ (3)	Based on $(F_y)_d$ (4)	$(P_u)_{test}$ kips (5)	(5)/(3) (6)	(5)/(4) (7)
2B1AA	0.0001	13.47	30.48	30.48	32.39	1.06	1.06
2B1BA	0.0001	13.24	30.23	30.23	31.56	1.04	1.04
2B3AA	0.1	13.20	30.12	35.45	38.64	1.28	1.09

Table 4.45

Buckling Coefficients Used to Calculate the Failure Moments of Channel Beams (Based on Tensile Yield Stress)

Spec.	w/t	K^*	K_e	K_p	K_{ys}	K_{yd}	K_s	K_d
(35XF Sheet Steel)								
4B0A	15.13	0.731	0.831	0.597	0.366	0.366	0.597	0.597
4B1A	15.16	0.733	0.832	0.597	0.368	0.378	0.597	0.597
4B1B	14.93	0.727	0.828	0.595	0.358	0.367	0.595	0.595
4B2A	15.04	0.730	0.830	0.596	0.363	0.413	0.596	0.596
4B2B	15.16	0.733	0.832	0.597	0.368	0.418	0.597	0.597
4C0A	20.93	0.754	0.850	0.607	0.650	0.650	0.630	0.630
4C1A	20.99	0.756	0.851	0.607	0.653	0.670	0.632	0.641
4C1B	20.93	0.755	0.851	0.607	0.650	0.667	0.630	0.639
4C2A	20.99	0.754	0.850	0.607	0.653	0.743	0.632	0.679
4C2B	20.93	0.754	0.850	0.607	0.650	0.739	0.630	0.677
(50XF Sheet Steel)								
4B0AX	15.28	0.738	0.836	0.599	0.581	0.581	0.599	0.599
4B1AX	15.31	0.737	0.835	0.599	0.582	0.591	0.599	0.599
4B1BX	15.31	0.736	0.834	0.599	0.582	0.591	0.599	0.599
4B2AX	15.39	0.739	0.838	0.600	0.588	0.621	0.600	0.611
4B2BX	15.35	0.738	0.836	0.600	0.585	0.618	0.600	0.610
4C0AX	20.48	0.750	0.847	0.605	0.969	0.969	0.799	0.799
4C1AX	20.48	0.749	0.846	0.605	0.967	0.983	0.799	0.806
4C1BX	20.50	0.750	0.847	0.605	0.971	0.985	0.800	0.808
4C2AX	20.57	0.751	0.847	0.605	0.977	1.032	0.803	0.833
4C2BX	20.54	0.750	0.847	0.605	0.974	1.030	0.802	0.832

Note: K^* : elastic buckling coefficient from Eq. 4.24
K_e : elastic buckling coefficient from Eq. 4.25
K_p : plastic buckling coefficient from Eq. 4.25
K_{ys} : yield buckling coefficient from Eq. 4.30 (based on static yield stress)
K_{yd} : yield buckling coefficient from Eq. 4.30 (based on dynamic yield stress)
K_s : buckling coefficient from Eq.4.29 for static condition
K_d : buckling coefficient from Eq.4.29 for dynamic condition

Table 4.46

Comparison of Computed and Tested Failure Moments
for Beams with Unstiffened Flanges
(35XF Sheet Steel)
(Based on Tensile Yield Stress)

Spec.	Strain Rate in./in./sec. (1)	w/t (2)	$(M_y)_{comp}$, kips Based on $(F_y)_s$ (3)	$(F_y)_d$ (4)	$(M_u)_{test}$ kips (5)	(5)/(3) (6)	(5)/(4) (7)
4A0A	0.00001	9.28	14.70*	14.70*	14.82	1.01	1.01
4A1A	0.0001	9.16	14.47*	14.76*	16.53	1.14	1.12
4A1B	0.0001	9.16	14.65*	14.94*	16.60	1.13	1.11
4A2A	0.01	9.22	14.57*	16.16*	17.41	1.20	1.08
4A2B	0.01	9.03	14.49*	16.07*	17.64	1.22	1.10
4B0A	0.00001	15.13	22.96	22.96	26.26	1.14	1.14
4B1A	0.0001	15.16	22.90	23.41	27.20	1.19	1.16
4B1B	0.0001	14.93	22.95	23.49	26.52	1.16	1.13
4B2A	0.01	15.04	22.94	25.55	29.48	1.29	1.15
4B2B	0.01	15.16	22.90	25.50	29.51	1.29	1.16
4C0A	0.00001	20.93	32.96	32.96	34.49	1.05	1.05
4C1A	0.0001	20.99	32.87	33.66	35.87	1.09	1.07
4C1B	0.0001	20.93	32.82	33.61	37.17	1.13	1.11
4C2A	0.01	20.99	33.15	37.26	41.56	1.25	1.12
4C2B	0.01	20.93	32.96	37.05	41.52	1.26	1.12
Mean						1.170	1.109
Standard Deviation						0.084	0.042

Note: The superscript * indicates that the value was computed by considering the cold-work of forming.

Table 4.47

Comparison of Computed and Tested Failure Moments
for Beams with Unstiffened Flanges
(50XF Sheet Steel)
(Based on Tensile Yield Stress)

Spec.	Strain Rate in./in./sec. (1)	w/t (2)	$(M_y)_{comp}$, kips Based on $(F_y)_s$ (3)	$(F_y)_d$ (4)	$(M_u)_{test}$ kips (5)	(5)/(3) (6)	(5)/(4) (7)
4A0AX	0.00001	9.28	18.29*	18.29*	17.13	0.94	0.94
4A1AX	0.0001	9.16	18.35*	18.55*	17.27	0.94	0.93
4A1BX	0.0001	9.16	18.33*	18.52*	16.94	0.92	0.92
4A2AX	0.01	9.22	18.37*	19.24*	18.31	1.00	0.95
4A2BX	0.01	9.03	18.27*	19.14*	18.13	0.99	0.95
4B0AX	0.00001	15.13	24.25	24.25	26.26	1.08	1.08
4B1AX	0.0001	15.16	24.43	24.67	27.20	1.11	1.10
4B1BX	0.0001	14.93	24.57	24.85	26.52	1.08	1.07
4B2AX	0.01	15.04	24.25	25.46	29.48	1.22	1.16
4B2BX	0.01	15.16	24.37	25.58	29.51	1.21	1.15
4C0AX	0.00001	20.93	36.26	36.26	32.96	0.91	0.91
4C1AX	0.0001	20.99	36.38	36.85	34.95	0.96	0.95
4C1BX	0.0001	20.93	36.26	36.74	34.20	0.94	0.93
4C2AX	0.01	20.99	36.34	38.27	35.67	0.98	0.93
4C2BX	0.01	20.93	36.38	38.32	36.03	0.99	0.94
Mean						1.018	0.994
Standard Deviation						0.100	0.090

Note: The superscript * indicates that the value was computed by considering the cold-work of forming.

This is because the computed yield moments neglected the effect of cold-work of forming. Again, the computed yield moments of channel beams fabricated from 50XF sheet steel are slightly less conservative than those fabricated from 35XF sheet steel as found previously for I-shaped stub column tests.

4. Strain Rates Measured in the Stub Column Tests. From Tables 4.19, 4.20, 4.42, and 4.43, it can be seen that for most cases, the values of $(P_u)_{test}/(P_u)_{comp}$ ratios (column (7) of these tables) increase with increasing strain rates for all groups having similar w/t ratios when the dynamic yield stresses were used in the calculation of computed ultimate loads. Figure 4.48 shows the strain-time relationships for specimen 2B3AA tested under the strain rate of 10^{-1} in./in./sec.. The strains used for this plot were obtained from the readings of the strain gages mounted on the unsupported edge of unstiffened flange. Gages 1, 2, and 3 are located at the top, central, and bottom portions of the unstiffened flange along the length of the stub column. It can be seen that the strain gage mounted at the central portion has a lower strain rate than the other two strain gages. Because the strain rates listed in each table were obtained from the readings of the strain gages mounted on the central portion of compression elements for box-shaped and I-shaped stub columns, the ultimate strengths of stub columns calculated according to these measured strain rates are conservative.

5. Comparison of Stub Column and Beam Test Data. Table 4.48 lists the ratios of the dynamic to static failure loads for box-shaped and I-shaped stub columns fabricated from 35XF sheet steel. The static

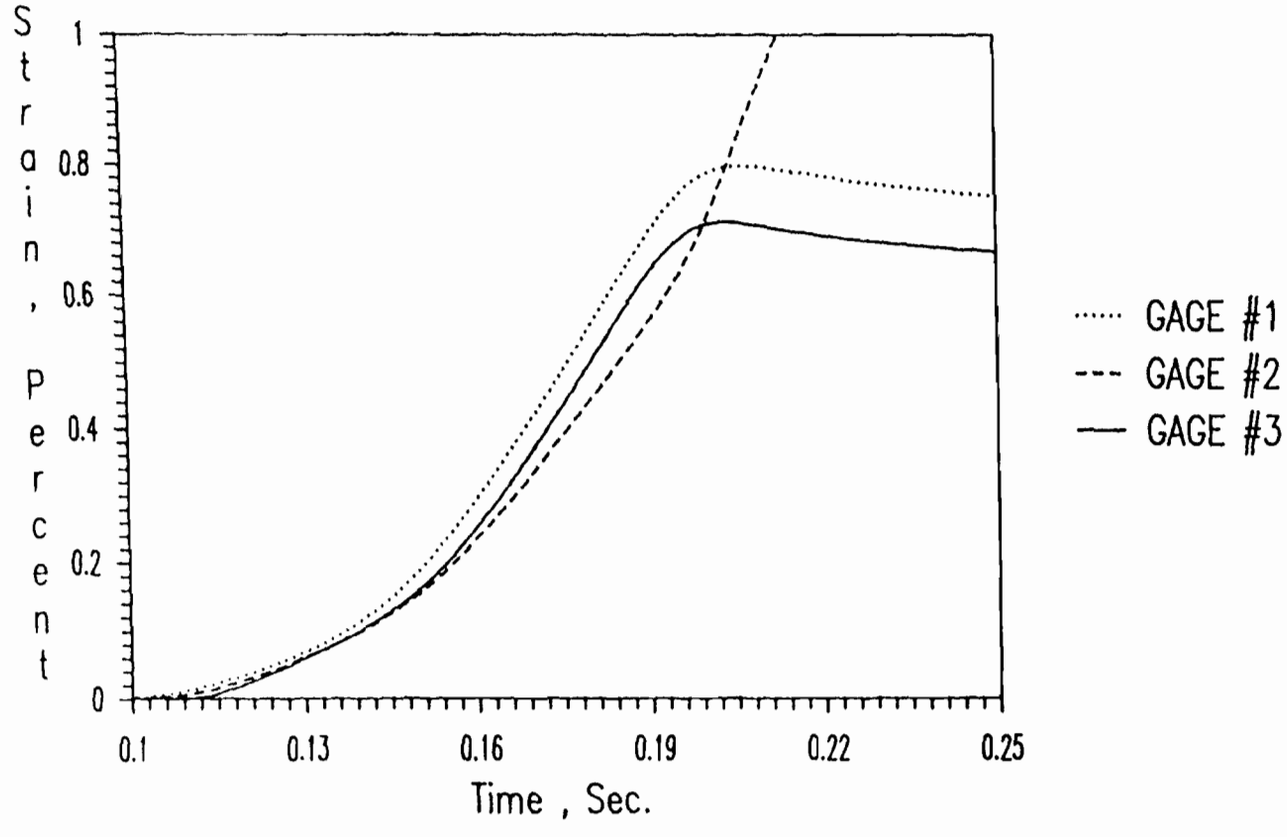

Figure 4.48 Strain-Time Curves of Specimen 2B3AA under a Strain Rate of 0.1 in./in./sec.

failure loads, $(P_u)_s$, were obtained from the stub column specimens tested under a strain rate of 10^{-4} in./in./sec., while the dynamic failure loads ,$(P_u)_{d1}$, were obtained from the stub column specimens tested under a strain rate of 10^{-2} in./in./sec.. The mean value of the $(P_u)_{d1}/(P_u)_s$ ratios listed in Table 4.48 are 1.101 and 1.087 for box-shaped stub columns and I-shaped stub columns, respectively. This indicates that the percentage increases in failure loads for box-shaped stub columns are similar to those for I-shaped stub columns. From the same table, it was also noted that the percentage increases in failure loads for both box-shaped and I-shaped stub columns are similar to the percentage increases in yield stresses.

Similar results can also be found from Table 4.49 which lists the ratios of dynamic to static failure loads for box-shaped and I-shaped stub columns fabricated from 50XF sheet steel. The mean values of $(P_u)_{d1}/(P_u)_s$ ratios listed in this table are 1.073 and 1.061 for box-shaped and I-shaped stub columns, respectively. For the stub columns fabricated from 35XF sheet steel, the percentage increases in failure loads are 9% to 10% for the tests conducted under strain rates ranged from 10^{-4} to 10^{-2} in./in./sec.. For the stub columns fabricated from 50XF sheet steel, the percentage increases in failure loads are 6% to 7% for the tests conducted under similar strain rates. In general, the percentage increases in failure loads for the stub columns fabricated from 50XF sheet steel are slightly less than the stub columns fabricated from 35XF sheet steel. This is because the strain-rate sensitivity of 35XF sheet steel is larger than that for 50XF sheet steel.

Table 4.48

Ratios of Dynamic to Static Tested Failure Loads

(a) Box-Shaped Stub Columns (35XF Sheet Steel)

	w/t			
	27.21	38.98	52.91	100.62
$(F_y)_{d1}/(F_y)_s$	1.107	1.107	1.107	1.107
$(P_u)_{d1}/(P_u)_s$	1.091	1.110	1.109	1.093

	Mean Value	Standard Deviation
$(P_u)_{d1}/(P_u)_s$	1.101	0.010

(b) I-Shaped Stub Columns (35XF Sheet Steel)

	w/t			
	8.98	13.38	20.87	44.57
$(F_y)_{d1}/(F_y)_s$	1.107	1.107	1.107	1.107
$(P_u)_{d1}/(P_u)_s$	1.061	1.079	1.104	1.103

	Mean Value	Standard Deviation
$(P_u)_{d1}/(P_u)_s$	1.087	0.021

Note: $(F_y)_s$: static yield stress (10^{-4} in./in./sec.)
$(F^y)_{d1}$: dynamic yield stress (10^{-2} in./in./sec.)
$(P^u)_s$: static failure load (10^{-4} in./in./sec.)
$(P_u)^s_{d1}$: dynamic failure load (10^{-2} in./in./sec.)

Table 4.49

Ratios of Dynamic to Static Tested Failure Loads

(a) Box-Shaped Stub Columns (50XF Sheet Steel)

	w/t			
	23.03	34.88	52.67	98.07
$(F_y)_{dl}/(F_y)_s$	1.042	1.042	1.042	1.042
$(P_u)_{dl}/(P_u)_s$	1.040	1.103	1.080	1.069

	Mean Value	Standard Deviation
$(P_u)_{dl}/(P_u)_s$	1.073	0.026

(b) I-Shaped Stub Columns (50XF Sheet Steel)

	w/t			
	8.37	11.59	22.77	35.27
$(F_y)_{dl}/(F_y)_s$	1.042	1.042	1.042	1.042
$(P_u)_{dl}/(P_u)_s$	1.040	1.079	1.061	1.065

	Mean Value	Standard Deviation
$(P_u)_{dl}/(P_u)_s$	1.061	0.016

Note: $(F_y)_s$: static yield stress (10^{-4} in./in./sec.)
$(F_y)_{dl}$: dynamic yield stress (10^{-2} in./in./sec.)
$(P_u)_s$: static failure load (10^{-4} in./in./sec.)
$(P_u)_{dl}$: dynamic failure load (10^{-2} in./in./sec.)

Table 4.50

Ratios of Dynamic to Static Tested Failure Moments

(a) Hat-Shaped Beams (35XF Sheet Steel)

	w/t		
	29.64	55.74	76.41
$(F_y)_{dl}/(F_y)_s$	1.107	1.107	1.107
$(M_u)_{dl}/(M_u)_s$	1.111	1.120	1.066

	Mean Value	Standard Deviation
$(M_u)_{dl}/(M_u)_s$	1.099	0.040

(b) Channel Beams (35XF Sheet Steel)

	w/t		
	9.17	15.08	20.95
$(F_y)_{dl}/(F_y)_s$	1.107	1.107	1.107
$(M_u)_{dl}/(M_u)_s$	1.058	1.098	1.137

	Mean Value	Standard Deviation
$(M_u)_{dl}/(M_u)_s$	1.098	0.040

Note: $(F_y)_s$: static yield stress (10^{-4} in./in./sec.)
$(F_y)_{dl}$: dynamic yield stress (10^{-2} in./in./sec.)
$(M_y)_{dl}$: static failure load (10^{-4} in./in./sec.)
$(M_u)_{dl}$: dynamic failure load (10^{-2} in./in./sec.)

Table 4.51

Ratios of Dynamic to Static Tested Failure Moments

(a) Hat-Shaped Beams (50XF Sheet Steel)

	w/t		
	26.68	46.09	65.77
$(F_y)_{dl}/(F_y)_s$	1.042	1.042	1.042
$(M_u)_{dl}/(M_u)_s$	1.060	1.038	1.054

	Mean Value	Standard Deviation
$(M_u)_{dl}/(M_u)_s$	1.051	0.011

(b) Channel Beams (50XF Sheet Steel)

	w/t		
	8.83	15.33	20.51
$(F_y)_{dl}/(F_y)_s$	1.042	1.042	1.042
$(M_u)_{dl}/(M_u)_s$	1.065	1.031	1.037

	Mean Value	Standard Deviation
$(M_u)_{dl}/(M_u)_s$	1.044	0.018

Note: $(F_y)_s$: static yield stress (10^{-4} in./in./sec.)
$(F_y)_{dl}$: dynamic yield stress (10^{-2} in./in./sec.)
$(M_u)_s$: static failure load (10^{-4} in./in./sec.)
$(M_u)_{dl}$: dynamic failure load (10^{-2} in./in./sec.)

Similar results were also found in the evaluation of failure moments of beam specimens. Table 4.50 lists the ratios of dynamic to static failure moments for hat-shaped and channel beams fabricated from 35XF sheet steel. Same as stub columns, the static failure moments of beams were obtained from the specimens tested under a strain rate of 10^{-4} in./in./sec. The mean values of $(M_u)_{dl}/(M_u)_s$ ratios are 1.099 and 1.098 for hat-shaped beams and channel beams, respectively. For beams fabricated from 50XF sheet steel, Tables 4.51(a) and 4.51(b) list the ratios of dynamic to static failure moments for hat-shaped and channel beams, respectively, with the mean values of $(M_u)_{dl}/(M_u)_s$ ratios to be 1.051 and 1.044. However, these values are slightly less than that found for the stub column tests.

V. CONCLUSIONS

Three selected sheet steels (35XF, 50XF, and 100XF) were tested in tension and compression for evaluating the effect of strain rate. In order to investigate the effect of strain rate on the structural strength of cold-formed members, 97 stub columns and 60 beams fabricated from two types of sheet steel (35XF and 50XF) were tested under different strain rates. Among these test specimens, box-shaped stub columns and hat-shaped beams were used to study the postbuckling strength of stiffened compression elements, while I-shaped stub columns and channel beams were used to study the postbuckling strength of unstiffened compression elements. The purpose of this investigation was to determine the validity of the current AISI effective width formulas for the design of cold-formed steel members subjected to dynamic loads.

Based on the test results obtained from this investigation, the following conclusions were drawn for the effect of strain rate on the mechanical properties of selected sheet steels:

1. The mechanical properties (proportional limit, yield strength, and ultimate tensile strength) increase with increasing strain rates.
2. For most cases, the mechanical properties of these selected sheet steels tested in transverse direction are slightly higher than those tested in longitudinal direction under the same strain rate.
3. Yield strength is more sensitive to strain rate than ultimate tensile strength.
4. The strain rate sensitivity values for yield strength in tension are similar to the values in compression.

5. The strain rate sensitivity value is not a constant for each material, it increases with increasing strain rate in most cases.
6. The mechanical properties of the sheet steels having lower yield strengths are more sensitive to strain-rate than the sheet steels having higher yield strengths.
7. A general equation (Equation 4.21) was developed to predict the tensile and compressive yield stresses for the strain rates from 10^{-4} to 10^{2} in./in./sec..

Based on the available test results of cold-formed steel structural members, the following conclusions can be drawn for the effect of strain rate on the strength of cold-formed steel stub columns and beams fabricated from 35XF and 50XF sheet steels:

1. For most cases, the ultimate loads of stub columns and the yield moments and ultimate moments of beams increase with increasing strain rates.
2. A better prediction for ultimate capacity of stub columns and beams can be achieved by using dynamic tensile yield stresses for the specimens fabricated from 35XF and 50XF sheet steels.
3. By considering the cold-work of forming, the predicted loads of compact sections (stub columns and beams) fabricated from 35XF sheet steel can be improved. However, it is not necessary to consider the cold-work effect for compact sections fabricated from 50XF sheet steel because of overestimation for some specimens.
4. For the compact sections of stub columns, the cold-work of forming is not the only reason to cause the discrepancies between the tested and computed ultimate loads. The tested loads are also

affected by the type of stress-strain relationship as discussed in Section E.2.

5. The percentage increases in ultimate loads for stub columns and ultimate moments for beams are slightly larger than the percentage increases of yield stresses.
6. For stub columns fabricated from the same sheet steel, the percentage increases in ultimate loads for box-shaped stub columns having stiffened elements are similar to those for I-shaped stub columns having unstiffened elements. Similar results were found for the beam specimens.
7. The percentage increases in ultimate moments for beams are slightly less than those for stub columns.
8. The computed ultimate loads for stub columns and the computed yield and ultimate moments for beams computed on the basis of the AISI Automotive Steel Design Manual were found to be conservative for most cases.
9. From test results, it was found that the computed ultimate loads of stub columns and ultimate moments of beams having stiffened compression elements are less conservative than the specimens with unstiffened compression elements by using the current design criteria.
10. For calculating the ultimate capacity of stub columns as well as beams, a local buckling coefficient of 4.0 for stiffened compression elements and the values computed from Kalyanaraman's equations for unstiffened compression elements can provide good agreements with test results.

APPENDIX A

NOTATION

The following symbols are used in this report:

a	Length of plate
A	Actual tensile or compressive coupon area
A_e	Effective cross-sectional area of stub columns
A_t	Total cross-sectional area of stub column
b	Effective width of a compression element
B_b	Width of bending element
B_r	Width of restraining element
b_c	Effective width of the compression flange
b_t	Total width of the tension flange
C	Ratio of the total corner cross-sectional area to the total cross-sectional area of the full section for stub column
	Ratio of the total corner cross-sectional area of the controlling flange to the full cross-sectional area of the controlling flange for beam
C_f	Correction factor
C_y	Compression strain factor for stiffened compression elements without intermediate stiffeners
D	Flexural rigidity of plate
d	Depth of the section
D_b	Flexural rigidity of the bending element
D_r	Flexural rigidity of the restraining element
$(d)_{comp}$	computed deflection of beam
E	Modulus of elasticity of steel, 29,500 ksi
E_t	Tangent modulus of steel
f	Edge stress in the compression element
f_{cr}	Critical local buckling stress
$(f_{cr})_E$	Elastic critical local buckling stress

$(f_{cr})_I$	Inelastic critical local buckling stress
f_x	Stress component normal to the edges of the plate
F_{pr}	Proportional limit
F_y	Yield stress
F_{ya}	Average tensile yield stress of steel
F_{yc}	Corner yield stress
F_{yf}	Weighted average tensile stress point of flat portions
F_{yv}	Tensile yield stress of virgin steel
F_u	Ultimate tensile strength
F_{uv}	Ultimate tensile strength of virgin steel
H	Thickness of the beam
I_e	Effective moment of inertia under service moment
k	Buckling coefficient
K_e	Elastic buckling coefficient
K_p	Plastic buckling coefficient
K_y	Yield buckling coefficient
K^*	Elastic buckling coefficient
L	Span length of beam
M	Dynamic bending moment
m	Strain-rate sensitivity
	Number of half sine waves in x-direction
M_o	Static collapse moment
M_s	Service moment
$(M_{cr})_{comp}$	Computed critical local buckling moment
$(M_{cr})_{test}$	Tested critical local buckling moment
$(M_s)_{test}$	Tested service moment
$(M_u)_{comp}$	Computed ultimate moment

$(M_u)_{test}$	Tested ultimate moment
$(M_y)_{comp}$	Computed yield moment
$(M_y)_{test}$	Tested yield moment
n	Number of half sine waves in y-direction
N_b	Number of buckling elements at the junction
P_{cr}	Critical local buckling load
$(P_{cr})_{comp}$	Computed critical local buckling load
$(P_{cr})_{test}$	Tested critical local buckling load
P_m	Mean crushing force
P_u	Ultimate load
$(P_u)_{comp}$	Computed ultimate load
$(P_u)_{test}$	Tested ultimate load
P_y	Yield load
$(P_y)_{test}$	Tested yield load
q	Lateral uniform load applied to the plate
R	Inside bend radius
	Dynamic correction factor
S_e	Elastic esction modulus of effective section
S''_r	Rotation edge stiffness
t	Thickness of element
t_b	Thickness of bending element
t_r	Thickness of restraining element
v	Crushing speed
w	Flat width of a compression element
ε	Engineering strain
$\bar{\varepsilon}$	True strain

$\dot{\varepsilon}$	Strain rate
$\dot{\kappa}$	Curvature rate
λ	Slenderness factor
ω	Lateral deflection of the plate
μ	Poisson's ratio
ρ	Reduction factor
σ	Engineering stress
$\overline{\sigma}$	True stress
τ_{xy}	Shear stress component on the edges of the plate in the x-z and y-z plane
ξ	Rotation edge restraint

APPENDIX B

SUPPLEMENTARY TABLES

Table 1

The Yield Stresses and Effective Cross-Sectional Areas Used for Calculating the Computed Failure Loads Listed in Table 4.11(a) (35XF Sheet Steel)

Spec.	Strain Rate in./in./sec.	w/t	$(F_y)_s$ ksi	$(A_e)_s$ kips	$(F_y)_d$ ksi	$(A_e)_d$ kips
1A1A	0.0001	27.15	32.87	1.2060	32.87	1.2060
1A1B	0.0001	27.39	32.87	1.2058	32.87	1.2058
1A2A	0.01	26.92	32.87	1.2007	36.40	1.2007
1A2B	0.01	27.06	32.87	1.2014	36.40	1.2014
1A3A	0.10	27.31	32.87	1.2009	39.08	1.2009
1A3B	0.10	27.40	32.87	1.2009	39.08	1.2009
1B1A	0.0001	38.93	32.87	1.5434	32.87	1.5434
1B1B	0.0001	39.17	32.87	1.5418	32.87	1.5418
1B2A	0.01	38.86	32.87	1.5373	36.40	1.5223
1B2B	0.01	39.10	32.87	1.5406	36.40	1.5253
1B3A	0.10	38.86	32.87	1.5424	39.08	1.5164
1B3B	0.10	38.96	32.87	1.5394	39.08	1.5131
1C1A	0.0001	52.69	32.87	1.7925	32.87	1.7925
1C1B	0.0001	52.96	32.87	1.7913	32.87	1.7913
1C2A	0.01	52.20	32.87	1.7913	36.40	1.7698
1C2B	0.01	53.06	32.87	1.7937	36.40	1.7714
1C3A	0.10	53.15	32.87	1.7953	39.08	1.7579
1C3B	0.10	53.39	32.87	1.7916	39.08	1.7544
1D1A	0.0001	100.68	32.87	2.0864	32.87	2.0864
1D1B	0.0001	100.35	32.87	2.0907	32.87	2.0907
1D2A	0.01	100.49	32.87	2.0852	36.40	2.0456
1D2B	0.01	100.62	32.87	2.0855	36.40	2.0544
1D3A	0.05	100.85	32.87	2.0837	38.21	2.0382
1D3B	0.05	100.72	32.87	2.0834	38.21	2.0379

Note: $(F_y)_s$: static tensile yield stress

$(F_y)_d$: dynamic tensile yield stress

Table 2

The Yield Stresses and Effective Cross-Sectional Areas Used for Calculating the Computed Failure Loads Listed in Table 4.12(a) (50XF Sheet Steel)

Spec.	Strain Rate in./in./sec.	w/t	$(F_y)_s$ ksi	$(A_e)_s$ kips	$(F_y)_d$ ksi	$(A_e)_d$ kips
1A1AX	0.0001	22.89	49.50	1.1569	49.50	1.1569
1A1BX	0.0001	23.15	49.50	1.1652	49.50	1.1652
1A2AX	0.01	23.15	49.50	1.1584	51.60	1.1584
1A2BX	0.01	22.94	49.50	1.1587	51.60	1.1587
1A3AX	0.05	23.10	49.50	1.1605	52.56	1.1605
1A3BX	0.05	22.92	49.50	1.1612	52.56	1.1612
1B1AX	0.0001	35.49	49.50	1.2786	49.50	1.2786
1B1BX	0.0001	34.59	49.50	1.2788	49.50	1.2788
1B2AX	0.01	34.50	49.50	1.2778	51.60	1.2731
1B2BX	0.01	34.96	49.50	1.2802	51.60	1.2754
1B3AX	0.04	34.97	49.50	1.2794	52.42	1.2728
1B3BX	0.04	34.79	49.50	1.2814	52.42	1.2747
1C1AX	0.0001	52.76	49.50	1.3305	49.50	1.3305
1C1BX	0.0001	53.40	49.50	1.3341	49.50	1.3341
1C2AX	0.01	53.06	49.50	1.3329	51.60	1.3260
1C2BX	0.01	52.23	49.50	1.3321	51.60	1.3236
1C3AX	0.04	51.67	49.50	1.3297	52.42	1.3203
1C3BX	0.04	52.90	49.50	1.3341	52.42	1.3245
1D1AX	0.0001	97.99	49.50	1.6394	49.50	1.6394
1D2AX	0.01	98.21	49.50	1.6380	51.60	1.6289
1D3AX	0.03	98.01	49.50	1.6424	52.24	1.6309
1D3BX	0.03	98.07	49.50	1.6430	52.24	1.6315

Note: $(F_y)_s$: static tensile yield stress

$(F_y)_d$: dynamic tensile yield stress

Table 3

The Yield Stresses and Effective Cross-Sectional Areas Used for Calculating the Computed Failure Loads Listed in Table 4.19(a) (35XF Sheet Steel)

Spec.	Strain Rate in./in./sec.	w/t	$(F_y)_s$ ksi	$(A_e)_s$ kips	$(F_y)_d$ ksi	$(A_e)_d$ kips
2A1A	0.0001	8.93	32.87	0.6220	32.87	0.6220
2A1B	0.0001	9.04	32.87	0.6285	32.87	0.6285
2A2A	0.01	8.93	32.87	0.6288	36.40	0.6288
2A2B	0.01	9.10	32.87	0.6275	36.40	0.6275
2A3A	0.10	8.93	32.87	0.6288	39.08	0.6288
2A3B	0.10	8.96	32.87	0.6254	39.08	0.6254
2B1A	0.0001	13.34	32.87	0.9118	32.87	0.9118
2B1B	0.0001	13.41	32.87	0.9051	32.87	0.9051
2B2A	0.01	13.40	32.87	0.9060	36.40	0.8953
2B2B	0.01	13.37	32.87	0.9090	36.40	0.8984
2B3A	0.10	13.34	32.87	0.9109	39.08	0.8925
2B3B	0.10	13.42	32.87	0.9096	39.08	0.8910
2C0A	0.00001	20.69	32.87	0.9665	32.02	0.9710
2C1A	0.0001	20.85	32.87	0.9635	32.87	0.9635
2C1B	0.0001	20.76	32.87	0.9699	32.87	0.9699
2C2A	0.01	20.97	32.87	0.9623	36.40	0.9459
2C2B	0.01	20.81	32.87	0.9699	36.40	0.9533
2C3A	0.10	20.93	32.87	0.9626	39.08	0.9347
2C3B	0.10	20.87	32.87	0.9635	39.08	0.9358
2D1A	0.0001	44.60	32.87	1.0754	32.87	1.0754
2D1B	0.0001	44.50	32.87	1.0767	32.87	1.0767
2D2A	0.01	44.62	32.87	1.0712	36.40	1.0492
2D2B	0.01	44.59	32.87	1.0730	36.40	1.0511
2D3A	0.05	44.51	32.87	1.0648	38.21	1.0327
2D3B	0.05	44.60	32.87	1.0751	38.21	1.0429

Note: $(F_y)_s$: static tensile yield stress

$(F_y)_d$: dynamic tensile yield stress

Table 4

The Yield Stresses and Effective Cross-Sectional Areas Used for Calculating the Computed Failure Loads Listed in Table 4.20(a) (50XF Sheet Steel)

Spec.	Strain Rate in./in./sec.	w/t	$(F_y)_s$ ksi	$(A_e)_s$ kips	$(F_y)_d$ ksi	$(A_e)_d$ kips
2A1AX	0.0001	8.41	49.50	0.5220	49.50	0.5220
2A1BX	0.0001	8.38	49.50	0.5227	49.50	0.5227
2A2AX	0.01	8.40	49.50	0.5228	51.60	0.5228
2A2BX	0.01	8.38	49.50	0.5224	51.60	0.5224
2A3AX	0.08	8.29	49.50	0.5232	52.86	0.5232
2A3BX	0.08	8.36	49.50	0.5227	52.86	0.5227
2B1AX	0.00001	11.68	49.50	0.7358	49.50	0.7358
2B1BX	0.0001	11.60	49.50	0.7400	49.50	0.7400
2B1CX	0.0001	11.63	49.50	0.7404	48.81	0.7414
2B2AX	0.01	11.58	49.50	0.7408	51.60	0.7376
2B2BX	0.01	11.54	49.50	0.7442	51.60	0.7411
2B2CX	0.001	11.53	49.50	0.7384	50.43	0.7371
2B3AX	0.08	11.65	49.50	0.7394	52.86	0.7344
2B3BX	0.08	11.50	49.50	0.7392	52.86	0.7344
2C1AX	0.0001	22.84	49.50	0.7990	49.50	0.7990
2C1BX	0.0001	22.73	49.50	0.8020	49.50	0.8020
2C2AX	0.01	22.77	49.50	0.7994	51.60	0.7942
2C2BX	0.01	22.76	49.50	0.8010	51.60	0.7957
2C3AX	0.05	22.72	49.50	0.7984	52.56	0.7907
2C3BX	0.05	22.79	49.50	0.8006	52.56	0.7932
2D1AX	0.0001	35.37	49.50	0.7675	49.50	0.7675
2D1BX	0.0001	35.33	49.50	0.7675	49.50	0.7675
2D2AX	0.01	35.26	49.50	0.7677	51.60	0.7616
2D2BX	0.01	35.21	49.50	0.7681	51.60	0.7620
2D3AX	0.04	35.29	49.50	0.7671	52.42	0.7589
2D3BX	0.04	35.15	49.50	0.7685	52.42	0.7602

Note: $(F_y)_s$: static tensile yield stress

$(F_y)_d$: dynamic tensile yield stress

Table 5

Average Tested Mechanical Properties of Sheet Steels
(Longitudinal Tension)

(a) 25AK Sheet Steel

Strain Rate in./in./sec.	F_y (ksi)	F_u (ksi)	Elongation (percent)
0.0001	24.60	42.76	-----
0.01	27.86	44.44	49.31*
0.1	31.72	47.35	50.98*
1.0	35.13	51.25	58.18*

(b) 50SK Sheet Steel

Strain Rate in./in./sec.	F_y (ksi)	F_u (ksi)	Elongation (percent)
0.0001	54.97	67.07	36.09
0.01	56.83	68.98	33.34
0.1	58.06	71.04	34.45
1.0	60.73	76.50	40.13

* : Because the maximum range for extensometer is 1.0 inch, these values were measured from the distance between the gage marks of tension coupons.

Table 6

Average Tested Mechanical Properties of Sheet Steels
(Longitudinal Compression)

(a) 25AK Sheet Steel

Strain Rate in./in./sec.	F_{pr} (ksi)	F_y (ksi)	F_{pr}/F_y
0.0001	15.93	21.66	0.74
0.01	19.55	24.77	0.79
0.1	22.81	29.80	0.76
1.0	-----	38.14	----

(b) 50SK Sheet Steel

Strain Rate in./in./sec.	F_{pr} (ksi)	F_y (ksi)	F_{pr}/F_y
0.0001	41.98	53.35	0.79
0.01	42.46	55.91	0.76
0.1	44.36	56.96	0.78
1.0	-----	59.41	----

Table 7

The Yield Stresses and Effective Cross-Sectional Areas Used for Calculating the Computed Failure Loads Listed in Table 4.42 (35XF Sheet Steel)

Spec.	Strain Rate in./in./sec.	w/t	$(F_y)_s$ ksi	$(A_e)_s$ kips	$(F_y)_d$ ksi	$(A_e)_d$ kips
2A1A	0.0001	8.93	36.60	0.6220	36.60	0.6220
2A1B	0.0001	9.04	36.56	0.6285	36.56	0.6285
2A2A	0.01	8.93	36.56	0.6288	40.02	0.6288
2A2B	0.01	9.10	36.57	0.6275	40.03	0.6275
2A3A	0.10	8.93	36.56	0.6288	42.67	0.6288
2A3B	0.10	8.96	36.58	0.6254	42.67	0.6254
2B1A	0.0001	13.34	35.38	0.9238	35.38	0.9238
2B1B	0.0001	13.41	35.40	0.9184	35.40	0.9184
2B2A	0.01	13.40	35.39	0.9190	38.88	0.9190
2B2B	0.01	13.37	35.39	0.9218	38.87	0.9218
2B3A	0.10	13.34	35.38	0.9229	41.53	0.9229
2B3B	0.10	13.42	35.38	0.9229	41.53	0.9229
2C0A	0.00001	20.69	32.87	1.0451	32.02	1.0496
2C1A	0.0001	20.85	32.87	1.0427	32.87	1.0427
2C1B	0.0001	20.76	32.87	1.0487	32.87	1.0487
2C2A	0.01	20.97	32.87	1.0423	36.40	1.0319
2C2B	0.01	20.81	32.87	1.0487	36.40	1.0372
2C3A	0.10	20.93	32.87	1.0424	39.08	1.0265
2C3B	0.10	20.87	32.87	1.0430	39.08	1.0267
2D1A	0.0001	44.60	32.87	1.3153	32.87	1.3153
2D1B	0.0001	44.50	32.87	1.3164	32.87	1.3164
2D2A	0.01	44.62	32.87	1.3115	36.40	1.2811
2D2B	0.01	44.59	32.87	1.3114	36.40	1.2827
2D3A	0.05	44.51	32.87	1.3052	38.21	1.2607
2D3B	0.05	44.60	32.87	1.3151	38.21	1.2706

Note: $(F_y)_s$: static tensile yield stress

$(F_y)_d$: dynamic tensile yield stress

Table 8

The Yield Stresses and Effective Cross-Sectional Areas Used for Calculating the Computed Failure Loads Listed in Table 4.43 (50XF Sheet Steel)

Spec.	Strain Rate in./in./sec.	w/t	$(F_y)_s$ ksi	$(A_e)_s$ kips	$(F_y)_d$ ksi	$(A_e)_d$ kips
2A1AX	0.0001	8.41	54.91	0.5220	54.91	0.5220
2A1BX	0.0001	8.38	54.90	0.5227	54.90	0.5227
2A2AX	0.01	8.40	54.90	0.5228	57.04	0.5228
2A2BX	0.01	8.38	54.90	0.5224	57.04	0.5224
2A3AX	0.08	8.29	54.90	0.5232	58.37	0.5232
2A3BX	0.08	8.36	54.90	0.5227	58.37	0.5227
2B1AX	0.00001	11.68	53.24	0.7554	53.24	0.7554
2B1BX	0.0001	11.60	53.22	0.7584	53.22	0.7584
2B1CX	0.0001	11.63	53.22	0.7593	52.56	0.7593
2B2AX	0.01	11.58	53.22	0.7588	55.35	0.7588
2B2BX	0.01	11.54	53.21	0.7618	55.33	0.7618
2B2CX	0.001	11.53	53.24	0.7558	54.16	0.7558
2B3AX	0.08	11.65	53.22	0.7587	56.66	0.7587
2B3BX	0.08	11.50	53.23	0.7562	56.68	0.7562
2C1AX	0.0001	22.84	49.50	0.9134	49.50	0.9134
2C1BX	0.0001	22.73	49.50	0.9152	49.50	0.9152
2C2AX	0.01	22.77	49.50	0.9131	51.60	0.9112
2C2BX	0.01	22.76	49.50	0.9145	51.60	0.9125
2C3AX	0.05	22.72	49.50	0.9115	52.56	0.9077
2C3BX	0.05	22.79	49.50	0.9145	52.56	0.9102
2D1AX	0.0001	35.37	49.50	0.9241	49.50	0.9241
2D1BX	0.0001	35.33	49.50	0.9240	49.50	0.9240
2D2AX	0.01	35.26	49.50	0.9241	51.60	0.9158
2D2BX	0.01	35.21	49.50	0.9244	51.60	0.9162
2D3AX	0.04	35.29	49.50	0.9236	52.42	0.9123
2D3BX	0.04	35.15	49.50	0.9246	52.42	0.9133

Note: $(F_y)_s$: static tensile yield stress

$(F_y)_d$: dynamic tensile yield stress

BIBLIOGRAPHY

1. American Iron and Steel Institute, "Automotive Steel Design Manual," 1986 Edition, Revision 3 - February 1991.

2. American Iron and Steel Institute, "Guide for Preliminary Design of Sheet Steel Automotive Structural Components," 1981 Edition.

3. Yu, W.W., C. Santaputra, and M.B. Parks, "Design of Automotive Structural Components Using High Strength Sheet Steels," First Progress Report, Civil Engineering Study 83-1, University of Missouri-Rolla, January 1983.

4. Parks, M.B. and W.W. Yu, "Design of Automotive Structural Components Using High Strength Sheet Steels: Mechanical Properties of Materials," Second Progress Report, Civil Engineering Study 83-3, University of Missouri-Rolla, August 1983.

5. Santaputra, C. and W.W. Yu, "Design of Automotive Structural Components Using High Strength Sheet Steels: Strength of Beam Webs," Third Progress Report, Civil Engineering Study 83-4, University of Missouri-Rolla, August 1983.

6. Parks, M.B. and W.W. Yu, "Design of Automotive Structural Components Using High Strength Sheet Steels: Strength of Curved Elements and Members Consisting of Curved Elements," Fourth Progress Report, Civil Engineering Study 83-5, University of Missouri-Rolla, August 1983.

7. Santaputra, C. and W.W. Yu, "Design of Automotive Structural Components Using High Strength Sheet Steels: Structural Behavior of Beam Webs Subjected to Web Crippling and a Combination of Web Crippling and Bending," Fifth Progress Report, Civil Engineering Study 84-1, University of Missouri-Rolla, October 1984.

8. Parks, M.B. and W.W. Yu, "Design of Automotive Structural Components Using High Strength Sheet Steels: Status Report on the Study of Members Consisting of Flat and Curved Elements," Sixth Progress Report, Civil Engineering Study 84-2, University of Missouri-Rolla, October 1984.

9. Parks, M.B. and W.W. Yu, "Design of Automotive Structural Components Using High Strength Sheet Steels: Results and Evaluation of Stub Column Tests for Unstiffened Curved Elements," Seventh Progress Report, Civil Engineering Study 85-1, University of Missouri-Rolla, September 1985.

10. Santaputra, C. and W.W. Yu, "Design of Automotive Structural Components Using High Strength Sheet Steels: Web Crippling of Cold-Formed Steel Beams," Eighth Progress Report, Civil Engineering Study 86-1, University of Missouri-Rolla, August 1986.

11. Parks, M.B. and W.W. Yu, "Design of Automotive Structural Components Using High Strength Sheet Steels: Structural Behavior of Members Consisting of Flat and Curved Elements," Ninth Progress Report, Civil Engineering Study 87-2, University of Missouri-Rolla, June 1987.

12. Lin, S.H., L.E. Hsiao, C.L. Pan, and W.W. Yu, "Design of Automotive Structural Components Using High Strength Sheet Steels: Structural Strength of Cold-Formed Steel I-Beams and Hat Sections Subjected to Web Crippling Load," Tenth Progress Report, Civil Engineering Study 88-5, University of Missouri-Rolla, June 1988.

13. Pan, L.C., "Effective Design Widths of High Strength Cold-Formed Steel Members," Ph.D. Thesis, University of Missouri-Rolla, 1987.

14. Kassar, M. and W.W. Yu, "Design of Automotive Structural Components Using High Strength Sheet Steels: The Effect of Strain Rate on Mechanical Properties of Sheet Steels," Eleventh Progress Report, Civil Engineering Study 89-2, University of Missouri-Rolla, January, 1989.

15. Kassar, M. and W.W. Yu, "Design of Automotive Structural Components Using High Strength Sheet Steels: The Effect of Strain Rate on Compressive Mechanical Properties of Sheet Steels," Twelfth Progress Report, Civil Engineering Study 89-4, University of Missouri-Rolla, August, 1989.

16. Kassar, M. and W.W. Yu, "Design of Automotive Structural Components Using High Strength Sheet Steels: Structural Strengths of Cold-Formed Steel Members under Dynamic loads," Thirteenth Progress Report, Civil Engineering Study 90-1, University of Missouri-Rolla, March, 1990.

17. Kassar, M, "Effect of Strain Rate on Material Properties of Sheet Steels and Structural Strengths of Cold-Formed Steel Members," Ph.D. Thesis, Also Published as "Design of Automotive Structural Components Using High Strength Sheet Steels: Effect of Strain Rate on Material Properties of Sheet Steels and Structural Strengths of Cold-Formed Steel Members," Fourteenth Progress Report, Civil Engineering Study 90-2, University of Missouri-Rolla, May, 1990.

18. Pan, C.L. and W.W. Yu, "Design of Automotive Structural Components Using High Strength Sheet Steels: Structural Strengths of Cold-Formed Steel Members under Dynamic Loads," Fifteenth Progress Report, Civil Engineering Study 90-3, University of Missouri-Rolla, November, 1990.

19. Pan, C.L. and W.W. Yu, "Design of Automotive Structural Components Using High Strength Sheet Steels: Structural Strengths of Cold-Formed Steel Beams under Dynamic Loads," Sixteenth Progress Report, Civil Engineering Study 91-4, University of Missouri-Rolla, September, 1991.

20. Hosford, W.F. and R.M. Caddel, Metal Forming-Mechanics and Metallurgy, Englewood Cliffs, N.J. : Prentice Hall, Inc., 1983, 80-84.

21. Timoshenko, S., Strength of Material - Part II. Princeton, N.J. : D. Van Nostrand Company, Inc., 1956, 400-428.

22. Meyers, M.A. and K.K. Chawla, Mechanical Metallurgy : Principles and Applications, Prentice Hall, Englewood Cliffs, N.J., 1984.

23. Singer, L.F. and A. Pytel, Strength of Materials, The Maple Press Company, Third Edition, 1980.

24. Yu, W.W., Cold-Formed Steel Design, Second Edition, Wiley-Interscience, New York, 1991.

25. American Iron and Steel Institute, "Cost-Effective Weight Reduction with Steel Sheet," SG-631 R.

26. Chatfield, D.A. and R.R. Rote, "Strain Rate Effects on the Properties of High Strength, Low Alloy Steel," Paper 740177, SAE Automotive Engineering Congress, Detroit, February 1974.

27. Staker, M.R., "High Strain Rate Testing," Metals Handbook, American Society for Metals, Ninth Edition, Volume 8, 1985.

28. Lindholm, U.S., "Techniques in Metal Research," Volume 5, Part 1, Wiley-Interscience, New York, 1971.

29. Zukas, J.A., T. Nicholas, H.F. Swift, L.B. Greszczuk, and D.R. Curran, Impact Dynamics, John Wiley & Sons, New York, 1982.

30. Grillis, P.P. and S.T. Gross, "Effect of Strain Rate on Flow Properties," Metals Handbook, American Society for Metals, Ninth Edition, Volume 8,1985.

31. Davis, E.A., "The Effect of the Speed of Stretching and the Rate of Loading on the Yielding of Mild Steel," Journal of Applied Mechanics, ASME Transactions, Volume 60, 1938.

32. Manjoine, M.J., "Influence of Rate of Strain and Temperature on Yield Stresses of Mild Steel," Journal of Applied Mechanics , ASME Transactions, Volume 66, 1944.

33. Norris, C.H., R.J. Hansen, M.J. Holley, J.M. Biggs, S. Mamyet, and J.K. Minami, Structural Design for Dynamic Loads, McGraw-Hill Book Company, New York, 1959.

34. Alder, J.F. and V.A. Phillips, "The Effect of Strain Rate and Temperature on the Resistance of Aluminum, Copper, and steel to Compression," Journal of the Institute of Metals, Volume 83, 1954-1955, pp.80-86.

35. Cook, P.M., "True Stress-Strain Curves for Steel in Compression at High Temperature and Strain Rate, for Application on the Calculation of Load and Torque in Hot Rolling," Conference on the Properties of Materials at High Rates of Strain, Institute of Mechanical Engineers, 1957, pp. 86-97.

36. Davies, E.D.H. and S.C. Hunter, "The Dynamic Compression Testing of Solids by the Method of the Split Hopkinson Pressure Bar," Journal of Mech. Phys. Solids, Volume 11, 1963, pp.155-172.

37. Holt, J.M., "The Effect of Strain Rate on the Tensile Properties of USS COR-TEN and USS TRI-TEN High-Strength Low-Alloy Steels'" United States Steel Corporation, Applied Research Center, Project Number 37.12-100(2), Pittsburgh, PA., 1962.

38. Duffy, J., "The J D Campbell Memorial Lecture : Testing Techniques and Material Behavior at High Rates of Strain," Institute of Physics Conf., Ser. No. 47, 1979.

39. Wilson, M.L., R.H. Hawley, and J. Duffy, "Strain Rate and Strain Rate History Effects in Two Mild Steels," Brown University, Rep. NSF ENG 75-18532/8, March 1979.

40. Eleiche, A.M. and J.D. Campbell, Tech. Report ARML-TR-76-90, Air Force Materials Laboratory, Wright-Patterson Air Force, 1976.

41. Watanabe, T., "Effect of Strain Rate on Yield Behavior of Cold-Rolled Sheet Steel," Transactions of the Iron and Steel Institute of Japan, Volume 22, 1982.

42. Meyer, L.W., "Dynamic Tension Studies of Strength and Formability Characteristic of a High Alloyed Steel with Repect to Thermal Activation," Mechanical Properties at High High Rate of Strain, Institute of Physics, London, No.70, 1984.

43. Sachdev, A.K. and R.H. Wagonar, "Uniaxial Strain Hardening at Large Strain in Several Sheet Steels," Novel Techniques in Metal Deformation Testing, The Metallurgical Society of AIME, 1983.

44. Nagorka, M.S., "The Effect of Microstructure and Strain Rate on the Stage III Strain Hardening and Ductility of Dual-Phase Steels," Material Science and Engineering, Vol. 94, 1987, pp.183-193.

45. Timoshenko, S.P. and J.M. Gere, Theory of Elastic Stability, Second Edition, McGraw-Hill Book Company, New York, 1961.

46. Bulson, P.S., The Stability of Flate Plates, American Elsevier Publishing Company, New York, 1969. 47. Saint Venant, "Discussion in Theorre de l'elasticte' des Corps Solids," by Clebsch, 1983, p.704.

48. Bleich, F., "Theorie und Berechnung der eisernen Brcicken," Julius Springer, Berlin, 1924.

49. Bijlaard, P.P., "Theory of Plastic Stability of Thin Plates," Pubs. International Association for Bridge and Structural Engineering, Volume VI, 1940-1941.

50. Bijlaard, P.P., "Theory of Tests on the Plastic Stability of Plates and Shells," Journal of the Aeronautical Sciences, Volume 16, 1949, pp.529-541.

51. Ilyushin, A.A., "The Elastic-Plastic Stability of Plates," Transcation in NACA Technical Memorandum 1188.

52. Stowell, E.Z., "A Unified Theory of Plastic Buckling of Columns and Plates," NACA Technical Note No. 1556, April 1948.

53. Von Karman, T., "Festigkeitsprobleme in Meschinenbau," Encyklpadie der Mathematischen, Volume 4, 1910, p.349.

54. Schnadel, G., "Die Uberschreitung der Knickgrenze bei dunnen Platlen," Proceedings of Third International Congress for Applied Mechanics, Stockholm, Volume 3, 1930.

55. Cox, H.L., "The Buckling of Thin Plates in Compression," Technical Report of the Aeronautical Committee, 1933-34.

56. Marguerre, K., "Die Mittrangende Breite der Gedrukten Platte," Luftfahrtforschung, Volume 14, 1937.

57. Levy, S., "Bending of Rectangular Plates with Large Deflections," NACA Technical Report 737, 1942, p.139.

58. Von Karman, T., E.E. Sechler, and L.H. Donnel, "The Strength of Thin Plates in Compression," Transcations, ASME, Volume 54, APM54-5, 1932.

59. Winter, G., "Strength of Thin Steel Compression Flanges," Bulletin No. 35, Part 3, Cornell University, Engineering Experiment Station, Ithaca, N.Y., 1947.

60. Winter, G., "Performance of Thin Steel Compression Flange," Preliminary Publication, 3rd Congress of the International Association for Bridge and Structural Engineering, 1948, p.137.

61. Winter, G., "Performance of Compression Plates as Parts of Structural Members," Bulletin No. 35, Cornell University, Engineering Experiment Station, Ithaca, N.Y., 1947.

62. Kalyanaraman, V., T. Pekoz, and G. Winter, "Analytical Study of Unstiffened Elements," Journal of Structural Division, ASCE, Volume 104, No. ST9, September 1978.

63. Kalyanaraman, V., T. Pekoz, and G. Winter, "Unstiffened Compression Elements," Journal of Structural Division, ASCE, Volume 103, No. ST9, September 1977.

64. Kalyanaraman, V., "Local Buckling of Cold-Formed Steel Members," Journal of Structural Division, ASCE, Volume 105, No. ST5, May 1979.

65. Pekoz, T., "Development of a Unified Approach to the Design of Cold-Formed Steel Members," Report SG86-4, AISI, Washington, D.C., May 1986.

66. American Iron and Institute, Cold-Formed Steel Design Manual,, 1986 Edition with the 1989 Addendum.

67. Parkes, E.W., "The Permanent Deformation of a Cantilevel Struck Transversely at Its Tip," Proceeding of the Royal Society, London, England, Series A, Vol. 228, 1955, p.462.

68. Parkes, E.W., "The Permanent Deformation of an Encastre Beam Struck Transversely at any Point in Its Span," Proc. Inst. Cilil Eng., July 1958.

69. Ezra, A.A., "The Plastic Response of a Simply Supported Beam to Impact Load at the Center," Proc. III U.S. Nat. Cong. Appl. Mech., 1958.

70. Ting, T.C.T. and P.S. Symonds, "Impact of a cantilevel Beam with Strain Rate Sensitivity," Proceeding of Fourth U.S. National Congress of Apllied Mechanics, 1962.

71. Bonder, S.R. and P.S. Symonds, "Experimental and Theoretical Investigation of the Plastic Deformation of Cantilevel Beams Subjected to Impulsive Loading," Journal of Applied Mechanics, Volume 29., December 1962.

72. Rawlings, B., "The Dynamic Behavior of Steel in Pure Flexure," Proceeding of Royal Society, Series A, Volume 275, 1963.

73. Ting, T.C.T., "Large Deformation of a Rigid-Ideally-Plastic Cantilevel Beam," Journal of Applied Mechanics, June 1965.

74. Florence, A.L. and R.D. Firth, "Rigid-Plastic Beams under Uniformly Distributed Impulses," Journal of Applied Mechanics, Volume 32, 1965, p.481.

75. Jones, N., "Influence of Strain-Hardening and Strain-Rate Sensitivity on the Permanent Deformation of Impulsively Loaded Rigid-Plastic Beam," Int. J. Mech. Sci., Volume 9, 1967, p.777.

76. Aspden, R.J. and J.D. Campbell, "The Effect of Loading Rate on the Elasto-Plastic Flexure of Steel Beams," Proceedings of Royal Society, Volume A290, 1966.

77. Culver, C.G., E.A. Zanoni, and A.H. Osgood, "Response of Thin-Walled Beams to Impact Loading," Proceedings of the First Specialty Conference on Cold-Formed Steel Structures, University of Missouri-Rolla, August 1971.

78. Symonds, P.S. and N. Jones, "Impulsive Loading of Fully Clamped Beams with Finite Plastic Deflection and Strain-Rate Sensitivity," Int. J. Mech. Sci., Volume 14, 1972.

79. Forrestal, M.J. and M.J. Sagartz, "Elastic-Plasric Response of 304 Stainless Steel Beams to Impulse Loads," Journal of Applied Mechanics, Volume 45., September 1978.

80. Forrestal, M.J. and D.L. Wesenberg, "Elastic Plastic Response of Simply Supported 1018 Steel Beams to Impulse Loads," Journal of Applied Mechanics, December 1977.

81. VanKuren R.C. and J.E. Scott, "Energy Absorption of High-Strength Steel Tubes under Impact Crush Conditions," Proceedings of International Automotive Engineering Congress and Exposition, Society of Automotive Engineers, 1977.

82. Calladine, C.R. and R.W. English, "Strain-Rate and Inertia Effects in the Collapse of Two Types of Energy-Absorbing Structure," Int. J. Mech. Sci., Volume 26, 1984, pp.689-701.

83. Rawlings, B., "Response of Structures to Dynamic Loads," Mechanical Properties at High Rates of Strain, Institute of Physics, London, No. 21, 1974.

84. Birch, R.S. and N. Jones, "Dynamic and Static Axial Crushing of Axially Stiffened Cylindical Shells," University of Livepool, Livepool, Australia.

85. Hoff, N., "Dynamic Stability of Structures," Proceedings of an International Conference on Dynamic Stability of Structures, Northwesten University, Evanston, Illinois, October 1965.

86. Culver, C.G. and N.R. Vaidya, "Impact Loading of Thin-Walled Columns," Proceedings of the First Specialty Conference on Cold-Formed Steel Structures, University of Missouri-Rolla, August 1971.

87. Logue, J.M., "Experimental Study of Thin-Walled Columns Subjected to Impact Loading," Master Thesis, Carnegie-Mellon University, April 1971.

88. Soden, P.D., S.T.S. Al-Hassani, and W. Johnson, "The Crumpling of Polyvinylchloride Tubes under Static and Dynamic Axial Loads," Mechanical Properties at High Rates of Strain, Institute of Physics, London, No. 21, 1974.

89. Van Kuren, R.C., "Energy Absorption of Plastic, Steel, and Aluminum Shells under Impact Conditions," Proceedings of International Automotive Engineering Congress and Exposition, Society of Automotive Engineers, 1980.

90. Wierzbicki, T., "Dynamic Crushing of Strain Rate Sensitive Box Columns," SAE Second International Conference on Vehicle Structural Mechanics, April 1977.

91. Wierzbicki, T. and W. Abramowicz, "Crushing of Thin-Walled Strain-Rate Sensitive Structures," Dynamic and Crushing Analysis of Plastic Structures, Euromech Colloquium No. 121, August 1979.

92. Abramowicz, W. and N. Jones, "Dynamic Axial Crushing of Square Tubes," Int. J. Impact Engng., Volume 2, 1984.

93. Alexander, J.M., "An Approximate Analysis of the Collapse on Thin Cylindrical Shells under Axial Loading," Quart J. Mech. Appl. Math., 1960.

94. Mahmood, H.F. and A. Paluszny, "Axial Collapse of Thin Wall Cylindrical Column," SAE Fifth International Conference on Vehicle Structural Mechanics, April 1984.

95. Mamalis, A.G., W. Johnson, and G.L. Viegelahn, "The Crumpling of Steel Thin-Walled Tubes and Frusta under Axial Compression at Elevated Strain-Rate: Some Experimental Results," Int. J. Mech. Sci., Volume 26, 1984, pp.537-547.

96. Galambos, T.V. (ed.), Guide to Stability Design Criteria for Metal Structures, 4th Edition, John Wiley & Sons Incs., New York, 1988.

97. Johnson, A.L. and G. Winter, "The Structural Performance of Austenitic Stainless Steel Members," Report No. 327, Cornell University, November 1966.

98. Chajes, A., S.J. Britvec, and G. Winter, "Effects of Cold-Straining on Structural Sheet Steels," Journal of the Structural Division, Proceedings of the American Society of Civil Engineers, Volume 89, No. ST2, April 1963.

99. Bleich, F., Buckling Strength of Metal Structures, New York: Mcgraw-Hill Book Company, 1952.

100. Gerard, G., and H. Becker, Handbook of Structural Stability, Part I - Buckling of Flat Plates, NACA Technical Note 3781, July, 1957.

101. Pan, C.L. and W.W. Yu, "Design of Automotive Structural Components Using High Strength Sheet Steels: Mechanical Properties of Materials," Seventeenth Progress Report, Civil Engineering Study 92-2, University of Missouri-Rolla, May, 1992.